The Convective Instability of BEK Family of Non-Newtonian Rotating Boundary-Layer Flows

Thesis submitted for the degree of

Doctor of Philosophy

at the University of Leicester

by

Mohammed Alaa Abdulameer

Department of Mathematics

University of Leicester

June 2018

Abstract

The BEK family of flows have many important practical applications such as centrifugal pumps, steam turbines, turbo-machinery and rotor-stator devices. The Bödewadt, Ekman and von Kármán flows are particular cases within this family. The convective instability of the BEK family of rotating boundary-layer flows has been considered for generalised Newtonian fluids, power-law and Carreau fluids. A linear stability analysis is conducted using a Chebyshev collocation method in order to investigate the effect of shear-thinning and shear-thickening fluids for generalised Newtonian fluids on the convective Type I (inviscid cross-flow) and Type II (viscous streamline curvature) modes of instability. The results reveal that shear-thinning power-law fluids have a universal stabilising effect across the entire BEK family of flows. However, the convective instability characteristics for the shear-thinning and shear-thickening Carreau fluids are affected by the value of the relaxation parameter k. The results reveal that Shear-thinning Carreau fluids have a small destabilising effect, while shear-thickening fluids have a slight stabilising effect on the Type I and Type II mode for the BEK family of flows when $k = 100$. On the other hand, shear-thinning and shear-thickening Carreau fluids are found to have stabilising and destabilising effect, respectively for optimal relaxation value ko. The results are presented in terms of neutral curves and growth rates. Furthermore, an energy analysis is presented to gain insight into the underlying physical mechanisms behind the stabilising effects of generalized Newtonian fluids. In conclusion, the use of shear-thinning power-law and Carreau fluids with optimal value ko can be recommended to reduce skin-friction drag in enclosed rotor-stator devices for the entire BEK family of flows.

I would like to dedicate this thesis to my loving parents ...

Acknowledgements

Contents

List of Figures

List of Tables

Nomenclature

Roman Symbols

$\bar{n}$ number of spiral vortices

η dimensionless similarity coordinate

$\hat{u}, \hat{v}, \hat{w}, \hat{p}$ spectral representations of the perturbation velocities and pressure, respectively

c_0 viscosity ratio for Carreau fluids

Co Coriolis parameter

K kinetic energy

k relaxation parameter

ko optimal relaxation parameter

L^* non-dimensional length scale

n power-law index

p, P perturbation and mean pressure, respectively

r radial coordinate

Re Reynolds number

Ro Rossby number

R_c critical Reynolds number at the onset of the Type I mode

t time

u, U perturbation and mean radial velocity, respectively

U_0, V_0, W_0 leading-order velocity components

v, V perturbation and mean azimuthal velocity, respectively

w, W perturbation and mean axial velocity, respectively

z axial coordinate

Greek Symbols

α radial wave-number

$\bar{\mu}_0$ zero-shear-rate viscosity

$\bar{\mu}_\infty$ infinite-shear-rate viscosity

β azimuthal wave-number

$\dot{\gamma}$ rate-of-strain tensor

κ, ϕ modified wavenumber and orientation angle, respectively

ν kinematic viscosity

ω frequency

Ω^* system rotation rate

ρ density

σ_{ij} anti-symmetric viscous stress terms

τ shear stress tensor

θ circumferential coordinate in the rotating frame

$\triangle \Omega^*$ differential rotation rate

Ω_D^*, Ω_F^* angular velocities of disk and fluid, respectively

Superscripts

$*$ dimensional quantity

Chapter 1

Introduction

1.1 Literature review

There has been significant interest in the stability and transition from laminar to turbulence of the three-dimensional boundary-layer flow due to the rotating-disk (that is the von Kármán flow) in recent decades. von Kármán (1921) was the first to investigate the three-dimensional problem theoretically. He considered the cylindrical Navier-Stokes equations for steady mean flow of an incompressible fluid induced by the rotation of an infinite plane with uniform angular velocity. These governing Navier-Stokes equations are transformed from partial differential equations to a set of ordinary differential equations using similarity variables that are referred to as the von Kármán similarity variables. von Kármán (1921) solved the equations numerically in order to obtain the solutions of steady mean velocity profiles of the flow. The problem was then verified by Cochran (1934) to obtain more accuracy for the results of mean velocity flow. Batchelor (1951) showed that the von Kármán flow is one particular case of a family of rotating flows that arises when the lower disk rotates under a stationary fluid. The other particular cases are the Ekman (1905) and Böedewadt (1940) flows.

The seminal study of the stability properties of the Newtonian rotating-disk boundary-layer was performed theoretically and experimentally by Gregory et al. (1955), and there the first

theoretical stability analysis are presented. However, Smith (1947) and Gray (1952) gave the first experimental observation of stationary cross-flow vortices for the flows of rotating-disk and flows over a swept wing, respectively. Gregory et al. (1955) used a china-clay technique and observed approximately 30 vortices on the disk surface in order to study the transition from laminar to turbulent flow where the angle between the normal of vortices and outward drawn radius was 14 degrees. It is found that cross-flow vortices appear at the Reynolds number of around $R \approx 430$, whilst $R \approx 530$ is reported in this experiment to initiate the transition to turbulence. Stuart conducted the theoretical part of the study by applying "a linear stability analysis" for high Reynolds numbers. Broad agreement between the theoretical and experimental parts was found for the angle of the vortices. However, he predicts that the number of stationary vortices was approximately 4 times the experimental observation, this is expected to be due to the neglect of viscous effects in the theoretical study. Work continues to this day in an attempt to clarify the full stability mechanics at play in this deceptively simple boundary layer.

Figure 1.1 shows the three main regions of the flow: laminar flow, spiral vortices and fully turbulent flow. This visualisation presents the spiral vortices as a transition process from laminar and turbulent flow caused by the appearance of an inviscid cross-flow instability or the mode that is referred to as the Type I mode. The occurrence of this mode is due to the inflectional point in the laminar radial velocity profile, under the well know Rayleigh inflection point rule.

The majority of this thesis is concerned with the stability characteristics for the family of boundary-layer flows attributed to a differential rotation rate between a lower disk and upper fluid in rigid-body rotation. Particular arrangements of this dual rotating system include the von Kármán (1921), Ekman (1905) and Böedewadt (1940) boundary-layer flows. The von Kármán layer arises when the lower disk rotates under a stationary fluid, the Ekman layer occurs when the disk and fluid rotate with approximately the same angular velocity, and the
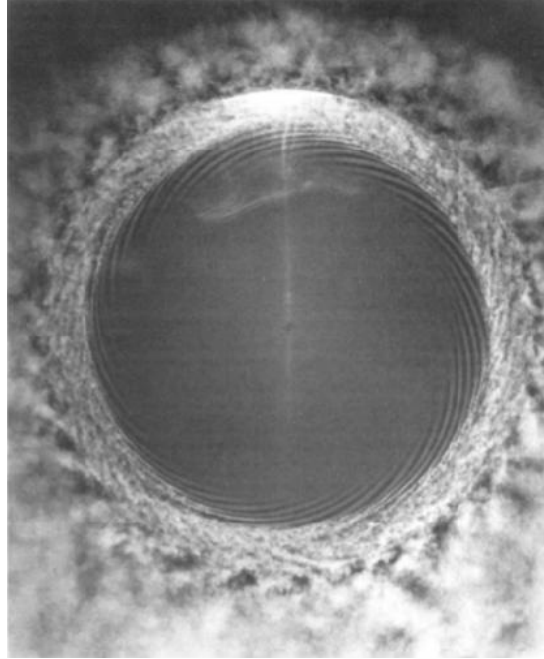
Figure 1.1: Experimental visualisation of the flow over a rotating-disk, taken from Kohama (1984).

Bödewadt layer occurs when the fluid rotates above a stationary disk. There is a continuum of intermediate cases between these standard configurations and collectively these form a wide class of boundary-layer flows is known to as "the BEK family".

The flows of BEK family for rotating-disk problem have many important practical applications such as centrifugal pumps, gas and steam turbines, turbo-machinery and rotor-stator devices and other machines related to rotating fluids. The rotating-disk in the von Kármán flow acts as a centrifugal fan, where the fluid at the disk surface is pulled circumferentially into azimuthal direction around the disk due to viscous stresses. Nevertheless, the fluid is thrown radially outwards caused by the centrifugal forces and the radial pressure gradient. Therefore, the radial and azimuthal components U and V, respectively play an important role to produce the flow in a spiral pattern, while the axial velocity W leads to replace fluid thrown away at the edge of the disk by an axial downward flow into all the disk surface as shown in Figure 1.2.

With regards to the Ekman flow, some investigations in meteorology and oceanography
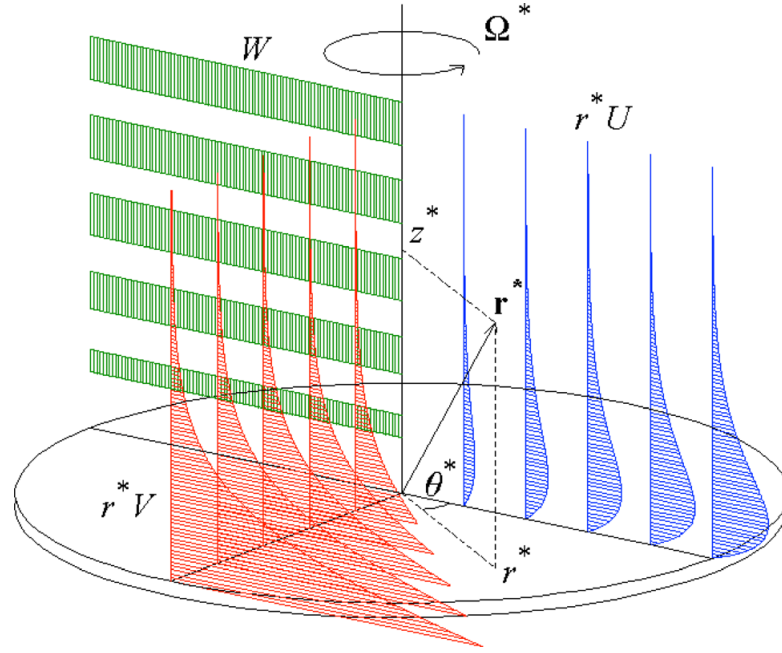
Figure 1.2: A sketch of the velocity profiles for the von Kármán boundary-layer on a rotating-disk, taken from Imayama et al. (2014).

use the Ekman boundary-layer. For example, the interaction of the oceans and atmosphere, hurricanes and typhoons. Ekman (1905) was the first to describe this flow and make the link to geophysical flows. He revealed that the earth's rotation affected the way that the currents of the ocean responded to the force of the wind. The effects of the radial pressure, Coriolis and viscous forces are balanced in the Ekman flow. The first investigation to study the stability analysis for the Ekman flow was performed experimentally by Faller (1963). A large cylindrical rotating tank was used to produce the Ekman layer and investigate the inviscid Type I instability mode noticed at Reynolds number of approximately $R \approx 125$. The Type I mode was also detected analytically by the study of Faller and Kaylor (1966) for Reynolds number of about $R \approx 118$. Furthermore, a viscous Type II instability mode attributed to the Coriolis force and streamline curvature effects was found to occur for $R \approx 55$. Further investigations of Type I and II modes for Ekman flow are conducted experimentally by Tatro and Mollo-Christensen (1967) and theoretically by Lilly (1966), Faller (1991) and Lingwood (1997).

The Bödewadt flow has a number of applications similar to the Ekman flow in the area of

meteorology and oceanography. Böedewadt (1940) was the first to obtain the solution of the steady mean flow profiles for a fluid rotates above a flat plate. The first experimental study of the Bödewadt flow was accomplished by Savaş (1987) who found that the structure of the laminar flow was in the form of circular waves with a critical Reynolds number for instability at $R = 25$. Further experimental study was performed by Lingwood and Alfredsson (2000) on the stability of the Bödewadt flow arising on the stator of an enclosed rotor-stator system. In general, the critical Reynolds number for Bödewadt flow is extremely small compared to critical values for the von Kármán and Ekman flows.

Malik (1986) presented an inclusive numerical study of the neutral stability curves for convective stationary disturbances using the sixth-order system of linear stability perturbation equations by utilising "a parallel-flow approximation". Malik identified the two distinct modes mentioned in the previous literature: inviscid Type I and viscous Type II instability modes that explain the numerical results as well as the regions of instability. The Type I mode was shown to be the dominant with a critical Reynolds number of 285.36, compared to 440.88 for the Type II mode. In the same year, Hall (1986) approached the problem rigorously and presented a high Reynolds number linear asymptotic analysis. Complete agreement between Hall and Malik's studies is found in the appropriate parameter limit.

Following these important milestones the seemingly simple system has continued to attract attention and it remains under active investigation to this day. The Type III mode that propagating energy towards the centre of the disk was discovered by Mack (1985); this mode was not observed in the previous stability investigations due to it being spatially damped. The Type III mode was investigated for the von Kármán flow by the study of Lingwood (1995). Lingwood discovered that the rotating-disk boundary-layer is locally absolutely unstable and suggested that the turbulent transition may be caused by absolute instability. Lingwood (1995) showed that the absolute instability in the rotating-disk flow is caused by the coalescence of the Type I and Type III for a complex frequency with positive imaginary part and non-zero real
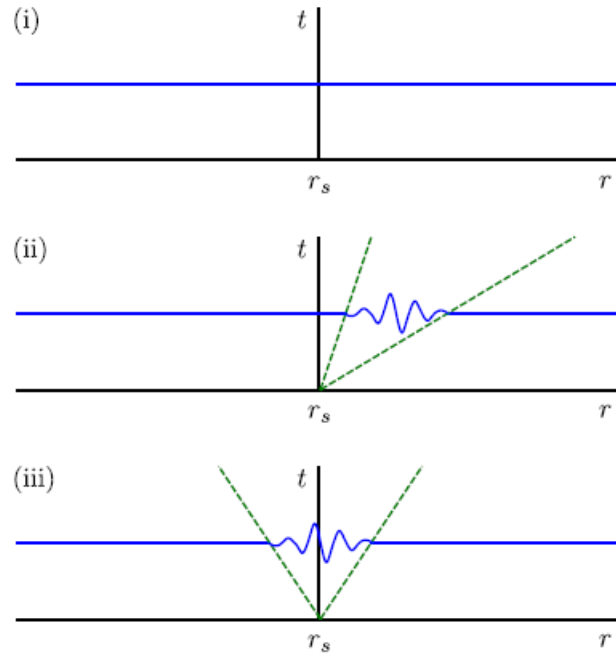
Figure 1.3: Space-time sketches of (i) stable, (ii) convectively unstable and (iii) absolutely unstable disturbances.

part by using "the Briggs-Bers method" (Bers, 1975; Briggs, 1964). This coalescence leads to pinch-points that exist within the region of the absolute instability. Lingwood (1995) reported the critical Reynolds number for the onset of absolute instability to be $R = 510$ which shows good agreement with the experimental value of Lingwood (1996) of $R = 513$.

A flow is absolutely unstable when unbounded localised disturbances for large time and propagate both upstream and downstream. However, in the case of convective unstable, the disturbances are swept away from the location where it generated either downstream or upstream. Figure 1.3 illustrates the concepts of (i) stable, (ii) convectively unstable and (iii) absolutely unstable. The two edges of the disturbance are propagating away from the source in the same direction for the convectively unstable, while the edges are propagating in the opposite direction toward infinity for the absolutely unstable.

Davies and Carpenter (2003) studied the global behaviour of the absolute instability for the rotating-disk problem. They showed by using direct numerical simulations of the linearised

governing equations that the local absolute instability does not produce a linear global instability. Furthermore, Davies and Carpenter (2003) found that the convective behaviour dominates at all Reynolds numbers. The interested reader is referred to the literature for full information on the latest developments concerning the transition to turbulence via the generation of a non-linear global mode (Appelquist et al., 2015; Imayama et al., 2014; Pier, 2003).

The study of the wider BEK family of flows has attracted the attention of many researchers in the last decades. The work of Lingwood (1997) is an important study that presented the local convective and absolute instability analyses for the BEK family of flows. Lingwood revealed that all flows of the BEK family are absolutely unstable. The critical Reynolds numbers of Type I mode for convective instability are reported for the von Kármán, Ekman and Bödewadt flow to be $R = 290.1$, 116.3, and 27.4, respectively. More recently, Lingwood and Garrett (2011) discussed the use of mass flux through the lower disk as a potential flow-control mechanism. Various experimental studies concerning the stability, transition and control of these types of flows has been an area of more recent active research (Imayama et al., 2014, 2016; Lingwood, 1996).

As explained below, the intention here is to generalise the original study by Lingwood (1997) of BEK family of flows to incorporate the effects of non-Newtonian fluids. The motivation in this thesis is to explore the potential for using such fluids to optimise the performance of rotor-stator systems in engineering applications by reducing skin-friction drag by maximising the region of laminar flow (that is, delaying the onset of instability).

The mechanisms of skin-friction drag reduction are interested by numerous researchers for the rotating-disk boundary-layer. Cooper and Carpenter (1997) presented the effects of wall compliance on the stability of the von Kármán flow theoretically. They revealed that there is a stabilizing effect the inviscid Type I mode, while the viscous Type II mode is found to be destabilizing. Recently, Cooper et al. (2015) studied the effects of anisotropic (concentric grooves and radial grooves) and isotropic roughness on boundary-layer flows applying a

partial-slip approach in order to delay the transition from laminar to turbulence. The effect of surface roughness leads to a stabilisation of the Type I and Type II mode with the exception of a disk with concentric grooves that has a strongly destabilizing effect on the Type II mode. The results of Cooper et al. (2015) are confirmed by the study of Garrett et al. (2016) using two different modelling approaches, MW (Miklavčič and Wang, 2004) and YHP (Yoon et al., 2007) models. More recently, Alveroglu et al. (2016) investigated the effect of both anisotropic and isotropic roughness on the BEK family flows.

Further research interests have related to the stability and the transition of the boundary-layer flow over rotating sphere and cones. Garrett and Peake (2002) showed that the cross-flow instability mode for the rotating sphere boundary-layer dominates below $\theta = 66°$, while the stream curvature mode is dominated above this latitude. The stability of the rotating cone boundary-layer have been investigated by Garrett et al. (2009). They reveal a convenient agreement with experimental results for half-angle $\psi > 40°$. An alternative formulation that focuses on centrifugal effects has been considered by Hussain et al. (2014) to study the stability of the rotating cone for half-angle $\psi < 40°$.

With regards to prior studies of the non-Newtonian boundary-layer flow over a rotating-disk, Mitschka (1964) was the first to extend the von Kármán similarity solution to incorporate fluids that adhere to a power-law governing viscosity relationship. One year later, Mitschka and Ulbrecht (1965) obtained steady mean flow solutions for both shear-thickening and shear-thinning fluids. That study was later verified by Andersson et al. (2001) in order to test the reliability of their numerical solutions. However, further to this, Denier and Hewitt (2004) readdressed the problem showing that asymptotic matching considerations need to be taken into account in order to able to accurately describe the flow of shear-thinning power-law fluids. In the shear-thickening regime it transpires that the boundary-layer solutions are complicated by a region of zero viscosity away from the wall. For these reasons, in the study of power-law fluids, we will restrict our attention to moderately shear-thinning fluids only. Ming et al.

(2011) extended the study of Andersson et al. (2001) in order to investigate the heat transfer supposed the thermal conductivity follows the same function as the power-law viscosity of fluid. For full details regarding the asymptotic structure of the solutions the interested reader is refereed to Denier and Hewitt (2004).

Much more recently, Griffiths et al. (2014b) considered a rigorous asymptotic stability analysis of the shear-thinning boundary-layer flow over a rotating-disk. This work was then extended by the same authors Griffiths et al. (2014a) to compute the neutral curves of convective instability (working under the boundary-layer approximation) and complete agreement was found with their prior asymptotic analysis. These two papers can be considered as the non-Newtonian generalisations of Hall (1986) and Malik (1986), respectively.

The Carreau fluid has been given less attention in the rotating-disk problem comparing to other rheological models of generalized Newtonian fluids. Carreau (1972) was the first to describe this type of fluid. Griffiths (2015) later extends the power-law studies to include the Bingham (1916) and Carreau (1972) models of non-Newtonian viscosity. He finds that a generalisation of the von Kármán similarity solution is applicable for a variety of different inelastic and viscoplastic non-Newtonian models. The convective instability analysis for Carreau model for shear-thinning and shear-thickening fluids was discussed in Griffiths (2016) for Kármán flow.

1.2   Contributions and Outline of thesis

The main aim of this thesis is to generalize the non-Newtonian study of Griffiths (2016) to the entire BEK family of rotating boundary-layer flows, as considered by Lingwood (1997) in the Newtonian case. A Chebyshev polynomial method is used after applying the linear convective instability to consider the effects of power-law and Carreau fluids on the Type I and Type II modes. In Chapter 2 an overview of the generalized Newtonian fluids is presented as a special case of non-Newtonian fluids. Furthermore, the governing boundary-layer equations

are considered for this problem by using boundary-layer approximation. These equations are solved to present the steady mean flow profiles of the BEK family for power-law and Carreau fluids in Chapter 3. The convective instabilities for the BEK family of flows of power-law and Carreau fluids are presented in Chapters 4 and 5, respectively. In these chapters, the linear perturbation equations are formulated by applying parallel-flow approximation and then solved them using Chebyshev collocation method in order to present the convective neutral curves. These curves are confirmed by presenting the growth rates and conducting an energy balance analysis. Finally, the conclusions of the findings are discussed in Chapter 6 including the comparison between the two generalised Newtonian fluid models. A view towards future work for the study is also presented.

The work related to power-law fluids has been published and appears in the literature as:

Abdulameer, M., Griffiths, P., Alveroğlu, B., Garrett, S. J., 2016. On the stability of the BEK family of rotating boundary-layer flows for power-law fluids. *Journal of Non-Newtonian Fluid Mechanics, 236*, 63–72.

Chapter 2

Formulation of the problem

In this chapter, the governing equations for non-Newtonian fluids over a rotating-disk have been derived in order to describe the boundary-layer flow and its stability properties. The behaviour of the fluid flow is affected by several physical properties, for instance, the viscosity which is the most important property for the nature of the fluid. There are many variables that determine the viscosity such as shear rate, temperature and pressure (Barnes et al., 1989). The change of the viscosity with the shear rate of the flow is represented by non-Newtonian fluids (generalised Newtonian fluids) in §2.1. The governing boundary-layer equations for generalized Newtonian fluids are derived in §2.2.

2.1 Generalised Newtonian fluids

In many industrial applications and flow problems such as lubrication and polymer processing, it was found that the shear rate dependence of fluid viscosity has several useful empiricisms summarized by Bird et al. (1977) as the generalised Newtonian fluids. The flow of a Newtonian fluid can be considered as a special case of the generalised Newtonian fluids. The constitutive relationship for a Newtonian fluid in a simple flow with velocity $\boldsymbol{u} = (u(y), 0, 0)$ is defined by

$$\tau = \mu_n \frac{du}{dy},$$ (2.1)

where τ is the shear stress tensor and μ_n is the constant viscosity.

The viscosity of the Newtonian fluid is constant at all shear rates, hence the shear stress is a linear function of the shear rate du/dy. However, the viscosity of a generalised Newtonian fluids is not constant and can be described as a function of the shear rate.

The fundamental relationship (2.1) can be extended for generalised Newtonian fluids to any arbitrary flow field in an arbitrary coordinate system $\boldsymbol{u} = \boldsymbol{u}(x,y,z,t)$ as follows

$$\boldsymbol{\tau} = \mu \dot{\boldsymbol{\gamma}},$$ (2.2)

where $\dot{\boldsymbol{\gamma}} = \nabla \boldsymbol{u} + (\nabla \boldsymbol{u})^T$ is the rate-of-strain tensor and μ is a scalar viscosity function depending on the invariants of the tensor $\dot{\boldsymbol{\gamma}}$. In other words, the generalised Newtonian viscosity can be written as $\mu = \mu(\dot{\gamma})$. The invariants of the tensor $\dot{\boldsymbol{\gamma}}$ are independent under a rotation of the coordinate system. Three invariants are defined in Bird et al. (1977) by selecting the following tensor component combinations:

$$I = \text{tr}\dot{\boldsymbol{\gamma}} = \sum_i \dot{\gamma}_{ii},$$ (2.3a)

$$II = \text{tr}\dot{\boldsymbol{\gamma}}^2 = \sum_i \sum_j \dot{\gamma}_{ij}\dot{\gamma}_{ji} = \sum_i \sum_j \dot{\gamma}_{ij}^2,$$ (2.3b)

$$III = \text{tr}\dot{\boldsymbol{\gamma}}^3 = \sum_i \sum_j \sum_k \dot{\gamma}_{ij}\dot{\gamma}_{jk}\dot{\gamma}_{ki}.$$ (2.3c)

It is clear to show that the first invariant $I = 2(\nabla.\boldsymbol{u})$, and hence I, is identically zero for incompressible fluids. The third invariant III vanishes to zero for shearing flow such as tube flow, axial annular flow and the flow between rotating disks. Therefore, the first and third invariants do not play a role in these flows (Bird et al., 1977). Thus, μ depends only on the second invariant which can be expressed in terms of $\dot{\gamma}$, the magnitude of $\dot{\boldsymbol{\gamma}}$:

$$\dot{\gamma} = \sqrt{\frac{\dot{\boldsymbol{\gamma}} : \dot{\boldsymbol{\gamma}}}{2}}, \tag{2.4}$$

where the double dot operation is defined by Griffiths (2016) to be

$$
\begin{aligned}
(\dot{\boldsymbol{\gamma}} : \dot{\boldsymbol{\gamma}}) &= \left[\left(\sum_i \sum_j \delta_i \delta_j \dot{\gamma}_{ij} \right) : \left(\sum_k \sum_l \delta_k \delta_l \dot{\gamma}_{kl} \right) \right] = \sum_i \sum_j \sum_k \sum_l \left(\delta_i \delta_j : \delta_k \delta_l \right) \dot{\gamma}_{ij} \dot{\gamma}_{kl} \\
&= \sum_i \sum_j \sum_k \sum_l \left(\delta_j . \delta_k \right) \left(\delta_i . \delta_l \right) \dot{\gamma}_{ij} \dot{\gamma}_{kl} = \sum_i \sum_j \sum_k \sum_l \delta_{il} \delta_{jk} \dot{\gamma}_{ij} \dot{\gamma}_{kl} \\
&= \sum_i \sum_j \dot{\gamma}_{ij} \dot{\gamma}_{ji} = \sum_i \sum_j \dot{\gamma}_{ij}^2 = II.
\end{aligned}
$$

In the generalised Newtonian fluids, there are several empiricisms for the non-Newtonian viscosity depending on the relation between the viscosity and the rate-of-strain tensor as follows (Bird et al., 1977)

Ostwald-de Waele model $\quad\quad \mu = m (\dot{\gamma})^{n-1}, \tag{2.5a}$

Carreau-Yasuda model $\quad\quad \mu = \bar{\mu}_\infty + (\bar{\mu}_0 - \bar{\mu}_\infty) \left[1 + (\lambda \dot{\gamma})^a \right]^{(n-1)/a}, \tag{2.5b}$

Powell-Eyring model $\quad\quad \mu = \bar{\mu}_\infty + (\bar{\mu}_0 - \bar{\mu}_\infty) (\lambda \dot{\gamma})^{-1} \operatorname{arcsinh} (\lambda \dot{\gamma}), \tag{2.5c}$

Bingham model $\quad\quad \mu = \begin{cases} \infty & \text{for} \quad \tau < \tau_y, \\ \bar{\mu}_p + \tau_y (\dot{\gamma})^{-1} & \text{for} \quad \tau \geq \tau_y. \end{cases} \tag{2.5d}$

Here m is the consistency coefficient and n is the dimensionless power-law index for the Ostwald-de Waele or power-law model. For the Carreau-Yasuda model, $\bar{\mu}_\infty$ is the infinite-shear-rate viscosity, $\bar{\mu}_0$ is the zero-shear-rate viscosity, λ is the characteristic time constant (relaxation time) and a is the power-law scale factor. By setting $a = 2$, the Carreau-Yasuda model that can reduces to the known Carreau model. For the Bingham model, $\bar{\mu}_p$ plastic-shear-rate viscosity, the magnitude of the shear stress tensor is $\tau = \sqrt{(\boldsymbol{\tau} : \boldsymbol{\tau})/2}$, and τ_y is the yield stress. These models are discussed at length in Bird et al. (1977).

The power-law and Carreau fluids are called shear-thinning (pseudoplastic) for $n < 1$

where the viscosity of these models decreases with increasing the shear rate. For the power-law index $n > 1$, the fluids are called shear-thickening (dilatant) where the viscosity increases with increasing shear rate of the fluids. The classical Newtonian viscosity relationship is recovered by setting $n = 1$ in (2.5) such that $m = \mu_n$ for power-law model, $\bar{\mu}_0 = \bar{\mu}_\infty$ for Carreau and Eyring models, and $\tau_y = 0$ for Bingam model. The viscosity of the Newtonian fluid flow is constant at all share rates as was mentioned before.

The power-law model was firstly defined by a British chemist Armand de Waele (De Waele, 1923) and then by the German biologist and chemist Friedrich Wilhelm Ostwald (Ostwald, 1925). The behaviour of the viscosity for the power-law fluids is described as follows

$$\lim_{\dot{\gamma} \to 0} \mu(\dot{\gamma}) \to \infty, \quad \lim_{\dot{\gamma} \to \infty} \mu(\dot{\gamma}) \to 0 \quad \text{for} \quad n < 1,$$

$$\lim_{\dot{\gamma} \to 0} \mu(\dot{\gamma}) \to 0, \quad \lim_{\dot{\gamma} \to \infty} \mu(\dot{\gamma}) \to \infty \quad \text{for} \quad n > 1.$$

It is clear to note that this behaviour is unphysical. Therefore, the relationship of power-law model is convenient for only finite shear rates.

The behaviour of the viscosity for the Carreau fluids, first introduced by a modern rheologist Pierre Carreau (Carreau, 1972) is expressed by

$$\lim_{\dot{\gamma} \to 0} \mu(\dot{\gamma}) \to \mu_0, \quad \lim_{\dot{\gamma} \to \infty} \mu(\dot{\gamma}) \to \mu_\infty \quad \text{for} \quad n < 1,$$

$$\lim_{\dot{\gamma} \to 0} \mu(\dot{\gamma}) \to \mu_0, \quad \lim_{\dot{\gamma} \to \infty} \mu(\dot{\gamma}) \to \infty \quad \text{for} \quad n > 1.$$

2.2 The governing boundary-layer equations for generalised Newtonian fluids

In this section the governing equations of the boundary-layer flow for both power-law and Carreau fluids are derived. The boundary-layer flow of an incompressible generalised Newtonian

fluid is considered above an infinite rotating-disk located at $z^* = 0$.

The continuity and Navier–Stokes equations in the frame of reference rotating with the angular velocity of the lower disk Ω_D^* can be considered as

$$\boldsymbol{\nabla}.\boldsymbol{u^*} = 0, \tag{2.6a}$$

$$\frac{\partial \boldsymbol{u^*}}{\partial t^*} + \boldsymbol{u^*}.\boldsymbol{\nabla}\boldsymbol{u^*} + 2\boldsymbol{\Omega_D^*} \times \boldsymbol{u^*} = -\frac{1}{\rho^*}\boldsymbol{\nabla}p^* + \frac{1}{\rho^*}\boldsymbol{\nabla}.\boldsymbol{\tau^*}. \tag{2.6b}$$

Here $\boldsymbol{u^*} = (u^*, v^*, w^*)$ are the steady velocity components in cylindrical polar coordinates (r^*, θ, z^*), t^* is time and $\boldsymbol{\Omega_D^*} = (0, 0, \Omega_D^*)$ is the angular velocity of the disk. Furthermore, ρ^* is the fluid density and p^* is the fluid pressure. The stress tensor $\boldsymbol{\tau^*}$ for generalised Newtonian models, is defined by

$$\boldsymbol{\tau^*} = \mu^*\boldsymbol{\dot{\gamma}^*} \quad \text{with} \quad \mu^* = \mu^*(\dot{\gamma}^*),$$

where $\boldsymbol{\dot{\gamma}^*} = \boldsymbol{\nabla}\boldsymbol{u^*} + (\boldsymbol{\nabla}\boldsymbol{u^*})^T$ is the rate-of-strain tensor and $\mu^*(\dot{\gamma}^*)$ is the non-Newtonian viscosity. The magnitude of the rate-of-strain tensor is given by

$$\dot{\gamma}^* = \sqrt{\frac{\boldsymbol{\dot{\gamma}^*} : \boldsymbol{\dot{\gamma}^*}}{2}}.$$

The system (2.6) can be written without using vector notation as follows

$$\frac{1}{r^*}\frac{\partial(r^* u^*)}{\partial r^*} + \frac{1}{r^*}\frac{\partial v^*}{\partial \theta} + \frac{\partial w^*}{\partial z^*} = 0, \tag{2.7}$$

$$\frac{\partial u^*}{\partial t^*} + u^*\frac{\partial u^*}{\partial r^*} + \frac{v^*}{r^*}\frac{\partial u^*}{\partial \theta} + w^*\frac{\partial u^*}{\partial z^*} - \frac{v^{*2}}{r^*} - 2\Omega_D^* v^* = -\frac{1}{\rho^*}\frac{\partial p^*}{\partial r^*}$$
$$+ \frac{1}{\rho^*}\left[\frac{1}{r^*}\frac{\partial(r^*\tau_{r^*r^*}^*)}{\partial r^*} + \frac{1}{r^*}\frac{\partial \tau_{r^*\theta}^*}{\partial \theta} + \frac{\partial \tau_{r^*z^*}^*}{\partial z^*} - \frac{\tau_{\theta\theta}^*}{r^*}\right], \tag{2.8a}$$

$$\frac{\partial v^*}{\partial t^*} + u^* \frac{\partial v^*}{\partial r^*} + \frac{v^*}{r^*} \frac{\partial v^*}{\partial \theta} + w^* \frac{\partial v^*}{\partial z^*} + \frac{u^* v^*}{r^*} + 2\Omega_D^* u^* = -\frac{1}{r^* \rho^*} \frac{\partial p^*}{\partial \theta}$$

$$+ \frac{1}{\rho^*} \left[\frac{1}{r^{*2}} \frac{\partial \left(r^{*2} \tau_{\theta r^*}^* \right)}{\partial r^*} + \frac{1}{r^*} \frac{\partial \tau_{\theta\theta}^*}{\partial \theta} + \frac{\partial \tau_{\theta z^*}^*}{\partial z^*} \right], \quad (2.8b)$$

$$\frac{\partial w^*}{\partial t^*} + u^* \frac{\partial w^*}{\partial r^*} + \frac{v^*}{r^*} \frac{\partial w^*}{\partial \theta} + w^* \frac{\partial w^*}{\partial z^*} = -\frac{1}{\rho^*} \frac{\partial p^*}{\partial z^*}$$

$$+ \frac{1}{\rho^*} \left[\frac{1}{r^*} \frac{\partial \left(r^* \tau_{z^* r^*}^* \right)}{\partial r^*} + \frac{1}{r^*} \frac{\partial \tau_{z^* \theta}^*}{\partial \theta} + \frac{\partial \tau_{z^* z^*}^*}{\partial z^*} \right]. \quad (2.8c)$$

The components of the stress tensor in (2.8) are expressed as

$$\tau_{r^* r^*}^* = 2\mu^* \left(\frac{\partial u^*}{\partial r^*} \right), \quad (2.9a)$$

$$\tau_{\theta\theta}^* = 2\mu^* \left(\frac{1}{r^*} \frac{\partial v^*}{\partial \theta} + \frac{u^*}{r^*} \right), \quad (2.9b)$$

$$\tau_{z^* z^*}^* = 2\mu^* \left(\frac{\partial w^*}{\partial z^*} \right), \quad (2.9c)$$

$$\tau_{r^* \theta}^* = \mu^* \left[r^* \frac{\partial}{\partial r^*} \left(\frac{v^*}{r^*} \right) + \frac{1}{r^*} \frac{\partial u^*}{\partial \theta} \right] = \tau_{\theta r^*}^*, \quad (2.9d)$$

$$\tau_{r^* z^*}^* = \mu^* \left(\frac{\partial u^*}{\partial z^*} + \frac{\partial w^*}{\partial r^*} \right) \qquad = \tau_{z^* r^*}^*, \quad (2.9e)$$

$$\tau_{\theta z^*}^* = \mu^* \left(\frac{\partial v^*}{\partial z^*} + \frac{1}{r^*} \frac{\partial w^*}{\partial \theta} \right) \qquad = \tau_{z^* \theta}^*. \quad (2.9f)$$

The rate-of-strain tensor $\dot{\gamma}^*$ can be written to be

$$\dot{\gamma}^* = \sqrt{\frac{II}{2}} = \left\{ 2 \left[\left(\frac{\partial u^*}{\partial r^*} \right)^2 + \left(\frac{1}{r^*} \frac{\partial v^*}{\partial \theta} + \frac{u^*}{r^*} \right)^2 + \left(\frac{\partial w^*}{\partial z^*} \right)^2 \right] \right.$$

$$\left. + \left[r^* \frac{\partial}{\partial r^*} \left(\frac{v^*}{r^*} \right) + \frac{1}{r^*} \frac{\partial u^*}{\partial \theta} \right]^2 + \left(\frac{\partial u^*}{\partial z^*} + \frac{\partial w^*}{\partial r^*} \right)^2 + \left(\frac{\partial v^*}{\partial z^*} + \frac{1}{r^*} \frac{\partial w^*}{\partial \theta} \right)^2 \right\}^{1/2} \quad (2.10)$$

where $II = \sum_i \sum_j \dot{\gamma}_{ij}^{*2} = \dot{\gamma}_{r^* r^*}^{*2} + \dot{\gamma}_{\theta\theta}^{*2} + \dot{\gamma}_{z^* z^*}^{*2} + 2 \left(\dot{\gamma}_{r^* \theta}^{*2} + \dot{\gamma}_{r^* z^*}^{*2} + \dot{\gamma}_{\theta z^*}^{*2} \right)$.

The dimensionless analysis for the system of equations (2.7) and (2.8) is organized into

two parts that dealing separately with the two models of the generalised Newtonian fluids used in this thesis; the power-law and Carreau fluids.

2.2.1 Power-law fluids

Now, the variables of the system (2.7) and (2.8) are defined for power-law fluids in non-dimensional form

$$r = \frac{r^*}{l^*}, \quad z = \frac{z^*}{Re^{-1/(n+1)}l^*}, \quad U(r,\theta,z) = \frac{u^*(r^*,\theta,z^*)}{l^*\Omega_D^*}, \quad V(r,\theta,z) = \frac{v^*(r^*,\theta,z^*)}{l^*\Omega_D^*},$$

$$W(r,\theta,z) = \frac{w^*(r^*,\theta,z^*)}{Re^{-1/(n+1)}l^*\Omega_D^*}, \quad t = \Omega_D^* t^*, \quad P(r,\theta,z) = \frac{p^*(r^*,\theta,z^*)}{\rho(l^*\Omega_D^*)^2}, \qquad (2.11)$$

where Ω_D^* is the angular velocity of the disk, l^* is length scale, $l^*\Omega_D^*$ is the natural velocity scale and Re is the dimensionless parameter referred to as the Reynolds number defined in (2.19).

Substituting (2.11) into (2.7) and (2.8) leads to the following dimensionless continuity and Navier-Stokes equations

$$\frac{1}{r}\frac{\partial(rU)}{\partial r} + \frac{1}{r}\frac{\partial V}{\partial \theta} + \frac{\partial W}{\partial z} = 0, \qquad (2.12)$$

$$\frac{\partial U}{\partial t} + U\frac{\partial U}{\partial r} + \frac{V}{r}\frac{\partial U}{\partial \theta} + W\frac{\partial U}{\partial z} - \frac{V^2}{r} - 2V = -\frac{\partial P}{\partial r}$$
$$+ \frac{1}{\rho^*(l^*\Omega_D^*)^2}\left[\frac{1}{r}\frac{\partial(r\tau_{rr})}{\partial r} + \frac{1}{r}\frac{\partial\tau_{r\theta}}{\partial \theta} + \frac{\partial\tau_{rz}}{\partial z} - \frac{\tau_{\theta\theta}}{r}\right], \quad (2.13a)$$

$$\frac{\partial V}{\partial t} + U\frac{\partial V}{\partial r} + \frac{V}{r}\frac{\partial V}{\partial \theta} + W\frac{\partial V}{\partial z} + \frac{UV}{r} + 2U = -\frac{1}{r}\frac{\partial P}{\partial \theta}$$

$$+ \frac{1}{\rho^*(l^*\Omega_D^*)^2}\left[\frac{1}{r^2}\frac{\partial\left(r^2\tau_{\theta r}\right)}{\partial r} + \frac{1}{r}\frac{\partial\tau_{\theta\theta}}{\partial\theta} + \frac{\partial\tau_{\theta z}}{\partial z}\right], \quad (2.13b)$$

$$Re^{-1/(n+1)}\left(\frac{\partial W}{\partial t} + U\frac{\partial W}{\partial r} + \frac{V}{r}\frac{\partial W}{\partial\theta} + W\frac{\partial W}{\partial z}\right) = -\frac{1}{Re^{-1/(n+1)}}\frac{\partial P}{\partial z}$$

$$+ \frac{1}{\rho^*(l^*\Omega_D^*)^2}\left[\frac{1}{r}\frac{\partial\left(r\tau_{zr}\right)}{\partial r} + \frac{1}{r}\frac{\partial\tau_{z\theta}}{\partial\theta} + \frac{\partial\tau_{zz}}{\partial z}\right], \quad (2.13c)$$

and the rate-of-strain tensor becomes

$$\dot{\gamma}^* = \Omega_D^*\left\{2\left[\left(\frac{\partial U}{\partial r}\right)^2 + \left(\frac{1}{r}\frac{\partial V}{\partial\theta} + \frac{U}{r}\right)^2 + \left(\frac{\partial W}{\partial z}\right)^2\right] + \left[r\frac{\partial}{\partial r}\left(\frac{V}{r}\right) + \frac{1}{r}\frac{\partial U}{\partial\theta}\right]^2\right.$$

$$\left. + \left(Re^{\frac{1}{(n+1)}}\frac{\partial U}{\partial z} + Re^{\frac{-1}{(n+1)}}\frac{\partial W}{\partial r}\right)^2 + \left(Re^{\frac{1}{(n+1)}}\frac{\partial V}{\partial z} + \frac{Re^{\frac{-1}{(n+1)}}}{r}\frac{\partial W}{\partial\theta}\right)^2\right\}^{1/2}. \quad (2.14)$$

In order to obtain the non-dimensional forms of the components of the stress tensor τ_{ij}, The dimensionless of the rate-of-strain tensor is written as follows

$$\dot{\gamma} = \dot{\gamma}^*\left(\frac{Re^{-1/(n+1)}}{\Omega_D^*}\right). \quad (2.15)$$

Substituting (2.15) into (2.14) we have

$$\dot{\gamma}^2 = \left(\frac{\partial U}{\partial z}\right)^2 + \left(\frac{\partial V}{\partial z}\right)^2 + Re^{-4/(n+1)}\left[\frac{1}{r}\left(\frac{\partial W}{\partial\theta}\right)^2 + \left(\frac{\partial W}{\partial r}\right)^2\right]$$

$$+ Re^{-2/(n+1)}\left\{2\left(\frac{\partial U}{\partial r}\right)^2 + 2\left(\frac{1}{r}\frac{\partial V}{\partial\theta} + \frac{U}{r}\right)^2 + 2\left(\frac{\partial W}{\partial z}\right)^2 + \left[r\frac{\partial}{\partial r}\left(\frac{V}{r}\right) + \frac{1}{r}\frac{\partial U}{\partial\theta}\right]^2\right.$$

$$\left. + \frac{2}{r}\frac{\partial V}{\partial z}\frac{\partial W}{\partial\theta} + 2\frac{\partial U}{\partial z}\frac{\partial W}{\partial r}\right\}.$$

Therefore, the non-dimensional viscosity function of the power-law fluids is defined in the following form

$$\mu^* = m^* \left(\frac{\Omega_D^* \dot{\gamma}}{Re^{-1/(n+1)}} \right)^{n-1} = m^* \left(\frac{\Omega_D^*}{Re^{-1/(n+1)}} \right)^{n-1} \mu. \tag{2.16}$$

Substituting (2.16) and (2.11) into the components of the stress tensor (2.9), we obtain that

$$\tau_{rr} = 2m^* \Omega_D^* \left(\frac{\Omega_D^*}{Re^{-1/(n+1)}} \right)^{n-1} \mu \left(\frac{\partial U}{\partial r} \right), \tag{2.17a}$$

$$\tau_{\theta\theta} = 2m^* \Omega_D^* \left(\frac{\Omega_D^*}{Re^{-1/(n+1)}} \right)^{n-1} \mu \left(\frac{1}{r} \frac{\partial V}{\partial \theta} + \frac{U}{r} \right), \tag{2.17b}$$

$$\tau_{zz} = 2m^* \Omega_D^* \left(\frac{\Omega_D^*}{Re^{-1/(n+1)}} \right)^{n-1} \mu \left(Re^{1/(n+1)} \frac{\partial W}{\partial z} \right), \tag{2.17c}$$

$$\tau_{r\theta} = m^* \Omega_D^* \left(\frac{\Omega_D^*}{Re^{-1/(n+1)}} \right)^{n-1} \mu \left[r \frac{\partial}{\partial r} \left(\frac{V}{r} \right) + \frac{1}{r} \frac{\partial U}{\partial \theta} \right] \qquad = \tau_{\theta r}, \tag{2.17d}$$

$$\tau_{rz} = m^* \Omega_D^* \left(\frac{\Omega_D^*}{Re^{-1/(n+1)}} \right)^{n-1} \mu \left(Re^{1/(n+1)} \frac{\partial U}{\partial z} + Re^{-1/(n+1)} \frac{\partial W}{\partial r} \right) = \tau_{zr}, \tag{2.17e}$$

$$\tau_{\theta z} = m^* \Omega_D^* \left(\frac{\Omega_D^*}{Re^{-1/(n+1)}} \right)^{n-1} \mu \left(Re^{1/(n+1)} \frac{\partial V}{\partial z} + \frac{Re^{-1/(n+1)}}{r} \frac{\partial W}{\partial \theta} \right) = \tau_{z\theta}. \tag{2.17f}$$

Hence (2.13) become

$$\frac{\partial U}{\partial t} + U \frac{\partial U}{\partial r} + \frac{V}{r} \frac{\partial U}{\partial \theta} + W \frac{\partial U}{\partial z} - \frac{V^2}{r} - 2V = -\frac{\partial P}{\partial r}$$
$$+ \frac{m^* \Omega_D^{*n-2}}{\rho^* l^{*2} Re^{-1}} \left\{ \frac{\partial}{\partial z} \left[\mu \left(\frac{\partial U}{\partial z} + Re^{\frac{-2}{(n+1)}} \frac{\partial W}{\partial r} \right) \right] + Re^{\frac{-2}{(n+1)}} \left[\frac{2}{r} \frac{\partial}{\partial r} \left(\mu r \frac{\partial U}{\partial r} \right) \right.\right.$$
$$\left.\left. + \frac{1}{r} \frac{\partial}{\partial \theta} \left(\mu r \frac{\partial}{\partial r} \left(\frac{V}{r} \right) + \frac{\mu}{r} \frac{\partial U}{\partial \theta} \right) - \frac{2\mu}{r} \left(\frac{1}{r} \frac{\partial V}{\partial \theta} + \frac{U}{r} \right) \right] \right\}, \tag{2.18a}$$

$$\frac{\partial V}{\partial t} + U \frac{\partial V}{\partial r} + \frac{V}{r} \frac{\partial V}{\partial \theta} + W \frac{\partial V}{\partial z} + \frac{UV}{r} + 2U = -\frac{1}{r} \frac{\partial P}{\partial \theta}$$
$$+ \frac{m^* \Omega_D^{*n-2}}{\rho^* l^{*2} Re^{-1}} \left\{ \frac{\partial}{\partial z} \left[\mu \left(\frac{\partial V}{\partial z} + Re^{\frac{-2}{(n+1)}} \frac{1}{r} \frac{\partial W}{\partial \theta} \right) \right] + Re^{\frac{-2}{(n+1)}} \left[\frac{1}{r} \frac{\partial}{\partial \theta} \left[\mu \left(\frac{1}{r} \frac{\partial V}{\partial \theta} + \frac{U}{r} \right) \right] \right.\right.$$
$$\left.\left. + \frac{1}{r^2} \frac{\partial}{\partial r} \left(\mu r^3 \frac{\partial}{\partial r} \left(\frac{V}{r} \right) + r\mu \frac{\partial U}{\partial \theta} \right) \right] \right\}, \tag{2.18b}$$

$$\frac{\partial W}{\partial t} + U\frac{\partial W}{\partial r} + \frac{V}{r}\frac{\partial W}{\partial \theta} + W\frac{\partial W}{\partial z} = -Re^{\frac{2}{(n+1)}}\frac{\partial P}{\partial z}$$
$$+ \frac{m^*\Omega_D^{*n-2}}{\rho^* l^{*2} Re^{-1}}\left\{\frac{1}{r}\frac{\partial}{\partial r}\left(r\mu\frac{\partial U}{\partial z} + Re^{\frac{-2}{(n+1)}}r\mu\frac{\partial W}{\partial r}\right) + 2\frac{\partial}{\partial z}\left(\mu\frac{\partial W}{\partial z}\right)\right.$$
$$\left. + \frac{1}{r}\frac{\partial}{\partial \theta}\left[\mu\left(\frac{\partial V}{\partial z} + Re^{\frac{-2}{(n+1)}}\frac{1}{r}\frac{\partial W}{\partial \theta}\right)\right]\right\}. \quad (2.18c)$$

Now, the Reynolds number for power-law fluids is defined in the following form

$$Re = \frac{\rho^*\Omega_D^{*2-n}l^{*2}}{m^*}. \quad (2.19)$$

By setting $n = 1$, the classical form of the Reynolds number for Newtonian fluid flow is recovered.

Therefore, by substituting the Reynolds number (2.19) into (2.18), the scaled governing Navier-Stokes equations are obtained for power-law fluids

$$\frac{\partial U}{\partial t} + U\frac{\partial U}{\partial r} + \frac{V}{r}\frac{\partial U}{\partial \theta} + W\frac{\partial U}{\partial z} - \frac{V^2}{r} - 2V \; = \; -\frac{\partial P}{\partial r} + \frac{\partial}{\partial z}\left(\mu\frac{\partial U}{\partial z}\right)$$
$$+ \; \mathcal{O}\left(Re^{\frac{-2}{(n+1)}}\right), \quad (2.20a)$$

$$\frac{\partial V}{\partial t} + U\frac{\partial V}{\partial r} + \frac{V}{r}\frac{\partial V}{\partial \theta} + W\frac{\partial V}{\partial z} + \frac{UV}{r} + 2U \; = \; -\frac{1}{r}\frac{\partial P}{\partial \theta} + \frac{\partial}{\partial z}\left(\mu\frac{\partial V}{\partial z}\right)$$
$$+ \; \mathcal{O}\left(Re^{\frac{-2}{(n+1)}}\right), \quad (2.20b)$$

$$\frac{\partial W}{\partial t} + U\frac{\partial W}{\partial r} + \frac{V}{r}\frac{\partial W}{\partial \theta} + W\frac{\partial W}{\partial z} \; = \; -Re^{\frac{2}{(n+1)}}\frac{\partial p}{\partial z} + \frac{1}{r}\frac{\partial}{\partial r}\left(\mu r\frac{\partial U}{\partial z}\right)$$
$$+ \; \frac{1}{r}\frac{\partial}{\partial \theta}\left(\mu\frac{\partial V}{\partial z}\right) + 2\frac{\partial}{\partial z}\left(\mu\frac{\partial W}{\partial z}\right)$$
$$+ \; \mathcal{O}\left(Re^{\frac{-2}{(n+1)}}\right), \quad (2.20c)$$

where

$$\mu = \left[\left(\frac{\partial U}{\partial z}\right)^2 + \left(\frac{\partial V}{\partial z}\right)^2 + \mathcal{O}\left(Re^{\frac{-2}{(n+1)}}\right) + \mathcal{O}\left(Re^{\frac{-4}{(n+1)}}\right)\right]^{(n-1)/2}, \quad (2.20d)$$

is the dimensionless viscosity function defined by

$$\mu = \frac{\left(Re^{1/n+1}\Omega_D^*\right)^{1-n}\mu^*}{m^*}.$$

The boundary-layer approximation is applied to the system of equations in order to neglect the terms that include inverse powers of the Reynolds number by considering $Re \gg 1$. Therefore, the components of velocity, pressure and viscosity in the Navier-Stokes equations (2.20) and the continuity equation (2.12) are assumed to have the asymptotic expansions as follows

$$U(r,\theta,\bar{z}) = U_0(r,\theta,z) + Re^{\frac{-2}{(n+1)}}U_1(r,\theta,z) + \cdots,$$

$$V(r,\theta,\bar{z}) = V_0(r,\theta,z) + Re^{\frac{-2}{(n+1)}}V_1(r,\theta,z) + \cdots,$$

$$W(r,\theta,\bar{z}) = W_0(r,\theta,z) + Re^{\frac{-2}{(n+1)}}W_1(r,\theta,z) + \cdots,$$

$$P(r,\theta,\bar{z}) = P_0(r,\theta,z) + Re^{\frac{-2}{(n+1)}}P_1(r,\theta,z) + \cdots,$$

$$\mu(r,\theta,\bar{z}) = \mu_0(r,\theta,z) + Re^{\frac{-2}{(n+1)}}\mu_1(r,\theta,z) + \cdots,$$

where $\bar{z} = z^*/l^* = Re^{-1/(n+1)}z$ is the outer region coordinate that corresponding to the region outside of the boundary-layer.

Thus, the zero-order boundary-layer equations are

$$\frac{1}{r}\frac{\partial(rU_0)}{\partial r} + \frac{1}{r}\frac{\partial V_0}{\partial\theta} + \frac{\partial W_0}{\partial z} = 0, \tag{2.21a}$$

$$\frac{\partial U_0}{\partial t} + U_0\frac{\partial U_0}{\partial r} + \frac{V_0}{r}\frac{\partial U_0}{\partial\theta} + W_0\frac{\partial U_0}{\partial z} - \frac{V_0^2}{r} - 2V_0 = -\frac{\partial P_0}{\partial r} + \frac{\partial}{\partial z}\left(\mu_0\frac{\partial U_0}{\partial z}\right),$$

$$\frac{\partial V_0}{\partial t} + U_0\frac{\partial V_0}{\partial r} + \frac{V_0}{r}\frac{\partial V_0}{\partial\theta} + W_0\frac{\partial V_0}{\partial z} + \frac{U_0V_0}{r} + 2U_0 = -\frac{1}{r}\frac{\partial P_0}{\partial\theta} + \frac{\partial}{\partial z}\left(\mu_0\frac{\partial V_0}{\partial z}\right), \tag{2.21b}$$

$$\frac{\partial W_0}{\partial t} + U_0\frac{\partial W_0}{\partial r} + \frac{V_0}{r}\frac{\partial W_0}{\partial\theta} + W_0\frac{\partial W_0}{\partial z} = -\frac{\partial P_1}{\partial z} + \frac{1}{r}\frac{\partial}{\partial r}\left(\mu_0 r\frac{\partial U_0}{\partial z}\right)$$

$$+ \frac{1}{r}\frac{\partial}{\partial\theta}\left(\mu_0\frac{\partial V_0}{\partial z}\right)$$

$$+ 2\frac{\partial}{\partial z}\left(\mu_0\frac{\partial W_0}{\partial z}\right), \tag{2.21c}$$

where

$$\mu_0 = \left[\left(\frac{\partial U_0}{\partial z} \right)^2 + \left(\frac{\partial V_0}{\partial z} \right)^2 \right]^{(n-1)/2}, \qquad (2.21d)$$

is the zero-order viscosity function of the power-law fluids.

The system of equations (2.21) is subject to the following boundary conditions

$$U_0(0) = V_0(0) = W_0(0) = 0, \qquad (2.22a)$$

$$U_0(z \to \infty) = 0, V_0(z \to \infty) = 1. \qquad (2.22b)$$

Equation (2.22a) reflects the no slip condition at the disk surface, while equation (2.22b) represents the quiescent flow condition at the upper edge of the boundary-layer.

2.2.2 Carreau fluids

For this model of fluid, the dimensionless variables of the system (2.7)-(2.8) are defined in the same way as the power-law model. However, the viscosity function for Carreau fluids defined in equation (2.5b) can be scaled in two ways by either the infinite-shear-rate viscosity $\bar{\mu}_{\infty}^*$ or the zero-shear-rate viscosity $\bar{\mu}_0^*$ as follows, respectively

$$\mu = 1 + c_0 \left[1 + \left(r^{-1} k \dot{\gamma} \right)^2 \right]^{(n-1)/2}, \qquad (2.23)$$

$$\mu = \left[1 + \left(r^{-1} k \dot{\gamma} \right)^2 \right]^{(n-1)/2}, \qquad (2.24)$$

where $c_0 = \left(\bar{\mu}_0^* - \bar{\mu}_{\infty}^* \right) / \bar{\mu}_{\infty}^*$ is the viscosity ratio and $k = r^* \lambda^* \Omega_D^* / l^* Re^{-1/2}$ is the dimensionless relaxation time parameter which is equivalent of the constant λ^*.

The viscosity function (2.24) scaled by $\bar{\mu}_0^*$ is used in this thesis in order to obtain the complete agreement with the familiar Newtonian mean flow profiles considered in Chapter 3 when $n = 1$.

Setting $n = 1$ and $m = \bar{\mu}_0^*$ in the system (2.18) in order to consider the flow of Carreau fluids. Therefore (2.18) becomes

$$
\frac{\partial U}{\partial t} + U \frac{\partial U}{\partial r} + \frac{V}{r} \frac{\partial U}{\partial \theta} + W \frac{\partial U}{\partial z} - \frac{V^2}{r} - 2V = -\frac{\partial P}{\partial r}
$$
$$
+ \frac{\bar{\mu}_0^* Re}{\rho^* l^{*2} \Omega_D^*} \left\{ \frac{\partial}{\partial z} \left[\mu \left(\frac{\partial U}{\partial z} + \frac{1}{Re} \frac{\partial W}{\partial r} \right) \right] + \frac{1}{Re} \left[\frac{2}{r} \frac{\partial}{\partial r} \left(\mu r \frac{\partial U}{\partial r} \right) \right. \right.
$$
$$
\left. \left. + \frac{1}{r} \frac{\partial}{\partial \theta} \left(\mu r \frac{\partial}{\partial r} \left(\frac{V}{r} \right) + \frac{\mu}{r} \frac{\partial U}{\partial \theta} \right) - \frac{2\mu}{r} \left(\frac{1}{r} \frac{\partial V}{\partial \theta} + \frac{U}{r} \right) \right] \right\}, \quad (2.25a)
$$

$$
\frac{\partial V}{\partial t} + U \frac{\partial V}{\partial r} + \frac{V}{r} \frac{\partial V}{\partial \theta} + W \frac{\partial V}{\partial z} + \frac{UV}{r} + 2U = -\frac{1}{r} \frac{\partial P}{\partial \theta}
$$
$$
+ \frac{\bar{\mu}_0^* Re}{\rho^* l^{*2} \Omega_D^*} \left\{ \frac{\partial}{\partial z} \left[\mu \left(\frac{\partial V}{\partial z} + \frac{1}{Re} \frac{1}{r} \frac{\partial W}{\partial \theta} \right) \right] + \frac{1}{Re} \left[\frac{1}{r} \frac{\partial}{\partial \theta} \left[\mu \left(\frac{1}{r} \frac{\partial V}{\partial \theta} + \frac{U}{r} \right) \right] \right. \right.
$$
$$
\left. \left. + \frac{1}{r^2} \frac{\partial}{\partial r} \left(\mu r^3 \frac{\partial}{\partial r} \left(\frac{V}{r} \right) + \mu r \frac{\partial U}{\partial \theta} \right) \right] \right\}, \quad (2.25b)
$$

$$
\frac{\partial W}{\partial t} + U \frac{\partial W}{\partial r} + \frac{V}{r} \frac{\partial W}{\partial \theta} + W \frac{\partial W}{\partial z} = -Re \frac{\partial P}{\partial z}
$$
$$
\frac{\bar{\mu}_0^* Re}{\rho^* l^{*2} \Omega_D^*} \left\{ \frac{1}{r} \frac{\partial}{\partial r} \left(r\mu \frac{\partial U}{\partial z} + \frac{1}{Re} r\mu \frac{\partial W}{\partial r} \right) + 2 \frac{\partial}{\partial z} \left(\mu \frac{\partial W}{\partial z} \right) \right.
$$
$$
\left. + \frac{1}{r} \frac{\partial}{\partial \theta} \left[\mu \left(\frac{\partial V}{\partial z} + \frac{1}{Re} \frac{1}{r} \frac{\partial W}{\partial \theta} \right) \right] \right\}. \quad (2.25c)
$$

Again, by fixing $n = 1$ and $m = \bar{\mu}_0^*$ in (2.19), the Reynolds number can be defined for Carreau fluids scaled by the zero-shear-rate viscosity

$$
Re = \frac{\rho^* \Omega_D^* l^{*2}}{\bar{\mu}_0^*}. \quad (2.26)
$$

Thus, by substituting the Reynolds number (2.26) into equations (2.25), the scaled governing Navier-Stokes equations for Carreau fluids are obtained as follows

$$\frac{\partial U}{\partial t} + U\frac{\partial U}{\partial r} + \frac{V}{r}\frac{\partial U}{\partial \theta} + W\frac{\partial U}{\partial z} - \frac{V^2}{r} - 2V = -\frac{\partial P}{\partial r} + \frac{\partial}{\partial z}\left(\mu\frac{\partial U}{\partial z}\right)$$
$$+ \quad \mathcal{O}\left(Re^{-1}\right), \tag{2.27a}$$

$$\frac{\partial V}{\partial t} + U\frac{\partial V}{\partial r} + \frac{V}{r}\frac{\partial V}{\partial \theta} + W\frac{\partial V}{\partial z} + \frac{UV}{r} + 2U = -\frac{1}{r}\frac{\partial P}{\partial \theta} + \frac{\partial}{\partial z}\left(\mu\frac{\partial V}{\partial z}\right)$$
$$+ \quad \mathcal{O}\left(Re^{-1}\right), \tag{2.27b}$$

$$\frac{\partial W}{\partial t} + U\frac{\partial W}{\partial r} + \frac{V}{r}\frac{\partial W}{\partial \theta} + W\frac{\partial W}{\partial z} = -Re\frac{\partial p}{\partial z} + \frac{1}{r}\frac{\partial}{\partial r}\left(\mu r\frac{\partial U}{\partial z}\right)$$
$$+ \quad \frac{1}{r}\frac{\partial}{\partial \theta}\left(\mu\frac{\partial V}{\partial z}\right) + 2\frac{\partial}{\partial z}\left(\mu\frac{\partial W}{\partial z}\right)$$
$$+ \quad \mathcal{O}\left(Re^{-1}\right), \tag{2.27c}$$

where

$$\mu = \left\{1 + \left(\frac{k}{r}\right)^2\left[\left(\frac{\partial U}{\partial z}\right)^2 + \left(\frac{\partial V}{\partial z}\right)^2 + \mathcal{O}\left(Re^{-1}\right) + \mathcal{O}\left(Re^{-2}\right)\right]\right\}^{(n-1)/2}, \tag{2.27d}$$

is the dimensionless viscosity function of the Carreau fluids.

By the same procedure used for the power-law model, using the boundary-layer approximation and considering $Re \gg 1$ in order to eliminate the terms that include inverse powers of the Reynolds number. The components of velocity, pressure and viscosity in the Navier-Stokes equations (2.27) and the continuity equation (2.12) are supposed to have the asymptotic expansions as follows

$$U\left(r,\theta,\bar{z}\right) = U_0\left(r,\theta,z\right) + Re^{-1}U_1\left(r,\theta,z\right) + \cdots,$$

$$V\left(r,\theta,\bar{z}\right) = V_0\left(r,\theta,z\right) + Re^{-1}V_1\left(r,\theta,z\right) + \cdots,$$

$$W\left(r,\theta,\bar{z}\right) = W_0\left(r,\theta,z\right) + Re^{-1}W_1\left(r,\theta,z\right) + \cdots,$$

$$P\left(r,\theta,\bar{z}\right) = P_0\left(r,\theta,z\right) + Re^{-1}P_1\left(r,\theta,z\right) + \cdots,$$

$$\mu\left(r,\theta,\bar{z}\right) = \mu_0\left(r,\theta,z\right) + Re^{-1}\mu_1\left(r,\theta,z\right) + \cdots,$$

where $\bar{z} = z^*/l^* = Re^{-1/2}z$ is the outer region coordinate that corresponding to the region

outside of the boundary-layer.

Thus the zero-order boundary-layer equations are

$$\frac{1}{r}\frac{\partial(rU_0)}{\partial r} + \frac{1}{r}\frac{\partial V_0}{\partial \theta} + \frac{\partial W_0}{\partial z} = 0, \tag{2.28a}$$

$$\frac{\partial U_0}{\partial t} + U_0\frac{\partial U_0}{\partial r} + \frac{V_0}{r}\frac{\partial U_0}{\partial \theta} + W_0\frac{\partial U_0}{\partial z} - \frac{V_0^2}{r} - 2V_0 = -\frac{\partial P_0}{\partial r} + \frac{\partial}{\partial z}\left(\mu_0\frac{\partial U_0}{\partial z}\right), \tag{2.28b}$$

$$\frac{\partial V_0}{\partial t} + U_0\frac{\partial V_0}{\partial r} + \frac{V_0}{r}\frac{\partial V_0}{\partial \theta} + W_0\frac{\partial V_0}{\partial z} + \frac{U_0 V_0}{r} + 2U_0 = -\frac{1}{r}\frac{\partial P_0}{\partial \theta} + \frac{\partial}{\partial z}\left(\mu_0\frac{\partial V_0}{\partial z}\right), \tag{2.28c}$$

$$\frac{\partial W_0}{\partial t} + U_0\frac{\partial W_0}{\partial r} + \frac{V_0}{r}\frac{\partial W_0}{\partial \theta} + W_0\frac{\partial W_0}{\partial z} = -\frac{\partial P_1}{\partial z} + \frac{1}{r}\frac{\partial}{\partial r}\left(\mu_0 r\frac{\partial U_0}{\partial z}\right) \tag{2.28d}$$

$$+ \frac{1}{r}\frac{\partial}{\partial \theta}\left(\mu_0\frac{\partial V_0}{\partial z}\right) \tag{2.28e}$$

$$+ 2\frac{\partial}{\partial z}\left(\mu_0\frac{\partial W_0}{\partial z}\right), \tag{2.28f}$$

where

$$\mu_0 = \left\{1 + \left(\frac{k}{r}\right)^2\left[\left(\frac{\partial U_0}{\partial z}\right)^2 + \left(\frac{\partial V_0}{\partial z}\right)^2\right]\right\}^{(n-1)/2}, \tag{2.28g}$$

is the zero-order viscosity function.

The system of equations (2.28) is subject to the following boundary conditions

$$U_0(0) = V_0(0) = W_0(0) = 0, \tag{2.29a}$$

$$U_0(z \to \infty) = 0, V_0(z \to \infty) = 1, \tag{2.29b}$$

which again represent the non-slip and quiescent flow conditions, respectively.

2.3   Summary

In this chapter, the generalized Newtonian fluids that describe the shear-rate dependence of the viscosity have been considered. Different empiricisms for the non-Newtonian viscosity are presented depending on the relation between the viscosity and the rate-of-strain tensor. The zero-order boundary-layer equations for generalized Newtonian fluid, power-law and Carreau fluids has been derived in order to describe the boundary-layer flow. The boundary-layer approximation is applied in the formulation of the governing leading order equations. This is by neglecting the terms that include inverse powers of the Reynolds number by considering $Re \gg 1$. These governing boundary-layer equations are important to obtain the steady mean flow solutions and study the transition from laminar to turbulence with stability properties of the flow.

Chapter 3

Steady mean BEK family flow solutions

In this chapter, the boundary-layer equations for the generalized non-Newtonian fluids have been solved to determine the steady mean BEK family of flow profiles. There are numerous investigations that present numerical results for the generalized non-Newtonian fluids. Mitschka and Ulbrecht (1965) was the first to obtain the solution of mean flow for the power-law fluids that is equivalent to the solution for the Newtonian fluid flow given by von Kármán (1921) when the power-law index n equal to unity. Andersson et al. (2001) revisited this study and improved the reliability of the numerical solution of Mitschka and Ulbrecht (1965) with better accuracy. Denier and Hewitt (2004) subsequently reconsidered the previous work to obtain the numerical solutions for power-law fluids and clarified their asymptotic behaviour in the far-field. Regarding Carreau models, Dabrowski (2009) studied the structure of the mean flow profiles for both power-law and Carreau models including shear thickening and shear-thinning fluids. Some years later, Griffiths (2016) presented a detailed solutions of the mean flow and an analysis of their stability using both asymptotic and numerical approaches. All these prior studies consider only the von Kármán flow within the more general BEK family.

Within this chapter, a brief description of the full BEK family of flows is introduced in §3.1. The solutions of the steady mean BEK flows family of flows for power-law fluids are given in §3.2. Steady mean BEK family of flows solutions for Carreau fluids are presented in

§3.3 . Finally, §3.4 provides the details of the MATLAB function solver used to obtain the steady mean flow profiles throughout this thesis.

3.1   BEK family of flows

The family of incompressible generalised Newtonian boundary-layer flows has been considered above an infinite rotating-disk located at the axis $z^* = 0$. Distinct flows within this family are generated by a differential rotation rate between this solid lower disk and an upper fluid in rigid-body rotation (Lingwood, 1997; Lingwood and Garrett, 2011). Particular cases within the family are Böedewadt (1940), Ekman (1905) and von Kármán (1921) boundary-layer flows. This family is referred to as the *BEK system* (Lingwood, 1997). Both rotating components (lower disk and upper fluid) are assumed to rotate in the same direction and about the same vertical axis z^* with angular velocities Ω_D^* and Ω_F^* indicating the disk D and upper fluid F, respectively. The von Kármán layer appears when the upper fluid is stationary and the lower disk rotates, i.e., $\Omega_F^* = 0$ and $\Omega_D^* \neq 0$; the Ekman layer arises when both upper fluid and lower disk rotates with the same angular velocity i.e., $\Omega_F^* = \Omega_D^* \neq 0$; and the Bödewadt layer occurs when the upper fluid is rotates and the lower disk stationary i.e., $\Omega_F^* \neq 0$ and $\Omega_D^* = 0$. Furthermore, there exists a continuum of cases between these three particular examples in which both the disk and fluid rotate with different angular velocities.

The system rotation rate is given by Lingwood (1997) in the following form

$$\Omega^* = \frac{\Omega_F^*}{2 - Ro} + \frac{\Omega_D^*}{2 + Ro} = \frac{\Omega_F^* + \Omega_D^*}{4} + \left(\left(\frac{\Omega_F^* + \Omega_D^*}{4} \right)^2 + \frac{(\triangle \Omega^*)^2}{2} \right)^{1/2}, \qquad (3.1)$$

where $\triangle \Omega^* = \Omega_F^* - \Omega_D^*$ is the differential rotation rate and Ro is the Rossby number which characterises each particular flow within the BEK family, .

The Rossby number Ro is defined in the following form
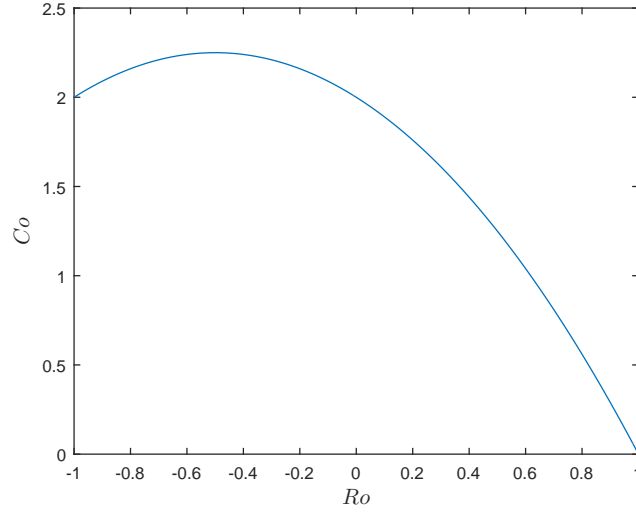
Figure 3.1: Variation in Coriolis parameter *Co* with Rossby number *Ro* for the BEK family flows

$$Ro = \frac{\triangle\Omega^*}{\Omega^*} = \frac{\Omega_F^* - \Omega_D^*}{\Omega^*}. \tag{3.2}$$

The Coriolis parameter which is related to the Rossby number is also defined as follows

$$Co = \frac{2\Omega_D^*}{\Omega^*} = 2 - Ro - Ro^2. \tag{3.3}$$

The frame of reference is assumed to be rotating with the lower disk Ω_D^*. Therefore, the Coriolis terms and centrifugal effects due to rotation appear in the governing equations.

The Rossby number *Ro* for BEK family of flows ranges from negative unity to positive unity, i.e., $Ro \in [-1, 1]$. The variation of the Coriolis parameter *Co* with the Rossby number *Ro* is plotted in Figure 3.1.

These parameters leads to the particular flow cases being identified by

Bödewadt flow:	$Ro = 1$	$Co = 0$	$\Omega^* = \Omega_F^*$
Ekman flow:	$Ro = 0$	$Co = 2$	$\Omega^* = \Omega_F^* = \Omega_D^*$
von Kármán flow:	$Ro = -1$	$Co = 2$	$\Omega^* = \Omega_D^*.$

3.2 Steady mean BEK family of flows for power-law fluids

Let us consider the governing boundary-layer equations obtained from (2.21) in dimensional form and expressed in a cylindrical-polar coordinates system (r^*, θ, z^*) as

$$\frac{1}{r^*}\frac{\partial(r^* U_0^*)}{\partial r^*} + \frac{1}{r^*}\frac{\partial V_0^*}{\partial \theta} + \frac{\partial W_0^*}{\partial z^*} = 0, \tag{3.4a}$$

$$\frac{\partial U_0^*}{\partial t^*} + U_0^*\frac{\partial U_0^*}{\partial r^*} + \frac{V_0^*}{r^*}\frac{\partial U_0^*}{\partial \theta} + W_0^*\frac{\partial U_0^*}{\partial z^*} - \frac{V_0^{*2}}{r^*} - 2\Omega_D^* V_0^* = -\frac{1}{\rho^*}\frac{\partial P_0^*}{\partial r^*}$$
$$+ \frac{1}{\rho^*}\frac{\partial}{\partial z^*}\left(\mu_0^*\frac{\partial U_0^*}{\partial z^*}\right), \tag{3.4b}$$

$$\frac{\partial V_0^*}{\partial t^*} + U_0^*\frac{\partial V_0^*}{\partial r^*} + \frac{V_0^*}{r^*}\frac{\partial V_0^*}{\partial \theta} + W_0^*\frac{\partial V_0^*}{\partial z^*} + \frac{U_0^* V_0^*}{r^*} + 2\Omega_D^* U_0^* = -\frac{1}{\rho^* r^*}\frac{\partial P_0^*}{\partial \theta}$$
$$+ \frac{1}{\rho^*}\frac{\partial}{\partial z^*}\left(\mu_0^*\frac{\partial V_0^*}{\partial z^*}\right), \tag{3.4c}$$

$$\frac{\partial W_0^*}{\partial t^*} + U_0^*\frac{\partial W_0^*}{\partial r^*} + \frac{V_0^*}{r^*}\frac{\partial W_0^*}{\partial \theta} + W_0^*\frac{\partial W_0^*}{\partial z^*} = -\frac{1}{\rho^*}\frac{\partial P_1^*}{\partial z^*} + \frac{1}{\rho^* r^*}\frac{\partial}{\partial r^*}\left(\mu_0^* r^*\frac{\partial U_0^*}{\partial z^*}\right)$$
$$+ \frac{1}{\rho^* r^*}\frac{\partial}{\partial \theta}\left(\mu_0^*\frac{\partial V_0^*}{\partial z^*}\right)$$
$$+ \frac{2}{\rho^*}\frac{\partial}{\partial z^*}\left(\mu_0^*\frac{\partial W_0^*}{\partial z^*}\right), \tag{3.4d}$$

where

$$\mu_0^* = m^*\left[\left(\frac{\partial U_0^*}{\partial z^*}\right)^2 + \left(\frac{\partial V_0^*}{\partial z^*}\right)^2\right]^{(n-1)/2}, \tag{3.5}$$

is the viscosity function, $\left(U_0^*, V_0^*, W_0^*\right)$ are the leading-order velocity components, and $\left(P_0^*, P_1^*\right)$ is the zero-order and first-order pressure, respectively.

A generalisation of von Kármán's exact similarity solution (von Kármán, 1921) is required in order to solve the steady mean flow equations relative to the lower disk. This is expressed in non-dimensional form as

$$U(\eta) = \frac{U_0^*}{r^* \triangle \Omega^*} = \frac{U_0^*}{r^* \Omega^* Ro}, \tag{3.6a}$$

$$V(\eta) = \frac{V_0^*}{r^* \triangle \Omega^*} = \frac{V_0^*}{r^* \Omega^* Ro}, \tag{3.6b}$$

$$W(\eta) = \frac{W_0^*}{\chi^*}, \tag{3.6c}$$

$$P(\eta) = \frac{P_1^*}{\rho^* (\chi^*)^2}, \tag{3.6d}$$

where

$$\chi^* = \left[\frac{\nu^*}{(r^*)^{1-n} (\Omega^*)^{1-2n} Ro^{-2n}} \right]^{1/(n+1)}.$$

Here (U, V, W) are the dimensionless radial, azimuthal and axial velocities, respectively, P is the pressure, and $\nu^* = m^*/\rho^*$ is the kinematic viscosity. The dimensionless similarity coordinate is defined by

$$\eta = \frac{(r^*)^{(1-n)/(n+1)} z^*}{(L^*)^{2/(n+1)}}, \tag{3.7}$$

where

$$L^* = \sqrt{\frac{\nu^*}{(\Omega^*)^{2-n} Ro^{1-n}}},$$

is the non-dimensional length scale.

The mean flow is assumed to be both steady and axisymmetric, i.e., the mean flow velocities and pressure term are independent of time t and azimuthal direction θ, respectively, i.e.,

$$\frac{\partial U_0^*}{\partial t^*} = \frac{\partial V_0^*}{\partial t^*} = \frac{\partial W_0^*}{\partial t^*} = 0,$$

$$\frac{\partial U_0^*}{\partial \theta} = \frac{\partial V_0^*}{\partial \theta} = \frac{\partial W_0^*}{\partial \theta} = \frac{\partial P_0^*}{\partial \theta} = 0.$$

The non-dimensional equations for the mean flow are obtained by substituting the dimensionless mean flow variables (3.6) in the governing boundary-layer equations (3.4) as follows

$$2U + \frac{1-n}{n+1}\eta U' + W' = 0,\tag{3.8a}$$

$$Ro\left[U^2 - (V^2 - 1) + \left(W + \frac{1-n}{n+1}\eta U\right)U'\right] - Co(V-1) - (\mu U')' = 0,\tag{3.8b}$$

$$Ro\left[2UV + \left(W + \frac{1-n}{n+1}\eta U\right)V'\right] + CoU - (\mu V')' = 0,\tag{3.8c}$$

$$Ro\left\{P' + WW' + \frac{1-n}{n+1}\left[U\left(\eta W' - W\right)\right]\right\} + \frac{2(1-n)}{n+1}\mu U' + 2\mu' U$$
$$- (\mu W')' = 0,\tag{3.8d}$$

where the primes denote derivatives with respect to η and $\mu = \left[(U')^2 + (V')^2\right]^{(n-1)/2}$ is the viscosity of power-law fluids.

When $n = 1$, the mean flow equations (3.8) are entirely consistent with the non-dimensional equations for the Newtonian mean flow given in Alveroglu et al. (2016); Lingwood (1997); Lingwood and Garrett (2011).

As discussed by Lingwood (1997), the radial zero-order pressure gradient term $-\partial P_0^*/\partial r^*$ in equation (3.4b) is determined from the relative circumferential flow as $\eta \to \infty$, i.e., $V \to 1$ in order to formulate (3.8b). By considering the assumptions $U(\eta) \to 0$, $U'(\eta) \to 0$ and $U''(\eta) \to 0$, as $\eta \to \infty$ gives

$$Ro + Co = \frac{1}{\rho^*\Omega^{*2}r^*Ro}\frac{\partial P_0^*}{\partial r^*},\tag{3.9}$$

which is taken as constant in η. The non-dimensional pressure P is not required to conduct the
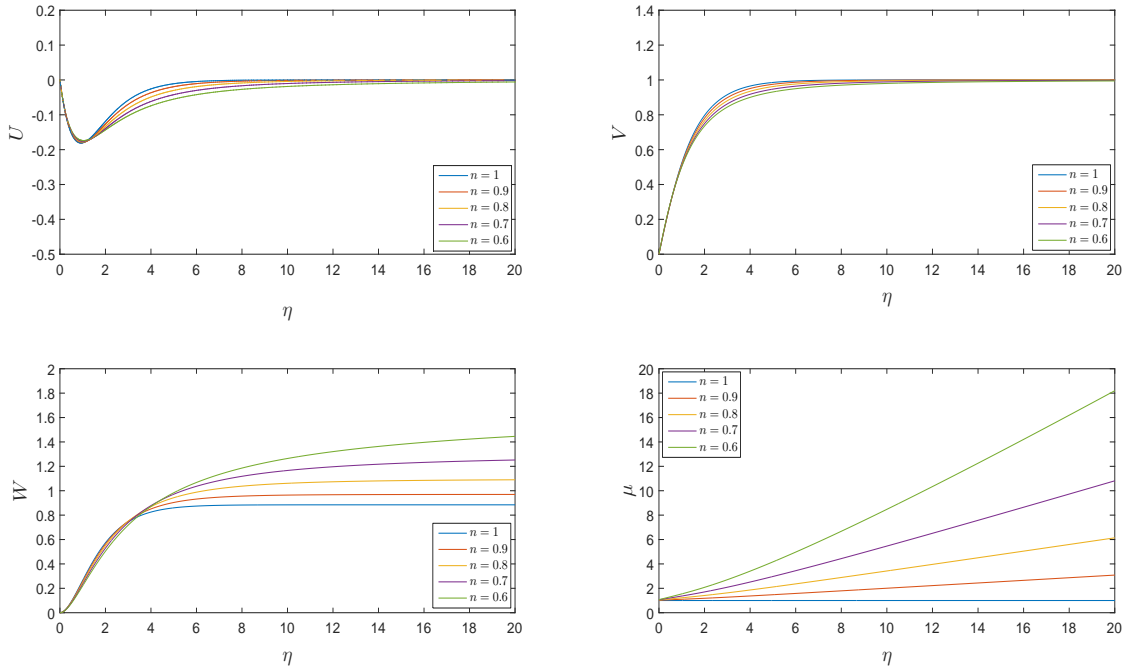
Figure 3.2: Steady mean flow profiles U, V and W and viscosity function μ versus η of the von Kármán flow, $Ro = -1$ for Newtonian $(n = 1)$ and shear-thinning power-law fluids with $n = 0.9, 0.8, 0.7, 0.6$.

instability analysis discussed later. Thus, the results of U, V and W are only presented here, and are completely defined by (3.8).

The system of equations (3.8) is subject to the following dimensionless boundary conditions

$$U(0) = V(0) = W(0) = 0, \tag{3.10a}$$

$$U(\eta \to \infty) = 0, V(\eta \to \infty) = 1. \tag{3.10b}$$

The MATLAB function solver and the numerical method applied to solve the system of equations (3.8) are explained later in §3.4. The initial values of mean velocity flow parameters $U'(0)$, $V'(0)$ and $W(\eta_\infty)$ are stated in Table 3.1 for various values of Ro.

n	$-U'(0)$	$V'(0)$	$W(\eta_\infty)$
1	0.5102	0.6159	0.8845
0.9	0.5069	0.6243	0.9698
0.8	0.5039	0.6362	1.0957
0.7	0.5017	0.6532	1.3051
0.6	0.5005	0.6778	1.7329

(a) von Kármán flow, $Ro = -1$

n	$-U'(0)$	$V'(0)$	$W(\eta_\infty)$
1	0.8570	0.9073	1.0219
0.9	0.8687	0.9434	1.0241
0.8	0.8831	0.9885	1.0250
0.7	0.9013	1.0461	1.0241
0.6	0.9245	1.1221	1.0205

(b) Flow for $Ro = -0.5$

n	$-U'(0)$	$V'(0)$	$W(\eta_\infty)$
1	1	1	1
0.9	1.0.189	1.0469	0.9814
0.8	1.0418	1.1050	0.9599
0.7	1.0697	1.1787	0.9348
0.6	1.1046	1.2755	0.9053

(c) Ekman flow, $Ro = 0$

n	$-U'(0)$	$V'(0)$	$W(\eta_\infty)$
1	1.0176	0.9612	1.0853
0.9	1.0346	1.0057	1.0567
0.8	1.0550	1.0607	0.9882
0.7	1.0798	1.1304	0.9890
0.6	1.1108	1.2212	0.9468

(d) Flow for $Ro = 0.5$

n	$-U'(0)$	$V'(0)$	$W(\eta_\infty)$
1	0.9420	0.7729	1.3494
0.9	0.9442	0.8021	1.3201
0.8	0.9475	0.8376	1.2855
0.7	0.9526	0.8821	1.2446
0.6	0.9599	0.9398	1.1962

(e) Bödewadt flow, $Ro = 1$

Table 3.1: Numerical values of the mean velocity flow parameters U', V' and W for Newtonian ($n = 1$) and shear-thinning power-law fluids with $n = 0.9, 0.8, 0.7, 0.6$ at various Ro.
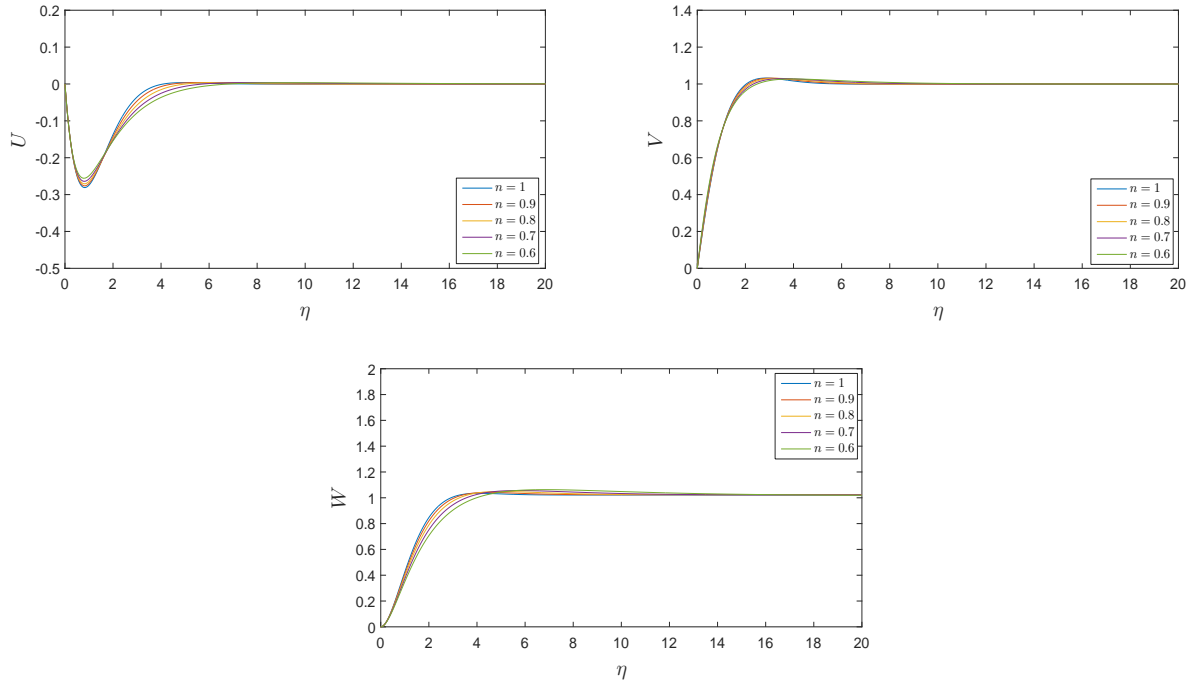
Figure 3.3: Steady mean flow profiles U, V and W versus η of the flow at $Ro = -0.5$ for Newtonian ($n = 1$) and shear-thinning power-law fluids with $n = 0.9, 0.8, 0.7, 0.6$.

The resulting steady mean flow profiles for shear-thinning power-law fluids are presented in Figures 3.2-3.6 for various Ro. The results of shear-thickening fluids ($n > 1$) are not included here because the trend of the viscosity function goes to zero at the outer-edge of the boundary-layer as n increased.

Figure 3.2 shows that the steady mean flow profiles (U, V, W) for the von Kármán flow ($Ro = -1$) and the plot of μ versus η are identical to those obtained by (Griffiths et al., 2014a,b).

There are several important properties that can be used to interpret the behaviour of the mean flow velocities. For example, the oscillation of the flow components, the thickness of the boundary-layer, the amount of fluid entrained into boundary-layer, and the size of the radial wall jet.

The behaviour of the mean flow profiles is influenced by the effect of shear-thinning fluids.
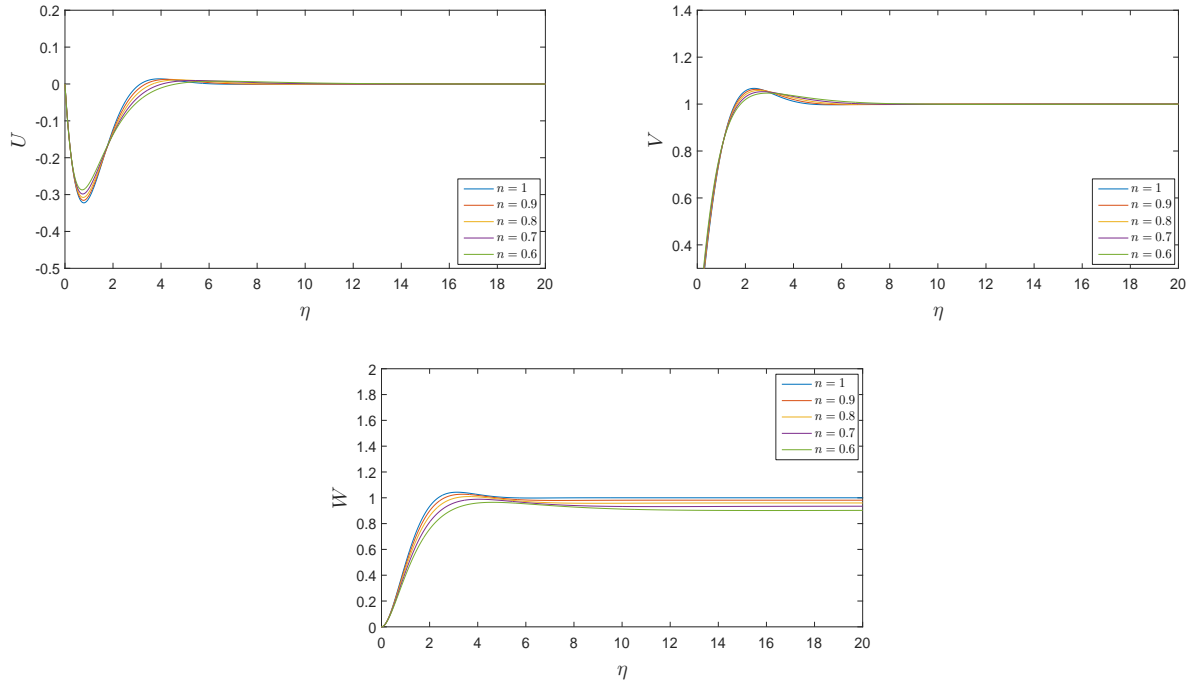
Figure 3.4: Steady mean flow profiles U, V and W versus η of the Ekman flow, $Ro = 0$ for Newtonian ($n = 1$) and shear-thinning power-law fluids with $n = 0.9, 0.8, 0.7, 0.6$.

The existence of inflectional points is crucial as this known to lead to the appearance of the Type I instability mechanism (cross-flow velocity)(Saric and Reed, 2003).

Figure 3.2 shows that only the radial mean flow is inflectional for all values of power-law index n. However, all mean flows (radial, azimuthal and axial) profiles become inflectional with increasing Ro from minus unity to unity for all n.

Figures 3.2-3.6 reveal that the behaviour of the oscillation is amplified as the flow changes from the von Kármán to the Bödewadt flows. Furthermore, it is interesting to note that the oscillation of the mean flows is damped as the power-law index n is reduced for all values of the Ro.

It is noted that the maximum value of the radial component U for all values of the Rossby number is decreased due to increase the effect of shear-thinning power-law fluids, i.e., the radial wall jet is reduced with decreasing n for all Ro. However, the radial wall jet is increased

Figure 3.5: Steady mean flow profiles U, V and W versus η of the flow at $Ro = 0.5$ for Newtonian ($n = 1$) and shear-thinning power-law fluids with $n = 0.9, 0.8, 0.7, 0.6$.

with increasing Ro from minus unity to unity for all n. Moreover, the location of the maximum value of U slightly approaches the disk surface as n reduced. Hence, the thickness of the boundary-layer for all values of Ro decreases with increased the effect of shear-thinning power-law fluids ($n < 1$).

In addition, Figure 3.2 demonstrates that the magnitude of the axial flow W in the far-field is increased for the von Kármán flow, $Ro = -1$ as n decreased. However, the magnitude of W is reduced for the flows at $Ro \geq -0.5$ as shown in Figures 3.3-3.6. In other words, the amount of fluid entrained into boundary-layer is increased with increasingly shear-thinning power-law fluids for the von Kármán flow, while this amount is reduced for the flows at $Ro \geq -0.5$ as n is decreased. On the other hand, it can be clearly seen that the magnitude of both radial and azimuthal flow in the far-field are unchanged.

Figure 3.6: Steady mean flow profiles U, V and W versus η of the Bödewadt flow, $Ro = 1$ for Newtonian ($n = 1$) and shear-thinning power-law fluids with $n = 0.9, 0.8, 0.7, 0.6$.

3.3 Steady mean BEK family of flows for Carreau fluids

Using equations (2.28), the governing boundary-layer equations (3.4) are obtained in the dimensional form with the viscosity function for Carreau fluids given by

$$
\mu_0^* = \left\{ 1 + \lambda^{*2} \left[\left(\frac{\partial U_0^*}{\partial z^*} \right)^2 + \left(\frac{\partial V_0^*}{\partial z^*} \right)^2 \right] \right\}^{(n-1)/2}.
\tag{3.11}
$$

Again, using the extension of von Kármán's exact similarity solution as Lingwood (1997) did, the dimensionless steady and axisymmetric mean flow components take the following form

$$U(z) = \frac{U_0^*}{r^* \triangle \Omega^*} = \frac{U_0^*}{r^* \Omega^* Ro}, \tag{3.12a}$$

$$V(z) = \frac{V_0^*}{r^* \triangle \Omega^*} = \frac{V_0^*}{r^* \Omega^* Ro}, \tag{3.12b}$$

$$W(z) = \frac{W_0^*}{L^* \triangle \Omega^*} = \frac{W_0^*}{L^* \Omega^* Ro}, \tag{3.12c}$$

$$P(z) = \frac{P_1^*}{\rho^* L^{*2} \triangle \Omega^{*2}} = \frac{P_1^*}{\rho^* L^{*2} \Omega^{*2} Ro^2}, \tag{3.12d}$$

where (U, V, W) are the non-dimensional radial, azimuthal and axial velocities, respectively, P is the pressure and $L^* = (v^*/\Omega^*)^{1/2}$.

By substituting the dimensionless mean flow variables (3.12) in the governing boundary-layer equations (3.4) with the viscosity function (3.11), the dimensionless steady mean flow equations are obtained as follows

$$2U + W' = 0, \tag{3.13a}$$

$$Ro\left(U^2 - \left(V^2 - 1\right) + WU'\right) - Co\left(V - 1\right) - \left(\mu U'\right)' = 0, \tag{3.13b}$$

$$Ro\left(2UV + WV'\right) + CoU - \left(\mu V'\right)' = 0, \tag{3.13c}$$

$$Ro\left(P' + WW'\right) - q\mu U' + 2\mu'U - \left(\mu W'\right)' = 0. \tag{3.13d}$$

Here the primes denote derivatives with respect to z, $\mu = \left\{1 + k^2\left[(U')^2 + (V')^2\right]\right\}^{(n-1)/2}$, $k = r^* \lambda^* \Omega^* Ro\left(v^*/\Omega^*\right)^{-1/2}$ and $q = \frac{k^2(n-1)\left(U'^2 + V'^2\right)}{1 + k^2\left(U'^2 + V'^2\right)}$.

The system of equations (3.13) is subject to the following dimensionless boundary conditions

$$U(0) = V(0) = W(0) = 0, \tag{3.14a}$$

$$U(z \to \infty) = 0, V(z \to \infty) = 1. \tag{3.14b}$$

Tables 3.2-3.3 state the initial values of mean velocity flow parameters $U'(0)$, $V'(0)$ and $W(z_\infty)$ for shear-thinning and shear-thickening fluids for various values of Ro, respectively.

n	$-U'(0)$	$V'(0)$	$W(z_\infty)$
1	0.5102	0.6159	0.8845
0.9	0.6440	0.7968	0.7659
0.8	0.8355	1.0644	0.6603
0.7	1.1197	1.4785	0.5686
0.6	1.5606	2.1544	0.4912

(a) von Kármán flow, $Ro = -1$

n	$-U'(0)$	$V'(0)$	$W(z_\infty)$
1	0.8570	0.9073	1.0219
0.9	1.1059	1.2028	0.8223
0.8	1.4701	1.6504	0.6457
0.7	2.0246	2.3607	0.4926
0.6	2.9092	3.5536	0.3631

(b) Flow for $Ro = -0.5$

n	$-U'(0)$	$V'(0)$	$W(z_\infty)$
1	1.000	1.000	1.0000
0.9	1.2984	1.3340	0.7910
0.8	1.7378	1.8432	0.6093
0.7	2.4110	2.6568	0.4549
0.6	3.4930	4.0334	0.3272

(c) Ekman flow, $Ro = 0$

n	$-U'(0)$	$V'(0)$	$W(z_\infty)$
1	1.0176	0.9612	1.0853
0.9	1.3198	1.2810	0.8538
0.8	1.7640	1.7679	0.6538
0.7	2.4433	2.5447	0.4848
0.6	3.5322	3.8565	0.3460

(d) Flow for $Ro = 0.5$

n	$-U'(0)$	$V'(0)$	$W(z_\infty)$
1	0.9420	0.7729	1.3494
0.9	1.2093	1.0206	1.0661
0.8	1.5975	1.3936	0.8203
0.7	2.2165	2.0649	0.5933
0.6	3.1063	2.9606	0.4394

(e) Bödewadt flow, $Ro = 1$

Table 3.2: Numerical values of the mean velocity flow parameters U', V' and W for Newtonian ($n = 1$) and shear-thinning Carreau fluids with $n = 0.9, 0.8, 0.7, 0.6$ and $k = 100$ at various Ro.

n	$-U'(0)$	$V'(0)$	$W(z_\infty)$
1	0.5102	0.6159	0.8845
1.1	0.4137	0.4892	1.0148
1.2	0.3422	0.3975	1.1557
1.3	0.2880	0.3293	1.3062
1.4	0.2460	0.2775	1.4651

(a) von Kármán flow, $Ro = -1$

n	$-U'(0)$	$V'(0)$	$W(z_\infty)$
1	0.8570	0.9073	1.0219
1.1	0.6812	0.7046	1.2436
1.2	0.5532	0.5608	1.4864
1.3	0.4578	0.4559	1.7489
1.4	0.3851	0.3774	2.0298

(b) Flow for $Ro = -0.5$

n	$-U'(0)$	$V'(0)$	$W(z_\infty)$
1	1.000	1.000	1.0000
1.1	0.7903	0.7721	1.2360
1.2	0.6385	0.6113	1.4981
1.3	0.5258	0.4945	1.7854
1.4	0.4403	0.4076	2.0967

(c) Ekman flow, $Ro = 0$

n	$-U'(0)$	$V'(0)$	$W(z_\infty)$
1	1.0176	0.9612	1.0853
1.1	0.8049	0.7427	1.3480
1.2	0.6508	0.5884	1.6411
1.3	0.5363	0.4763	1.9638
1.4	0.4493	0.3928	2.3148

(d) Flow for $Ro = 0.5$

n	$-U'(0)$	$V'(0)$	$W(z_\infty)$
1	0.9420	0.7729	1.3494
1.1	0.7518	0.6021	1.6698
1.2	0.6127	0.4804	2.0265
1.3	0.5085	0.3913	2.4183
1.4	0.4287	0.3244	2.8436

(e) Bödewadt flow, $Ro = 1$

Table 3.3: Numerical values of the mean velocity flow parameters U', V' and W for Newtonian ($n = 1$) and shear-thickening Carreau fluids with $n = 1.1, 1.2, 1.3, 1.4$ and $k = 100$ at various Ro.
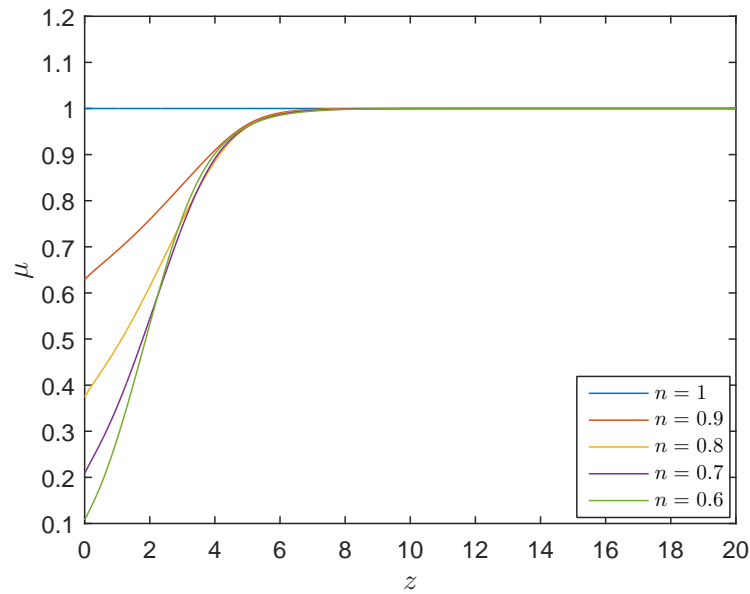
(a) Shear-thinning fluids with $n = 1, 0.9, 0.8, 0.7, 0.6$ and $k = 100$.
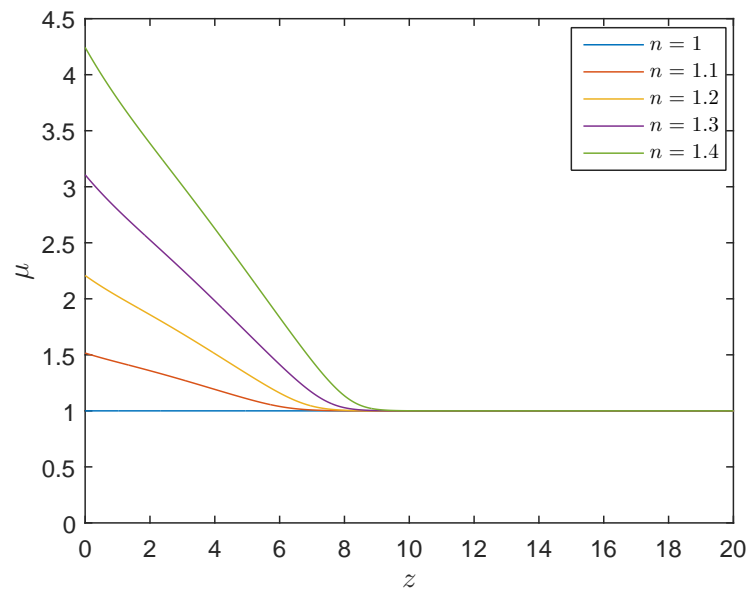
(b) Shear-thickening fluids with $n = 1, 1.1, 1.2, 1.3, 1.4$ and $k = 100$.

Figure 3.7: Viscosity function μ versus z for Carreau fluids.
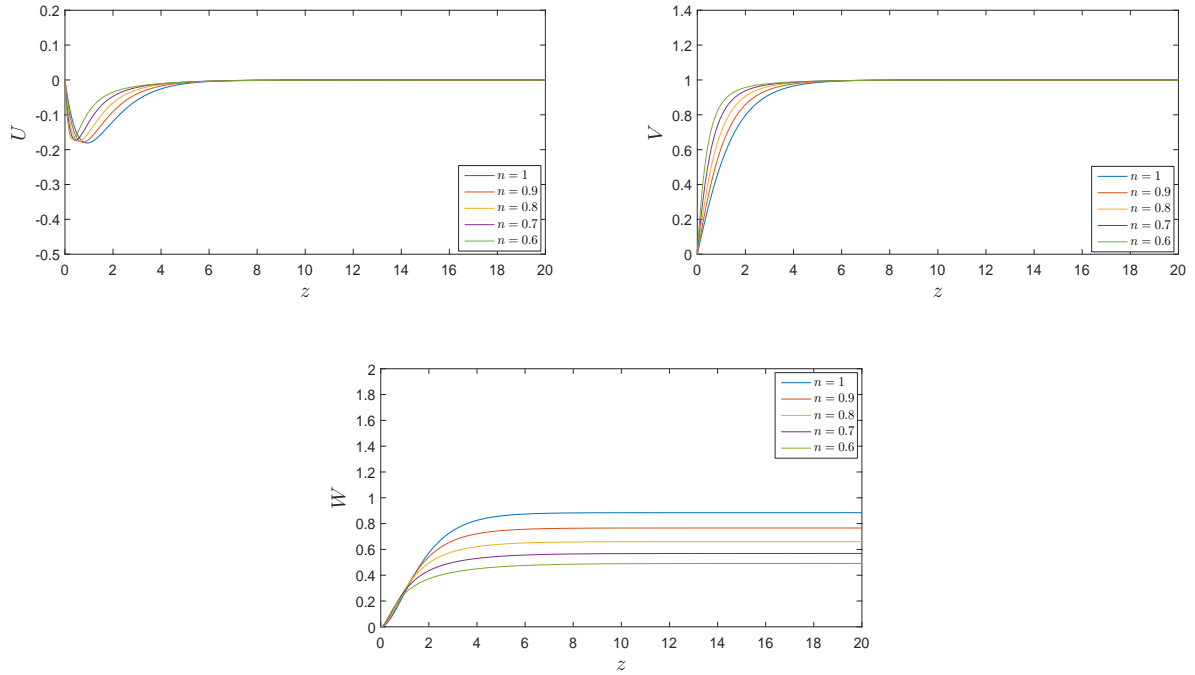
Figure 3.8: Steady mean flow profiles U, V and W versus z of the von Kármán flow, $Ro = -1$ for Newtonian ($n = 1$) and shear-thinning Carreau fluids with $n = 0.9, 0.8, 0.7, 0.6$ and $k = 100$.

The steady mean flow profiles of shear-thinning and shear-thickening fluids for Carreau model are presented in Figures 3.8-3.17 at various values of Ro. The value of relaxation time parameter k is selected here as 100 for all cases. However, there is some sensitivity in the flows resulting from the choice of k and, while this is not significant to the appearance of the steady flows, it does have an effect on their stability behaviour. This is considered in Chapter 5. In contrast to the solutions for shear-thinning power-law fluids, it can be noted that the results for shear-thinning and shear-thickening fluids have converged on the boundary-layer region $0 \leq z \leq 20$. Figure 3.7 presents the variation of the viscosity μ for both cases of Carreau fluids versus z. It can be seen that the steady mean flow profiles are not consistent to those obtained by Griffiths (2015) due to apply the viscosity function (2.24) scaled by $\bar{\mu}_0^*$, while the viscosity function (2.23) scaled by $\bar{\mu}_\infty^*$ is used by Griffiths (2015). Therefore, the mean flow profiles
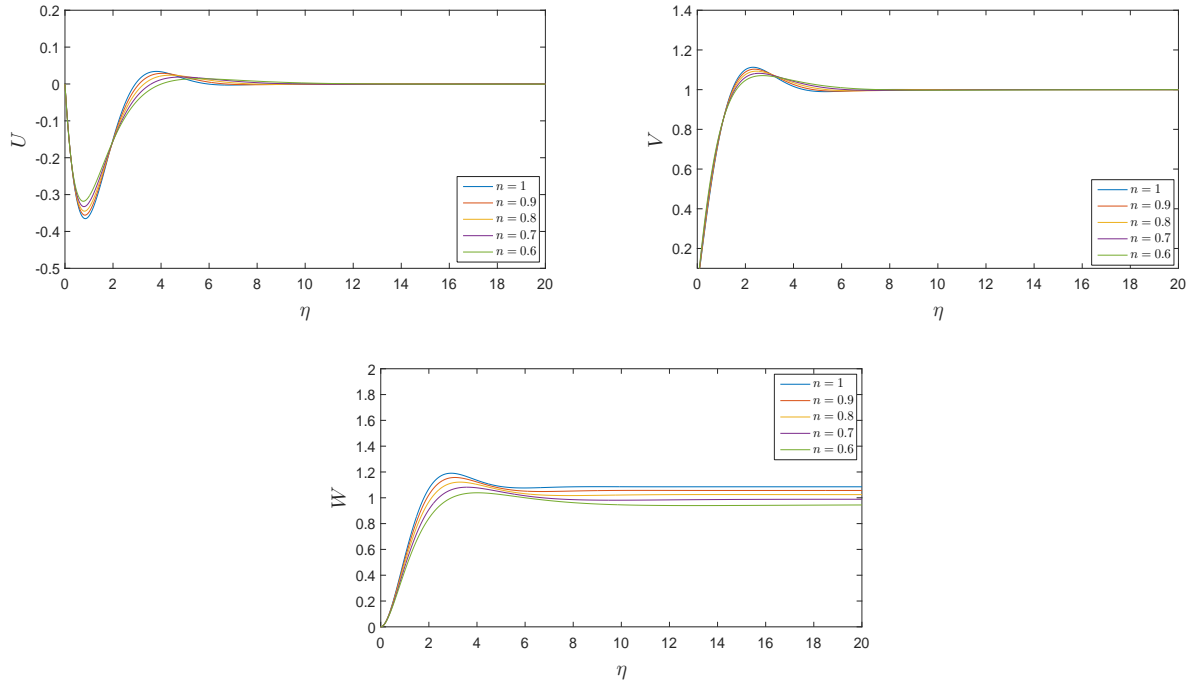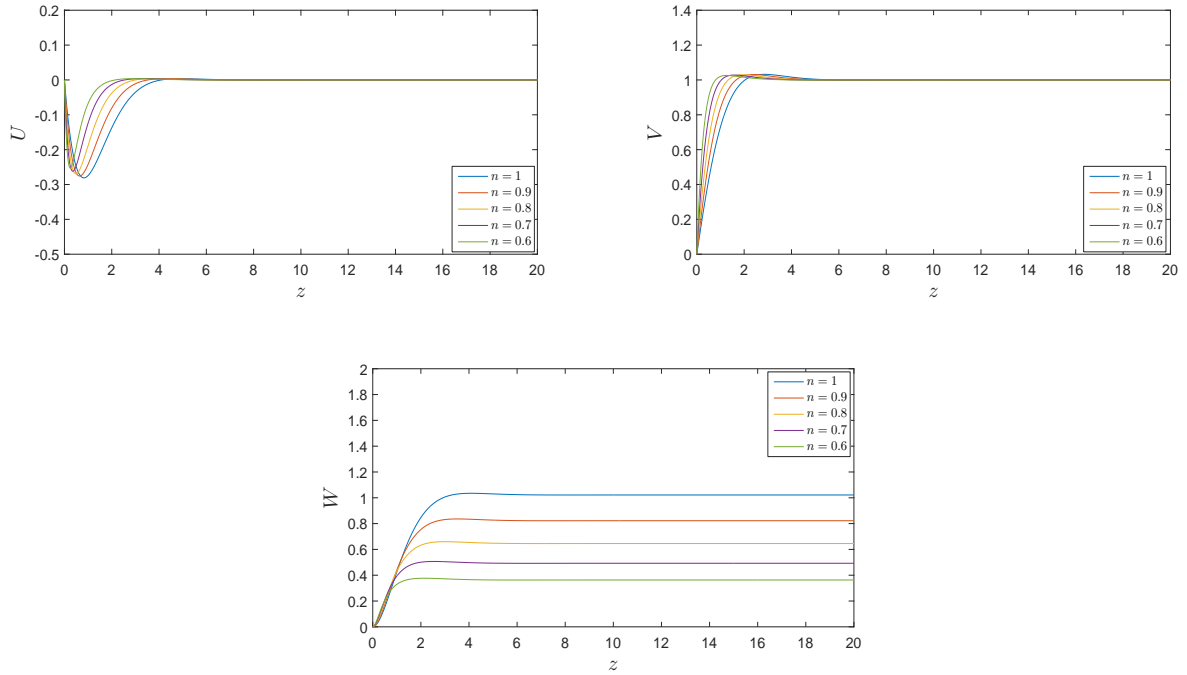
Figure 3.9: Steady mean flow profiles U, V and W versus z of the flow at $Ro = -0.5$ for Newtonian ($n = 1$) and shear-thinning Carreau fluids with $n = 0.9, 0.8, 0.7, 0.6$ and $k = 100$.

for $n = 1$ in Figures 3.8-3.17 are identical to the Newtonian mean flow profiles in Lingwood (1997).

It is interesting to note that the location of the maximum value of radial cross-flow profile U for shear-thinning Carreau fluids clearly approaches the disk surface as n is reduced as shown in Figures 3.8-3.12. This effect is more significant that for the radial profiles of shear-thinning power-law fluids. On the other hand, the peak of U for shear-thickening Carreau fluids is shifted along the z-axis toward the far-field for all the values of Ro. In other words, the thickness of the boundary-layer reduces with increased shear-thinning Carreau fluids while, increasingly the effect of shear-thickening Carreau fluids lead to an increase in the the thickness of the boundary-layer at all Ro. Furthermore, Figures 3.8-3.12 present that the maximum value for the radial flow profile U (the radial wall jet) is reduced for increasingly shear-thinning Carreau fluids, whereas it can be seen in Figures 3.13-3.17 it is increased for
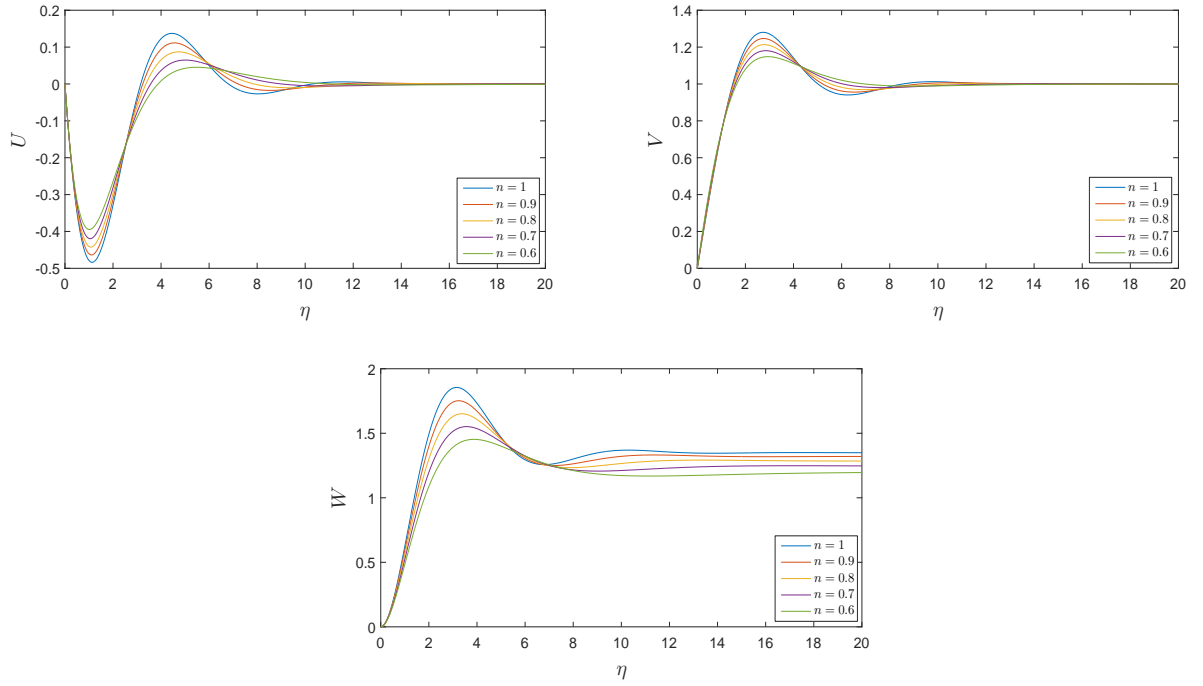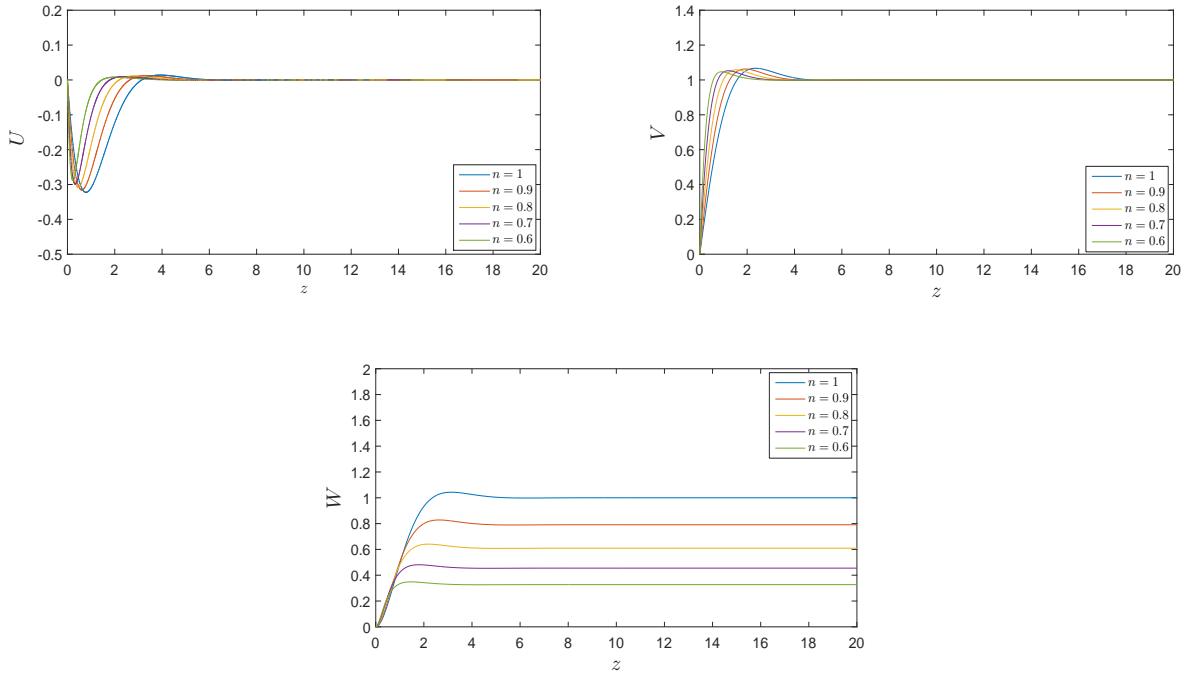
Figure 3.10: Steady mean flow profiles U, V and W versus z of the Ekman flow, $Ro = 0$ for Newtonian $(n = 1)$ and shear-thinning Carreau fluids with $n = 0.9, 0.8, 0.7, 0.6$ and $k = 100$.

increasingly shear-thickening Carreau fluids.

The oscillation for both shear-thinning and shear-thickening Carreau fluids is increased for all n as the Rossby number increased from minus unity to unity for all mean flows profiles. It can be noted that the oscillation of the flow is dampened for increased shear-thinning Carreau fluids, while it is amplified for increased shear-thickening Carreau fluids for all values of Ro. Furthermore, the radial mean flow is inflectional for all n. Nevertheless, all mean flows radial, azimuthal and axial velocities become inflectional with increasing Ro from minus unity to unity for all n. This behaviour is consistent with that seen from power-law fluids.

The magnitude of axial flow W in the far-field is reduced for all Ro as n is decreased for shear-thinning fluids. However, the magnitude of axial flow W for shear-thickening fluids in the far-field is increased for all values of Ro as n is decreased. The magnitude of both radial and azimuthal flows remain unchanged for all n.
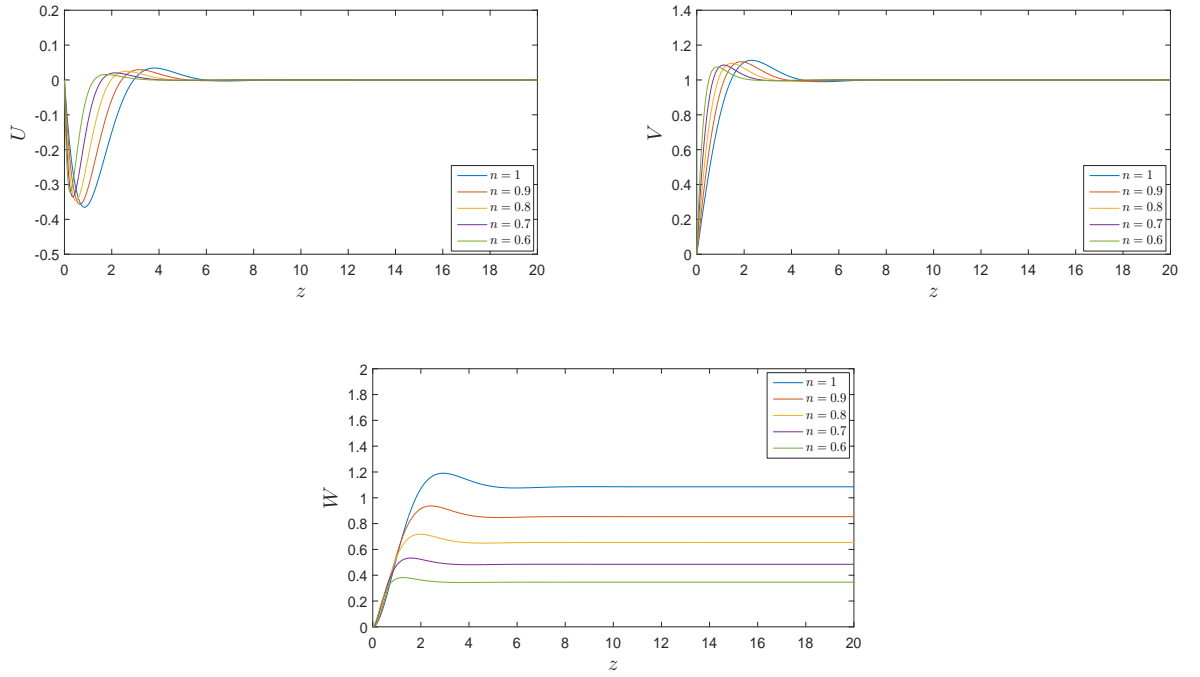
Figure 3.11: Steady mean flow profiles U, V and W versus z of the flow at $Ro = 0.5$ for Newtonian ($n = 1$) and shear-thinning Carreau fluids with $n = 0.9, 0.8, 0.7, 0.6$ and $k = 100$.
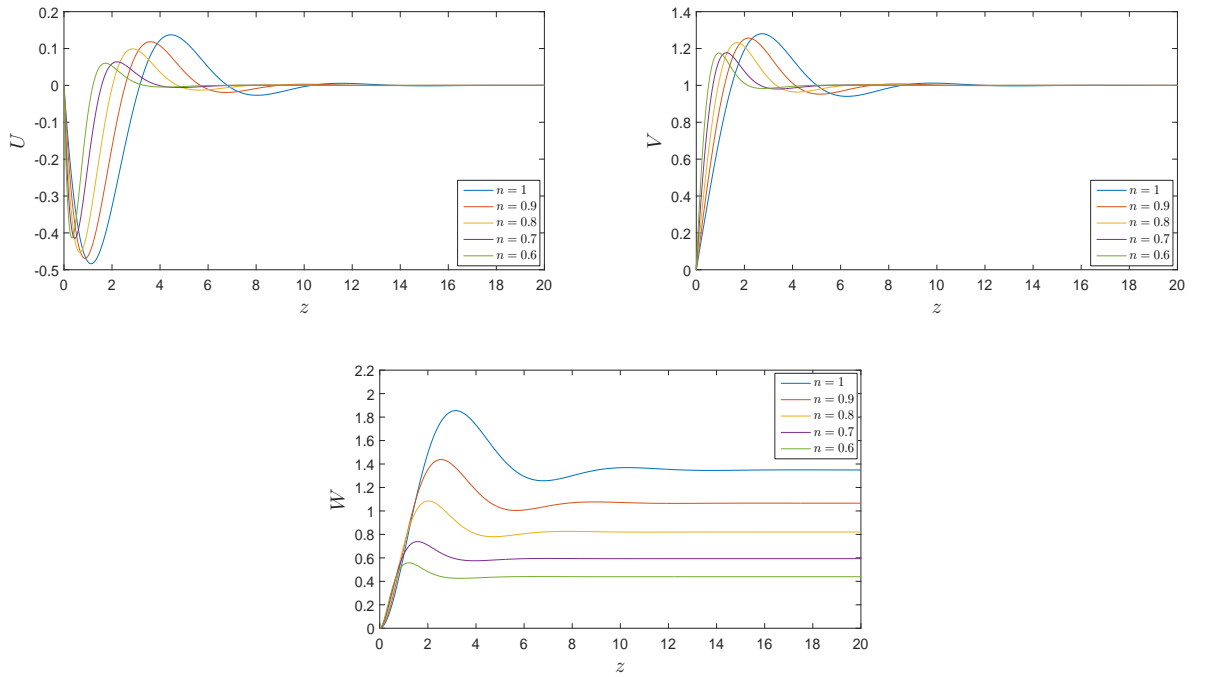
Figure 3.12: Steady mean flow profiles U, V and W versus z of the Bödewadt flow, $Ro = 1$ for Newtonian ($n = 1$) and shear-thinning Carreau fluids with $n = 0.9, 0.8, 0.7, 0.6$ and $k = 100$.
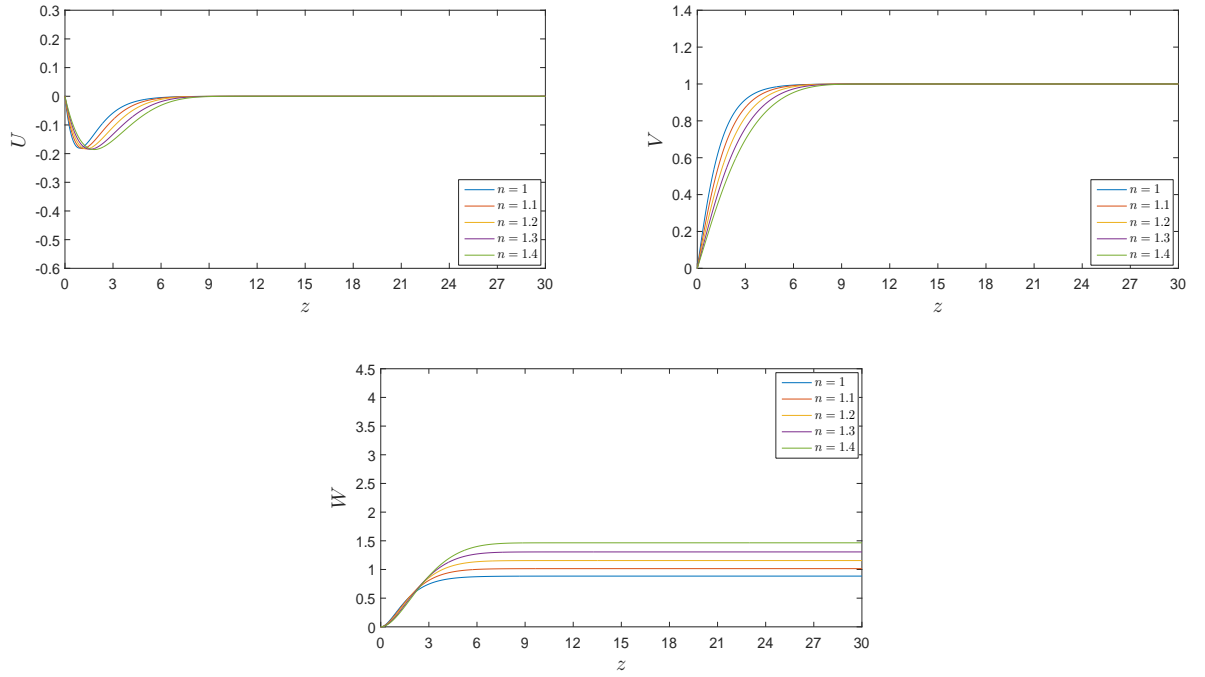
Figure 3.13: Steady mean flow profiles U, V and W versus z of the von Kármán flow, $Ro = -1$ for Newtonian ($n = 1$) and shear-thickening Carreau fluids with $n = 1.1, 1.2, 1.3, 1.4$ and $k = 100$.
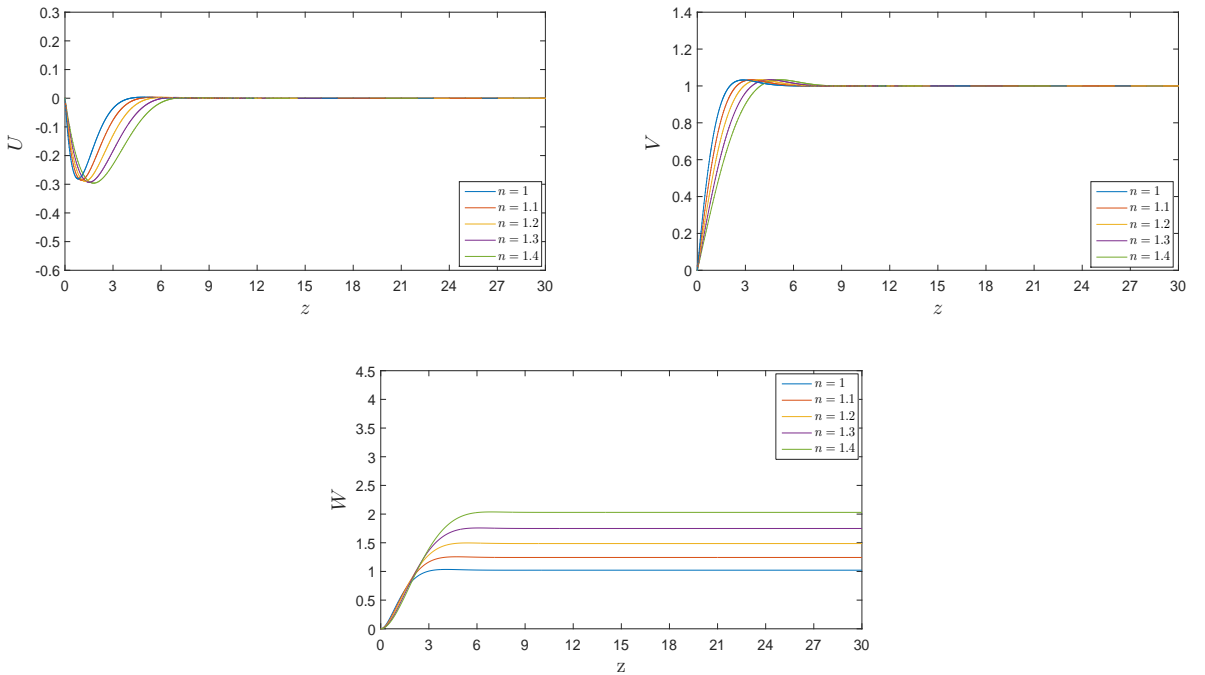
Figure 3.14: Steady mean flow profiles U, V and W versus z of the flow at $Ro = -0.5$ for Newtonian ($n = 1$) and shear-thickening Carreau fluids with $n = 1.1, 1.2, 1.3, 1.4$ and $k = 100$.
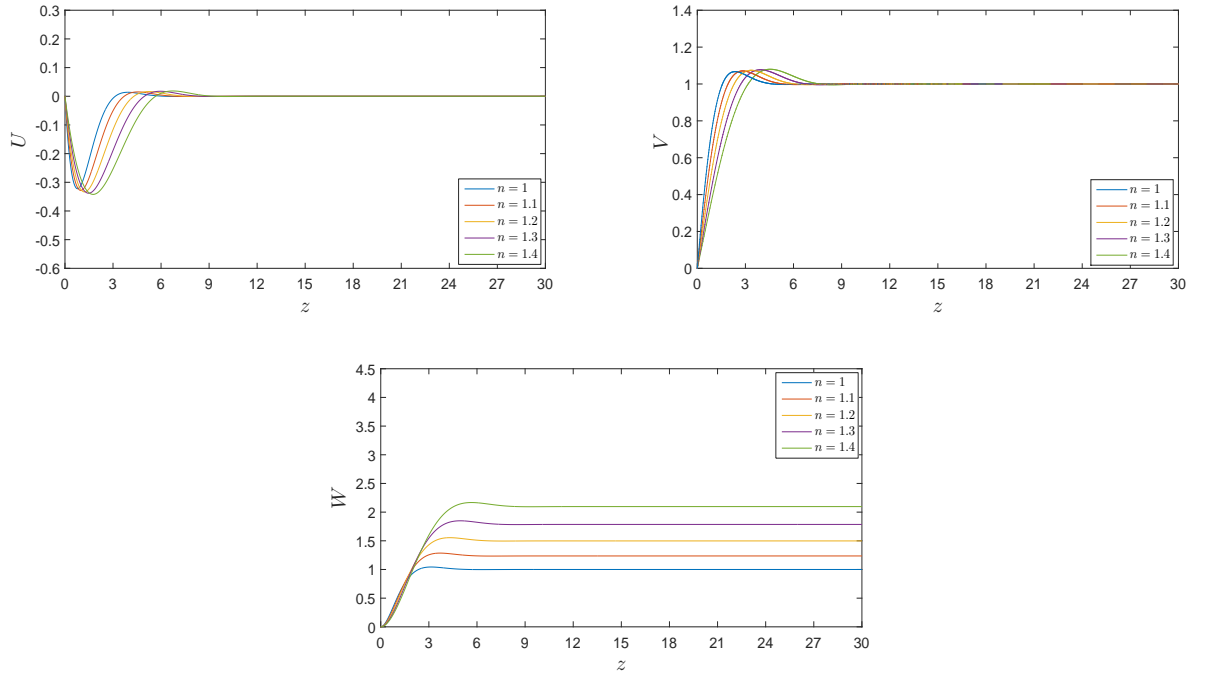
Figure 3.15: Steady mean flow profiles U, V and W versus z of the Ekman flow, $Ro = 0$ for Newtonian ($n = 1$) and shear-thickening Carreau fluids with $n = 1.1, 1.2, 1.3, 1.4$ and $k = 100$.
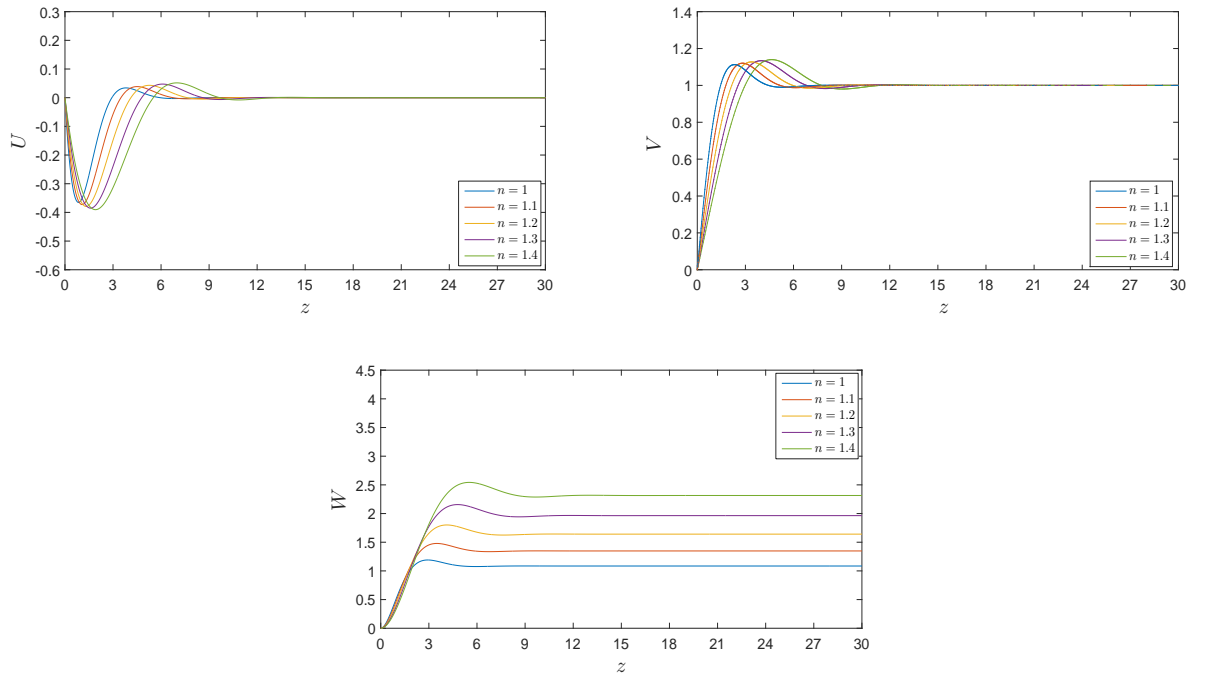
Figure 3.16: Steady mean flow profiles U, V and W versus z of the flow at $Ro = 0.5$ for Newtonian ($n = 1$) and shear-thinning power-law fluids with $n = 1.1, 1.2, 1.3, 1.4$ and $k = 100$.
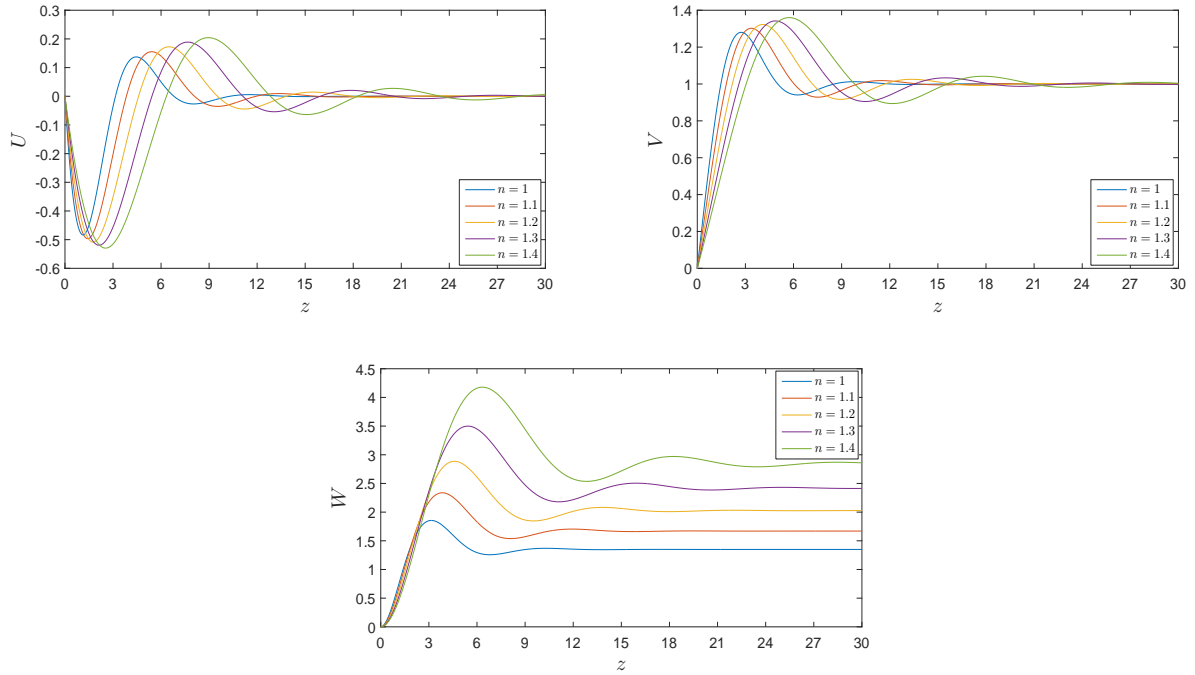
Figure 3.17: Steady mean flow profiles U, V and W versus z of the Bödewadt flow, $Ro = 1$ for Newtonian ($n = 1$) and shear-thinning power-law fluids with $n = 1.1, 1.2, 1.3, 1.4$ and $k = 100$.

3.4 Matlab solver for the steady mean flow

The MATLAB solver function **bvp4c** is opted to obtain the solution of the non-linear steady mean flow equations considered throughout this chapter. This solver function consists a finite difference method implementing the 3-stage Lobatto IIIa formula that can be introduced as one of the implicit Rung-kutta methods (Kierzenka and Shampine, 2001). The Lobatto IIIa formula is a collocation method that provides a C^1-continuous solution that is fourth-order accurate uniformly in the interval of integration. This interval is divided into subintervals by using mesh selection points. The error control and mesh selection are based on the residual of the continuous solution. Furthermore, the points of the initial mesh and an initial approximation of the solution at the mesh points are used to solve the equations.

Firstly, to obtain the solution of the mean flow profiles U, V and W, it is important to express the governing non-dimensional mean flow equations (3.8) and (3.13) for power-law

and Carreau fluids, respectively, as a system of first order ordinary differential equations. This system of equations is written as a five coupled first order equations in terms of the new five dependent transformation variables ϕ_n $(n = 1, 2, ...5)$ where

$$\phi_1 = U, \quad \phi_2 = U', \quad \phi_3 = V, \quad \phi_4 = V', \quad \text{and} \quad \phi_5 = W. \tag{3.15}$$

The transformed first order ODE system with no-slip boundary conditions for power-law fluids is given by

$$
\begin{aligned}
\phi_1' &= \phi_2, \\
\phi_2' &= \frac{\left(\phi_2^2 + n\phi_4^2\right) F - (1-n)\,\phi_2\phi_4 G}{n\mu\left[\phi_2^2 + \phi_4^2\right]}, \\
\phi_3' &= \phi_4, \\
\phi_4' &= \frac{\left[n\phi_2^2 + \phi_4^2\right] G + (1-n)\,\phi_2\phi_4 F}{n\mu\left[\phi_2^2 + \phi_4^2\right]}, \\
\phi_5' &= -2\phi_1 - \left(\frac{1-n}{n+1}\right)\eta\phi_2,
\end{aligned}
\tag{3.16a}
$$

$$\phi_1(0) = \phi_3(0) = \phi_5(0) = 0,$$

$$\phi_1(\eta \to \infty) = 0, \phi_3(\eta \to \infty) = 1. \tag{3.16b}$$

where

$$
\begin{aligned}
F &= Ro\left[\phi_1^2 - (\phi_3^2 - 1) + \left(\phi_5 + \left(\frac{1-n}{n+1}\right)\eta\phi_1\right)\phi_2\right] - Co\,(\phi_3 - 1), \\
G &= Ro\left[2\phi_1\phi_3 + \left(\phi_5 + \left(\frac{1-n}{n+1}\right)\eta\phi_1\right)\phi_4\right] + Co\phi_1, \\
\mu &= \left[(U')^2 + (V')^2\right]^{(n-1)/2}.
\end{aligned}
$$

Regarding to Carreau model, the transformed first order ODE system with no-slip boundary conditions for Carreau fluids is given by

$$\phi_1' = \phi_2,$$

$$\phi_2' = \frac{\left\{1 + k^2 \left(\phi_2^2 + n\phi_4^2\right)\right\} F - (1-n) k^2 \phi_2 \phi_4 G}{\mu \left\{1 + nk^2 \left(\phi_2^2 + \phi_4^2\right)\right\}},$$

$$\phi_3' = \phi_4, \qquad\qquad (3.17a)$$

$$\phi_4' = \frac{\left\{1 + k^2 \left(n\phi_2^2 + \phi_4^2\right)\right\} G + (1-n) k^2 \phi_2 \phi_4 F}{\mu \left\{1 + nk^2 \left(\phi_2^2 + \phi_4^2\right)\right\}},$$

$$\phi_5' = -2\phi_1,$$

$$\phi_1(0) = \phi_3(0) = \phi_5(0) = 0,$$

$$\phi_1(z \to \infty) = 0, \phi_3(z \to \infty) = 1, \qquad\qquad (3.17b)$$

where

$$F = Ro\left[\phi_1^2 - \left(\phi_3^2 - 1\right) + \phi_5\phi_2\right] - Co\left(\phi_3 - 1\right),$$

$$G = Ro\left[2\phi_1\phi_3 + \phi_5\phi_4\right] + Co\phi_1,$$

$$\mu = \left\{1 + k^2 \left[\left(U'\right)^2 + \left(V'\right)^2\right]\right\}^{(n-1)/2}.$$

The procedure of the solver function **bvp4c** is outlined firstly by obtaining a solution guess in an initial finite interval using the MATLAB function **bvpinit**, and then solving the system of equations (3.16) and (3.17) for power-law and Carreau fluids, respectively resulting from the boundary conditions in this interval. The solution is continued over larger intervals depending on the mesh selection points. The solver function approximates the error of the numerical solution on each interval. The process is repeated if the solution does not satisfy the tolerance criteria until it applies for the entire domain.

3.5   Summary

In this chapter, the profiles of steady mean BEK family of flows have been obtained by solving the boundary-layer equations for generalized Newtonian fluid; power-law and Carreau fluids. These governing equations are solved numerically by using fourth-order Runge-Kutta method. The properties of the mean flow velocities has been interpreted in order to describe the behaviour of the boundary-layer flow. These properties are the oscillation of the flow components, the thickness of the boundary-layer, the amount of fluid entrained into boundary-layer, and the size of the radial wall jet.

Chapter 4

Convective instabilities for the BEK family of flows for power-law fluids

In this chapter, the linear perturbation equations applicable to power-law fluids for the BEK family of flows are formulated with a view to studying the occurrence of linear convective instabilities. The Chebyshev collocation method described in Appendix B is applied to solve these perturbation equations. Alveroglu et al. (2016) and Abdulameer et al. (2016) used this numerical method to compute the neutral curves for the convective instability of Newtonian and power-law fluids, respectively. Much of the content of this chapter has been previously published in Abdulameer et al. (2016).

The derivation of the perturbation equations is given in §4.1. The neutral stability curves are presented in §4.2 and the growth rates are discussed in §4.3. Finally, the results of an energy analysis are presented in §4.4.

4.1   The perturbation equations

The dimensional governing boundary-layer equations (3.4) are used to derive the perturbation equations for power-law fluids. A local linear stability analysis is applied at a local radius

of the disk r_a^* by imposing infinitesimally small disturbances on the steady-mean flow at that position. Here the local Reynolds number is defined as

$$
\begin{aligned}
R &= (r_a^*)^{2/(n+1)} \left[\frac{(\triangle\Omega^*)^{2-n} L^*}{\nu^*} \right]^{2/(n+1)} = (r_a^*)^{2/(n+1)} \left[\frac{Ro^{2-n} (\Omega^*)^{2-n} L^*}{\nu^*} \right]^{2/(n+1)} \\
&= (r_a^*)^{2/(n+1)} \left[\frac{RoRo^{1-n} (\Omega^*)^{2-n} L^*}{\nu^*} \right]^{2/(n+1)} = \left(\frac{r_a^* Ro}{L^*} \right)^{2/(n+1)} \\
&= (r_a Ro)^{2/(n+1)}.
\end{aligned}
\tag{4.1}
$$

Note that this definition leads to negative Reynolds number for Newtonian flow ($n = 1$) when the Rossby number is negative. However, this is simply a consequence of the formulation and all results will be given in terms of positive R for all Ro and n. The Reynolds number can be interpreted as the non-dimensional location of the local analysis, and increasing R in magnitude corresponds to moving radially outwards from the axis of rotation (irrespective of the sign of the Rossby number) (Lingwood, 1997).

The non-dimensionalised velocity, pressure and time scales are $r_a^* \Omega^* Ro$, $\rho^* r_a^{*2} \Omega^{*2} Ro^2$ and $L^* / (r_a^* \Omega^* Ro)$, respectively. The steady mean flows and small perturbing quantities are denoted by upper-case and lower-case symbols, respectively. The non-dimensional velocities and pressure of a perturbed flow are defined as

$$
U_0(\eta, r, \theta, t) = \frac{rRo}{R^{(n+1)/2}} U(\eta) + u(\eta, r, \theta, t),
\tag{4.2a}
$$

$$
V_0(\eta, r, \theta, t) = \frac{rRo}{R^{(n+1)/2}} V(\eta) + v(\eta, r, \theta, t),
\tag{4.2b}
$$

$$
W_0(\eta, r, \theta, t) = \frac{r^{(n-1)/(n+1)} Ro}{R^{(n+1)/2}} W(\eta) + w(\eta, r, \theta, t),
\tag{4.2c}
$$

$$
P_{0,1}(\eta, r, \theta, t) = \frac{r^{2(n-1)/(n+1)} Ro^2}{R^{(n+1)}} P(\eta) + p(\eta, r, \theta, t),
\tag{4.2d}
$$

where $\eta = \eta(r,z) = r^{(1-n)/(n+1)} z$.

Note that the scalings used in equations (3.6), (3.7) and (4.2) are a generalisation of the

similarity solution introduced by Mitschka and Ulbrecht (1965) and Griffiths et al. (2014a) for the von Kármán flow under the power-law model. When $Ro = -1$, these expressions are consistent with those used by Griffiths et al. (2014a,b) for all n and when $n = 1$, they are consistent with those used in the Newtonian study of the BEK family of flows by Lingwood (1997) for all Ro.

The dimensionless Navier-Stokes equations in cylindrical-polar coordinates are linearised with respect to the perturbation quantities. The parallel-flow approximation is applied in the same way as Lingwood (1997) to ensure that the linearised equations are separable in r, θ and t. In practice, this involves ignoring variations in the Reynolds number with radius by replacing the variable r with $R^{(n+1)/2}/Ro$, and by neglecting all $\mathcal{O}((Ro/R)^2)$ terms. Furthermore, it has been necessary to set each factor Ro^j that appear in disturbance equations to unity, where j is some expression involving $n - 1$. This approximation is necessary to ensure continuity as Ro is varied from -1 to 1. The derivation of the perturbation equations for power-law fluids is presented in Appendix A. Therefore, the resulting linear disturbance equations are given by

$$R^{(n-1)/2}\frac{\partial u}{\partial r} + \frac{Ro}{R}\left[\eta\frac{(1-n)}{(n+1)}\frac{\partial u}{\partial \eta} + u + \frac{\partial v}{\partial \theta}\right] + \frac{\partial w}{\partial \eta} = 0, \tag{4.3a}$$

$$R^{(n-1)/2}\left(\frac{\partial u}{\partial t} + U\frac{\partial u}{\partial r}\right) + \frac{Ro}{R}\left(V\frac{\partial u}{\partial \theta} + W\frac{\partial u}{\partial \eta} + Uu\right) + U'w$$
$$- \left(2\frac{Ro}{R}V + \frac{Co}{R}\right)v + \frac{Ro}{R}\eta\frac{(1-n)}{(n+1)}\left(U\frac{\partial u}{\partial \eta} + U'u + \frac{\partial p}{\partial \eta}\right)$$
$$= -R^{(n-1)/2}\frac{\partial p}{\partial r} + \frac{1}{R}\frac{\partial}{\partial \eta}\left[\mu\frac{\partial u}{\partial \eta} + \hat{\mu}\left(U'\frac{\partial u}{\partial \eta} + V'\frac{\partial v}{\partial \eta}\right)U'\right], \tag{4.3b}$$

$$R^{(n-1)/2} \left(\frac{\partial v}{\partial t} + U \frac{\partial v}{\partial r} \right) + \frac{Ro}{R} \left(V \frac{\partial v}{\partial \theta} + W \frac{\partial v}{\partial \eta} + Uv \right) + V'w$$
$$+ \left(2\frac{Ro}{R}V + \frac{Co}{R} \right) u + \frac{Ro}{R} \eta \frac{(1-n)}{(n+1)} \left(U \frac{\partial v}{\partial \eta} + V'u \right)$$
$$= -\frac{Ro}{R} \frac{\partial p}{\partial \theta} + \frac{1}{R} \frac{\partial}{\partial \eta} \left[\mu \frac{\partial v}{\partial \eta} + \hat{\mu} \left(U' \frac{\partial u}{\partial \eta} + V' \frac{\partial v}{\partial \eta} \right) V' \right], \quad (4.3c)$$

$$R^{(n-1)/2} \left(\frac{\partial w}{\partial t} + U \frac{\partial w}{\partial r} \right) + \frac{Ro}{R} V \frac{\partial w}{\partial \theta} + \frac{Ro}{R} W \frac{\partial w}{\partial \eta} + \frac{Ro}{R} W'w$$
$$+ \frac{Ro}{R} \eta \frac{(1-n)}{(n+1)} U \frac{\partial w}{\partial \eta} = -\frac{\partial p}{\partial \eta} + \frac{1}{R} \frac{\partial}{\partial \eta} \left(\mu \frac{\partial w}{\partial \eta} \right) = 0, \quad (4.3d)$$

where the viscosity and the disturbance viscosity functions of power-law fluids is given respectively by

$$\mu \quad = \quad \left[(U')^2 + (V')^2 \right]^{(n-1)/2}, \tag{4.3e}$$

$$\hat{\mu} \quad = \quad \frac{(n-1)\,\mu}{\left[(U')^2 + (V')^2 \right]}. \tag{4.3f}$$

The perturbation quantities are supposed now to have the form consistent with the prior Newtonian analysis (Alveroglu et al., 2016; Lingwood, 1997; Lingwood and Garrett, 2011)

$$u \quad = \quad \hat{u}(\eta; \alpha, \beta, \omega; R, Ro) e^{i(\alpha r + \widetilde{\beta}\theta - \omega t)}, \tag{4.4a}$$

$$v \quad = \quad \hat{v}(\eta; \alpha, \beta, \omega; R, Ro) e^{i(\alpha r + \widetilde{\beta}\theta - \omega t)}, \tag{4.4b}$$

$$w \quad = \quad \hat{w}(\eta; \alpha, \beta, \omega; R, Ro) e^{i(\alpha r + \widetilde{\beta}\theta - \omega t)}, \tag{4.4c}$$

$$p \quad = \quad \hat{p}(\eta; \alpha, \beta, \omega; R, Ro) e^{i(\alpha r + \widetilde{\beta}\theta - \omega t)}. \tag{4.4d}$$

Here $\hat{u}, \hat{v}, \hat{w}$ and $\hat{p}$ are the spectral representations of the perturbation velocities and pressure, respectively, $\alpha = \alpha_r + i\alpha_i$ and $\widetilde{\beta} = \beta/Ro$ are the complex radial and real azimuthal wavenumbers, and ω is the frequency of the disturbance in the frame rotating with the lower disk. The perturbation equations now reduce to

$$\left(i\bar{\alpha} + \frac{Ro}{R}\right)\hat{u} + i\bar{\beta}\hat{v} + \frac{Ro}{R}\eta\frac{(1-n)}{(n+1)}\frac{\partial\hat{u}}{\partial\eta} + \frac{\partial\hat{w}}{\partial\eta} = 0, \tag{4.5a}$$

$$\left[i\left(\bar{\alpha}U + \bar{\beta}V - \bar{\omega}\right) + \frac{Ro}{R}U\right]\hat{u} - \left(2\frac{Ro}{R}V + \frac{Co}{R}\right)\hat{v} + \frac{Ro}{R}W\frac{\partial\hat{u}}{\partial\eta}$$
$$+ U'\hat{w} + \frac{Ro}{R}\eta\frac{(1-n)}{(n+1)}\left(U\frac{\partial\hat{u}}{\partial\eta} + U'\hat{u} + \frac{\partial\hat{p}}{\partial\eta}\right) + i\bar{\alpha}\hat{p}$$
$$- \frac{1}{R}\frac{\partial}{\partial\eta}\left[\mu\frac{\partial\hat{u}}{\partial\eta} + \hat{\mu}\left(U'\frac{\partial\hat{u}}{\partial\eta} + V'\frac{\partial\hat{v}}{\partial\eta}\right)U'\right] = 0, \tag{4.5b}$$

$$\left[i\left(\bar{\alpha}U + \bar{\beta}V - \bar{\omega}\right) + \frac{Ro}{R}U\right]\hat{v} + \left(2\frac{Ro}{R}V + \frac{Co}{R}\right)\hat{u} + \frac{Ro}{R}W\frac{\partial\hat{v}}{\partial\eta}$$
$$+ V'\hat{w} + \frac{Ro}{R}\eta\frac{(1-n)}{(n+1)}\left(U\frac{\partial\hat{v}}{\partial\eta} + V'\hat{u}\right) + i\bar{\beta}\hat{p}$$
$$- \frac{1}{R}\frac{\partial}{\partial\eta}\left[\mu\frac{\partial\hat{v}}{\partial\eta} + \hat{\mu}\left(U'\frac{\partial\hat{u}}{\partial\eta} + V'\frac{\partial\hat{v}}{\partial\eta}\right)V'\right] = 0, \tag{4.5c}$$

$$\left[i\left(\bar{\alpha}U + \bar{\beta}V - \bar{\omega}\right) + \frac{Ro}{R}W'\right]\hat{w} + \frac{Ro}{R}\left[W\frac{\partial\hat{w}}{\partial\eta} + \eta\frac{(1-n)}{(n+1)}U\frac{\partial\hat{w}}{\partial\eta}\right]$$
$$+ \frac{\partial\hat{p}}{\partial\eta} - \frac{1}{R}\frac{\partial}{\partial\eta}\left(\mu\frac{\partial\hat{w}}{\partial\eta}\right) = 0, \tag{4.5d}$$

where $\bar{\alpha} = R^{(n-1)/2}\alpha$, $\bar{\beta} = \beta/R$, $\bar{\omega} = R^{(n-1)/2}\omega$. The frequency ω is setted to be zero in order to study the occurrence of stationary instability in this thesis.

The modified wavenumber and orientation angle typically used in asymptotic analysis are then given by Griffiths et al. (2014a) in the following form

$$\kappa = \sqrt{\bar{\alpha}^2 + \bar{\beta}^2} = r^{(n-1)/(n+1)}\sqrt{\alpha^2 + \frac{\beta^2}{r^2}}, \tag{4.6}$$

and

$$\phi = \tan^{-1}\left(\frac{\bar{\beta}}{\bar{\alpha}}\right) = \frac{\pi}{2} - \tan^{-1}\left(\frac{\alpha r}{\beta}\right). \tag{4.7}$$

Note that additional viscous terms $\hat{\mu}U'\left(U'\frac{\partial \hat{u}}{\partial \eta} + V'\frac{\partial \hat{v}}{\partial \eta}\right)$ and $\hat{\mu}V'\left(U'\frac{\partial \hat{u}}{\partial \eta} + V'\frac{\partial \hat{v}}{\partial \eta}\right)$ appear in the perturbation equations (4.5) and these are due to the first-order terms of the cross-product associated with the generalised binomial expansion of the perturbed viscosity function. The study of Griffiths et al. (2014a) neglects these terms along with other η/R terms. However, the solution method used here is such that all $\hat{\mu}U'\left(U'\frac{\partial \hat{u}}{\partial \eta} + V'\frac{\partial \hat{v}}{\partial \eta}\right), \hat{\mu}V'\left(U'\frac{\partial \hat{u}}{\partial \eta} + V'\frac{\partial \hat{v}}{\partial \eta}\right)$ and η/R terms can be retained. This represents a small deviation from Griffiths' prior study of the von Kármán flow ($Ro = -1$) but should be considered an improvement.

Consistent with Griffiths' analyses, it is noted that the perturbation equations when $n = 1$ are not entirely consistent with the Newtonian set of transformed perturbation equations used by Lingwood (1997); Lingwood and Garrett (2011) for Newtonian flow. This minor discrepancy is due to the boundary-layer approximation used to construct the steady mean flow solutions in this general non-Newtonian formulation. Further details on this are given in the literature (Griffiths et al., 2014a).

In much the same way as presented by Alveroglu et al. (2016), the perturbation equations (4.5) are written as the eigenvalue problem (B.20) and solved by using a Galerkin projection in terms of Chebyshev polynomials described in Appendix B. This enables solutions of the dispersion relation $D(\alpha, \beta, \omega; R, n, Ro) = 0$ to be obtained at each (n, Ro) with the aim of studying the occurrence of local convective instability of power-law fluids at each parameter triple. Chebyshev polynomials permit significantly higher accuracy than standard finite-difference methods and this motivates their use here. Furthermore, as discussed by Alveroglu et al. (2016), this approach has two additional advantages over the shooting method used previously in the literature (Griffiths et al., 2014a; Lingwood, 1997; Lingwood and Garrett, 2011). Firstly, the perturbation equations are solved in terms of primitive variables not transformed to a ODE system; this permits the retention of a number of terms otherwise neglected (as

discussed previously). Secondly, all eigenvalues can be obtained simultaneously instead of searching iteratively from some initial guess. However, the shooting method used the transformed new system in order to calculates a single eigenvalue at each run. Appelquist (2014) presents a comparison between the shooting and Chebyshev methods in full details for the von Kármán flow.

The perturbation equations (4.5) are subject to boundary conditions

$$\hat{u}(\eta = 0) = \hat{v}(\eta = 0) = \hat{w}(\eta = 0) = 0 \tag{4.8a}$$

$$\hat{u}(\eta \to \eta_\infty) = \hat{v}(\eta \to \eta_\infty) = \hat{w}(\eta \to \eta_\infty) = 0 \tag{4.8b}$$

These represent the no-slip condition on the disk surface and also ensure that the disturbances are contained within the boundary-layer. All calculations use a Gauss–Lobatto grid with 100 points distributed via an exponential map between the lower disk surface $\eta = 0$ and the top of the domain $\eta = \eta_\infty$. Further increases in the resolution and spatial extent of this grid were found to have no numerical effect on the stability results.

4.2 Neutral curves

Neutral curves, defined by neutral spatial growth $\alpha_i = 0$, have been calculated for $0.6 \leq n \leq 1$ in increments of 0.1 at $Ro = -1, -0.5, 0, 0.5$ and 1. This range is deemed sufficient to capture the convective instability characteristics of shear-thinning power-law fluids within the BEK family of flows. Figures 4.1-4.6 presents the neutral curves in the R–$\bar{\alpha}_r$, R–$\bar{\beta}$, R–κ and R–ϕ planes where $\bar{\alpha}_r$ and $\bar{\beta}$ represent the real radial and the azimuthal wavenumbers, respectively, κ and ϕ denote the wavenumber and wave angle, and are defined in (4.6) and (4.7), respectively. These curves enclose a region in which the boundary-layer is convectively unstable.
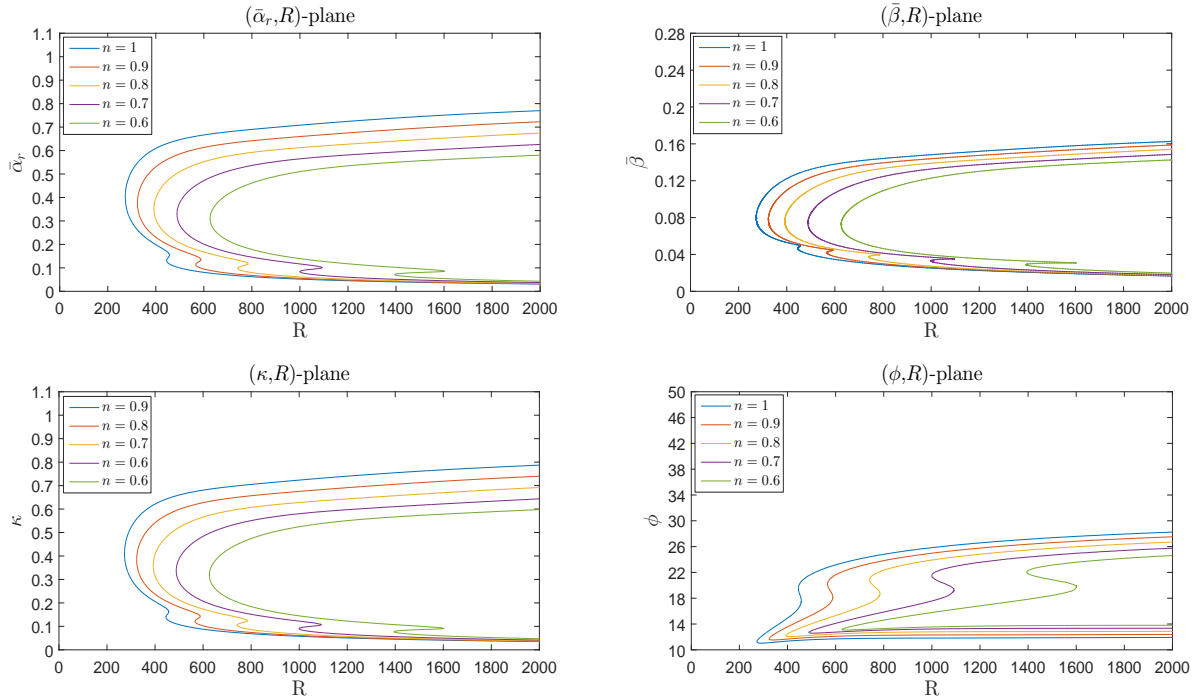
Figure 4.1: Neutral curves of the von Kármán flow, $Ro = -1$ for shear-thinning power-law fluids with $n = 1, 0.9, 0.8, 0.7, 0.6$.

The neutral curves are seen to have a two-lobed structure demonstrating that both the Type I and Type II modes exist in the non-Newtonian system. In particular, the upper branch lobe (in the R–wavenumbers planes) correspond to the Type I mode of instability (due to an inflectional crossflow velocity component) and the smaller lower branch lobe to the Type II mode of instability (due to streamline curvature). Critical Reynolds numbers for the onset of both modes are presented in Table 4.1.

Figure 4.2 shows the structure of the two spatial branches in the complex α–plane for the flow of $Ro = -0.5$ when $n = 0.6$, for $R = 380$ and $R = 762$. The convective instability is determined by a branch region lying below the line $\alpha_i = 0$. Figure 4.2(a) shows that branch 1 now defines the region of convective instability. Increasing the value of R affects the minimum of branch 1 that moves downwards and the points of the branch crossing the line $\alpha_i = 0$ move apart. Therefore, branch 1 results in an extension of the region of instability as R is increased.
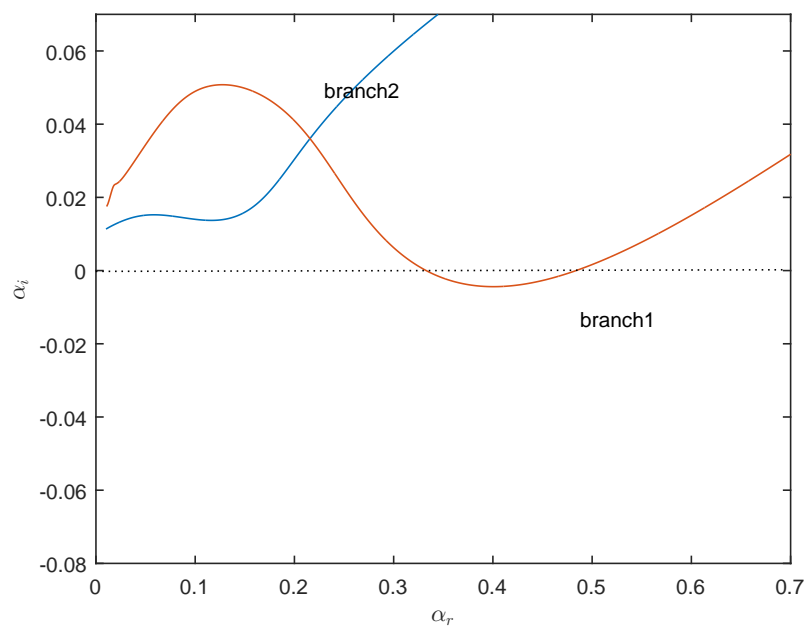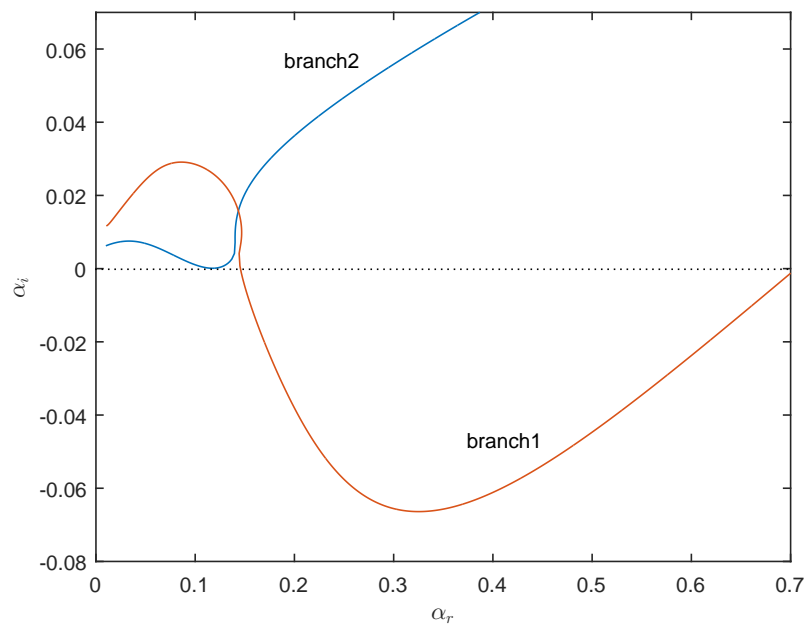
Figure 4.2: The two spatial branches for the flow at $Ro = -0.5$ in the case of $n = 0.6$ showing Type I instability at; (a) at $R = 380$ and (b) $R = 762$.

n	R	$\bar{\alpha}$	$\bar{\beta}$	κ	ϕ
1	272.90(445.21)	0.4029(0.1319)	0.0802(0.0467)	0.4108(0.1400)	11.26(19.48)
0.9	323.60(566.41)	0.3768(0.1142)	0.0781(0.0419)	0.3848(0.1216)	11.71(20.16)
0.8	392.36(741.16)	0.3518(0.0982)	0.0760(0.0374)	0.3599(0.1051)	12.19(20.83)
0.7	488.20(999.78)	0.3298(0.0841)	0.0743(0.0331)	0.3380(0.0903)	12.69(21.46)
0.6	626.06(1394.57)	0.3103(0.0717)	0.0725(0.0290)	0.3186(0.0773)	13.15(22.01)

(a) von Kármán, $Ro = -1$

n	R	$\bar{\alpha}$	$\bar{\beta}$	κ	ϕ
1	149.74(-)	0.5098(-)	0.1237(-)	0.5246(-)	13.64(-)
0.9	180.37(-)	0.4780(-)	0.1185(-)	0.4924(-)	13.92(-)
0.8	221.84(-)	0.4495(-)	0.1139(-)	0.4637(-)	14.22(-)
0.7	279.54(-)	0.4253(-)	0.1102(-)	0.4393(-)	14.52(-)
0.6	362.69(763.26)	0.4065(0.1179)	0.1075(0.0527)	0.4204(0.1291)	15.81(24.08)

(b) $Ro = -0.5$

n	R	$\bar{\alpha}$	$\bar{\beta}$	κ	ϕ
1	105.88(-)	0.5805(-)	0.1444(-)	0.5982(-)	13.97(-)
0.9	127.54(-)	0.5466(-)	0.1386(-)	0.5639(-)	14.23(-)
0.8	157.52(-)	0.5163(-)	0.1336(-)	0.5333(-)	14.51(-)
0.7	200.20(-)	0.4891(-)	0.1293(-)	0.5059(-)	14.81(-)
0.6	263.00(496.81)	0.4677(0.1569)	0.1263(0.0704)	0.4845(0.1720)	15.11(24.15)

(c) Ekman, $Ro = 0$

n	R	$\bar{\alpha}$	$\bar{\beta}$	κ	ϕ
1	67.21(-)	0.5861(-)	0.1455(-)	0.6039(-)	13.94(-)
0.9	81.28(-)	0.5521(-)	0.1402(-)	0.5696(-)	14.25(-)
0.8	101.40(-)	0.5187(-)	0.1351(-)	0.5360(-)	14.60(-)
0.7	131.08(-)	0.4892(-)	0.1306(-)	0.5063(-)	14.95(-)
0.6	176.36(-)	0.4646(-)	0.1271(-)	0.4816(-)	15.30(-)

(d) $Ro = 0.5$

n	R	$\bar{\alpha}$	$\bar{\beta}$	κ	ϕ
1	22.40(-)	0.5404(-)	0.1185(-)	0.5532(-)	12.37(-)
0.9	27.22(-)	0.5119(-)	0.1189(-)	0.5256(-)	13.07(-)
0.8	34.51(-)	0.4803(-)	0.1179(-)	0.4946(-)	13.79(-)
0.7	46.08(-)	0.4470(-)	0.1155(-)	0.4616(-)	14.49(-)
0.6	65.71(-)	0.4108(-)	0.1117(-)	0.4257(-)	15.21(-)

(e) Bödewadt, $Ro = 1$

Table 4.1: The values of the critical Reynolds number R, wavenumbers α, β and κ and wave angle ϕ for shear-thinning power-law fluids at various Ro on the both modes Type I and (Type II).
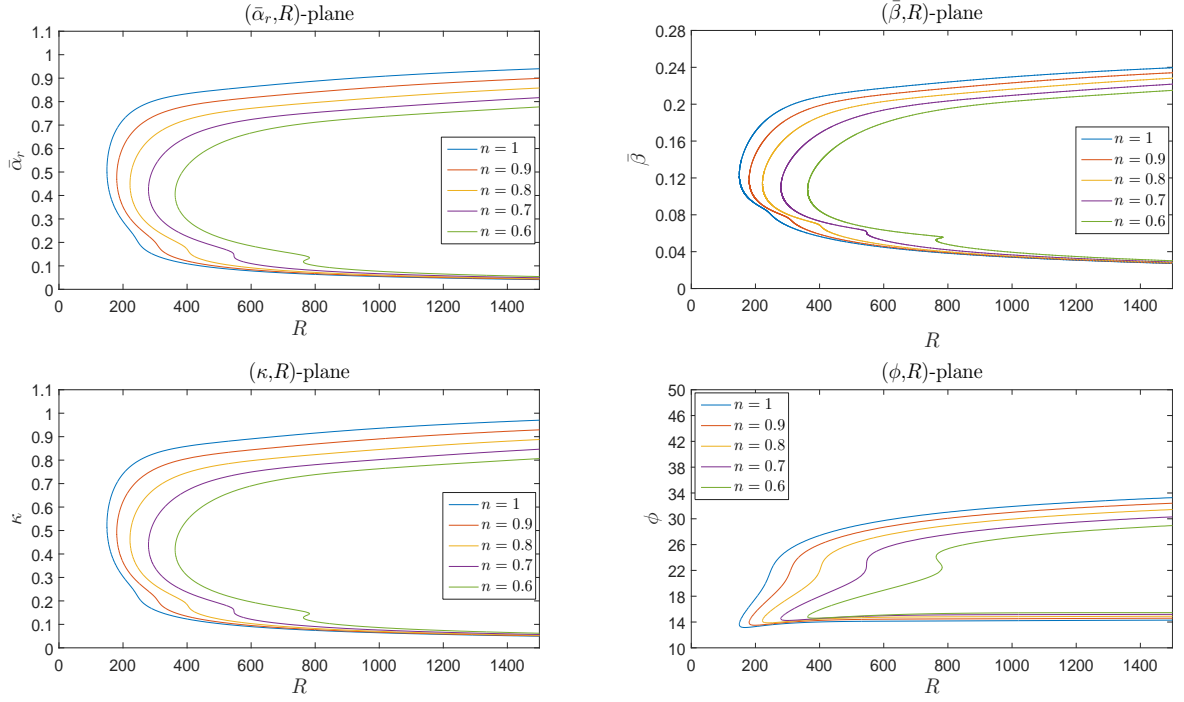
Figure 4.3: Neutral curves of the flow at $Ro = -0.5$ for shear-thinning power-law fluids with $n = 1, 0.9, 0.8, 0.7, 0.6$.

Furthermore, branch 2 eventually also crosses the line $\alpha_i = 0$ thereby mapping out the upper and lower branch of the neutral curve, as shown in Figure 4.2(b).

It is noted that Figure 4.1 is consistent with the neutral curves generated by Griffiths et al. (2014a) for Newtonian von Kármán flow, $Ro = -1$ and $n = 1$. However, slight differences in the numerical values of the critical Reynolds numbers are found owing to the inclusion of the additional viscous terms $\hat{\mu} U' \left(U' \frac{\partial \hat{u}}{\partial \eta} + V' \frac{\partial \hat{v}}{\partial \eta} \right)$, $\hat{\mu} V' \left(U' \frac{\partial \hat{u}}{\partial \eta} + V' \frac{\partial \hat{v}}{\partial \eta} \right)$ and η/R in the perturbation equations. Figure 4.1 shows that shear-thinning fluids for the von Kármán flow have a strong stabilising effect on both the Type I and Type II in terms of the critical Reynolds number and the region of instability from the upper branch. It is interesting to note that these terms lead to growth in the relative size of the Type II mode as n is decreased (as compared to Griffiths' results). In addition, the critical Reynolds numbers are reduced in comparison with Griffiths' numerical results as predicted in Griffiths et al. (2014a).
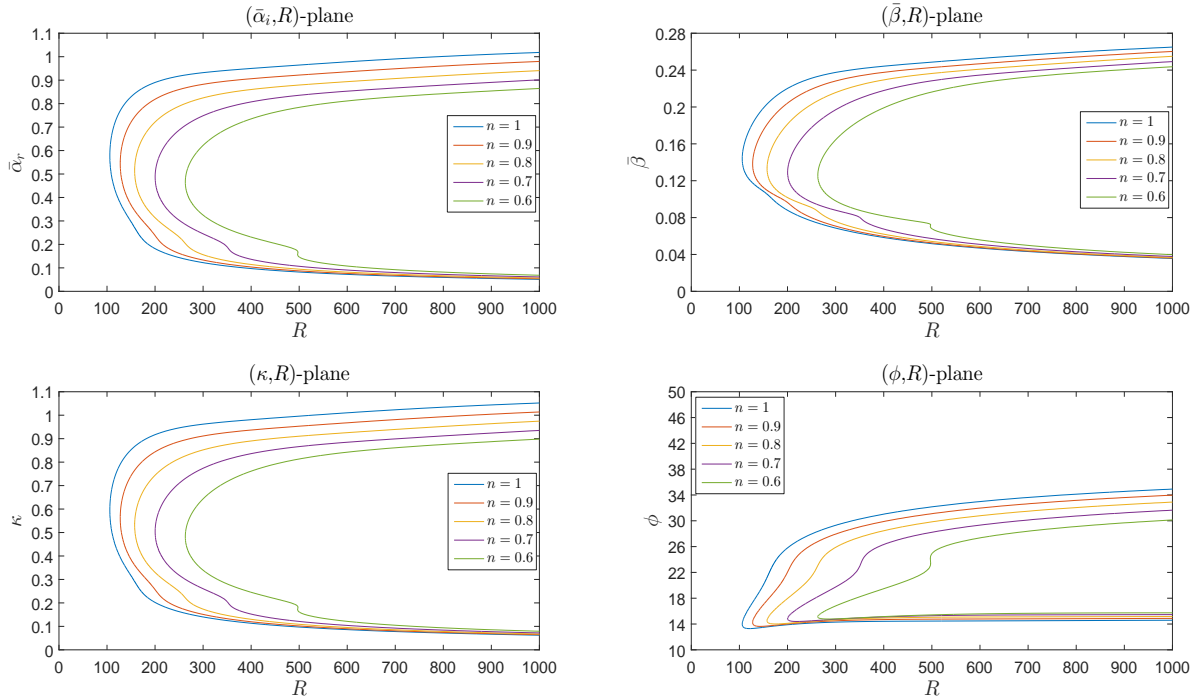
Figure 4.4: Neutral curves of the Ekman flow, $Ro = 0$ for shear-thinning power-law fluids with $n = 1, 0.9, 0.8, 0.7, 0.6$.

Figure 4.3 reveals the neutral curves of the related flow of the BEK family for $Ro = -0.5$. It shows that decreasing the power-law index $(n < 1)$ has a stabilising effect on both the Type I and Type II modes in terms of the critical Reynolds number and the region of instability from the upper branch. Furthermore, the Type II mode begins to appear as the power-law index n is decreased and it can be seen this clearly at $n = 0.6$.

The neutral curves for the Ekman flow, $Ro = 0$ are then presented in Figure 4.4. It shows that the behaviour of the Ekman flow is similar to the flow for $Ro = -0.5$ in terms of the stabilising effect on the Type I mode and appearance of the Type II mode as n is reduced.

Figure 4.5 shows the neutral curves of the related flow of the BEK family for $Ro = 0.5$. It is noted from this figure that there is a stabilising effect for decreasing power-law index n in terms of the critical Reynolds number as well as the region of instability from the upper branch.
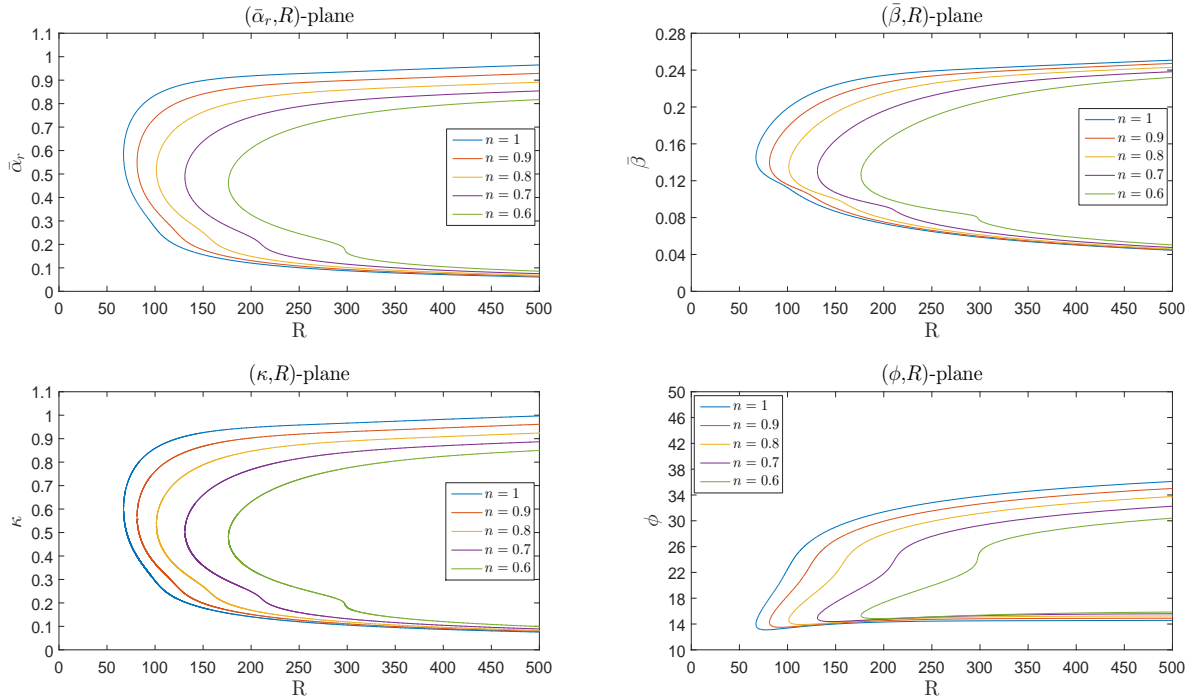
Figure 4.5: Neutral curves of the flow at $Ro = 0.5$ for shear-thinning power-law fluids with $n = 1, 0.9, 0.8, 0.7, 0.6$.

The neutral curves for Bödewadt flow are then produced at $Ro = 1$. Figure 4.6 reveals that shear-thinning fluids have a stabilising effect on Type I mode for the Bödewadt flow in terms of the critical Reynolds number and the region of instability from the upper branch. However, the stabilising effect is weaker compared to the effect of the other flows of BEK family. In other words, the stabilising effect is decreasing gradually depending on the value of Rossby number changed from von Kármán flow, $Ro = -1$ towards Bödewadt flow, $Ro = 1$.

In general, all neutral curves in Figures 4.1-4.6 and critical Reynolds numbers in Table 4.1 suggest that decreasing the power-law index $(n < 1)$ has a stabilising effect on both the dominant Type I mode and secondary Type II mode for all Ro. That is, shear-thinning fluids act to stabilise the von Kármán, the Ekman, the Bödewadt, and all intermediate boundary-layers. Figures 4.1-4.6 further suggest that, while reducing the associated critical Reynolds number, reductions in n act to promote the appearance of the distinct Type II mode.
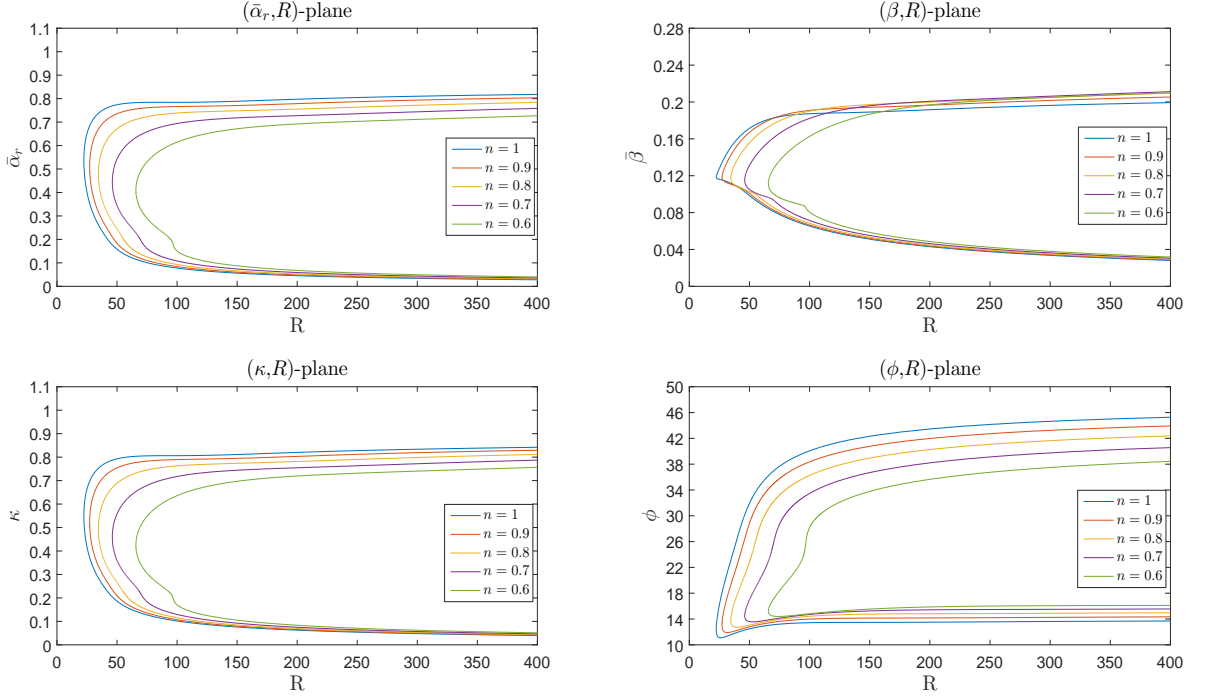
Figure 4.6: Neutral curves of the Bödewadt flow, $Ro = 1$ for shear-thinning power-law fluids with $n = 1, 0.9, 0.8, 0.7, 0.6$.

4.3 Growth rates

In this section, the growth rates of the Type I instability mode of the BEK family of boundary-layer flows are presented for power-law fluids. These growth rates are plotted as a variation of the absolute value of the imaginary part of the negative radial wavenumber, $|\alpha_i|$, at particular number of spiral vortices $\bar{n}$. The growth rates of the secondary Type II mode are not included here, owing to their very small value in comparison with the dominant Type I mode. In addition, the power-law fluids have only a slight effect on the Type II mode.

Figure 4.7 shows the convective growth rates of the dominant Type I mode at $R = R_c + 25$ against $\bar{n}$ at $Ro = -1, -0.5$ and 0 for various value of n. Here $\bar{n} = \bar{\beta}R$ is the number of spiral vortices around the disk surface, and R_c denotes the critical Reynolds number at the onset of the Type I mode presented in Table 4.1 for the particular n and Ro. That is, the growth rate is sampled a fixed distance ($R = 25$) into the convectively unstable region for a variety of flow
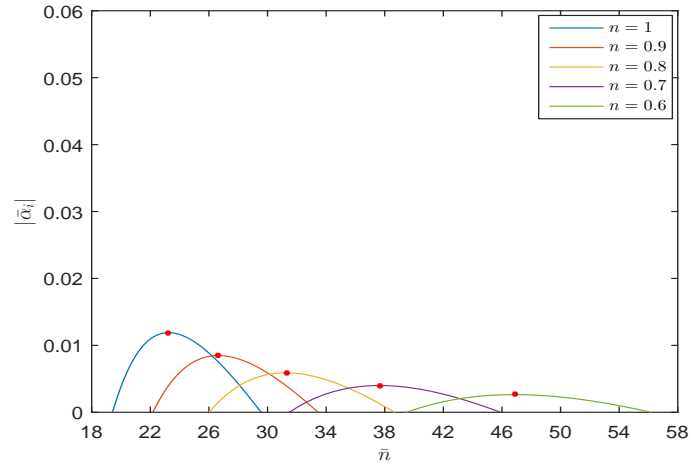
(a) von Kármán, $Ro = -1$
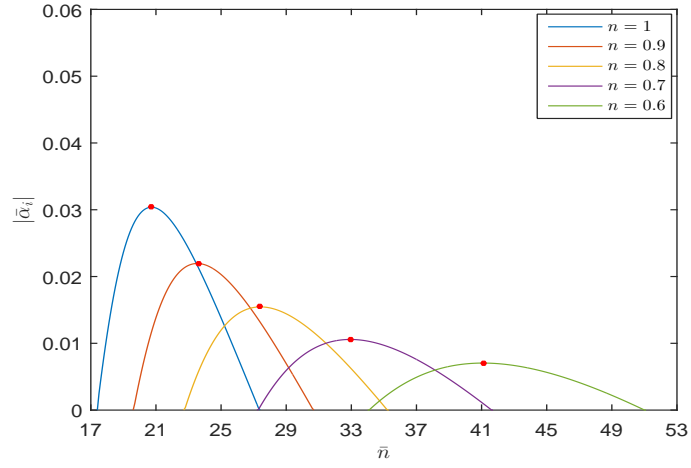
(b) $Ro = -0.5$
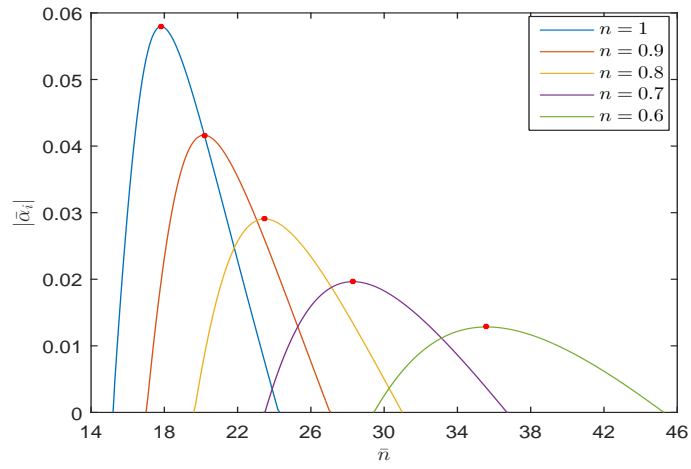
(c) Ekman, $Ro = 0$

Figure 4.7: Growth rates for Type I mode for shear-thinning power-law fluids with $n = 1, 0.9, 0.8, 0.7, 0.6$.

configurations.

Figure 4.7 reveals a universal stabilising effect on the growth rates of the Type I mode for each flow as n decreases; this is in addition to the stabilising increase in R_c with reduced n as identified previously. The stabilising results seen here are consistent with the critical values for each flow reported in Table 4.1.

It is interesting to note that the maximum growth rate (identified with a red dot) is pushed to higher $\bar{n}$. That is, although it might be expected the delayed onset and weaker growth of the disturbances for shear-thinning fluids, the number of spiral vortices at the maximum growth rate location is predicted to increase compared to the Newtonian case. Furthermore, the maximum growth rate for all values of n is increased as the Rossby number reduced from -1 to 0. These maximum rates are used later in the energy analysis of §4.4.

Note that it is not possible to show convective growth rates for $Ro \geq 0.5$. This is due to the very early onset of absolute instability and associated "branch exchange" between Type I and Type III modes. Therefore, it is impossible to find the location of maximum growth rate at such positive Ro. Further information on this can be found for the Newtonian case performed by Lingwood and Garrett (2011).

4.4   Energy analysis

Following the work of Cooper and Carpenter (1997), Cooper et al. (2015) and Garrett et al. (2016) for the von Kármán flow, an integral energy equation for the disturbances within the power-law BEK family of flows is derived here in order to gain insight into the underlying physical mechanisms behind the stabilising effects determined previously.

Cooper's approach are followed by derive the governing energy equations by multiplying the linearised momentum equations (4.3) by the disturbance quantities u, v and w, respectively. These are then summed to obtain the following kinetic-energy equation for the disturbances

$$
\left\{ R^{(n-1)/2} \left(\frac{\partial}{\partial t} + U \frac{\partial}{\partial r} \right) + \frac{Ro}{R} \left(V \frac{\partial}{\partial \theta} - W \frac{\partial}{\partial \eta} \right) \right\} K
$$
$$
= -uw \frac{\partial U}{\partial \eta} - vw \frac{\partial V}{\partial \eta} + \frac{Ro}{R} w^2 \frac{\partial W}{\partial \eta} + \frac{Ro}{R} U u^2 + \frac{Ro}{R} U v^2
$$
$$
- \left[R^{(n-1)/2} \frac{\partial (up)}{\partial r} + \frac{Ro}{R} \frac{\partial (vp)}{\partial \theta} + \frac{\partial (wp)}{\partial \eta} - \frac{Ro}{R} up \right] + \left[\frac{\partial (u_j \sigma_{ij})}{\partial x_i} - \sigma_{ij} \frac{\partial u_j}{\partial x_i} \right]
$$
$$
+ \frac{1}{R} \frac{\partial}{\partial \eta} \left(\mu \frac{\partial u}{\partial \eta} \right) u + \frac{1}{R} \frac{\partial}{\partial \eta} \left(\mu \frac{\partial v}{\partial \eta} \right) v + \frac{1}{R} \frac{\partial}{\partial \eta} \left(\mu \frac{\partial w}{\partial \eta} \right) w. \quad (4.9)
$$

Here $K = (1/2) \left(u^2 + v^2 + w^2 \right)$ is the kinetic energy, σ_{ij} are anti-symmetric viscous stress terms

$$
\sigma_{ij} = \frac{\mu}{R} \left(\frac{\partial u_i}{\partial x_j} - \frac{\partial u_j}{\partial x_i} \right). \quad (4.10)
$$

Note that $\mathcal{O} \left(1/R^2 \right)$ viscous terms have been omitted to ensure consistency with the linearised governing stability equations. Furthermore, the derivatives with respect to t and θ are removed to capture the steady, rotationally-symmetric nature of the energy. In practice this is done by averaging the perturbations over a single time period and azimuthal mode. The equations are then integrated across the entire boundary-layer to obtain the following expressions:

$$\int_0^\infty \left[R^{(n-1)/2} \left\{ \underbrace{U \frac{\partial \overline{K}}{\partial r}}_{a} + \underbrace{\frac{\partial \left(\overline{up} \right)}{\partial r}}_{b} - \underbrace{\frac{\partial}{\partial r} \left(\overline{u\sigma_{11}} + \overline{v\sigma_{12}} + \overline{w\sigma_{13}} \right)}_{c} \right\} \right] d\eta$$

$$= \underbrace{\int_0^\infty \left[\left(-\overline{uw} \frac{\partial U}{\partial \eta} \right) + \left(-\overline{vw} \frac{\partial V}{\partial \eta} \right) + \left(\frac{Ro}{R} \overline{w^2} \frac{\partial W}{\partial \eta} \right) \right] d\eta}_{\text{I}}$$

$$\underbrace{- \int_0^\infty \left(\overline{\sigma_{ij} \frac{\partial u_j}{\partial x_i}} \right) d\eta}_{\text{II}} + \underbrace{\int_0^\infty \left(\frac{Ro}{R} \overline{up} \right) d\eta + (\overline{wp})_{\bar{W}}}_{\text{III}} - \underbrace{(\overline{u\sigma_{31}} + \overline{v\sigma_{32}} + \overline{w\sigma_{33}})_{\bar{W}}}_{\text{IV}}$$

$$+ \underbrace{\int_0^\infty \frac{Ro}{R} \frac{\partial \bar{K}}{\partial \eta} W d\eta + \int_0^\infty \frac{Ro}{R} \overline{u^2} U d\eta + \int_0^\infty \frac{Ro}{R} \overline{v^2} U d\eta}_{\text{V}}$$

$$\underbrace{+ \frac{1}{R} \int_0^\infty \left[\mu \overline{\frac{\partial^2 u}{\partial \eta^2}} u + \frac{\partial \mu}{\partial \eta} \overline{\frac{\partial u}{\partial \eta}} u \right] d\eta + \frac{1}{R} \int_0^\infty \left[\mu \overline{\frac{\partial^2 v}{\partial \eta^2}} v + \frac{\partial \mu}{\partial \eta} \overline{\frac{\partial v}{\partial \eta}} v \right] d\eta_{N_2} + \frac{1}{R} \int_0^\infty \left[\mu \overline{\frac{\partial^2 w}{\partial \eta^2}} w + \frac{\partial \mu}{\partial \eta} \overline{\frac{\partial w}{\partial \eta}} w \right] d\eta}_{VI}.$$

$$(4.11)$$

Note that overbars denote a period-averaged quantity; for example, $\overline{uv} = uv^* + u^* v$ (where * indicates a complex conjugate) and $\bar{W}$ subscripts denote quantities evaluated at the wall.

Substituting (4.4) into the left-hand-side of equation (4.11) and then derive the terms with respect to r gives

$$\int_0^\infty \left[R^{(n-1)/2} i (\alpha - \alpha^*) \left\{ U (uu^* + vv^* + ww^*) + (up^* + u^* p) \right. \right.$$
$$\left. \left. - (u\sigma_{11}^* + u^* \sigma_{11} + v\sigma_{12}^* + v^* \sigma_{12} + w\sigma_{13}^* + w^* \sigma_{13}) \right\} \right] d\eta = RHS.$$

It is clear that $\alpha = \alpha_r + i\alpha_i$ and $\alpha^* = \alpha_r - i\alpha_i$, gives
$$-2\bar{\alpha}_i \int_0^\infty \left[U\overline{K} + \overline{up} - (\overline{u\sigma_{11}} + \overline{v\sigma_{12}} + \overline{w\sigma_{13}}) \right] d\eta = RHS$$

where $\bar{\alpha} = R^{(n-1)/2}\alpha$.

Therefore, The energy equation is normalized for any eigenmode against the integrated

mechanical energy flux as follows

$$-2\bar{\alpha}_i = \underbrace{(P_1 + P_2 + P_3)}_{I} + \underbrace{D}_{II} + \underbrace{(PW_1 + PW_2)}_{III} + \underbrace{(S_1 + S_2 + S_3)}_{IV}$$

$$+ \underbrace{(G_1 + G_2 + G_3)}_{V} + \underbrace{(N_1 + N_2 + N_3)}_{VI}. \quad (4.12)$$

Note that the mathematical origin of each term is indicated by the numbered underbracing in equations (4.11) and (4.12).

As discussed by Cooper and Carpenter (1997); Cooper et al. (2015), particular terms in equation (4.12) can be interpreted physically as originating from the following effects,

(a) average kinetic energy convected by the radial mean flow,

(b) work done by the perturbation pressure,

(c) work done by the viscous stress inside the boundary-layer,

(I) Reynolds stress energy production terms, P_i,

(II) viscous dissipation energy removal term, D,

(III) pressure work terms, PW_i,

(IV) contributions from work done on the wall by viscous stresses, S_i,

(V) terms arising from the streamline curvature effects and the three dimensionality of the mean flow, G_i,

(VI) non-Newtonian viscosity terms, N_i.

The terms PW_2, S_1, S_2 and S_3 in the energy balance equation (4.12) are equal to zero. This is because of the boundary conditions (4.8) for all flows of the BEK family. Furthermore, for the Ekman flow, $Ro = 0$, PW_1 and G_i are identically zero.

The positive terms in the equation (4.12) contribute to energy production while the negative terms remove energy from the disturbances. A mode is therefore amplified when energy production outweighs the energy dissipation. That is, the instability is occurred when $\bar{\alpha}_i < 0$ from equation (4.12), which is consistent with the definition of instability used to generate the neutral curves in §4.2 and growth rates in §4.3.

The total energy of the system, (the sum of the energy production and the dissipation terms) is very useful to interpret the stability effects of power-law fluids. Increased total energy leads to a destabilising effect on the Type I mode. On the other hand, reduced total energy lead to stabilising effect on the mode.

As discussed previously in §4.3, the maximum growth rate is used here to calculate the energy balance for the flow of BEK family. All calculations within the energy analysis are performed at $R = R_c + 25$. Here R_c is the critical Reynolds number presented in Table 4.1 at the onset of the Type I mode. Again, as predicted by Lingwood and Garrett (2011), it is not possible to find the location of maximum growth rate for $Ro \geq 0.5$ due to the very early onset of absolute instability and associated "branch exchange". Thus, it is impossible to present the energy balance calculations at these positive Ro.

Figure 4.8 presents the energy balance calculations for the dominant Type I mode at $Ro = -1$, -0.5 and 0 for various value of n. It can be seen that there is a stabilising effect on the Type I mode for the von Kármán, Ekman and the flow of $Ro = -0.5$. This is due to decrease in the total energy that comes from the sum of the energy production and the dissipation terms. Furthermore, it is interesting to note that both the Reynolds stress energy production term P_2 and the viscous dissipation energy term D are reduced as n is decreased; this is primary cause of the reduction in total energy. It is interesting to note that non-Newtonian viscosity effects (indicated by N_i) are found to play a negligible role in the generation of the instability. That is, non-Newtonian viscosity acts to modify the steady flow but the stability response to this is predominantly inviscid in nature.
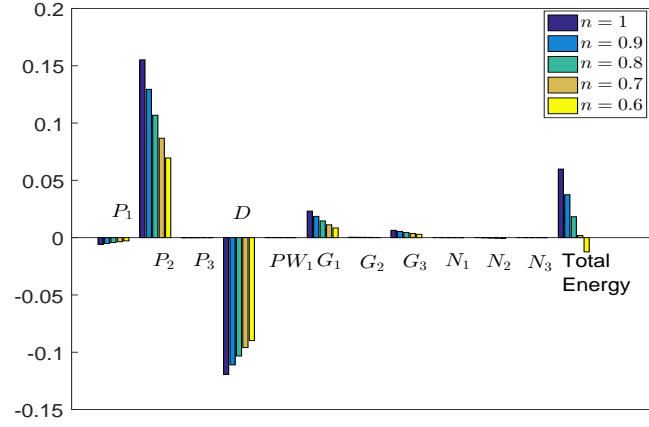
(a) von Kármán, $Ro = -1$
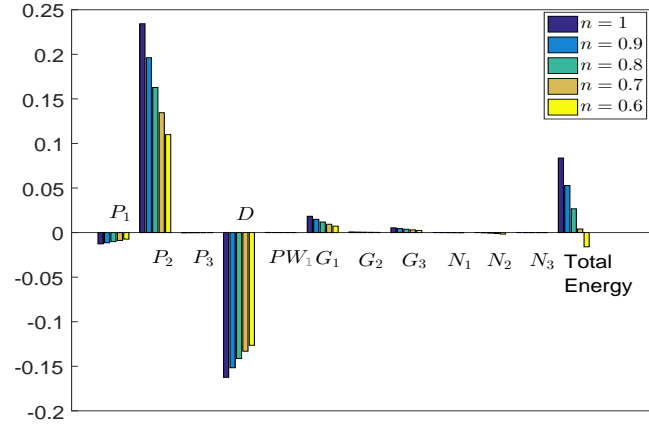
(b) $Ro = -0.5$
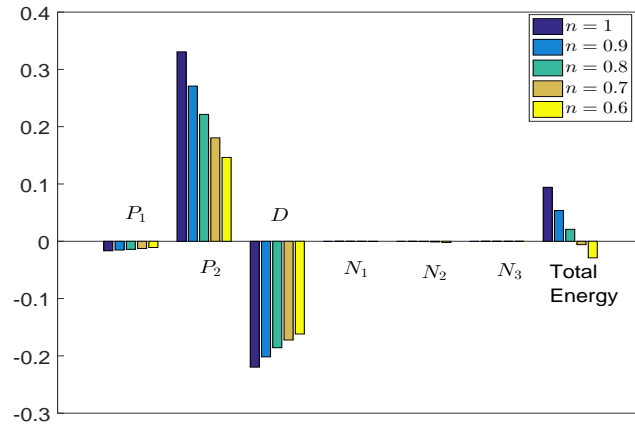
(c) Ekman, $Ro = 0$

Figure 4.8: Type I energy balance at $Re = R_c + 25$ for shear-thinning power-law fluids with $n = 1, 0.9, 0.8, 0.7, 0.6$.

4.5 Conclusion

In this chapter, the stability of stationary convective disturbances in the BEK family of boundary-layer flows has been investigated for shear-thinning power-law fluids. The work of Griffiths et al. (2014a) has been generalised successfully to this broader class of flows and also allowed for a number of mathematical terms that had been previously neglected in that analysis. As with Griffiths' study, the analysis has required the use of the so-called boundary-layer and parallel-flow approximations. Although this may lead to some slight inaccuracies in the qualitative predictions, the use of this approximation is common in the community and is not expected to affect the quantitative conclusions made here.

The newly-derived steady-flow solutions presented in Chapter 3 were perturbed to derive the perturbation equations. Linear stability analysis has been conducted to study the occurrence of convective instability. The governing equations are controlled by the power-law index (defining the extent of shear thinning) and the Rossby number (defining the global rotation rate). The results presented show that shear-thinning power-law fluids are expected to be stabilising for the entire BEK family of flows. In particular, there is a stabilising effect on both the Type I and Type II modes. This is evident through a delayed onset of convective instability to higher Reynolds numbers and also qualitatively 'weaker' modes. Furthermore, the growth rates of Type I instability mode have been considered to find the maximum rates for particular flows in the system.

The results have been confirmed by energy-balance calculations at the maximum growth rates in order to obtain the underlying physical mechanisms behind the stabilising effects. This approach suggests that all physical processes (both energy production and dissipation) are weakened by the introduction of shear-thinning fluids. Furthermore, non-Newtonian viscosity is expected to play very little role in the dominant instability mechanisms. Rather the results suggest that their benefit comes from a modification of the steady flow profiles which, in turn, are more stable to inviscid Type I effects.

With regards to motivating industrial aims in this thesis, the skin-friction drag in enclosed rotor-stator devices can be reduced through the use of shear-thinning lubricants. This would work by delaying laminar-turbulent transition, thereby utilising the lower drag forces arising from laminar flow.

Chapter 5

Convective instabilities for the BEK family of flows for Carreau fluids

In this chapter, the linear perturbation equations relevant to Carreau fluids for the BEK family of flows are formulated in order to study the occurrence of linear convective instability. Again, as mentioned in the previous chapter, the Chebyshev collocation method used by Alveroglu et al. (2016) and Abdulameer et al. (2016) is applied to solve these perturbation equations. The stability neutral curves in this chapter are computed by this numerical method in order to present the properties of convective instability for shear-thinning and shear-thickening Carreau fluids. While the structure of this chapter follows that of Chapter 4, it is important to note that this chapter considers an entirely different model for non-Newtonian viscosity. Significant differences have been found between the two models in the case of the von Kármán flow (Griffiths, 2016) and this motivates its consideration here.

The derivation of the perturbation equations is given in §5.1. The neutral stability curves are presented that based on the solutions of the perturbation equations in §5.2 and §5.3 while the effects of Carreau fluids on the growth rates are described in §5.4. Finally, the results of the energy analysis are presented in §5.5.

5.1   The perturbation equations

The same procedure detailed in §4.1 for the power-law fluids is followed in this section, except now using the viscosity of Carreau fluids (3.11) in the governing boundary-layer equations (3.4). A local linear stability analysis is conducted at a local radius of the disk r_a^* by assuming sufficiently small disturbances on the steady-mean flow at that position.

The local Reynolds number for Carreau fluids is defined by setting $n = 1$ in (4.1) as follows

$$R \;\; = \;\; \frac{r_a^* \triangle \Omega^* L^*}{v^*} = \frac{r_a^* Ro \Omega^* L^*}{v^*} = \frac{r_a^* Ro}{L^*} = r_a Ro. \tag{5.1}$$

This definition of Reynolds number is entirely consistent with the Newtonian formulation of Lingwood (1997). The Reynolds number is negative when the Rossby number is negative, however this is merely a consequence of the formulation and all results will be presented in terms of positive R for all Ro. The local Reynolds number can be interpreted as the non-dimensional location of the local analysis (Lingwood, 1997).

The velocity, pressure and time in the dimensionless form are given by $r_a^* \Omega^* Ro$, $\rho^* r_a^{*2} \Omega^{*2} Ro^2$ and $L^* / (r_a^* \Omega^* Ro)$, respectively. The steady mean flow and small perturbing quantities are indicated by upper-case and lower-case symbols, respectively. The instantaneous dimensionless velocities and pressure of a perturbed flow are defined by setting $n = 1$ in the non-dimensional components (4.2) as follows

$$U_0(z, r, \theta, t) \;\; = \;\; \frac{rRo}{R} U(z) + u(z, r, \theta, t), \tag{5.2a}$$

$$V_0(z, r, \theta, t) \;\; = \;\; \frac{rRo}{R} V(z) + v(z, r, \theta, t), \tag{5.2b}$$

$$W_0(z, r, \theta, t) \;\; = \;\; \frac{Ro}{R} W(z) + w(z, r, \theta, t), \tag{5.2c}$$

$$P_{0,1}(z, r, \theta, t) \;\; = \;\; \frac{Ro^2}{R^2} P(z) + p(z, r, \theta, t). \tag{5.2d}$$

It is noted that the scalings (3.12) and (5.2) are an extension of the exact similarity solution introduced by von Kármán (1921) and Lingwood (1995) for the von Kármán flow. The

scalings (5.2) are consistent with those used in the Newtonian study of the BEK family by Lingwood (1997). When $Ro = -1$, these expressions are consistent with those used by Griffiths (2016). However, Carreau fluids are controlled by two parameters: the power-law index n and relaxation parameter k, these arise from the viscosity function (3.11) and so appear in the perturbation equations.

The non-dimensional Navier-Stokes equations are linearised with respect to the perturbation quantities. The parallel-flow approximation is applied in the same way as Lingwood (1997) to ensure that the linearised equations are separable in r, θ and t. Therefore, variations in the Reynolds number with radius are neglected by replacing the variable r with R/Ro. Furthermore, all $\mathscr{O}((Ro/R)^2)$ terms are also ignored. The derivation of perturbation equations for Carreau fluids is presented in Appendix A. Thus, the linearised disturbance equations take the following form

$$\frac{\partial u}{\partial r} + \frac{Ro}{R}\left(u + \frac{\partial v}{\partial \theta}\right) + \frac{\partial w}{\partial z} = 0, \tag{5.3a}$$

$$\frac{\partial u}{\partial t} + U\frac{\partial u}{\partial r} + \frac{Ro}{R}\left(V\frac{\partial u}{\partial \theta} + W\frac{\partial u}{\partial z} + Uu\right) + U'w - \left(2\frac{Ro}{R}V + \frac{Co}{R}\right)v$$
$$= -\frac{\partial p}{\partial r} + \frac{1}{R}\frac{\partial}{\partial z}\left[\mu\frac{\partial u}{\partial z} + \hat{\mu}\left(U'\frac{\partial u}{\partial z} + V'\frac{\partial v}{\partial z}\right)U'\right], \tag{5.3b}$$

$$\frac{\partial v}{\partial t} + U\frac{\partial v}{\partial r} + \frac{Ro}{R}V\frac{\partial v}{\partial \theta} + \frac{Ro}{R}W\frac{\partial v}{\partial z} + \frac{Ro}{R}Uv + V'w + \left(2\frac{Ro}{R}V + \frac{Co}{R}\right)u$$
$$= -\frac{Ro}{R}\frac{\partial p}{\partial \theta} + \frac{1}{R}\frac{\partial}{\partial z}\left[\mu\frac{\partial v}{\partial z} + \hat{\mu}\left(U'\frac{\partial u}{\partial z} + V'\frac{\partial v}{\partial z}\right)V'\right],$$

$$\frac{\partial w}{\partial t} + U\frac{\partial w}{\partial r} + \frac{Ro}{R}V\frac{\partial w}{\partial \theta} + \frac{Ro}{R}W\frac{\partial w}{\partial z} + \frac{Ro}{R}W'w = -\frac{\partial p}{\partial z} + \frac{1}{R}\frac{\partial}{\partial z}\left(\mu\frac{\partial w}{\partial z}\right), \tag{5.3c}$$

where the viscosity and the disturbance viscosity function of Carreau fluids is given by, re-

spectively

$$\mu = \left\{1+k^2\left[(U')^2+(V')^2\right]\right\}^{(n-1)/2}, \tag{5.3d}$$

$$\hat{\mu} = \frac{k^2(n-1)\mu}{\left\{1+k^2[(U')^2+(V')^2]\right\}}. \tag{5.3e}$$

where n is the power-law index and k is the relaxation parameter.

Following the procedure applied for power-law fluids, the perturbation quantities are assumed to have the normal-mode form

$$u = \hat{u}(z;\alpha,\beta,\omega;R,Ro,k)e^{i(\alpha r+\widetilde{\beta}\theta-\omega t)}, \tag{5.4a}$$

$$v = \hat{v}(z;\alpha,\beta,\omega;R,Ro,k)e^{i(\alpha r+\widetilde{\beta}\theta-\omega t)}, \tag{5.4b}$$

$$w = \hat{w}(z;\alpha,\beta,\omega;R,Ro,k)e^{i(\alpha r+\widetilde{\beta}\theta-\omega t)}, \tag{5.4c}$$

$$p = \hat{p}(z;\alpha,\beta,\omega;R,Ro,k)e^{i(\alpha r+\widetilde{\beta}\theta-\omega t)}. \tag{5.4d}$$

Here $\hat{u},\hat{v},\hat{w}$ and $\hat{p}$ are the spectral representations of the perturbation velocities and pressure, respectively, $\alpha = \alpha_r + i\alpha_i$ and $\widetilde{\beta} = \beta/Ro$ are the complex radial and real azimuthal wave-numbers, and ω is the frequency of the disturbance in the frame rotating with the lower disk. Substituting the normal-mode forms (5.4) into (5.3) gives

$$\left(i\alpha+\frac{Ro}{R}\right)\hat{u}+i\bar{\beta}\hat{v}+\frac{\partial\hat{w}}{\partial z}=0, \tag{5.5a}$$

$$\left[i\left(\alpha U+\bar{\beta}V-\omega\right)+\frac{Ro}{R}U\right]\hat{u}-\left(2\frac{Ro}{R}V+\frac{Co}{R}\right)\hat{v}+\frac{Ro}{R}W\frac{\partial\hat{u}}{\partial z}$$
$$+U'\hat{w}+i\bar{\alpha}\hat{p}-\frac{1}{R}\frac{\partial}{\partial z}\left[\mu\frac{\partial\hat{u}}{\partial z}+\hat{\mu}\left(U'\frac{\partial\hat{u}}{\partial z}+V'\frac{\partial\hat{v}}{\partial z}\right)U'\right]=0, \tag{5.5b}$$

$$\left[i\left(\alpha U+\bar{\beta}V-\omega\right)+\frac{Ro}{R}U\right]\hat{v}+\left(2\frac{Ro}{R}V+\frac{Co}{R}\right)\hat{u}+\frac{Ro}{R}W\frac{\partial\hat{v}}{\partial z}$$

$$+V'\hat{w}+i\bar{\beta}\hat{p}-\frac{1}{R}\frac{\partial}{\partial z}\left[\mu\frac{\partial\hat{v}}{\partial z}+\hat{\mu}\left(U'\frac{\partial\hat{u}}{\partial z}+V\frac{\partial\hat{v}}{\partial z}\right)V'\right]=0, \quad (5.5c)$$

$$\left[i\left(\alpha U+\bar{\beta}V-\omega\right)+\frac{Ro}{R}W\right]\hat{w}+\frac{Ro}{R}W\frac{\partial\hat{w}}{\partial z}+\frac{\partial\hat{p}}{\partial z}-\frac{1}{R}\frac{\partial}{\partial z}\left(\mu\frac{\partial\hat{w}}{\partial z}\right)=0, \quad (5.5d)$$

where $\bar{\beta}=\beta/R$. The neutral wavenumber κ and orientation angle ϕ typically used in asymptotic analyses are then given by

$$\kappa=\sqrt{\alpha^2+\bar{\beta}^2}=\sqrt{\alpha^2+\frac{\beta^2}{r^2}}, \quad (5.6)$$

and

$$\phi=\tan^{-1}\left(\frac{\bar{\beta}}{\alpha}\right)=\frac{\pi}{2}-\tan^{-1}\left(\frac{\alpha r}{\beta}\right). \quad (5.7)$$

It is noted that additional viscous terms $\hat{\mu}U'\left(U'\frac{\partial\hat{u}}{\partial z}+V'\frac{\partial\hat{v}}{\partial z}\right)$ and $\hat{\mu}V'\left(U'\frac{\partial\hat{u}}{\partial z}+V'\frac{\partial\hat{v}}{\partial z}\right)$ appear in the perturbation equations (5.5) which are also neglected in Griffiths (2016). The perturbation equations (5.5) are written as the eigenvalue problem (B.23) by implementing the Chebyshev collocation method. This eigenvalue problem is solved to obtain the solutions of the dispersion relation $D\left(\alpha,\beta,\omega;R,n,Ro,k\right)=0$ with the aim of studying the occurrence of convective instability of Carreau fluids at each parameter set (n,Ro,k). The Chebyshev collocation method is applied by Alveroglu et al. (2016) for Newtonian fluids to study the effects of surface roughness and also in the Chapter 4 of this thesis to determine neutral curves for power-law fluids. The details of this numerical method are explained in Appendix B.

The boundary conditions for perturbation equations (5.5) are given by

$$\hat{u}(z=0)=\hat{v}(z=0)=\hat{w}(z=0)=0, \quad (5.8a)$$

$$\hat{u}\left(z\to z_\infty\right)=\hat{v}\left(z\to z_\infty\right)=\hat{w}\left(z\to z_\infty\right)=0 \quad (5.8b)$$

5.2 Neutral curves for the case $k = 100$

In this section, the neutral curves defined by neutral spatial growth $\alpha_i = 0$ are presented for
$0.6 \le n \le 1.4$ in increments of 0.1 at $Ro = -1, -0.5, 0, 0.5$ and 1 for the case $k = 100$. These
curves have been calculated to determine the convective instability properties of both shear-
thinning and shear-thickening Carreau fluids within the BEK family of flows. All the neutral
curves in this thesis are presented in the R–α_r, R–$\bar{\beta}$, R–κ and R–ϕ planes where α_r and $\bar{\beta}$
denote the real radial and the azimuthal wavenumbers, respectively, κ and ϕ represent the
wavenumber and wave angle defined in (5.6) and (5.7), respectively. Each curve encloses
a region in which the boundary-layer is convectively unstable. Two parameters, n and k,
determine the characteristics of a Carreau fluid. The relaxation parameter is fixed here by
choosing $k = 100$ and varying the power-law index n, and consider the effect of k in section
5.3.

As mentioned in a previous chapter, two instability modes contribute to the neutral curves
for the non-Newtonian system. The upper branch is the Type I mode of instability that is at-
tributed to an inflectional crossflow velocity component, and the smaller lower branch Type II
mode of instability that is attributed to external streamline curvature and other viscous effects.

The two spatial branches in the complex α–plane are presented in Figure 5.1 for the flow
at $Ro = -0.5$ with $k = 100$ for shear-thinning ($n = 0.6$) and shear-thickening ($n = 1.4$) fluids
at the same value of Reynolds number at $R = 235$. A branch region lying below the line
$\alpha_i = 0$ determines the convective instability. The region of convective instability is indicated
by branch 1 for both shear-thinning and shear-thickening fluids. Figure 5.1(a) shows that
branch 2 crosses the line $\alpha_i = 0$, mapping out the Type II mode in the case of $n = 0.6$. However,
the Type II mode does not appear in the neutral curves for shear-thickening fluids because the
branch 2 has not crossed the line $\alpha_i = 0$, as shown in Figure 5.1(b). Moreover, the regions of
convective instability determined by both branch 1 and branch 2 are extended by increasing
the value of R.
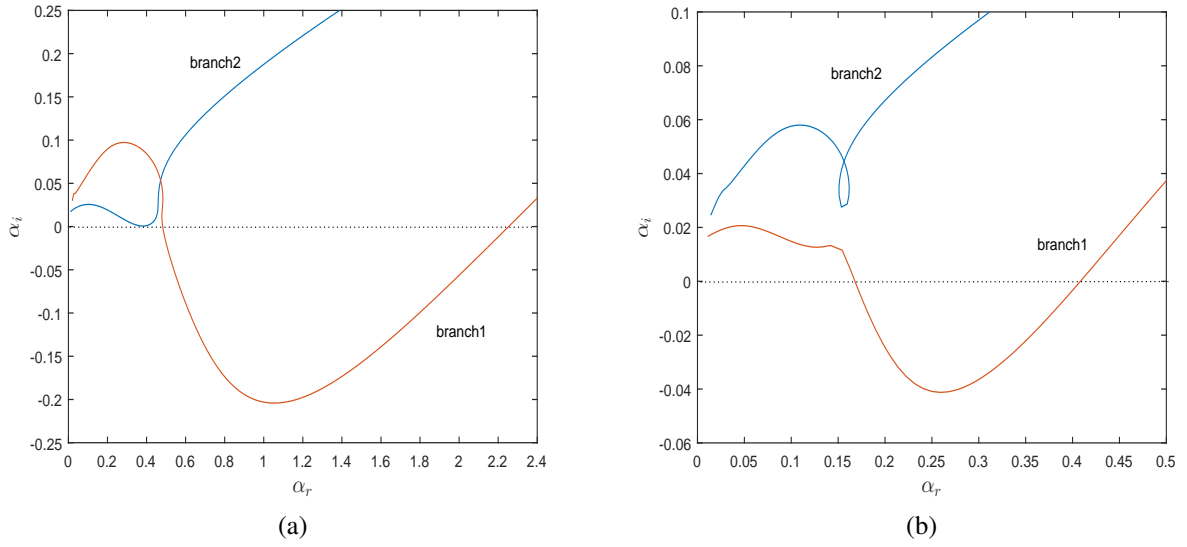
Figure 5.1: The two spatial branches for the flow at $Ro = -0.5$ with $k = 100$ showing Type I instability at $R = 235$ for; (a) shear-thinning, $n = 0.6$ and (b) shear- thickening, $n = 1.4$.

The neutral curves of the von Kármán flow, $Ro = -1$ for both shear-thinning and shear-thickening Carreau fluids with $k = 100$ are presented here in Figures 5.2-5.3. The neutral curves for other related flows of BEK family are shown in Appendix C.

Figure 5.2 shows that shear-thinning fluids for the von Kármán flow with $k = 100$ have a slight destabilising effect on both the Type I and Type II modes in terms of the critical Reynolds number. It is noted that the size of Type II mode is increased as n is reduced. Furthermore, a strong destabilising effect has been observed in terms of the region of instability from the upper branch. The other related flows of BEK family for shear thinning fluids have found to display the same behaviour in terms of the critical Reynolds number for Type I mode and the region of instability from the upper branch.

On the other hand, Figure 5.3 shows that shear-thickening fluids with $k = 100$ for the von Kármán flow have a small stabilising effect on both Type I and Type II modes in terms of the critical Reynolds number. However, the convectively unstable region is strongly reduced from the upper branch of the neutral curve. The same behaviour has been noticed for other related flows of BEK family in terms of the critical Reynolds number at the onset of Type I mode and
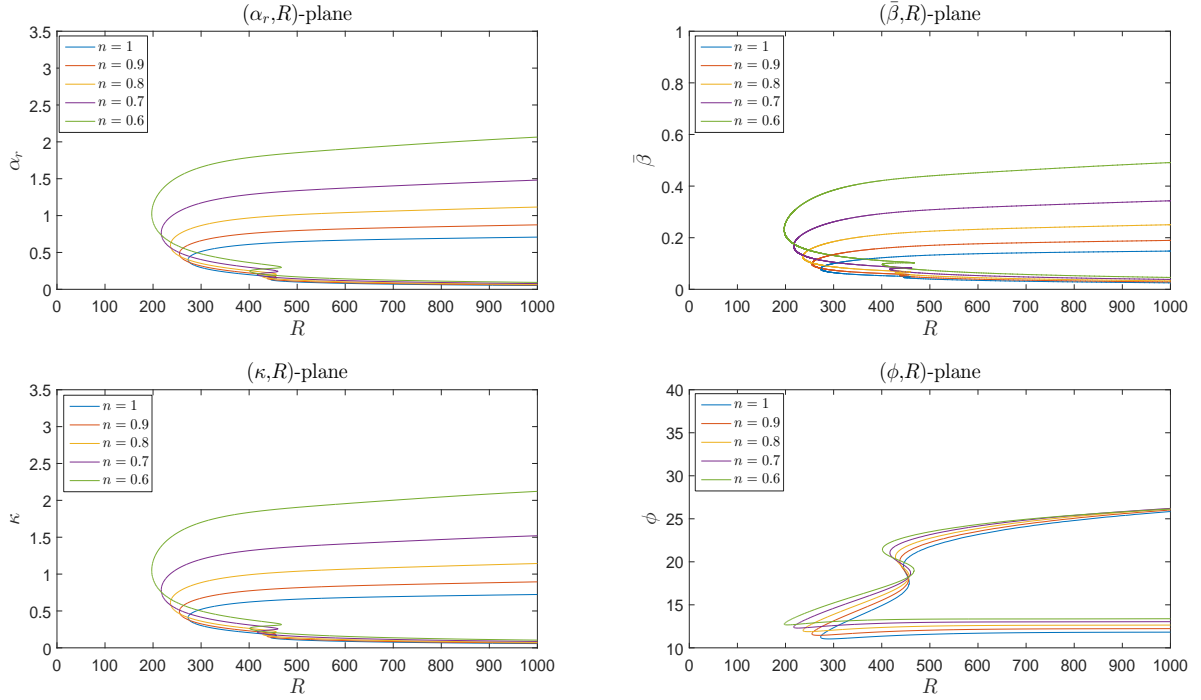
Figure 5.2: Neutral curves of the von Kármán flow, $Ro = -1$ for shear-thinning Carreau fluids with $n = 1, 0.9, 0.8, 0.7, 0.6$ and $k = 100$.

the region of instability from the upper branch. Moreover, it has been seen that the Type II mode does not appear for flows with $Ro \geq -0.5$.

It is interesting to note that there is a remarkable difference between equivalent results of shear-thinning power-law and Carreau fluids in terms of their convective instability characteristics. The neutral curves reveal that the unstable region is increased for Carreau fluids as n is reduced for $k = 100$. In other words, shear-thinning Carreau fluids have a destabilising effect on both the dominant Type I mode and distinct Type II mode for all value of Ro by setting the parameter $k = 100$.

The findings in this thesis regarding the differences between the two non-Newtonian models across all Ro are consistent with those of Griffiths (2016) in the limiting case of $Ro = -1$. However, it is noted that where comparisons can be made between the Carreau studies at $Ro = -1$, there is a difference in the values of critical Reynolds numbers for both Type I
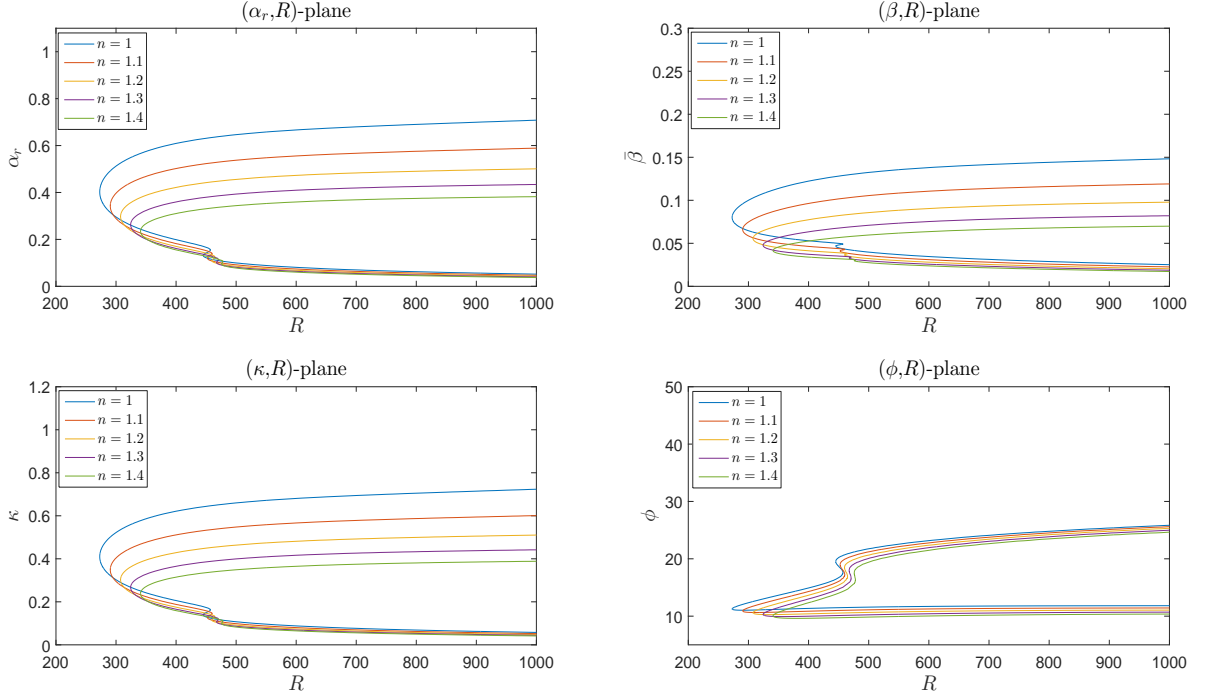
Figure 5.3: Neutral curves of the von Kármán flow, $Ro = -1$ for shear-thickening Carreau fluids with $n = 1, 1.1, 1.2, 1.3, 1.4$ and $k = 100$.

and Type II modes and in the instability region form the upper branch. This is due to using the viscosity function (2.24) scaled by $\bar{\mu}_0^*$ in the perturbation equations (5.5) while Griffiths (2016) used the viscosity function (2.23) scaled by $\bar{\mu}_\infty^*$ in the perturbation equations. This scaling leads to some deviation from the neutral curve of Newtonian fluids. Furthermore, the additional viscous terms $\hat{\mu}U'\left(U'\frac{\partial \hat{u}}{\partial z} + V'\frac{\partial \hat{v}}{\partial z}\right)$ and $\hat{\mu}V'\left(U'\frac{\partial \hat{u}}{\partial z} + V'\frac{\partial \hat{v}}{\partial z}\right)$ are included in the perturbation equations (5.5) as the same as power-law fluids whilst these terms are removed in Griffiths (2016). Tables 5.1-5.2 show the values of critical Reynolds numbers for the onset of Type I and Type II mode for shear-thinning and shear-thickening Carreau fluids, respectively.

The relaxation parameter k in the viscosity function of Carreau fluids has also been investigated. This parameter is found to play a significant role in the stability characteristics of the flow to the extent that the value of k can determine whether Carreau fluids have a stabilising or destabilising effect on the Type I and Type II modes. Therefore, the variation of the critical

n	R	α	$\bar{\beta}$	κ	ϕ
1	272.90(445.21)	0.4029(0.1319)	0.0802(0.0467)	0.4108(0.1400)	11.26(19.48)
0.9	254.86(437.51)	0.4853(0.1479)	0.0999(0.0539)	0.4954(0.1574)	11.63(20.04)
0.8	236.27(428.50)	0.5988(0.1698)	0.1276(0.0637)	0.6123(0.1813)	12.03(20.55)
0.7	217.08(416.98)	0.7676(0.2005)	0.1690(0.0771)	0.7860(0.2148)	12.41(21.03)
0.6	197.31(401.39)	1.0300(0.2457)	0.2332(0.0964)	1.0561(0.2639)	12.76(21.42)

(a) von Kármán, $Ro = -1$

n	R	α	$\bar{\beta}$	κ	ϕ
1	149.74(-)	0.5098(-)	0.1237(-)	0.5246(-)	13.64(-)
0.9	142.19(-)	0.6128(-)	0.1517(-)	0.6313(-)	13.90(-)
0.8	134.10(-)	0.7565(-)	0.1913(-)	0.7803(-)	14.19(-)
0.7	125.39(-)	0.9729(-)	0.2511(-)	1.0048(-)	14.47(-)
0.6	116.09(234.89)	1.3175(0.3823)	0.3463(0.1696)	1.3622(0.4182)	14.73 (23.92)

(b) $Ro = -0.5$

n	R	α	$\bar{\beta}$	κ	ϕ
1	105.88(-)	0.5805(-)	0.1444(-)	0.5982(-)	13.97(-)
0.9	100.08(-)	0.6980(-)	0.1768(-)	0.7200(-)	14.21(-)
0.8	94.43(-)	0.8623(-)	0.2230(-)	0.8907(-)	14.50(-)
0.7	88.84(-)	1.1084(-)	0.2926(-)	1.1464(-)	14.79(-)
0.6	83.20(-)	1.4736(-)	0.3980(-)	1.5550(-)	15.07(-)

(c) Ekman, $Ro = 0$

n	R	α	$\bar{\beta}$	κ	ϕ
1	67.21(-)	0.5861(-)	0.1455(-)	0.6039(-)	13.94(-)
0.9	63.14(-)	0.7037(-)	0.1782(-)	0.7259(-)	14.21(-)
0.8	59.59(-)	0.8679(-)	0.2246(-)	0.8964(-)	14.51(-)
0.7	56.53(-)	1.0815(-)	0.2887(-)	1.1194(-)	14.95(-)
0.6	53.90(-)	1.4312(-)	0.3918(-)	1.4839(-)	15.31(-)

(d) $Ro = 0.5$

n	R	α	$\bar{\beta}$	κ	ϕ
1	22.40(-)	0.5404(-)	0.1185(-)	0.5532(-)	12.37(-)
0.9	20.36(-)	0.6499(-)	0.1481(-)	0.6666(-)	12.84(-)
0.8	18.68(-)	0.8099(-)	0.1900(-)	0.8319(-)	13.20(-)
0.7	20.65 (-)	1.0301(-)	0.2529 (-)	1.0607 (-)	13.80 (-)
0.6	16.81(-)	1.2700(-)	0.3296(-)	1.3121(-)	14.55(-)

(e) Bödewadt, $Ro = 1$

Table 5.1: The values of the critical Reynolds number R, wave numbers α, β, κ and wave angle ϕ shear-thinning Carreau fluids with $k = 100$ at various Ro on the both modes Type I and (Type II).

n	R	α	$\bar{\beta}$	κ	ϕ
1	272.90(445.21)	0.4029(0.1319)	0.0802(0.0467)	0.4108(0.1399)	11.26(19.48)
1.1	290.44(452.44)	0.3428(0.1191)	0.0661(0.0410)	0.3491(0.1259)	10.91(18.98)
1.2	307.58(459.77)	0.2984(0.1096)	0.0558(0.0365)	0.3036(0.1155)	10.59(18.44)
1.3	324.36(467.53)	0.2633(0.1013)	0.0479(0.0329)	0.2676(0.1065)	10.30(17.98)
1.4	340.85(475.91)	0.2354(0.0955)	0.0417(0.0300)	0.2390(0.1001)	10.05(17.43)

(a) von Kármán, $Ro = -1$

n	R	α	$\bar{\beta}$	κ	ϕ
1	149.74(-)	0.5098(-)	0.1237(-)	0.5246(-)	13.64(-)
1.1	156.88(-)	0.4342(-)	0.1035(-)	0.4464(-)	13.41(-)
1.2	163.77(-)	0.3785(-)	0.0887(-)	0.3888(-)	13.19(-)
1.3	170.56(-)	0.3336(-)	0.0772(-)	0.3424(-)	13.03(-)
1.4	177.41(-)	0.2997(-)	0.0684(-)	0.3074(-)	12.86(-)

(b) $Ro = -0.5$

n	R	α	$\bar{\beta}$	κ	ϕ
1	105.88(-)	0.5805(-)	0.1444(-)	0.5981 (-)	13.97(-)
1.1	111.94(-)	0.4930(-)	0.1207(-)	0.5075 (-)	13.76(-)
1.2	118.32(-)	0.4272(-)	0.1031(-)	0.4395 (-)	13.56 (-)
1.3	125.05(-)	0.3744(-)	0.0893(-)	0.3849 (-)	13.42 (-)
1.4	132.15(-)	0.3326(-)	0.0785(-)	0.3418 (-)	13.29 (-)

(c) Ekman, $Ro = 0$

n	R	α	$\bar{\beta}$	κ	ϕ
1	67.21(-)	0.5861(-)	0.1455(-)	0.6039 (-)	13.94 (-)
1.1	71.76(-)	0.4960(-)	0.1211(-)	0.5105(-)	13.72 (-)
1.2	76.77(-)	0.4268(-)	0.1026(-)	0.4390 (-)	13.52(-)
1.3	82.17(-)	0.3737(-)	0.0884(-)	0.3840 (-)	13.30 (-)
1.4	87.90(-)	0.3297(-)	0.0769(-)	0.3385 (-)	13.14 (-)

(d) $Ro = 0.5$

n	R	α	$\bar{\beta}$	κ	ϕ
1	22.40(-)	0.5404(-)	0.1185(-)	0.5532 (-)	12.37 (-)
1.1	24.82 (-)	0.4579(-)	0.0965(-)	0.4680(-)	11.90 (-)
1.2	27.55 (-)	0.4114(-)	0.0800(-)	0.4191(-)	11.01(-)
1.3	36.5 (-)	0.4129(-)	0.0700(-)	0.4188(-)	9.63(-)
1.4	34.5 (-)	0.3144(-)	0.0555(-)	0.3192(-)	10.01(-)

(e) Bödewadt, $Ro = 1$

Table 5.2: The values of the critical Reynolds number R, wave numbers α, β, κ and wave angle ϕ for shear-thickening Carreau fluids with $k = 100$ at various Ro on the both modes Type I and (Type II).

Reynolds numbers with the parameter k is required to identify the optimal value of k denoted in this thesis by ko. This optimization is also important to enable a comparison of equivalent results between the power-law and Carreau models. The neutral curves for the parameter ko will be considered in the following section.

5.3 Neutral curves for the case $k = ko$

In this section, the neutral curves for $0.6 \leq n \leq 1.4$ in increments of 0.1 at $Ro = -1, -0.5, 0, 0.5$ are presented for the case $k = ko$. As discussed in the previous section, the variation of critical Reynolds numbers with the parameter k is necessary in order to select the optimal values of $k = ko$ for each value of n and Ro. Figures 5.4 and 5.5 present the critical Reynolds numbers versus the parameter k for both shear-thinning and shear-thickening Carreau fluids, respectively. These figures are plotted by firstly calculating the steady mean flow velocities in the range $[0, 100]$ of the parameter k, and then solving the perturbation equations in order to determine the critical Reynolds number in $k \in [0, 100]$. The variation in R_c versus k for the Rossby number $Ro = 1$ are not performed here due to inconsistency of the numerical code calculated mean flow velocities for all k. The steady mean flow profiles of shear-thinning and shear-thickening Carreau fluids with $k = ko$ are presented in Appendix C. Furthermore, the numerical values of these mean flow parameters $U'(0)$, $V'(0)$ and $W(z_\infty)$ calculated at the optimal value ko for each n and Ro are also reported in Tables C.1-C.2 in Appendix C. It has been noticed from these tables that the optimal values of relaxation parameter ko for each Ro are approximately close to each other for all n where the values are between $6.42 < ko < 6.16$ and $5.17 < ko < 4.82$ for von Kármán and Ekman flows, respectively.

(a) von Kármán, $Ro = -1$

(b) $Ro = -0.5$

(c) Ekman, $Ro = 0$

(d) $Ro = 0.5$
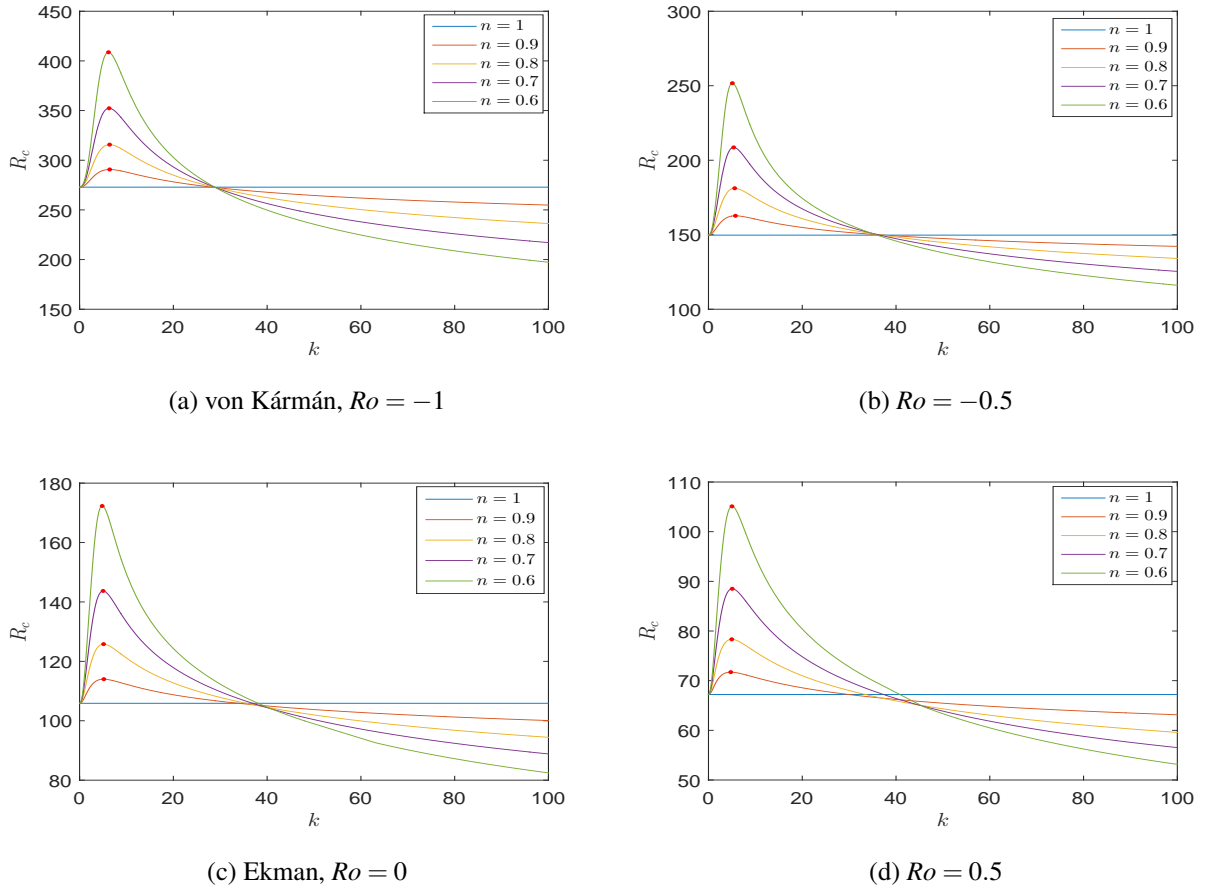
Figure 5.4: Variation in the critical Reynolds number R_c with the relaxation parameter k for shear-thinning Carreau fluids.

Figure 5.4 reveals that the critical Reynolds numbers for shear-thinning Carreau fluids sharply increase with k until reaching a maximum value for all $n < 1$ and Ro, and then there is a gradual drop passing the critical Reynolds number for Newtonian fluid ($R = 272.90$). The optimal values of the parameter k are selected at the maximum value of R_c indicated by the red dots in the Figure 5.4. This selection is to ensure that shear-thinning Carreau fluids have a maximum stabilising effect on both Type I and Type II modes. In contrast, Figure 5.5 shows that the critical Reynolds numbers for shear-thickening Carreau fluids are markedly decreased approaching its minimum value for each $n > 1$ and Ro followed by regular rise until $k = 100$. The minimum values of R_c are identified as the "optimal" values of the parameter k denoted by

(a) von Kármán, $Ro = -1$ (b) $Ro = -0.5$

(c) Ekman, $Ro = 0$ (d) $Ro = 0.5$
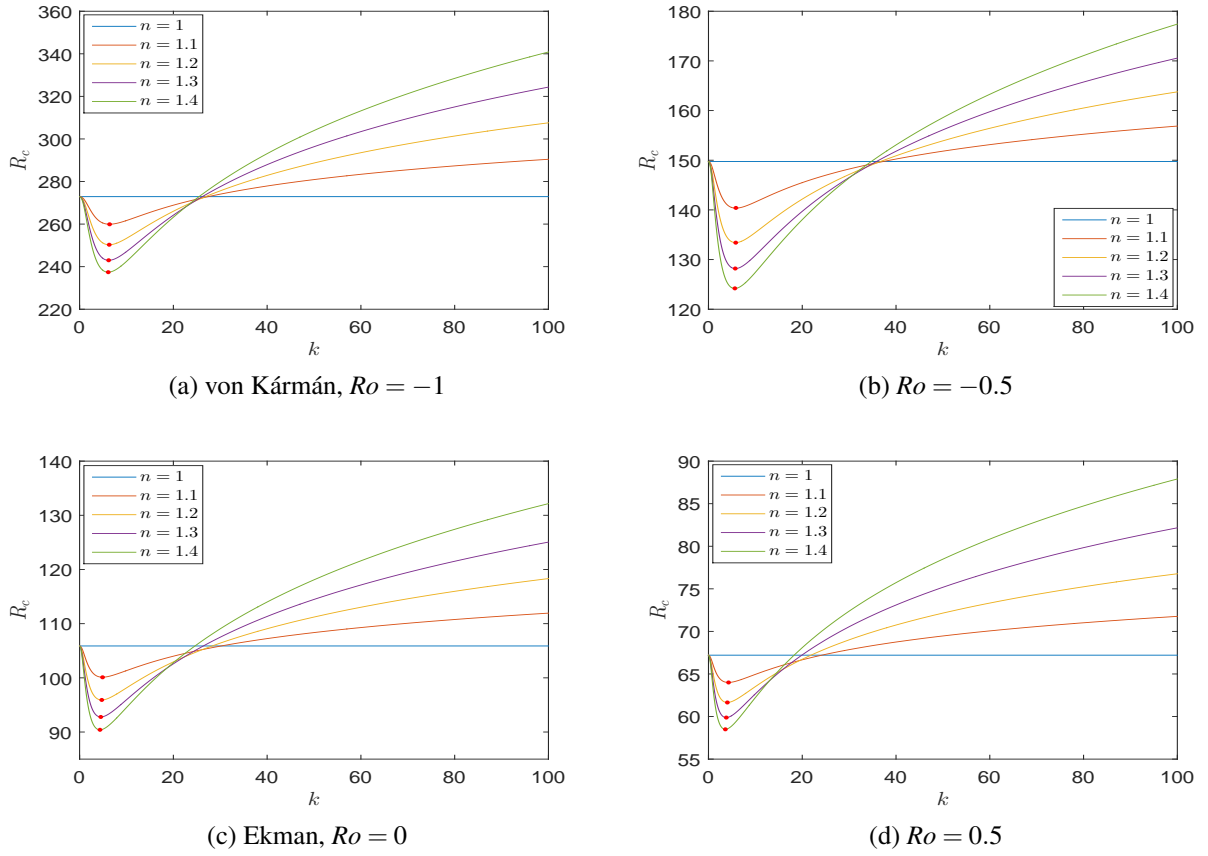
Figure 5.5: Variation in the critical Reynolds number R_c with the relaxation parameter k for shear-thickening Carreau fluids.

the red dots to ensure that the shear-thickening Carreau fluids have the maximum destabilising effect on both Type I and Type II modes.

Figure 5.6 shows the two spatial branches in the complex α–plane for the flow of $Ro = -0.5$ with $k = ko$ for a shear-thinning fluid ($n = 0.6$) at $R = 523$ and a shear-thickening fluid ($n = 1.4$) at $R = 224$. The convective instability is determined by a branch region lying below the line $\alpha_i = 0$. The branch 1 indicates the region of convective instability for both shear-thinning and shear-thickening fluids. It has been seen that branch 2 started to pass the line $\alpha_i = 0$ to produce the Type II lobe as shown in Figure 5.6(a). However, the branch 2 in Figure 5.6(b) is far away from the line. Thus, the Type II lobe does not exist in the neutral curve. The regions of convective instability determined by both branch 1 and branch 2 are extended by
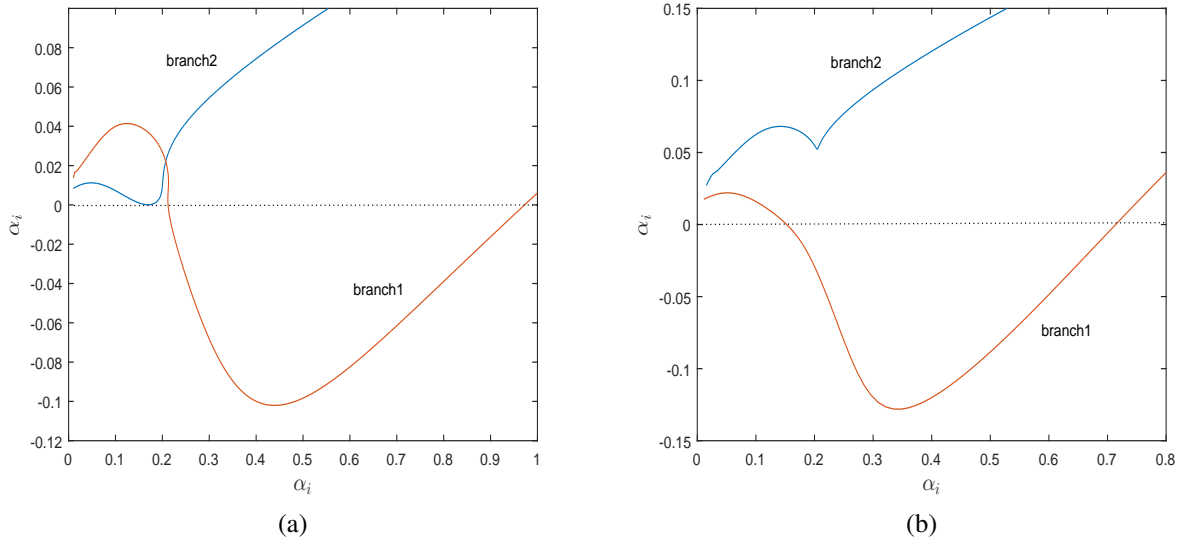
Figure 5.6: The two spatial branches for the flow at $Ro = -0.5$ with $k = ko$ showing Type I instability for; (a) shear-thinning and $n = 0.6$ at $R = 523$, (b) shear- thickening, $n = 1.4$ at $R = 224$.

increasing the value of R.

The neutral curves of the von Kármán flow, $Ro = -1$ for both shear-thinning and shear-thickening Carreau fluids with $k = ko$ are revealed here in Figures 5.7 and 5.8. All other neutral curves for related flows of BEK family are presented in Appendix C.

Figure 5.7 shows that shear-thinning Carreau fluids for the von Kármán flow with $k = ko$ have a stabilising effect on both the Type I and Type II modes in terms of the critical Reynolds number. However, it is noted that there is a slight destabilising effect in terms of the region of instability from the upper branch. Furthermore, it is found that the Type II mode is expanded as n is decreased which is similar to the effect of the shear-thinning power-law fluids. The same stability behaviour of the von Kármán flow has been observed for other related flows of BEK family in terms of the critical Reynolds number, the region of instability and the growth of Type II mode. Furthermore, it is interesting to note that the growth of the distinct Type II mode is gradually increased as n is reduced.
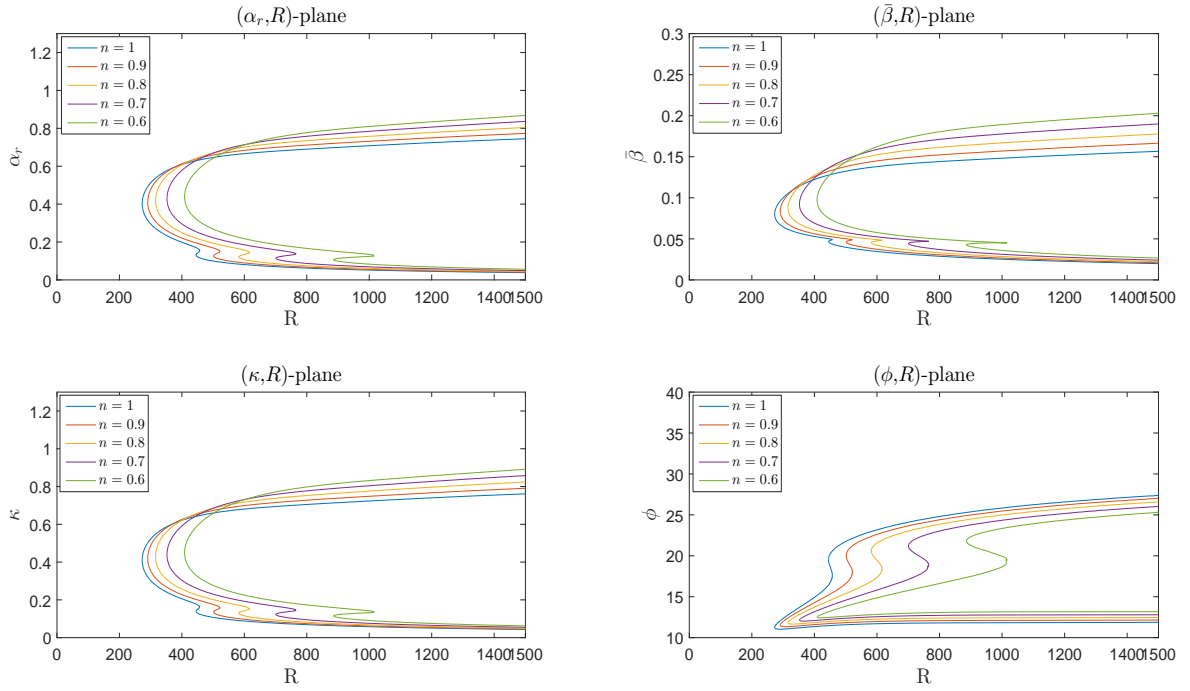
Figure 5.7: Neutral curves of the von Kármán flow, $Ro = -1$ for shear-thinning Carreau fluids with $n = 1, 0.9, 0.8, 0.7, 0.6$ and $k = ko$.

On the other hand, Figure 5.8 shows that shear-thickening Carreau fluids for the von Kármán flow with $k = ko$ have a slight destabilising effect on both the Type I and Type II modes in terms of the critical Reynolds number. Nevertheless, a small stabilising effect is observed in terms of the region of instability from the upper branch. Moreover, very slight promotion has been accrued on the Type II mode as n increased. All other related flows of BEK family for shear-thickening fluids have the same stability behaviour of the von Kármán flow in terms of the critical Reynolds number for Type I mode and the region of instability from the upper branch. However, the Type II mode for the related flows of $Ro \geq -0.5$ does not appear obviously. The critical Reynolds numbers of shear-thinning and shear-thickening for the onset of both modes are reported in Tables 5.3-5.4, respectively.

Returning back to the variation of R_c versus k, it is clear that the Non-Newtonian Carreau fluids have Newtonian critical Reynolds number R_c^N for particular values of relaxation

n	R	α	$\bar{\beta}$	κ	ϕ
1	272.90(445.21)	0.4029(0.1319)	0.0802(0.0467)	0.4108(0.1400)	11.26(19.48)
0.9	290.66(501.72)	0.4118(0.1268)	0.0839(0.0462)	0.4203(0.1349)	11.51(20.02)
0.8	315.68(581.97)	0.4209(0.1212)	0.0880(0.0455)	0.4300(0.1295)	11.81(20.57)
0.7	352.29(700.81)	0.4307(0.1145)	0.0926(0.0443)	0.4405(0.1227)	12.14(21.18)
0.6	408.66(885.98)	0.4396(0.1068)	0.0975(0.0427)	0.4503(0.1150)	12.51(21.79)

(a) von Kármán, $Ro = -1$

n	R	α	$\bar{\beta}$	κ	ϕ
1	149.74(-)	0.5098(-)	0.1237(-)	0.5246(-)	13.64(-)
0.9	162.70(-)	0.5201(-)	0.1281(-)	0.5356(-)	13.83(-)
0.8	181.18(-)	0.5325(-)	0.1332(-)	0.5489(-)	14.05(-)
0.7	208.62(-)	0.5423(-)	0.1384(-)	0.5597(-)	14.31(-)
0.6	251.74(522.34)	0.5495(0.1695)	0.1432(0.0765)	0.5679(0.1860)	14.61(24.28)

(b) $Ro = -0.5$

n	R	α	$\bar{\beta}$	κ	ϕ
1	105.88(-)	0.5805(-)	0.1444(-)	0.5982(-)	13.97(-)
0.9	114.00(-)	0.5948(-)	0.1496(-)	0.6134(-)	14.12(-)
0.8	125.80(-)	0.6114(-)	0.1558(-)	0.6310(-)	14.29(-)
0.7	143.68(-)	0.6279(-)	0.1625(-)	0.6485(-)	14.51(-)
0.6	172.34(335.55)	0.6417(0.2235)	0.1693(0.1011)	0.6637(0.2453)	14.78(24.33)

(c) Ekman, $Ro = 0$

n	R	α	$\bar{\beta}$	κ	ϕ
1	67.21(-)	0.5861(-)	0.1455(-)	0.6039(-)	13.94(-)
0.9	71.72(-)	0.6028(-)	0.1512	0.6215(-)	14.09(-)
0.8	78.33(-)	0.6203(-)	0.1580(-)	0.6401(-)	14.29(-)
0.7	88.50(-)	0.6403(-)	0.1659(-)	0.6615(-)	14.52(-)
0.6	105.12(-)	0.6602(-)	0.1744(-)	0.6828(-)	14.80(-)

(d) $Ro = 0.5$

Table 5.3: The values of the critical Reynolds number R, wave numbers α, β and κ and wave angle ϕ for shear-thinning Carreau fluids with $k = ko$ at various Ro on the both modes Type I and (Type II).

n	R	α	$\bar{\beta}$	κ	ϕ
1	272.90(445.21)	0.4029(0.1319)	0.0802(0.0467)	0.4108(0.1400)	11.26(19.48)
1.1	259.94(404.14)	0.3955(0.1359)	0.0771(0.0469)	0.4030(0.1437)	11.03(19.03)
1.2	250.28(373.52)	0.3886(0.13912)	0.0744(0.0469)	0.3957(0.1468)	10.8347(18.64)
1.3	242.99(350.24)	0.3831(0.1423)	0.0721(0.0470)	0.3898(0.1499)	10.6654(18.27)
1.4	237.41(332.22)	0.3768(0.1442)	0.0700(0.0468)	0.3833(0.1516)	10.5246(17.99)

(a) von Kármán, $Ro = -1$

n	R	α	$\bar{\beta}$	κ	ϕ
1	149.74(-)	0.5098(-)	0.1237(-)	0.5246(-)	13.64(-)
1.1	140.36(-)	0.4986(-)	0.1197(-)	0.5128(-)	13.49(-)
1.2	133.41(-)	0.4888(-)	0.1162(-)	0.5024(-)	13.37(-)
1.3	128.18(-)	0.4788(-)	0.1131(-)	0.4920(-)	13.29(-)
1.4	124.18(-)	0.4715(-)	0.1106(-)	0.4843(-)	13.20(-)

(b) $Ro = -0.5$

n	R	α	$\bar{\beta}$	κ	ϕ
1	105.88(-)	0.5805(-)	0.1444(-)	0.5982(-)	13.97(-)
1.1	100.12(-)	0.5666(-)	0.1398(-)	0.5836(-)	13.86(-)
1.2	95.92(-)	0.5538(-)	0.1359(-)	0.5702(-)	13.79(-)
1.3	92.78(-)	0.5437(-)	0.1328(-)	0.5597(-)	13.73(-)
1.4	90.41(-)	0.5362(-)	0.1304(-)	0.5518(-)	13.67(-)

(c) Ekman, $Ro = 0$

n	R	α	$\bar{\beta}$	κ	ϕ
1	67.21(-)	0.5861(-)	0.1455(-)	0.6039(-)	13.94(-)
1.1	64.00(-)	0.5713(-)	0.1406(-)	0.5884(-)	13.83(-)
1.2	61.65(-)	0.5598(-)	0.1367(-)	0.5762(-)	13.73(-)
1.3	59.88(-)	0.5507(-)	0.1336(-)	0.5667(-)	13.64(-)
1.4	58.50(-)	0.5424(-)	0.1310(-)	0.5580(-)	13.57(-)

(d) $Ro = 0.5$

Table 5.4: The values of the critical Reynolds number R, wave numbers α, β and κ and wave angle ϕ for shear-thickening Carreau fluids with $k = ko$ at various Ro on the both modes Type I and (Type II).

Figure 5.8: Neutral curves of the von Kármán flow, $Ro = -1$ for shear-thickening Carreau fluids with $n = 1, 1.1, 1.2, 1.3, 1.4$ and $k = ko$.

parameter k for each $0.6 < n < 1.4$ as shown in Figures 5.4-5.5. The neutral curves of shear-thinning and shear-thickening Carreau fluids are presented for the von Kármán flow, $Ro = -1$ that have $R_c^N = 272.90$ for each n. It is observed that the shear-thinning Carreau fluids have a slight stabilising effect on the Type II mode that is promoted as n is decreased; this is in contrast to shear-thickening Carreau fluids that have a destabilising effect on this mode as presented in Figures 5.9-5.10. Furthermore, a stark destabilising effect has been noticed for shear thinning fluids such that the instability region is expanded via the upper branch as n is reduced, while shear-thickening fluids are observed to have a strong stabilising effects on this region. The critical Reynolds numbers at the onset of Type II mode for both shear-thinning and shear-thickening fluids that have $R_c^N = 272.90$ at the onset of Type I mode for the Kármán flow, $Ro = -1$ are reported in Table 5.5.

Figure 5.9: Neutral curves of the von Kármán flow, $Ro = -1$ for shear-thinning Carreau fluids with $n = 1, 0.9, 0.8, 0.7, 0.6$ and $R_c^N = 272.90$ at the onset of Type I mode.
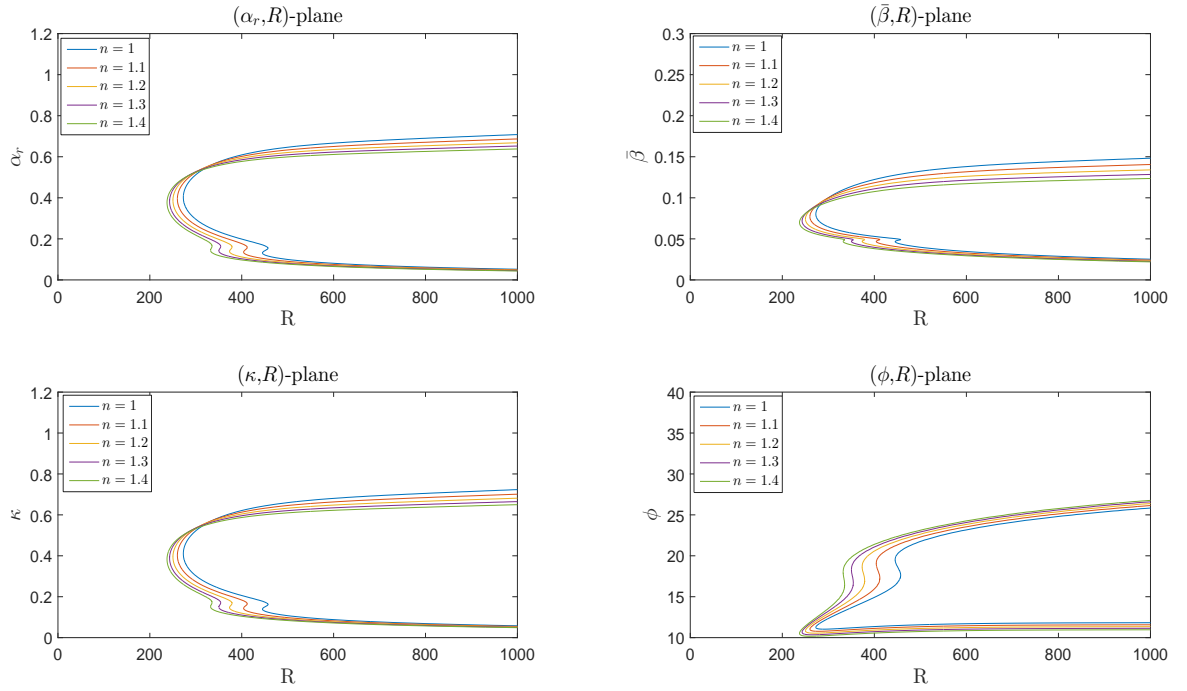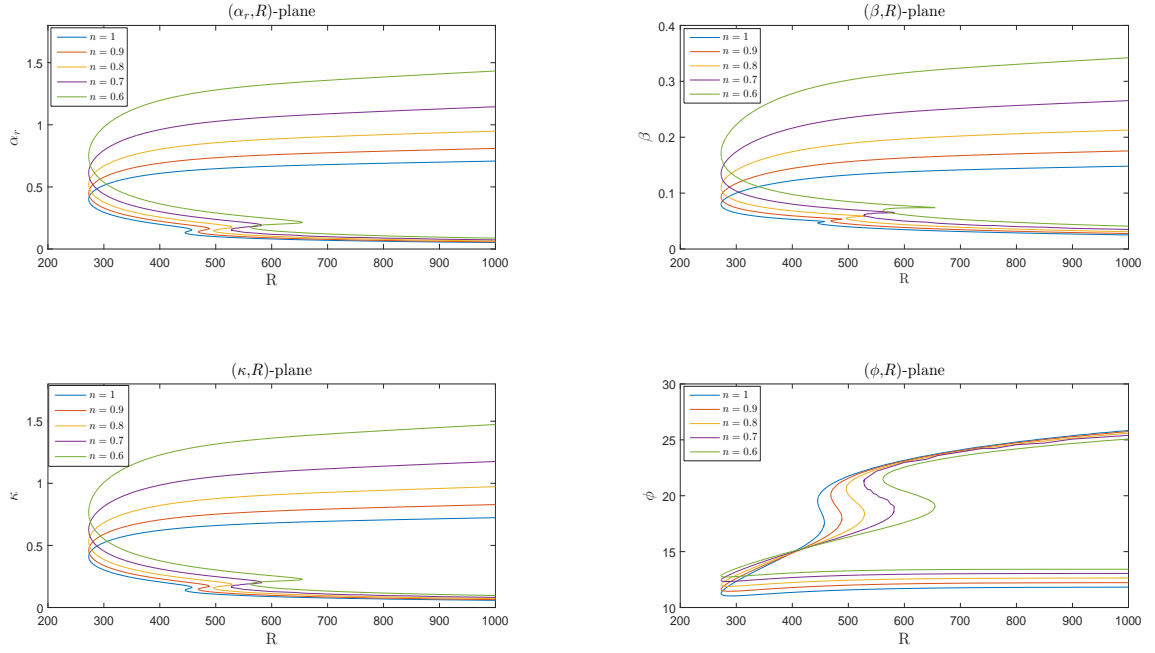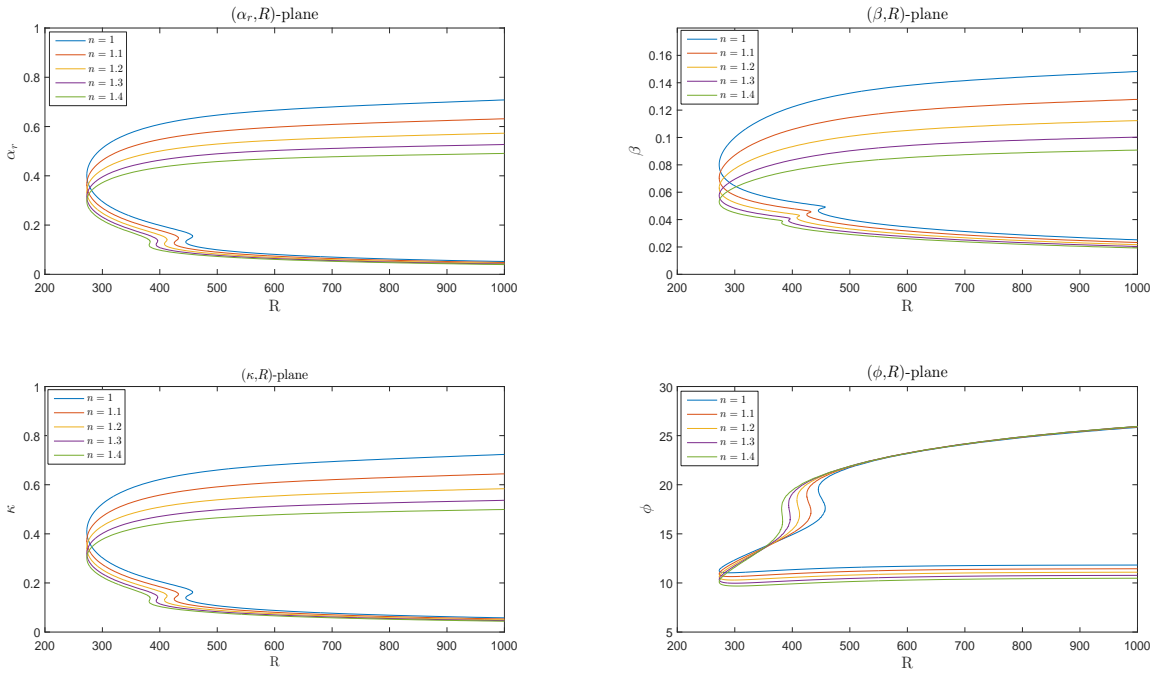

Figure 5.10: Neutral curves of the von Kármán flow, $Ro = -1$ for shear-thickening Carreau fluids with $n = 1, 1.1, 1.2, 1.3, 1.4$ and $R_c^N = 272.90$ at the onset of Type I mode.

n	R	α	$\bar{\beta}$	κ	ϕ	k
1	445.21	0.1319	0.0467	0.1400	19.48	-
0.9	468.81	0.1379	0.0503	0.1468	20.04	28.4
0.8	496.28	0.1463	0.0549	0.1562	20.5879	28.6
0.7	527.60	0.1539	0.0600	0.1651	21.3046	28.8
0.6	561.80	0.1762	0.0693	0.1893	21.4875	28.8

(a) Shear-thinning fluids

n	R	α	$\bar{\beta}$	κ	ϕ	k
1	445.21	0.1319	0.0467	0.1400	19.48	-
1.1	425.11	0.1270	0.0437	0.1343	18.9805	27.4
1.2	408.08	0.1240	0.0413	0.1308	18.4317	26.8
1.3	393.65	0.1213	0.0393	0.1276	17.9669	26.2
1.4	381.42	0.1192	0.0377	0.1250	17.5445	25.5

(b) Shear-thickening fluids

Table 5.5: The values of the critical Reynolds number of Type II mode R, wave numbers α, β, κ, wave angle ϕ and relaxation parameter k that have $R_c^N = 272.90$ for each n at the onset of Type I mode for the von Kármán flow, $Ro = -1$.

5.4   Growth rates

In this section, the growth rates of the Type I instability mode are presented for the BEK family of shear-thinning and shear-thickening Carreau fluids for both cases $k = 100$ and $k = ko$. The growth rates of the Type I instability mode are plotted as a variation of the absolute value of the imaginary part of the negative radial wavenumber, $|\alpha_i|$, at particular values of number of spiral vortices $\bar{n}$. The growth rates of the secondary Type II mode are not involved here, due to their very small value as compared to the dominant Type I mode and also because Carreau fluids have only a slight effect on the Type II mode.

For the case $k = 100$, Figures 5.11-5.12 present the convective growth rates of the dominant Type I mode at $R = R_c + 25$ against $\bar{n}$ at $Ro = -1$, -0.5 and 0 for shear-thinning and shear-thickening fluids, respectively. Here $\bar{n} = \bar{\beta} R$ is the number of spiral vortices around the disk surface, and R_c denotes the critical Reynolds number reported in Tables 5.1-5.2 for the onset of the Type I mode for the particular n and Ro.

Figure 5.11 shows a destabilising effect on the growth rates of the Type I mode and the

maximum values identified by red dotes are pushed to higher values of $\bar{n}$ for each shear-thinning flow as n is decreased. However, shear-thickening fluids have a stabilising effect on the growth rates of the Type mode I and the maximum values shift to lower values of $\bar{n}$ as presented in Figure 5.12.

Regarding the optimal case $k = ko$, the convective growth rates of the dominant Type I mode at $R = R_c + 25$ against $\bar{n}$ at $Ro = -1$, -0.5 and 0 for both shear-thinning and shear-thickening fluids are presented in Figures 5.13-5.14, respectively. The critical Reynolds numbers R_c for the onset of the Type I mode for each flow are stated in Tables 5.3-5.4.

In contrast to the case of fixed $k = 100$, Figure 5.13 reveals a stabilising effect on the growth rates of the Type I mode for each shear-thinning flow when $k = ko$, while Figure 5.14 shows a destabilising effect on the growth rates of the Type I for these flows of shear-thickening fluids. On the other hand, it is interesting to note that the behaviour of the shifting maximum growth rates with number of spiral vortices $\bar{n}$ for Carreau fluids is the same for $k = ko$ and $k = 100$. However, this behaviour is different between shear-thinning and shear thickening Carreau fluids. In other words, the number of spiral vortices $\bar{n}$ is increased for shear-thinning Carreau fluids, whilst it is decreased for shear-thickening fluids for all k.

Moreover, it has been seen that the maximum growth rate for all values of n for both cases of k is increased as the Rossby number Ro reduced from -1 to 0. In general, All the results of growth rates are consistent with the critical Reynolds numbers for each flow presented previously.

As mentioned in the Chapter 4, absolute instability onsets at very small Reynolds numbers for $Ro \geq 0.5$ leading to "branch exchange". Therefore, it is impossible to find the location of maximum growth rate (Lingwood and Garrett, 2011).

(a) von Kármán, $Ro = -1$

(b) $Ro = -0.5$

(c) Ekman, $Ro = 0$

Figure 5.11: Growth rates for Type I mode for shear-thinning Carreau fluids with $n = 1, 0.9, 0.8, 0.7, 0.6$ and $k = 100$.

(a) von Kármán, $Ro = -1$

(b) $Ro = -0.5$

(c) Ekman, $Ro = 0$

Figure 5.12: Growth rates for Type I mode for shear-thickening Carreau fluids with $n = 1, 1.1, 1.2, 1.3, 1.4$ and $k = 100$.
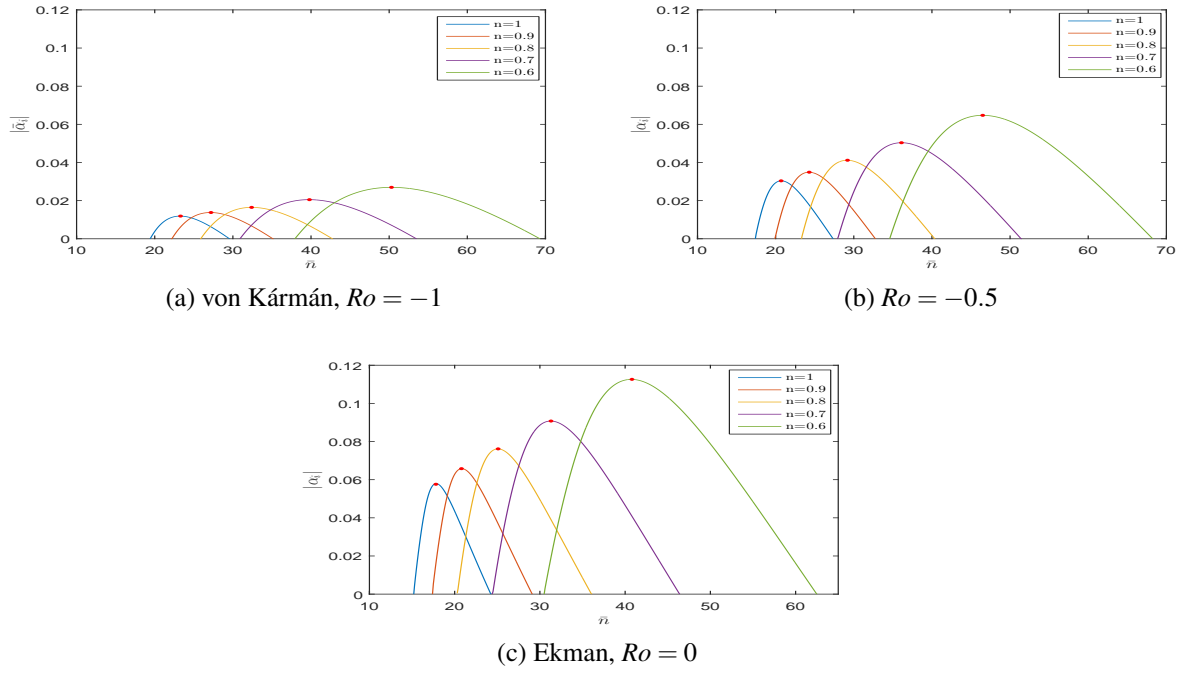
(a) von Kármán, $Ro = -1$

(b) $Ro = -0.5$

(c) Ekman, $Ro = 0$

Figure 5.13: Growth rates for Type I mode for shear-thinning Carreau fluids with $n = 1, 0.9, 0.8, 0.7, 0.6$ and $k = ko$.

(a) von Kármán, $Ro = -1$

(b) $Ro = -0.5$

(c) Ekman, $Ro = 0$
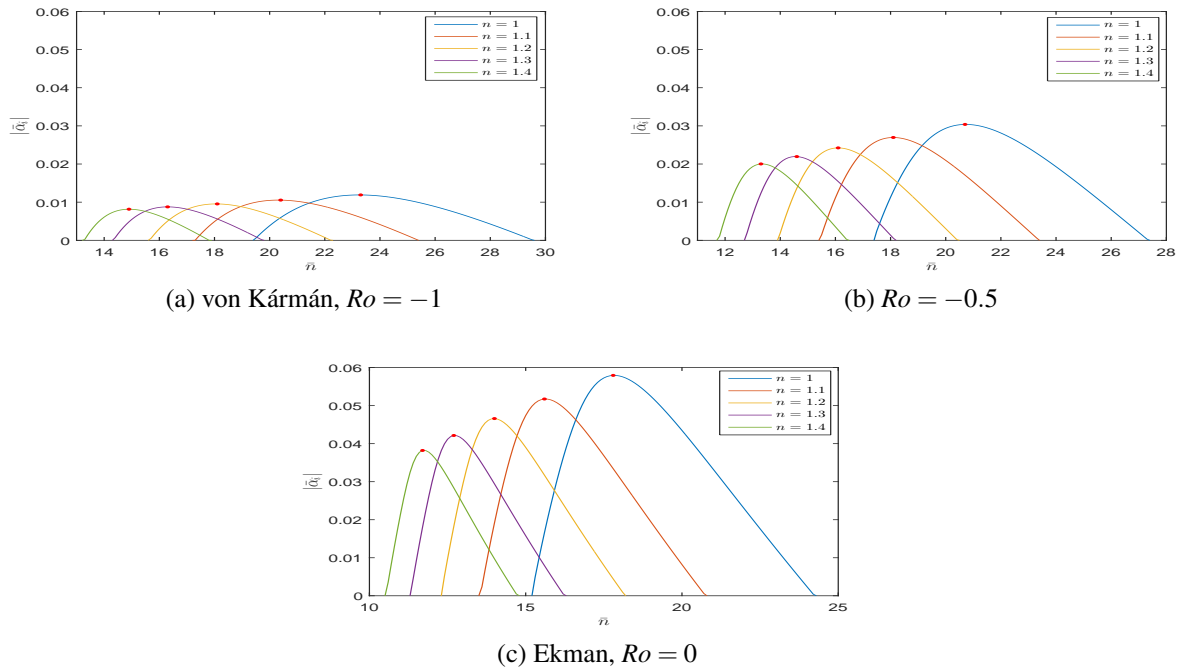
Figure 5.14: Growth rates for Type I mode for shear-thickening Carreau fluids with $n = 1, 1.1, 1.2, 1.3, 1.4$ and $k = ko$.
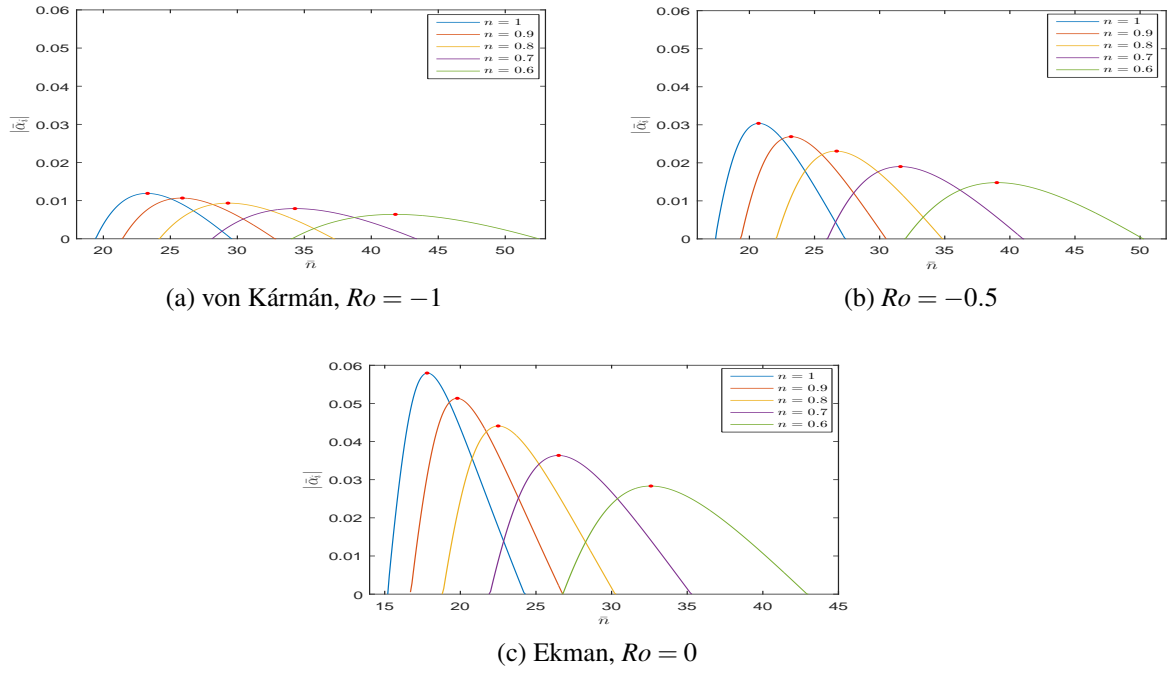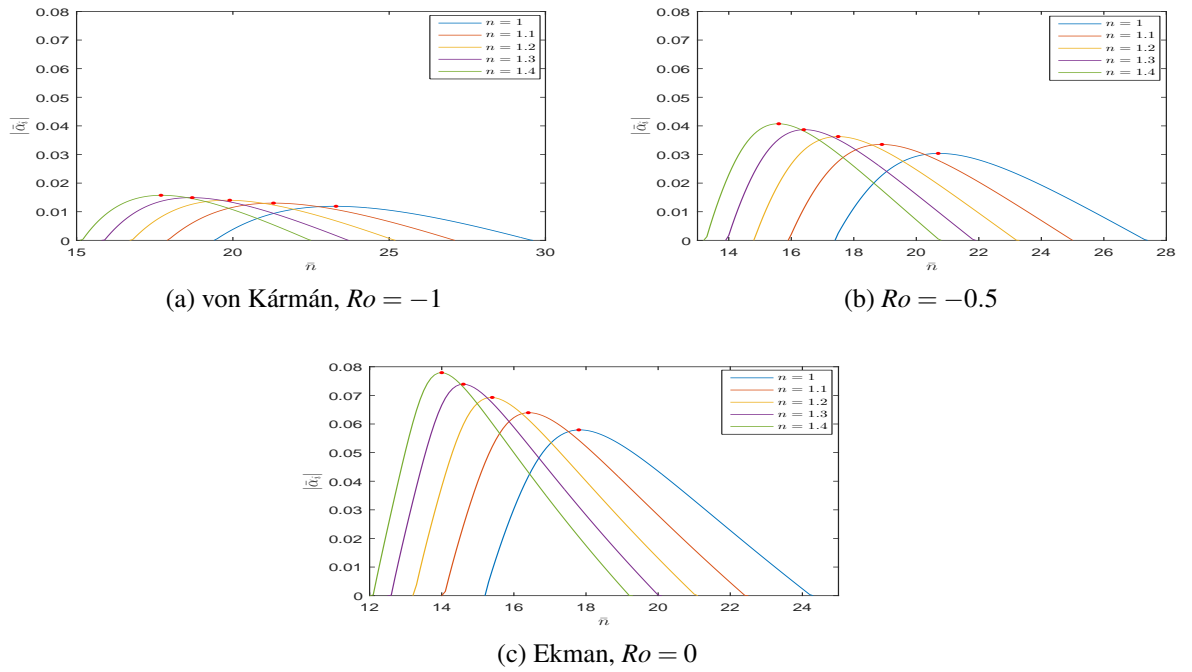
5.5   Energy analysis

By the same procedure as in §4.4, the studies of Cooper and Carpenter (1997), Cooper et al. (2015) and Garrett et al. (2016) for the von Kármán flow are followed in this section, and derive an integral energy equation for the disturbances within the Carreau BEK family of flows. This will enable us to establish the underlying physical mechanisms behind the stabilising effects determined previously.

The approach of Cooper and Carpenter (1997) is applied here to derive the governing energy equations by multiplying the linearised momentum equations (5.3) by the disturbance quantities u, v and w, respectively. The kinetic energy equation is then obtained by summing the momentum equations and is given as follows

$$
\left\{ \frac{\partial}{\partial t} + U \frac{\partial}{\partial r} + \frac{Ro}{R} \left(V \frac{\partial}{\partial \theta} - W \frac{\partial}{\partial z} \right) \right\} K
$$
$$
= -uw \frac{\partial U}{\partial z} - vw \frac{\partial V}{\partial z} + \frac{Ro}{R} w^2 \frac{\partial W}{\partial z} + \frac{Ro}{R} U u^2 + \frac{Ro}{R} U v^2
$$
$$
- \left[\frac{\partial (up)}{\partial r} + \frac{Ro}{R} \frac{\partial (vp)}{\partial \theta} + \frac{\partial (wp)}{\partial z} - \frac{Ro}{R} up \right] + \left[\frac{\partial (u_j \sigma_{ij})}{\partial x_i} - \sigma_{ij} \frac{\partial u_j}{\partial x_i} \right]
$$
$$
+ \frac{1}{R} \frac{\partial}{\partial z} \left(\mu \frac{\partial u}{\partial z} \right) u + \frac{1}{R} \frac{\partial}{\partial z} \left(\mu \frac{\partial v}{\partial z} \right) v + \frac{1}{R} \frac{\partial}{\partial z} \left(\mu \frac{\partial w}{\partial z} \right) w. \quad (5.9)
$$

Note that $K = (1/2) \left(u^2 + v^2 + w^2 \right)$ is the kinetic energy, μ is the viscosity function of the Carreau fluids, and σ_{ij} are anti-symmetric viscous stress terms

$$
\sigma_{ij} = \frac{\mu}{R} \left(\frac{\partial u_i}{\partial x_j} - \frac{\partial u_j}{\partial x_i} \right). \quad (5.10)
$$

The viscous terms $\mathscr{O} \left(1/R^2 \right)$ have been neglected to ensure consistency with the linearised governing stability equations. Moreover, the steady, rotationally-symmetric nature of the energy is ensured by removing the derivatives with respect to both t and θ. The perturbations are averaging over a single time period and azimuthal mode. The energy integral equation is

then obtained by integrate the entire boundary-layer as follows

$$
\int_0^\infty \left[\underbrace{U \frac{\partial \overline{K}}{\partial r}}_{a} + \underbrace{\frac{\partial (\overline{up})}{\partial r}}_{b} - \underbrace{\frac{\partial}{\partial r} \left(\overline{u\sigma_{11}} + \overline{v\alpha\sigma_{12}} + \overline{w\sigma_{13}} \right)}_{c} \right] dz
$$

$$
= \underbrace{\int_0^\infty \left[\left(-\overline{uw} \frac{\partial U}{\partial z} \right) + \left(-\overline{vw} \frac{\partial V}{\partial z} \right) + \left(\frac{Ro}{R} \overline{w^2} \frac{\partial W}{\partial z} \right) \right] dz}_{\text{I}}
$$

$$
\underbrace{- \int_0^\infty \left(\overline{\sigma_{ij} \frac{\partial u_j}{\partial x_i}} \right) dz}_{\text{II}} + \underbrace{\int_0^\infty \left(\frac{Ro}{R} \overline{up} \right) dz}_{\text{III}} + \underbrace{(\overline{wp})_{\bar{W}} - \underbrace{(\overline{u\sigma_{31}} + \overline{v\sigma_{32}} + \overline{w\sigma_{33}})_{\bar{W}}}_{\text{IV}}}_{}
$$

$$
+ \underbrace{\int_0^\infty \frac{Ro}{R} \frac{\partial \bar{K}}{\partial z} W dz + \int_0^\infty \frac{Ro}{R} \overline{u^2} U dz + \int_0^\infty \frac{Ro}{R} \overline{v^2} U dz}_{\text{V}}
$$

$$
+ \underbrace{\frac{1}{R} \int_0^\infty \left[\mu \overline{\frac{\partial^2 u}{\partial z^2} u} + \overline{\frac{\partial \mu}{\partial z} \frac{\partial u}{\partial z} u} \right] dz + \frac{1}{R} \int_0^\infty \left[\mu \overline{\frac{\partial^2 v}{\partial z^2} v} + \overline{\frac{\partial \mu}{\partial z} \frac{\partial v}{\partial z} v} \right] dz + \frac{1}{R} \int_0^\infty \left[\mu \overline{\frac{\partial^2 w}{\partial z^2} w} + \overline{\frac{\partial \mu}{\partial z} \frac{\partial w}{\partial z} w} \right] dz}_{VI}.
$$

$$(5.11)$$

Here overbars denote a period-averaged quantity, such that $\overline{uv} = uv^* + u^*v$ where * indicates a complex conjugate and $\bar{W}$ subscripts denote quantities evaluated at the wall.

Substituting (5.4) on the left-hand-side of equation (5.11) and then derive the terms with respect to r gives

$$
\int_0^\infty \left[i(\alpha - \alpha^*) \left\{ U (uu^* + vv^* + ww^*) + (up^* + u^*p) \right. \right.
$$

$$
\left. \left. - (u\sigma_{11}^* + u^*\sigma_{11} + v\sigma_{12}^* + v^*\sigma_{12} + w\sigma_{13}^* + w^*\sigma_{13}) \right\} \right] d\eta = RHS.
$$

It is clear that $\alpha = \alpha_r + i\alpha_i$ and $\alpha^* = \alpha_r - i\alpha_i$, gives

$$
-2\alpha_i \int_0^\infty \left[U\overline{K} + \overline{up} - (\overline{u\sigma_{11}} + \overline{v\sigma_{12}} + \overline{w\sigma_{13}}) \right] d\eta = RHS
$$

Thus, the energy equation is normalized for any eigenmode against the integrated mech-

anical energy flux in the following form

$$-2\alpha_i = \underbrace{(P_1 + P_2 + P_3)}_{I} + \underbrace{D}_{II} + \underbrace{(PW_1 + PW_2)}_{III} + \underbrace{(S_1 + S_2 + S_3)}_{IV}$$
$$+ \underbrace{(G_1 + G_2 + G_3)}_{V} + \underbrace{(N_1 + N_2 + N_3)}_{VI}, \quad (5.12)$$

The mathematical origin of each term is indicated by the numbered underbracing in equations (5.11) and (5.12) and explained physically in §4.4.

The terms PW_2, S_1, S_2 and S_3 in the energy balance equation (5.12) are identically zero due to the boundary conditions (5.8) for all flows of the BEK family. Furthermore, for the Ekman flow, $Ro = 0$, PW_1 and G_i are equal to zero due to the appearance of Ro in these terms.

The stability effect of both shear-thinning and shear-thickening Carreau fluids can be interpreted by calculating the total energy of the system which is the sum of the energy production and dissipation terms. In other words, increased total energy reveals a destabilising effect on the modes, while decreased total energy indicates a stabilising effect on the mode.

The maximum growth rates obtained in §5.4 for each flow are used here to obtain the energy balance for flows within the BEK family. The calculations of the energy analysis are applied at $R = R_c + 25$, where R_c is the critical Reynolds number for the onset of the Type I mode. Again, as predicted by Lingwood and Garrett (2011), it is not possible to find the location of maximum growth rate for $Ro \geq 0.5$ due to the very early onset of absolute instability and associated "branch exchange". Therefore, the energy balance calculations at these positive Ro are not shown here.

The energy balance calculations of the dominant Type I mode for BEK family of shear-thinning and shear-thickening Carreau fluids are presented for cases $k = 100$ and $k = ko$.

For the case $k = 100$, Figures 5.15-5.16 show the energy balance calculations of Type I mode for the von Kármán, Ekman and the flow of $Ro = -0.5$ for both shear-thinning and shear-thickening fluids, respectively. A very slight destabilising effect can be found on the

(a) von Kármán, $Ro = -1$

(b) $Ro = -0.5$

(c) Ekman, $Ro = 0$

Figure 5.15: Type I energy balance at $Re = R_c + 25$ for shear-thinning Carreau fluids with $n = 1, 0.9, 0.8, 0.7, 0.6$ and $k = 100$.

(a) von Kármán, $Ro = -1$

(b) $Ro = -0.5$

(c) Ekman, $Ro = 0$

Figure 5.16: Type I energy balance at $Re = R_c + 25$ for shear-thickening Carreau fluids with $n = 1, 1.1, 1.2, 1.3, 1.4$ and $k = 100$.

(a) von Kármán, $Ro = -1$

(b) $Ro = -0.5$

(c) Ekman, $Ro = 0$

Figure 5.17: Type I energy balance at $Re = R_c + 25$ for shear-thinning Carreau fluids with $n = 1, 0.9, 0.8, 0.7, 0.6$ and $k = ko$.
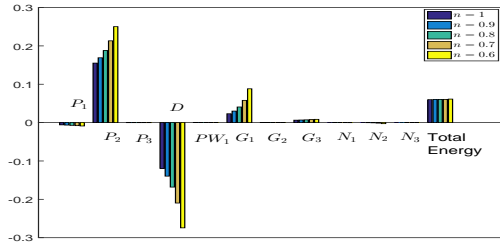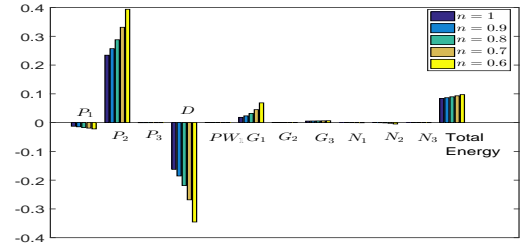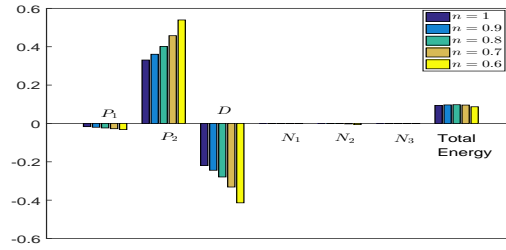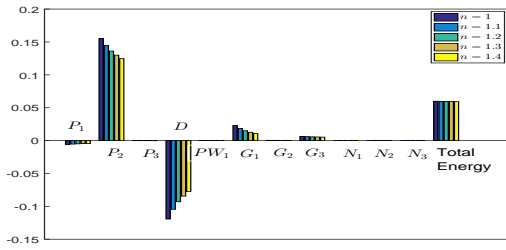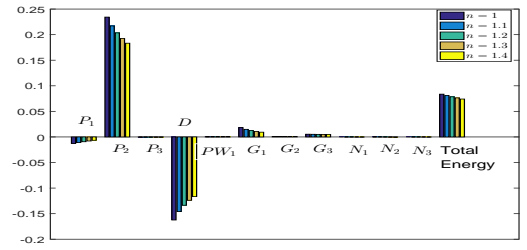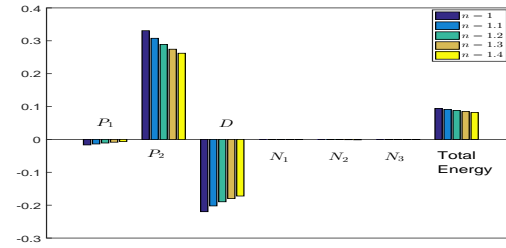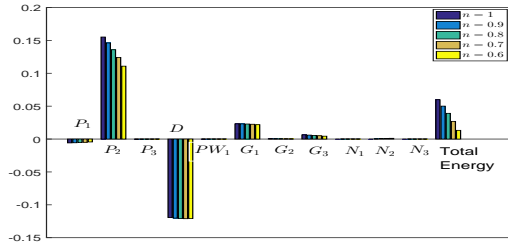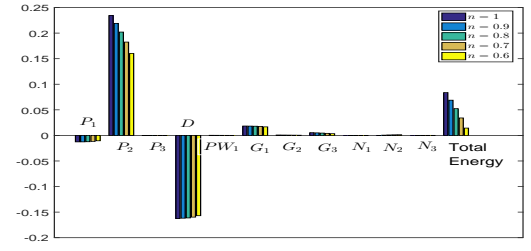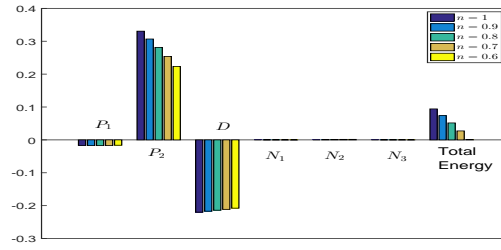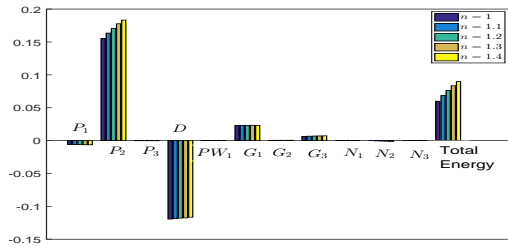

(a) von Kármán, $Ro = -1$
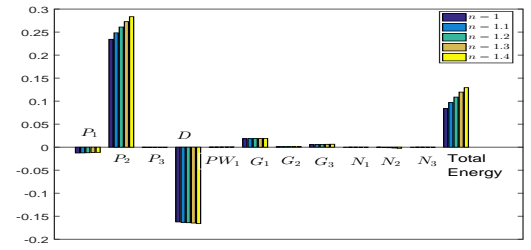
(b) $Ro = -0.5$
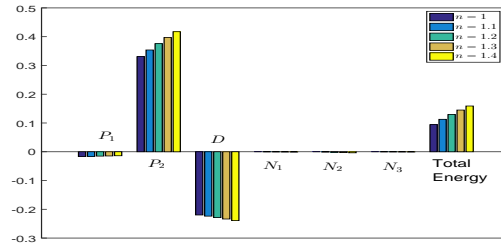
(c) Ekman, $Ro = 0$

Figure 5.18: Type I energy balance at $Re = R_c + 25$ for shear-thickening Carreau fluids with $n = 1, 1.1, 1.2, 1.3, 1.4$ and $k = ko$.

Type I mode for shear-thinning fluids due to rise the total energy that come from the sum of the energy production and the dissipation term. Furthermore, it has been noticed that the terms of both energy production P_2 and dissipation energy D are increased as n decreased. However, a small stabilising effect can be observed for shear-thickening fluids due to a reduction in the total energy. Moreover, the energy production term P_2 and the dissipation energy term D are reduced as n increased.

Figures 5.17-5.18 present the energy balance calculations of the Type I mode at $Ro = -1, -0.5$ and 0 for both shear-thinning and shear-thickening fluids with the case $k = ko$, respectively. It has been seen that there is a stabilising effect on the Type I mode for shear-thinning fluids where the term of energy production P_2 is reduced as n decreased. On the other hand, shear-thickening fluids have a destabilising effect on the Type I mode where the term P_2 is increased as n raised. It is observed that the term of energy production P_2 has a primary effect on the total energy that indicates the stability behaviour of the flow while the term of dissipation energy D has a slight effect on the total energy in the case $k = ko$. As found in Chapter 4 for the power-law flows, no direct effects on the energy balance are found for non-Newtonian terms. The modified viscosity is therefore again seen to act to establish new steady flows which are unstable through inviscid effects. This is as expected for the inviscid Type I mode.

5.6   Conclusion

In this chapter, the stability of stationary convective disturbances in the BEK family of boundary-layer flows have been investigated for both shear-thinning and shear-thickening Carreau fluids for the case of $k = 100$ and the optimal value of $k = ko$. The steady mean flow velocities derived in Chapter 3 are perturbed to obtain the perturbation equations. The linear stability analysis are conducted to investigate the occurrence of convective instability. The power-law index n indicates whether a Carreau fluid is shear-thinning when $n < 1$ or shear-thickening

when $n > 1$. The Rossby number Ro identifies the particular flow within the BEK family such that the von Kármán flow is obtained when $Ro = -1$, Ekman flow when $Ro = 0$, and Bödewadt flow when $Ro = 1$. Furthermore, the stability behaviour of Curreau fluids is determined by the value of relaxation parameter k. Therefore, the governing perturbation equations are controlled by these three parameters n, Ro and k. The optimal values of the parameter k mentioned in 5.3 are obtained as a variation of the critical Reynolds number with k that presented in Figures 5.4-5.5 for each n and Ro. Physically the parameter k determines the stability behaviour of Carreau fluids such that k represents as a key to decide whether the fluid has a stabilising or destabilising effect.

The neutral curves have revealed that shear-thinning fluids have a slight destabilising effect on both Type I and Type II modes for the BEK family of flows when $k = 100$, while shear-thickening fluids have a small stabilising effect on these modes for the same case. In direct contrast to these results, the selection of the optimal value ko reveals that shear-thinning fluids have a stabilising effect on both Type I and Type II modes for the BEK family of flows. However, shear-thickening fluids have a destabilising effect. It is found that the results in the shear-thinning for the case $k = ko$ have the same stability characteristics as the results of shear-thinning power-law fluids which is in contrast to the results for the case $k = 100$.

The growth rates of the Type I instability mode have been considered in order to find the maximum rates for particular flows in the system. The results obtained are confirmed by conducting an energy balance analysis at the locations of the maximum growth rates to obtain the underlying physical mechanisms behind the stabilising effects. The total energy of the system is affected by the physical processes energy production and dissipation terms. The results of the energy analysis are consistent with the results of the neutral curves for both shear-thinning and shear- thickening fluids.

In conclusion, the shear-thinning Carreau fluids at ko can be used to reduce skin-friction drag and delay transition from laminar to turbulence in many industrial applications.

Chapter 6

Conclusions

6.1 Completed work

This thesis is concerned with the convective instability analysis in the BEK family of rotating boundary-layer flows for two types of generalised Newtonian fluid models: power-law and Carreau fluids. The non-Newtonian study of Griffiths (2016) has been generalized to the entire BEK family of rotating boundary-layer flows. The boundary-layer approximation is applied to the Navier-Stokes equations in order to construct the governing leading order equations. The non-dimensionalised governing continuity and boundary-layer equations are solved to obtain the solutions of steady mean BEK family of flows. The flows of this family are governed by the Rossby number, Ro. The particular cases of this family are von Kármán $(Ro = -1)$, Ekman $(Ro = 0)$ and Bödewadt $(Ro = 1)$ flows. The viscosity function of power-law fluids are parametrised by a power-law index n, while the viscosity of Carreau fluids are controlled by two parameters, n and the relaxation parameter k. Two cases for Carreau fluids have been investigated depending on the value of the relaxation parameter: $k = 100$ and the optimal value of $k = ko$.

A comparison between shear-thinning power-law and Carreau fluids has been accomplished for the mean flow profiles, convective neutral curves, growth rates, and energy bal-

(a)

(b)
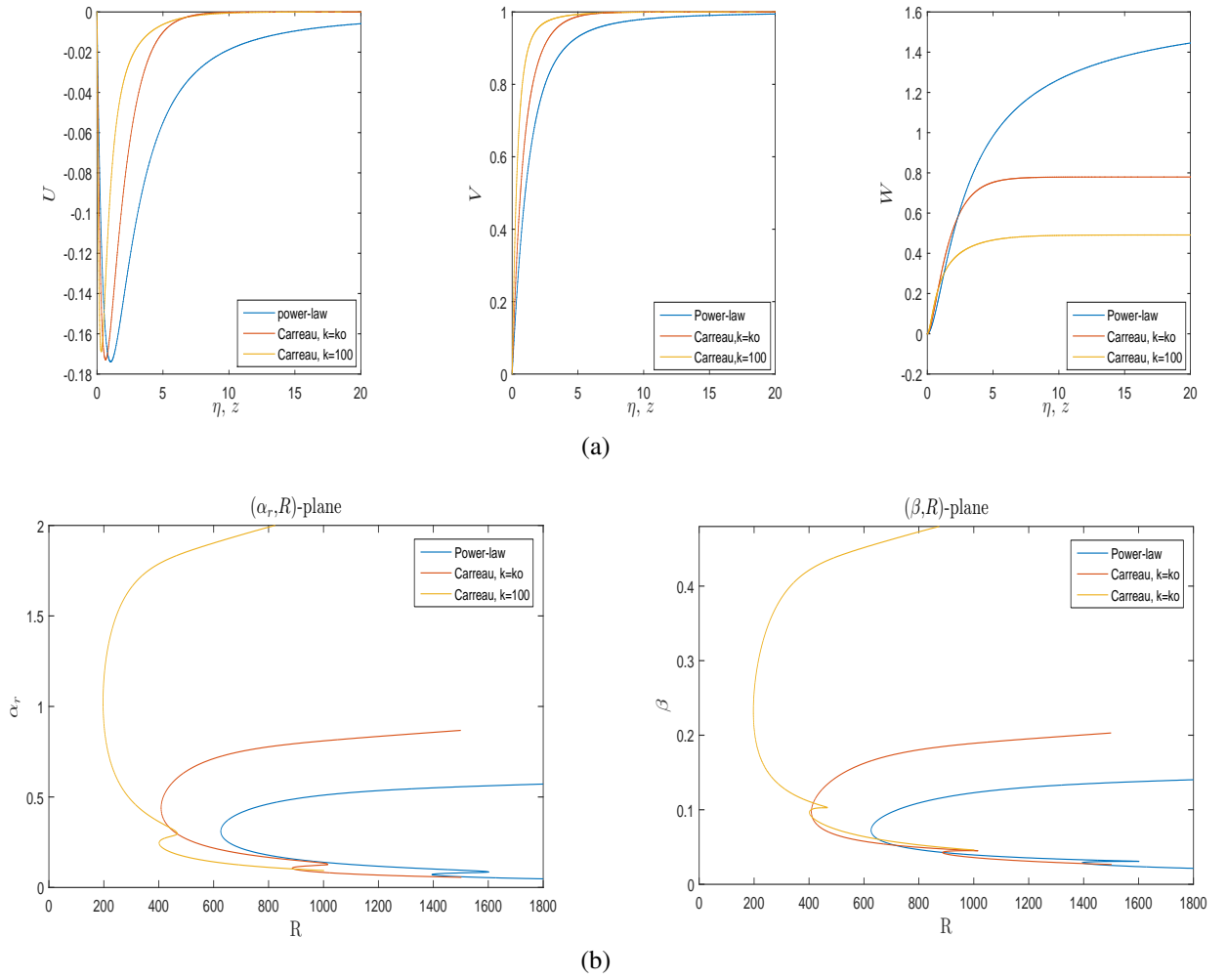
Figure 6.1: Comparison of shear-thinning power-law and Carreau fluids for the von Kármán flow, $Ro = -1$ when $n = 0.6$ for; (a) mean flow profiles and (b) neutral curves.

ance for von Kármán flow, $Ro = -1$ with the power-law index, $n = 0.6$. Figure 6.1(a) shows that the maximum value of the radial component U slightly approaches the disk surface for Carreau fluids. Therefore, the thickness of the boundary-layer reduces by using Carreau fluids instead of power-law fluids. Furthermore, the magnitude of the axial flow W in the far-field is decreased by using Carreau fluids, especially for larger values of the k as shown in figure 6.1(a). The viscosity function for shear-thinning power-law fluids is unbounded in the far-field of the boundary-layer. This behaviour is unphysical in contrast to the behaviour of the viscosity function for Carreau fluids which is limited in the region of the boundary-layer.

Therefore, the study of Carreau fluids presents a good description of the real nature of the shear-thinning and shear-thickening boundary-layer flows. Furthermore, the viscosity function of shear-thickening power-law fluids tends to zero at the outer-edge of the boundary-layer. Thus, the study is restricted here to investigate only shear-thinning fluids for the power-law model.

The solutions of the steady mean flows across the BEK family are perturbed in order to obtain the perturbation equations for both power-law and Carreau fluids. A linear stability analysis was conducted in order to study the occurrence of convective instability. The Chebyshev collocation method was applied here to calculate the neutral curves for each of the BEK family of flows. The results reveal that shear-thinning power-law fluids have a stabilising effect on both the Type I and Type II modes for the BEK family of flows in terms of the critical Reynolds number and the region of instability from the upper branch. Furthermore, the effect of shear-thinning fluids lead to growth in the size of the Type II mode. With respect to Carreau fluids, the shear-thinning Carreau fluids have a slight destabilising effect on both the Type I and Type II modes for $k = 100$ in terms of the critical Reynolds number. Furthermore, these fluids are found to have a strongly destabilising effect from upper branch of neutral curve. Therefore, the results suggest that the stability behaviour of shear-thinning Carreau fluids for $k = 100$ is not consistent with the behaviour of shear-thinning power-law fluids. In contrast, the shear-thickening Carreau fluids have a small stabilising effect in terms of the critical Reynolds number, while the region of instability is starkly decreased from upper branch of neutral curve.

The investigation shows that the value of relaxation parameter k plays a crucial role in the stability properties of Carreau fluids. The results reveal that the optimal value of $k = ko$ changes the behaviour of previous results of Carreau fluids as shown previously in §5.3. The value ko is obtained by plotting the variation of critical Reynolds numbers versus k as presented in Figures 5.4-5.5 in Chapter 5. The values of ko are different for each value of

(a)   (b)
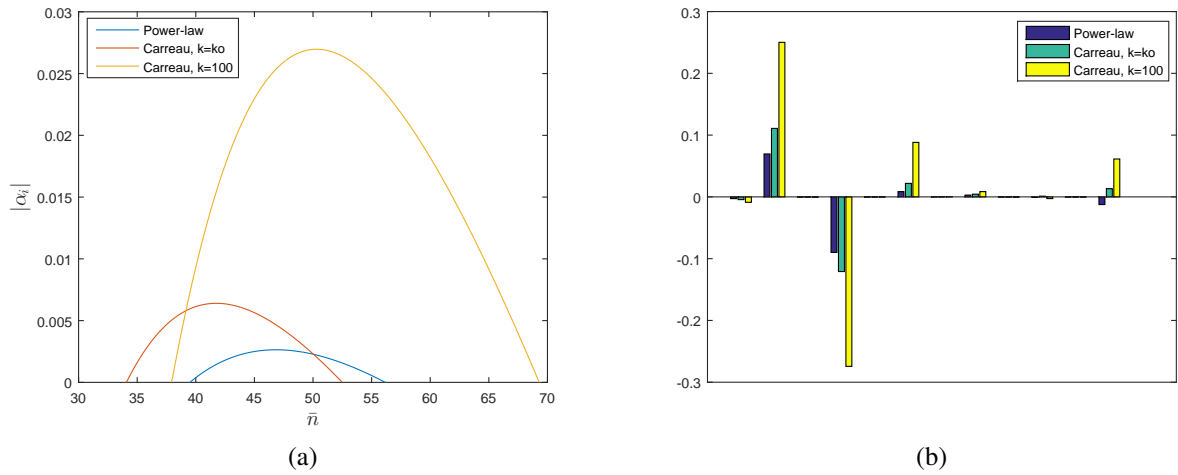
Figure 6.2: Comparison of shear-thinning power-law and Carreau fluids when $n = 0.6$ and $Ro = -1$ for (a) Growth rates of Type I mode and (b)Type I energy balance at $Re = R_c + 25$.

n and Ro. However, these values are approximately very close to each other. It is found that shear-thinning Carreau fluids have a stabilising effect which is consistent with those of power-law fluids, while shear-thickening Carreau fluids have a destabilising effect at ko.

Figure 6.1(b) shows that shear-thinning Carreau fluids for $k = 100$ have very strong destabilising effects on Type I and II modes in comparison to fluids that are otherwise the same but with $k = ko$ in terms of critical Reynolds number and the region of instability from the upper branch. The results of convective neutral curves have been confirmed by an investigation of the growth rates of the Type I instability mode to present the effects of power-law and Carreau fluids. As expected, agreement has been found between the results of neutral curves and the growth rates as shown in Figure 6.2(a).

The results of growth rates are obtained for only von Kármán and Ekman flows. This is due to very early onset of absolute instability for $Ro \geq 0.5$ that leads to "branch exchange" between Type I and Type III modes. Thus, it is impossible to detect maximum growth rate at such positive Ro (Lingwood and Garrett, 2011). The study of the energy analysis supports the results obtained for neutral curves and growth rates. The energy-balance calculations are obtained to provide the underlying physical mechanisms behind the stabilising effects by ap-

plying the approach of Cooper and Carpenter (1997). The results of the energy analysis are consistent with the results obtained from the neutral curves. Figure 6.2(b) shows a comparative Type I energy balance between shear-thinning power-law and Carreau fluids for von Kármán flow with the power-law index $n = 0.6$. The comparative mean flow profiles, neutral curves, growth rates and energy balance for other related flows of BEK family have the same behaviour of those for von Kármán flow, $Ro = -1$. Comparative results for Ekman flow are shown in Appendix C.5.

In conclusion, the use of shear-thinning power-law and Carreau fluids with optimal values of relaxation parameter is crucial to delay the transition from laminar to turbulence for the entire BEK family of flows. In other words, these fluids led to reduce skin-friction drag in enclosed rotor-stator devices in industrial applications.

6.2   Future work

There are several areas of research for future work on the current study of this thesis. Firstly, the experimental study is needed in order to compare and validate the theoretical analysis. The results presented here could be extended to other non-Newtonian viscosity models. Furthermore, this current study has been limited to stationary disturbances that are to expected to be observed in all practical engineering applications where they are continuously excited by unavoidable surface roughness. However, where great care is taken to use high polished surfaces, it is known that non-stationary convective instabilities can become dominant in the sense of both larger growth rates and lower critical Reynolds numbers (Balakumar and Malik, 1990; Hussain et al., 2011). The study of absolute instability is also a potential area of future interest. Previous studies of absolute instability has been performed for BEK family of Newtonian flows by Lingwood (1997) and Lingwood and Garrett (2011). Chapters 4 and 5 could be generalized to observe the absolute instability characteristics of the BEK family of flows for power-law and Carreau fluids, respectively, which will give an insight into the onset

of turbulence within the boundary layers. The results were obtained here by applying a linear stability analysis with local parallel-flow approximation. Thus, non-parallel mean flow could be involved in the work by following the study of Davies and Carpenter (2003). Finally, the asymptotic linear stability analysis would also be valuable to confirm the results in the limit of high Reynolds number behaviour.

Appendix A

Derivation of the perturbation equations

In this appendix, the governing boundary-layer equations are presented in the non-dimensional form and the calculations for adding small perturbing quantities to the mean flow velocities to generate the governing perturbation equations. Furthermore, these equations are rearranged and presented in a form consistent with the Chebyshev collocation method of solution. §A.1 and §A.2 present the form of the perturbation equations for power-law and Carreau fluids, respectively.

A.1 Power-law fluids

The dimensionless form for the boundary-layer equations are obtained with respect to the following variable

$$r = \frac{r^*}{L^*}, \quad z = \frac{z^*}{L^*}, \quad (U,V,W) = \frac{(U^*,V^*,W^*)}{r_a^*\Omega^* Ro}, \quad P = \frac{P^*}{\rho^*(r_a^*\Omega^* Ro)^2}, \quad t = \frac{t^* r_a^*\Omega^*}{L^*}. \quad \text{(A.1)}$$

The local Reynolds number is defined as:

$$
\begin{aligned}
R &= r_a^{*2/(n+1)} \left[\frac{\triangle \Omega^{2-n} L^*}{\nu^*} \right]^{2/(n+1)} = r_a^{*2/(n+1)} \left[\frac{Ro^{2-n} \Omega^{2-n} L^*}{\nu^*} \right]^{2/(n+1)} \\
&= r_a^{*2/(n+1)} \left[\frac{Ro Ro^{1-n} \Omega^{2-n} L^*}{\nu^*} \right]^{2/(n+1)} = \left[\frac{r_a^* Ro}{L^*} \right]^{2/(n+1)} \\
&= [r_a Ro]^{2/(n+1)}.
\end{aligned}
\tag{A.2}
$$

Therefore the governing boundary-layer equations (3.4) become

$$
\frac{1}{r} \frac{\partial (r U_0)}{\partial r} + \frac{1}{r} \frac{\partial V_0}{\partial \theta} + \frac{\partial W_0}{\partial z} = 0,
\tag{A.3}
$$

$$
\frac{\partial U_0}{\partial t} + U_0 \frac{\partial U_0}{\partial r} + \frac{V_0}{r} \frac{\partial U_0}{\partial \theta} + W_0 \frac{\partial U_0}{\partial z} - \frac{V_0^2}{r} - \frac{Co V_0}{R^{(n+1)/2}} = -\frac{\partial P_0}{\partial r} + \frac{1}{R^{(2-n)(n+1)/2}} \left(\frac{\partial}{\partial z} \left(\mu_0 \frac{\partial U_0}{\partial z} \right) \right),
\tag{A.4}
$$

$$
U_0 \frac{\partial V_0}{\partial r} + \frac{V_0}{r} \frac{\partial V_0}{\partial \theta} + W_0 \frac{\partial V_0}{\partial z} + \frac{U_0 V_0}{r} + \frac{Co U_0}{R^{(n+1)/2}} = -\frac{1}{r} \frac{\partial P_0}{\partial \theta} + \frac{1}{R^{(2-n)(n+1)/2}} \left(\frac{\partial}{\partial z} \left(\mu_0 \frac{\partial V_0}{\partial z} \right) \right),
\tag{A.5}
$$

$$
\begin{aligned}
U_0 \frac{\partial W_0}{\partial r} + \frac{V_0}{r} \frac{\partial W_0}{\partial \theta} + W_0 \frac{\partial W_0}{\partial z} &= -\frac{\partial P_1}{\partial z} + \frac{1}{R^{(2-n)(n+1)/2}} \left[\frac{1}{r} \frac{\partial}{\partial r} \left(\mu_0 r \frac{\partial U_0}{\partial z} \right) \right. \\
&\left. + \frac{1}{r} \frac{\partial}{\partial \theta} \left(\mu_0 \frac{\partial V_0}{\partial z} \right) + 2 \frac{\partial}{\partial z} \left(\mu_0 \frac{\partial W_0}{\partial z} \right) \right],
\end{aligned}
\tag{A.6}
$$

where

$$
\mu_0 = \frac{\mu_0^*}{m^*} \left(\frac{r_a^* \Omega^* Ro}{L^*} \right)^{1-n} = \left[\left(\frac{\partial U_0}{\partial z} \right)^2 + \left(\frac{\partial V_0}{\partial z} \right)^2 \right]^{(n-1)/2}.
\tag{A.7}
$$

The instantaneous non-dimensional velocities and pressure are given by

$$
\begin{aligned}
U_0(\eta, r, \theta, t) &= \frac{rRo}{R^{(n+1)/2}} U(\eta) + u(\eta, r, \theta, t), \\
V_0(\eta, r, \theta, t) &= \frac{rRo}{R^{(n+1)/2}} V(\eta) + v(\eta, r, \theta, t), \\
W_0(\eta, r, \theta, t) &= \frac{r^{(n-1)/(n+1)} Ro}{R^{(n+1)/2}} W(\eta) + w(\eta, r, \theta, t), \\
P_{0,1}(\eta, r, \theta, t) &= \frac{r^{2(n-1)/(n+1)} Ro^2}{R^{(n+1)}} P(\eta) + p(\eta, r, \theta, t).
\end{aligned}
$$

The continuity equation becomes

$$
\frac{1}{r} \frac{\partial}{\partial r} \left[\frac{r^2 Ro U(\eta)}{R^{(n+1)/2}} + ru(r, \eta, \theta, t) \right] + \frac{1}{r} \frac{\partial}{\partial \theta} \left[\frac{rRo V(\eta)}{R^{(n+1)/2}} + v(r, \eta, \theta, t) \right]
$$
$$
+ \frac{\partial}{\partial z} \left[\frac{r^{(n-1)/(n+1)} Ro W(\eta)}{R^{(n+1)/2}} + w(r, \eta, \theta, t) \right] = 0,
$$
$$
\implies \frac{1}{r} \frac{\partial (ru)}{\partial r} + \frac{1-n}{n+1} \frac{\eta}{r} \frac{\partial u}{\partial \eta} + \frac{1}{r} \frac{\partial v}{\partial \theta} + r^{(1-n)/(n+1)} \frac{\partial w}{\partial \eta} = 0.
$$

We have

$$
R^{(n-1)/2} \frac{\partial u}{\partial r} + \frac{Ro}{R} \frac{(1-n)}{(n+1)} \eta \frac{\partial u}{\partial \eta} + \frac{Ro}{R} u + \frac{Ro}{R} \frac{\partial v}{\partial \theta} + Ro^{(n-1)/(n+1)} \frac{\partial w}{\partial \eta} = 0. \tag{A.8}
$$

The viscosity function becomes

$$
\mu_0 = \left(\left\{ \frac{\partial}{\partial z} \left[\frac{rRo U(\eta)}{R^{(n+1)/2}} + u(r, \eta, \theta, t) \right] \right\}^2 + \left\{ \frac{\partial}{\partial z} \left[\frac{rRo V(\eta)}{R^{(n+1)/2}} + v(r, \eta, \theta, t) \right] \right\}^2 \right)^{(n-1)/2},
$$
$$
= \left\{ \left[\frac{rr^{(1-n)/(n+1)} U' Ro}{R^{(n+1)/2}} + r^{(1-n)/(n+1)} \frac{\partial u}{\partial \eta} \right]^2 + \left[\frac{rr^{(1-n)/(n+1)} V' Ro}{R^{(n+1)/2}} + r^{(1-n)/(n+1)} \frac{\partial v}{\partial \eta} \right]^2 \right\}^{(n-1)/2},
$$
$$
= \left\{ \left[\frac{r^2 r^{2(1-n)/(n+1)} (U')^2 Ro^2}{R^{n+1}} + \frac{2rr^{2(1-n)/(n+1)} Ro}{R^{(n+1)/2}} U' \frac{\partial u}{\partial \eta} \right] \right.
$$
$$
\times \left. \left[\frac{r^2 r^{2(1-n)/(n+1)} (V')^2 Ro^2}{R^{n+1}} + \frac{2rr^{2(1-n)/(n+1)} Ro}{R^{(n+1)/2}} V' \frac{\partial v}{\partial \eta} \right] \right\}^{(n-1)/2},
$$

$$= \left\{ \frac{r^2 r^{2(1-n)/(n+1)} Ro^2}{R^{n+1}} [(U')^2 + (V')^2] + \frac{2rr^{2(1-n)/(n+1)} Ro}{R^{(n+1)/2}} \left(U'\frac{\partial u}{\partial \eta} + V'\frac{\partial v}{\partial \eta} \right) \right\}^{(n-1)/2},$$

$$= \left\{ \frac{r^{4/(n+1)} Ro^2}{R^{n+1}} [(U')^2 + (V')^2] \right\}^{(n-1)/2} \left(1 + \frac{2r^{(3-n)/(n+1)} Ro}{R^{(n+1)/2}} \left\{ \frac{r^{4/(n+1)} Ro^2}{R^{n+1}} [(U')^2 + (V')^2] \right\}^{-1} \right.$$

$$\times \left. \left(U'\frac{\partial u}{\partial \eta} + V'\frac{\partial v}{\partial \eta} \right) \right)^{(n-1)/2},$$

$$= \frac{r^{2(n-1)/(n+1)} Ro^{n-1}}{R^{(n-1)(n+1)/2}} [(U')^2 + (V')^2]^{(n-1)/2} \left\{ 1 + \frac{2R^{(n+1)/2}}{r[(U')^2 + (V')^2] Ro} \left(U'\frac{\partial u}{\partial \eta} + V'\frac{\partial v}{\partial \eta} \right) \right\}^{(n-1)/2},$$

$$= \frac{r^{2(n-1)/(n+1)} Ro^{n-1}}{R^{(n-1)(n+1)/2}} \left\{ \mu + \frac{R^{(n+1)/2}}{rRo} \frac{(n-1)\mu}{[(U')^2 + (V')^2]} \left(U'\frac{\partial u}{\partial \eta} + V'\frac{\partial v}{\partial \eta} \right) \right\},$$

$$= \frac{r^{2(n-1)/(n+1)} Ro^{n-1}}{R^{(n-1)(n+1)/2}} \left\{ \mu + \frac{R^{(n+1)/2}}{rRo} \frac{(n-1)\mu U'}{[(U')^2 + (V')^2]} \frac{\partial u}{\partial \eta} + \frac{R^{(n+1)/2}}{rRo} \frac{(n-1)\mu V'}{[(U')^2 + (V')^2]} \frac{\partial v}{\partial \eta} \right\},$$

$$= \frac{r^{2(n-1)/(n+1)} Ro^{n-1}}{R^{(n-1)(n+1)/2}} \left[\mu + \frac{R^{(n+1)/2}}{rRo} \hat{\mu} U' \frac{\partial u}{\partial \eta} + \frac{R^{(n+1)/2}}{rRo} \hat{\mu} V' \frac{\partial v}{\partial \eta} \right],$$

where

$$\hat{\mu} = \frac{(n-1)\mu}{[(U')^2 + (V')^2]} = (n-1)[(U')^2 + (V')^2]^{(n-3)/2}.$$

The derivatives of the viscosity and disturbance viscosity functions are given by

$$\frac{\partial \mu}{\partial z} = \mu',$$

$$\frac{\partial \hat{\mu}}{\partial z} = \frac{(n-3)\mu'}{[(U')^2 + (V')^2]},$$

$$\frac{\partial \mu}{\partial r} = \frac{1-n}{n+1} \frac{\eta}{r} \mu',$$

$$\frac{\partial \hat{\mu}}{\partial r} = \frac{1-n}{n+1} \frac{\eta}{r} \frac{(n-3)\mu'}{[(U')^2 + (V')^2]}.$$

The *r*-momentum equation becomes

$$
\frac{\partial}{\partial t}\left[\frac{rRoU(\eta)}{R^{(n+1)/2}}+u(r,\eta,\theta,t)\right]+\left[\frac{rRoU(\eta)}{R^{(n+1)/2}}+u(r,\eta,\theta,t)\right]\frac{\partial}{\partial r}\left[\frac{rRoU(\eta)}{R^{(n+1)/2}}+u(r,\eta,\theta,t)\right]
$$

$$
+\frac{1}{r}\left[\frac{rRoV(\eta)}{R^{(n+1)/2}}+v(r,\eta,\theta,t)\right]\frac{\partial}{\partial\theta}\left[\frac{rRoU(\eta)}{R^{(n+1)/2}}+u(r,\eta,\theta,t)\right]
$$

$$
+\left[\frac{r^{(n-1)/(n+1)}RoW(\eta)}{R^{(n+1)/2}}+w(r,\eta,\theta,t)\right]\frac{\partial}{\partial z}\left[\frac{rRoU(\eta)}{R^{(n+1)/2}}+u(r,\eta,\theta,t)\right]
$$

$$
-\frac{1}{r}\left[\frac{rRoV(\eta)}{R^{(n+1)/2}}+v(r,\eta,\theta,t)\right]^2-\frac{Co}{R^{(n+1)/2}}\left[\frac{rRoV(\eta)}{R^{(n+1)/2}}+v(r,\eta,\theta,t)\right]
$$

$$
=-\frac{\partial}{\partial r}\left[\frac{r^{2(n-1)/(n+1)}Ro^2P(\eta)}{R^{n+1}}+p(r,\eta,\theta,t)\right]+\frac{X_1}{R^{(2-n)(n+1)/2}},
$$

$$
\implies \frac{\partial u}{\partial t}+\frac{rU^2Ro^2}{R^{n+1}}+\frac{r}{R^{n+1}}\frac{1-n}{n+1}\eta UU'Ro^2+\frac{rURo}{R^{(n+1)/2}}\frac{\partial u}{\partial r}+\frac{\eta Ro}{R^{(n+1)/2}}\frac{1-n}{n+1}U\frac{\partial u}{\partial\eta}+\frac{RoUu}{R^{(n+1)/2}}
$$

$$
+\frac{\eta Ro}{R^{(n+1)/2}}\frac{1-n}{n+1}U'u+\frac{VRo}{R^{(n+1)/2}}\frac{\partial u}{\partial\theta}+\frac{rU'WRo^2}{R^{n+1}}+\frac{WRo}{R^{(n+1)/2}}\frac{\partial u}{\partial\eta}+\frac{rr^{(1-n)/(n+1)}U'wRo}{R^{(n+1)/2}}
$$

$$
-\frac{rV^2Ro^2}{R^{n+1}}-\frac{2VvRo}{R^{(n+1)/2}}-\frac{Cov}{R^{(n+1)/2}}
$$

$$
=-\frac{r^{2(n-1)/(n+1)}Ro^2}{rR^{n+1}}\frac{1-n}{n+1}\left(\eta P'-2P\right)-\frac{\partial p}{\partial r}-\frac{1-n}{n+1}\frac{\eta}{r}\frac{\partial p}{\partial\eta}+\frac{X_1}{R^{(2-n)(n+1)/2}},
$$

where

$$
X_1=\frac{\partial}{\partial z}\left(\frac{r^{2(n-1)/(n+1)}Ro^{n-1}}{R^{(n-1)(n+1)/2}}\left(\mu+\frac{R^{(n+1)/2}}{rRo}\hat{\mu}U'\frac{\partial u}{\partial\eta}+\frac{R^{(n+1)/2}}{rRo}\hat{\mu}V'\frac{\partial v}{\partial\eta}\right)\right.
$$

$$
\left.\left\{\frac{\partial}{\partial z}\left[\frac{rU(\eta)Ro}{R^{(n+1)/2}}+u(r,\eta,\theta,t)\right]\right\}\right),
$$

$$
=\frac{r^{2(n-1)/(n+1)}Ro^{n-1}}{R^{(n-1)(n+1)/2}}\frac{\partial}{\partial z}\left[\left(\mu+\frac{R^{(n+1)/2}}{rRo}\hat{\mu}U'\frac{\partial u}{\partial\eta}+\frac{R^{(n+1)/2}}{rRo}\hat{\mu}V'\frac{\partial u}{\partial\eta}\right)\right.
$$

$$
\left.\times\left(\frac{rr^{(1-n)/(n+1)}U'Ro}{R^{(n+1)/2}}+r^{(1-n)/(n+1)}\frac{\partial u}{\partial\eta}\right)\right],
$$

$$= \frac{r^{2(n-1)/(n+1)}Ro^{n-1}}{R^{(n-1)(n+1)/2}}\frac{\partial}{\partial z}\left[\frac{rr^{(1-n)/(n+1)}\mu U'Ro}{R^{(n+1)/2}} + r^{(1-n)/(n+1)}\mu\frac{\partial u}{\partial \eta}\right.$$

$$\left. + r^{(1-n)/(n+1)}\hat{\mu}U'\left(U'\frac{\partial u}{\partial \eta} + V'\frac{\partial v}{\partial \eta}\right)\right],$$

$$= \frac{r^{2(n-1)/(n+1)}Ro^{n-1}}{R^{(n-1)(n+1)/2}}\left\{\frac{rr^{2(1-n)/(n+1)}(\mu U')'Ro}{R^{(n+1)/2}} + r^{2(1-n)/(n+1)}\left(\mu'\frac{\partial u}{\partial \eta} + \mu\frac{\partial^2 u}{\partial \eta^2}\right)\right.$$

$$\left. + r^{2(1-n)/(n+1)}\left[\hat{\mu}U'\left(U'\frac{\partial u}{\partial \eta} + V'\frac{\partial v}{\partial \eta}\right)\right]'\right\},$$

$$= \frac{Ro^{n-1}}{R^{(n-1)(n+1)/2}}\left\{\frac{r(\mu U')'Ro}{R^{(n+1)/2}} + \left(\mu'\frac{\partial u}{\partial \eta} + \mu\frac{\partial^2 u}{\partial \eta^2}\right)\right.$$

$$\left. + \left[\hat{\mu}U'\left(U'\frac{\partial u}{\partial \eta} + V'\frac{\partial v}{\partial \eta}\right)\right]'\right\},$$

$$\implies \frac{X_1 Ro^{n-1}}{R^{(2-n)(n+1)/2}} = \frac{r(\mu U')'Ro}{R^{(n+1)}} + \frac{1}{R^{(n+1)/2}}\frac{\partial}{\partial \eta}\left(\mu\frac{\partial u}{\partial \eta} + \hat{\mu}U'\left(U'\frac{\partial u}{\partial \eta} + V'\frac{\partial v}{\partial \eta}\right)\right).$$

Apply parallel-flow approximation, we have

$$R^{(n-1)/2}\left(\frac{\partial u}{\partial t} + U\frac{\partial u}{\partial r}\right) + \frac{Ro}{R}V\frac{\partial u}{\partial \theta} + \frac{Ro}{R}W\frac{\partial u}{\partial \eta} + \frac{Ro}{R}Uu + Ro^{(n-1)/(n+1)}U'w$$

$$- \left(2\frac{Ro}{R}V + \frac{Co}{R}\right)v + \frac{Ro}{R}\eta\frac{(1-n)}{(n+1)}\left(U\frac{\partial u}{\partial \eta} + U'u + \frac{\partial p}{\partial \eta}\right)$$

$$= -R^{(n-1)/2}\frac{\partial p}{\partial r} + \frac{Ro^{n-1}}{R}\frac{\partial}{\partial \eta}\left(\mu\frac{\partial u}{\partial \eta} + \hat{\mu}U'\left(U'\frac{\partial u}{\partial \eta} + V'\frac{\partial v}{\partial \eta}\right)\right), \quad \text{(A.9)}$$

where

$$\hat{\mu} = \frac{(n-1)\mu}{[(U')^2 + (V')^2]}. \tag{A.10}$$

The θ-momentum equation becomes

$$\frac{\partial}{\partial t}\left[\frac{rRoV(\eta)}{R^{(n+1)/2}}+v(r,\eta,\theta,t)\right]+\left[\frac{rRoU(\eta)}{R^{(n+1)/2}}+u(r,\eta,\theta,t)\right]\frac{\partial}{\partial r}\left[\frac{rRoV(\eta)}{R^{(n+1)/2}}+v(r,\eta,\theta,t)\right]$$

$$+\frac{1}{r}\left[\frac{rRoV(\eta)}{R^{(n+1)/2}}+v(r,\eta,\theta,t)\right]\frac{\partial}{\partial\theta}\left[\frac{rRoV(\eta)}{R^{(n+1)/2}}+v(r,\eta,\theta,t)\right]$$

$$+\left[\frac{r^{(n-1)/(n+1)}RoW(\eta)}{R^{(n+1)/2}}+w(r,\eta,\theta,t)\right]\frac{\partial}{\partial z}\left[\frac{rRoV(\eta)}{R^{(n+1)/2}}+v(r,\eta,\theta,t)\right]$$

$$+\frac{1}{r}\left[\frac{rRoU(\eta)}{R^{(n+1)/2}}+u(r,\eta,\theta,t)\right]\left[\frac{rRoV(\eta)}{R^{(n+1)/2}}+v(r,\eta,\theta,t)\right]+\frac{Co}{R^{(n+1)/2}}\left[\frac{rRoU(\eta)}{R^{(n+1)/2}}+u(r,\eta,\theta,t)\right]$$

$$=-\frac{1}{r}\frac{\partial}{\partial\theta}\left[\frac{r^{2(n-1)/(n+1)}Ro^2P(\eta)}{R^{n+1}}+p(r,\eta,\theta,t)\right]+\frac{X_2}{R^{(2-n)(n+1)/2}},$$

$$\implies\frac{\partial v}{\partial t}+\frac{rUVRo^2}{R^{n+1}}+\frac{r}{R^{n+1}}\frac{1-n}{n+1}\eta UV'Ro^2+\frac{rURo}{R^{(n+1)/2}}\frac{\partial v}{\partial r}+\frac{\eta Ro}{R^{(n+1)/2}}\frac{1-n}{n+1}U\frac{\partial v}{\partial\eta}+\frac{RoVu}{R^{(n+1)/2}}$$

$$+\frac{\eta Ro}{R^{(n+1)/2}}\frac{1-n}{n+1}V'u+\frac{VRo}{R^{(n+1)/2}}\frac{\partial v}{\partial\theta}+\frac{rV'WRo^2}{R^{n+1}}+\frac{RoW}{R^{(n+1)/2}}\frac{\partial v}{\partial\eta}+\frac{rr^{(1-n)/(n+1)}V'wRo}{R^{(n+1)/2}}$$

$$+\frac{rUVRo^2}{R^{n+1}}+\frac{Ro(Uv+Vu)}{R^{(n+1)/2}}+\frac{rCoRoU}{R^{n+1}}+\frac{Cou}{R^{(n+1)/2}}=-\frac{1}{r}\frac{\partial p}{\partial\theta}+\frac{X_2}{R^{(2-n)(n+1)/2}},$$

where

$$X_2=\frac{\partial}{\partial z}\left(\frac{r^{2(n-1)/(n+1)}Ro^{n-1}}{R^{(n-1)(n+1)/2}}\left(\mu+\frac{R^{(n+1)/2}}{rRo}\hat{\mu}U'\frac{\partial u}{\partial\eta}+\frac{R^{(n+1)/2}}{rRo}\hat{\mu}V'\frac{\partial v}{\partial\eta}\right)\right.$$

$$\left.\left\{\frac{\partial}{\partial z}\left[\frac{rV(\eta)Ro}{R^{(n+1)/2}}+v(r,\eta,\theta,t)\right]\right\}\right)$$

$$=\frac{r^{2(n-1)/(n+1)}Ro^{n-1}}{R^{(n-1)(n+1)/2}}\frac{\partial}{\partial z}\left[\left(\mu+\frac{R^{(n+1)/2}}{rRo}\hat{\mu}U'\frac{\partial u}{\partial\eta}+\frac{R^{(n+1)/2}}{rRo}\hat{\mu}V'\frac{\partial v}{\partial\eta}\right)\right.$$

$$\left.\times\left(\frac{rr^{(1-n)/(n+1)}V'Ro}{R^{(n+1)/2}}+r^{(1-n)/(n+1)}\frac{\partial v}{\partial\eta}\right)\right],$$

$$=\frac{r^{2(n-1)/(n+1)}Ro^{n-1}}{R^{(n-1)(n+1)/2}}\frac{\partial}{\partial z}\left[\frac{rr^{(1-n)/(n+1)}\mu V'Ro}{R^{(n+1)/2}}+r^{(1-n)/(n+1)}\mu\frac{\partial v}{\partial\eta}\right.$$

$$\left.+r^{(1-n)/(n+1)}\hat{\mu}V'\left(U'\frac{\partial u}{\partial\eta}+V'\frac{\partial v}{\partial\eta}\right)\right],$$

$$= \frac{r^{2(n-1)/(n+1)}Ro^{n-1}}{R^{(n-1)(n+1)/2}} \left\{ \frac{rr^{2(1-n)/(n+1)}(\mu V')'Ro}{R^{(n+1)/2}} + r^{2(1-n)/(n+1)} \left(\mu' \frac{\partial v}{\partial \eta} + \mu \frac{\partial^2 v}{\partial \eta^2} \right) \right.$$

$$\left. + r^{2(1-n)/(n+1)} \left[\hat{\mu} V' \left(U' \frac{\partial u}{\partial \eta} + V' \frac{\partial v}{\partial \eta} \right) \right]' \right\},$$

$$= \frac{Ro^{n-1}}{R^{(n-1)(n+1)/2}} \left\{ \frac{r(\mu V')'Ro}{R^{(n+1)/2}} + \left(\mu' \frac{\partial v}{\partial \eta} + \mu \frac{\partial^2 v}{\partial \eta^2} \right) \right.$$

$$\left. + \left[\hat{\mu} V' \left(U' \frac{\partial u}{\partial \eta} + V' \frac{\partial v}{\partial \eta} \right) \right]' \right\},$$

$$\implies \frac{X_2 Ro^{n-1}}{R^{(2-n)(n+1)/2}} = \frac{r(\mu V')'Ro}{R^{(n+1)}} + \frac{1}{R^{(n+1)/2}} \frac{\partial}{\partial \eta} \left(\mu \frac{\partial v}{\partial \eta} + \hat{\mu} V' \left(U' \frac{\partial u}{\partial \eta} + V' \frac{\partial v}{\partial \eta} \right) \right).$$

Apply parallel-flow approximation, we have

$$R^{(n-1)/2} \left(\frac{\partial v}{\partial t} + U \frac{\partial v}{\partial r} \right) + \frac{Ro}{R} V \frac{\partial v}{\partial \theta} + \frac{Ro}{R} W \frac{\partial v}{\partial \eta} + \frac{Ro}{R} Uv + Ro^{(n-1)/(n+1)} V' w$$

$$+ \left(2 \frac{Ro}{R} V + \frac{Co}{R} \right) u + \frac{Ro}{R} \eta \frac{(1-n)}{(n+1)} \left(U \frac{\partial v}{\partial \eta} + V' u \right)$$

$$= -\frac{Ro}{R} \frac{\partial p}{\partial \theta} + \frac{Ro^{n-1}}{R} \frac{\partial}{\partial \eta} \left(\mu \frac{\partial v}{\partial \eta} + \hat{\mu} V' \left(U' \frac{\partial u}{\partial \eta} + V' \frac{\partial v}{\partial \eta} \right) \right). \quad \text{(A.11)}$$

The *z*-momentum equation becomes

$$\frac{\partial}{\partial t} \left[\frac{r^{(n-1)/(n+1)}RoW(\eta)}{R^{(n+1)/2}} + w(r,\eta,\theta,t) \right] + \left[\frac{rRoU(\eta)}{R^{(n+1)/2}} + u(r,\eta,\theta,t) \right]$$

$$\times \frac{\partial}{\partial r} \left[\frac{r^{(n-1)/(n+1)}RoW(\eta)}{R^{(n+1)/2}} + w(r,\eta,\theta,t) \right]$$

$$+ \frac{1}{r} \left[\frac{rRoV(\eta)}{R^{(n+1)/2}} + v(r,\eta,\theta,t) \right] \frac{\partial}{\partial \theta} \left[\frac{r^{(n-1)/(n+1)}RoW(\eta)}{R^{(n+1)/2}} + w(r,\eta,\theta,t) \right]$$

$$+ \left[\frac{r^{(n-1)/(n+1)}RoW(\eta)}{R^{(n+1)/2}} + w(r,\eta,\theta,t) \right] \frac{\partial}{\partial z} \left[\frac{r^{(n-1)/(n+1)}RoW(\eta)}{R^{(n+1)/2}} + w(r,\eta,\theta,t) \right]$$

$$= -\frac{\partial}{\partial z} \left[\frac{r^{2(n-1)/(n+1)}Ro^2 P(\eta)}{R^{n+1}} + p(r,\eta,\theta,t) \right] + \frac{X_3}{R^{(2-n)(n+1)/2}},$$

$$\implies \frac{\partial w}{\partial t} + \frac{r^{(n-1)/(n+1)}Ro^2}{R^{n+1}}\frac{1-n}{n+1}\left[U\left(\eta W' - W\right)\right] + \frac{rURo}{R^{(n+1)/2}}\frac{\partial w}{\partial r} + \frac{\eta Ro}{R^{(n+1)/2}}\frac{1-n}{n+1}U\frac{\partial w}{\partial \eta}$$

$$+ \frac{r^{(n-1)/(n+1)}Ro}{rR^{(n+1)/2}}\frac{1-n}{n+1}[u(\eta W' - W)] + \frac{VRo}{R^{(n+1)/2}}\frac{\partial w}{\partial \theta} + \frac{r^{(n-1)/(n+1)}WW'Ro^2}{R^{n+1}} + \frac{WRo}{R^{(n+1)/2}}\frac{\partial w}{\partial \eta}$$

$$+ \frac{W'wRo}{R^{(n+1)/2}} = -\frac{r^{(n-1)/(n+1)}P'Ro^2}{R^{n+1}} - r^{(1-n)/(n+1)}\frac{\partial p}{\partial \eta} + \frac{X_3}{R^{(2-n)(n+1)/2}},$$

where

$$X_3 = \frac{\partial}{\partial z}\left(\frac{r^{2(n-1)/(n+1)}Ro^{n-1}}{R^{(n-1)(n+1)/2}}\left(\mu + \frac{R^{(n+1)/2}}{rRo}\hat{\mu}U'\frac{\partial u}{\partial \eta} + \frac{R^{(n+1)/2}}{rRo}\hat{\mu}V'\frac{\partial v}{\partial \eta}\right)\right.$$

$$\left. \times \left\{\frac{\partial}{\partial z}\left[\frac{r^{(n-1)/(n+1)}W(\eta)Ro}{R^{(n+1)/2}} + w(r,\eta,\theta,t)\right]\right\}\right)$$

$$= \frac{r^{2(n-1)/(n+1)}Ro^{n-1}}{R^{(n-1)(n+1)/2}}\frac{\partial}{\partial z}\left[\left(\mu + \frac{R^{(n+1)/2}}{rRo}\hat{\mu}U'\frac{\partial u}{\partial \eta} + \frac{R^{(n+1)/2}}{rRo}\hat{\mu}V'\frac{\partial v}{\partial \eta}\right)\right.$$

$$\left. \times \left(\frac{W'Ro}{R^{(n+1)/2}} + r^{(1-n)/(n+1)}\frac{\partial w}{\partial \eta}\right)\right],$$

$$= \frac{r^{2(n-1)/(n+1)}Ro^{n-1}}{R^{(n-1)(n+1)/2}}\frac{\partial}{\partial z}\left[\frac{\mu W'Ro}{R^{(n+1)/2}} + r^{(1-n)/(n+1)}\mu\frac{\partial w}{\partial \eta} + \frac{\hat{\mu}W'}{r}\left(U'\frac{\partial u}{\partial \eta} + V'\frac{\partial v}{\partial \eta}\right)\right],$$

$$= \frac{r^{(n-1)/(n+1)}Ro^{n-1}}{R^{(n-1)(n+1)/2}}\left\{\frac{(\mu W')'Ro}{R^{(n+1)/2}} + r^{(1-n)/(n+1)}\left(\mu'\frac{\partial w}{\partial \eta} + \mu\frac{\partial^2 w}{\partial \eta^2}\right)\right.$$

$$\left. + \left[\frac{\hat{\mu}W'}{r}\left(U'\frac{\partial u}{\partial \eta} + V'\frac{\partial v}{\partial \eta}\right)\right]'\right\},$$

$$= \frac{Ro^{n-1}}{R^{(n-1)(n+1)/2}}\left\{\frac{r^{(n-1)/(n+1)}(\mu W')'Ro}{R^{(n+1)/2}} + \left(\mu'\frac{\partial w}{\partial \eta} + \mu\frac{\partial^2 w}{\partial \eta^2}\right)\right.$$

$$\left. + \frac{r^{(n-1)/(n+1)}}{r}\left[\hat{\mu}W'\left(U'\frac{\partial u}{\partial \eta} + V'\frac{\partial v}{\partial \eta}\right)\right]'\right\},$$

$$\implies \frac{X_3 Ro^{n-1}}{R^{(2-n)(n+1)/2}} = \frac{r^{(n-1)/(n+1)}(\mu W')'Ro}{R^{(n+1)}} + \frac{1}{R^{(n+1)/2}}\frac{\partial}{\partial \eta}\left(\mu\frac{\partial w}{\partial \eta}\right)$$

$$+ \frac{r^{(n-1)/(n+1)}}{rR^{(n+1)/2}}\left[\hat{\mu}W'\left(U'\frac{\partial u}{\partial \eta} + V'\frac{\partial v}{\partial \eta}\right)\right]'.$$

Apply parallel-flow approximation, we have

$$R^{(n-1)/2}\left(\frac{\partial w}{\partial t}+U\frac{\partial w}{\partial r}\right)+\frac{Ro}{R}V\frac{\partial w}{\partial\theta}+\frac{Ro}{R}W\frac{\partial w}{\partial\eta}+\frac{Ro}{R}W'w$$

$$+\frac{Ro}{R}\eta\frac{(1-n)}{(n+1)}U\frac{\partial w}{\partial\eta}=-Ro^{(n-1)/(n+1)}\frac{\partial p}{\partial\eta}+\frac{Ro^{n-1}}{R}\frac{\partial}{\partial\eta}\left(\mu\frac{\partial w}{\partial\eta}\right)=0. \quad \text{(A.12)}$$

It has been necessary to set each factor Ro^j that appear in disturbance equations to unity, where j is some expression involving $n-1$. This approximation is necessary to ensure the continuity as Ro is varied from -1 to 1. Then the continuity equation A.8 and the linear disturbance equations A.9, A.11 and A.12 become

$$R^{(n-1)/2}\frac{\partial u}{\partial r}+\frac{Ro}{R}\left[\eta\frac{(1-n)}{(n+1)}\frac{\partial u}{\partial\eta}+u+\frac{\partial v}{\partial\theta}\right]+\frac{\partial w}{\partial\eta}=0, \quad \text{(A.13a)}$$

$$R^{(n-1)/2}\left(\frac{\partial u}{\partial t}+U\frac{\partial u}{\partial r}\right)+\frac{Ro}{R}\left(V\frac{\partial u}{\partial\theta}+W\frac{\partial u}{\partial\eta}+Uu\right)+U'w$$

$$-\frac{(2RoV+Co)v}{R}+\frac{Ro}{R}\eta\frac{(1-n)}{(n+1)}\left(U\frac{\partial u}{\partial\eta}+U'u+\frac{\partial p}{\partial\eta}\right)$$

$$=-R^{(n-1)/2}\frac{\partial p}{\partial r}+\frac{1}{R}\frac{\partial}{\partial\eta}\left[\mu\frac{\partial u}{\partial\eta}+\hat{\mu}\left(U'\frac{\partial u}{\partial\eta}+V'\frac{\partial v}{\partial\eta}\right)U'\right], \quad \text{(A.13b)}$$

$$R^{(n-1)/2}\left(\frac{\partial v}{\partial t}+U\frac{\partial v}{\partial r}\right)+\frac{Ro}{R}V\frac{\partial v}{\partial\theta}+\frac{Ro}{R}W\frac{\partial v}{\partial\eta}+\frac{Ro}{R}Uv+V'w$$

$$+\left(2\frac{Ro}{R}V+\frac{Co}{R}\right)u+\frac{Ro}{R}\eta\frac{(1-n)}{(n+1)}\left(U\frac{\partial v}{\partial\eta}+V'u\right)$$

$$=-\frac{Ro}{R}\frac{\partial p}{\partial\theta}+\frac{1}{R}\frac{\partial}{\partial\eta}\left[\mu\frac{\partial v}{\partial\eta}+\hat{\mu}\left(U'\frac{\partial u}{\partial\eta}+V'\frac{\partial v}{\partial\eta}\right)V'\right], \quad \text{(A.13c)}$$

$$R^{(n-1)/2}\left(\frac{\partial w}{\partial t}+U\frac{\partial w}{\partial r}\right)+\frac{Ro}{R}V\frac{\partial w}{\partial\theta}+\frac{Ro}{R}W\frac{\partial w}{\partial\eta}+\frac{Ro}{R}W'w$$

$$+\frac{Ro}{R}\eta\frac{(1-n)}{(n+1)}U\frac{\partial w}{\partial\eta}=-\frac{\partial p}{\partial\eta}+\frac{1}{R}\frac{\partial}{\partial\eta}\left(\mu\frac{\partial w}{\partial\eta}\right)=0. \quad \text{(A.13d)}$$

Assume the disturbances have the normal mode form:

$$u = \hat{u}(\eta;\alpha,\beta,\omega;R,Ro)e^{i(\alpha r+\widetilde{\beta}\theta-\omega t)}, \tag{A.14a}$$

$$v = \hat{v}(\eta;\alpha,\beta,\omega;R,Ro)e^{i(\alpha r+\widetilde{\beta}\theta-\omega t)}, \tag{A.14b}$$

$$w = \hat{w}(\eta;\alpha,\beta,\omega;R,Ro)e^{i(\alpha r+\widetilde{\beta}\theta-\omega t)}, \tag{A.14c}$$

$$p = \hat{p}(\eta;\alpha,\beta,\omega;R,Ro)e^{i(\alpha r+\widetilde{\beta}\theta-\omega t)}. \tag{A.14d}$$

where $\widetilde{\beta} = \beta/Ro$.

Set $\omega = 0$ so that

$$\bar{\alpha}(i\hat{u}) + \frac{Ro}{R}\left(\hat{u}+\eta\frac{(1-n)}{(n+1)}\hat{u}'\right) + i\bar{\beta}\hat{v} + \hat{w}' = 0,$$

$$\left(i\bar{\alpha}U + i\bar{\beta}V + \frac{Ro}{R}U\right)\hat{u} + \frac{Ro}{R}W\hat{u}' - \frac{(2RoV+Co)\hat{v}}{R} + U'\hat{w} + \frac{Ro}{R}\eta\frac{(1-n)}{(n+1)}\left(U\hat{u}'+U'\hat{u}+\hat{p}'\right)$$

$$= -i\bar{\alpha}\hat{p} + \frac{1}{R}\{\mu\hat{u}'' + \mu'\hat{u}' + \hat{u}'[\hat{\mu}'U'U' + \hat{\mu}(U'U''+U'U'')] + \hat{v}'[\hat{\mu}'U'V' + \hat{\mu}(V'U''+U'V'')]$$

$$+ \hat{u}''\hat{\mu}U'U' + \hat{v}''\hat{\mu}U'V'\},$$

$$\left(i\bar{\alpha}U + i\bar{\beta}V + \frac{Ro}{R}U\right)\hat{v} + \frac{Ro}{R}W\hat{v}' + \frac{(2RoV+Co)\hat{u}}{R} + V'\hat{w} + \frac{Ro}{R}\eta\frac{(1-n)}{(n+1)}\left(U\frac{\partial\hat{v}}{\partial\eta}+V'\hat{u}\right)$$

$$= -i\bar{\beta}\hat{p} + \frac{1}{R}\{\mu\hat{v}'' + \mu'\hat{v}' + \hat{u}'[\hat{\mu}'U'V' + \hat{\mu}(U'V''+V'U'')] + \hat{v}'[\hat{\mu}'V'V' + \hat{\mu}(V'V''+V'V'')]$$

$$+ \hat{u}''\hat{\mu}U'V' + \hat{v}''\hat{\mu}V'V'\},$$

$$\left(i\bar{\alpha}U + i\bar{\beta}V + \frac{Ro}{R}W'\right)\hat{w} + \frac{Ro}{R}\left(W+\eta\frac{(1-n)}{(n+1)}U\right)\hat{w}' = -\hat{p}' + \frac{1}{R}\{\mu\hat{w}''+\mu'\hat{w}'\}.$$

Rearranging the equations in a way that it makes easy to solve by using the Chebyshev spectral method as in the following form

$$\bar{\alpha}(i\hat{u}) + \frac{Ro}{R}\left(\hat{u}+\hat{\eta}\hat{u}'\right) + i\bar{\beta}\hat{v} + \hat{w}' = 0, \tag{A.15a}$$

$$\bar{\alpha}\left[i\left(U\hat{u}+\hat{p}\right)\right] + r_0 = 0, \tag{A.15b}$$

$$\bar{\alpha}(iU\hat{v}) + \theta_0 = 0, \tag{A.15c}$$

$$\bar{\alpha}(iU\hat{w}) + z_0 = 0. \tag{A.15d}$$

Here

$$
\begin{aligned}
r_0 &= \left[\mathrm{i}\bar{\beta}V + \frac{Ro}{R}\left(U + \hat{\eta}U'\right)\right]\hat{u} + \frac{1}{R}\left(RoW + Ro\hat{\eta}U - \mu' - \hat{\mu}'\left(U'\right)^2 - 2\hat{\mu}U'U''\right)\hat{u}' \\
&\quad - \frac{(2RoV + Co)}{R}\hat{v} - \frac{1}{R}\left[\hat{\mu}'U'V' + \hat{\mu}\left(U'V'' + V'U''\right)\right]\hat{v}' - \frac{1}{R}\left[\mu + \hat{\mu}\left(U'\right)^2\right]\hat{u}'' \\
&\quad - \frac{1}{R}\left(\hat{\mu}U'V'\right)\hat{v}'' + U'\hat{w} + \left(\frac{Ro}{R}\hat{\eta}\right)\hat{p}, \\
\theta_0 &= \left[\frac{(2RoV + Co)}{R} + Ro\hat{\eta}V'\right]\hat{u} - \frac{1}{R}\left[\hat{\mu}'U'V' + \hat{\mu}\left(U'V'' + V'U''\right)\right]\hat{u}' + \left(\mathrm{i}\bar{\beta}V + \frac{Ro}{R}U\right)\hat{v} \\
&\quad + \frac{1}{R}\left[RoW + Ro\hat{\eta}U - \mu' - \hat{\mu}'\left(V'\right)^2 - 2\hat{\mu}V'V''\right]\hat{v}' - \frac{1}{R}\left(\hat{\mu}U'V'\right)\hat{u}'' \\
&\quad - \frac{1}{R}\left[\mu + \hat{\mu}\left(V'\right)^2\right]\hat{v}'' + V'\hat{w} + \mathrm{i}\bar{\beta}\hat{p}, \\
z_0 &= \left(\mathrm{i}\bar{\beta}V + \frac{Ro}{R}W'\right)\hat{w} + \frac{1}{R}\left(RoW + Ro\hat{\eta}U - \mu'\right)\hat{w}' - \frac{\mu}{R}\hat{w}'' + \hat{p}',
\end{aligned}
$$

where $\hat{\eta} = \eta \frac{(1-n)}{(n+1)}$ and $\hat{\mu} = \frac{(n-1)\mu}{U'^2 + V'^2}$.

A.2   Carreau fluids

The non-dimensionalising velocity, pressure and time scales for Carreau fluids are similar to those for Power-law fluids given in A.1. The local Reynolds number is defined as:

$$
R = \frac{r_a^*\triangle\Omega^* L^*}{\nu^*} = \frac{r_a^* Ro\Omega^* L^*}{\nu^*} = \frac{r_a^* Ro}{L^*} = r_a Ro. \tag{A.16}
$$

Therefore the governing boundary-layer equations (3.4) and the viscosity function (3.11) become

$$\frac{1}{r}\frac{\partial (rU_0)}{\partial r} + \frac{1}{r}\frac{\partial V_0}{\partial \theta} + \frac{\partial W_0}{\partial z} = 0, \tag{A.17}$$

$$\frac{\partial U_0}{\partial t} + U_0\frac{\partial U_0}{\partial r} + \frac{V_0}{r}\frac{\partial U_0}{\partial \theta} + W_0\frac{\partial U_0}{\partial z} - \frac{V_0^2}{r} - \frac{CoV_0}{R} = -\frac{\partial P_0}{\partial r} + \frac{1}{R}\left[\frac{\partial}{\partial z}\left(\mu_0\frac{\partial U_0}{\partial z}\right)\right], \tag{A.18}$$

$$\frac{\partial V_0}{\partial t} + U_0\frac{\partial V_0}{\partial r} + \frac{V_0}{r}\frac{\partial V_0}{\partial \theta} + W_0\frac{\partial V_0}{\partial z} + \frac{U_0V_0}{r} + \frac{CoU_0}{R} = -\frac{1}{r}\frac{\partial P_0}{\partial \theta} + \frac{1}{R}\left[\frac{\partial}{\partial z}\left(\mu_0\frac{\partial V_0}{\partial z}\right)\right], \tag{A.19}$$

$$\frac{\partial W_0}{\partial t} + U_0\frac{\partial W_0}{\partial r} + \frac{V_0}{r}\frac{\partial W_0}{\partial \theta} + W_0\frac{\partial W_0}{\partial z} = -\frac{\partial P_1}{\partial z} + \frac{1}{R}\left[\frac{1}{r}\frac{\partial}{\partial r}\left(\mu_0 r\frac{\partial U_0}{\partial z}\right)\right.$$
$$\left.\frac{1}{r}\frac{\partial}{\partial \theta}\left(\mu_0\frac{\partial V_0}{\partial z}\right) + \frac{\partial}{\partial z}\left(2\mu_0\frac{\partial W_0}{\partial z}\right)\right], \tag{A.20}$$

where

$$\mu_0 = \left\{1 + \frac{k^2 R^2}{r^2 Ro^2}\left[\left(\frac{\partial U}{\partial z}\right)^2 + \left(\frac{\partial V}{\partial z}\right)^2\right]\right\}^{(n-1)/2}. \tag{A.21}$$

The instantaneous non-dimensional velocities and pressure are given by

$$\begin{aligned}
U_0(r,z,\theta,t) &= \frac{rRo}{R}U(z) + u(r,z,\theta,t), \\
V_0(r,z,\theta,t) &= \frac{rRo}{R}V(z) + v(r,z,\theta,t), \\
W_0(r,z,\theta,t) &= \frac{Ro}{R}W(z) + w(r,z,\theta,t), \\
P_1(r,,\theta,t) &= \frac{Ro^2}{R^2}P(z) + p(r,z,\theta,t).
\end{aligned}$$

The continuity equation becomes

$$\frac{1}{r}\frac{\partial}{\partial r}\left[\frac{r^2 RoU(z)}{R} + ru(r,z,\theta,t)\right] + \frac{1}{r}\frac{\partial}{\partial \theta}\left[\frac{rRoV(z)}{R} + v(r,z,\theta,t)\right] + \frac{\partial}{\partial z}\left[\frac{RoW(z)}{R} + w(r,z,\theta,t)\right] = 0,$$

$$\implies \frac{1}{r}\frac{\partial (ru)}{\partial r} + \frac{1}{r}\frac{\partial v}{\partial \theta} + \frac{\partial w}{\partial z} = 0.$$

We have

$$\frac{\partial u}{\partial r} + \frac{Ro}{R}u + \frac{Ro}{R}\frac{\partial v}{\partial \theta} + \frac{\partial w}{\partial z} = 0. \tag{A.23}$$

The viscosity function becomes

$$
\begin{aligned}
\mu_0 &= \left[1 + \frac{k^2 R^2}{r^2 Ro^2} \left(\left\{ \frac{\partial}{\partial z}\left[\frac{rRoU(z)}{R} + u(r,z,\theta,t) \right] \right\}^2 + \left\{ \frac{\partial}{\partial z}\left[\frac{rRoV(z)}{R} + v(r,z,\theta,t) \right] \right\}^2 \right) \right]^{(n-1)/2}, \\
&= \left\{ 1 + \frac{k^2 R^2}{r^2 Ro^2}\left[\left(\frac{rRoU'}{R} + \frac{\partial u}{\partial z} \right)^2 + \left(\frac{rRoV'}{R} + \frac{\partial v}{\partial z} \right)^2 \right] \right\}^{(n-1)/2}, \\
&= \left\{ 1 + \frac{k^2 R^2}{r^2 Ro^2}\left[\left(\frac{r^2 Ro^2 (U')^2}{R^2} + \frac{2rRoU'}{R}\frac{\partial u}{\partial z} \right) + \left(\frac{r^2 Ro^2 (V')^2}{R^2} + \frac{2rRoV'}{R}\frac{\partial v}{\partial z} \right) \right] \right\}^{(n-1)/2}, \\
&= \left\{ 1 + k^2[(U')^2 + (V')^2] + \frac{2k^2 R}{rRo}\left(U'\frac{\partial u}{\partial z} + V'\frac{\partial v}{\partial z} \right) \right\}^{(n-1)/2}, \\
&= \{ 1 + k^2[(U')^2 + (V')^2] \}^{(n-1)/2}\left(1 + \frac{2k^2 R}{rRo\{1 + k^2[(U')^2 + (V')^2]\}}\left(U'\frac{\partial u}{\partial z} + V'\frac{\partial v}{\partial z} \right) \right)^{(n-1)/2}, \\
&= \{ 1 + k^2[(U')^2 + (V')^2] \}^{(n-1)/2}\left(1 + \frac{(n-1)k^2 R}{rRo\{1 + k^2[(U')^2 + (V')^2]\}}\left(U'\frac{\partial u}{\partial z} + V'\frac{\partial v}{\partial z} \right) \right), \\
&= \mu + \frac{k^2(n-1)\mu R}{rRo\{1 + k^2[(U')^2 + (V')^2]\}}\left(U'\frac{\partial u}{\partial z} + V'\frac{\partial v}{\partial z} \right), \\
&= \mu + \frac{k^2(n-1)\mu U' R}{Ro\{1 + k^2[(U')^2 + (V')^2]\}}\frac{1}{r}\frac{\partial u}{\partial z} + \frac{k^2(n-1)\mu V' R}{Ro\{1 + k^2[(U')^2 + (V')^2]\}}\frac{1}{r}\frac{\partial v}{\partial z}, \\
&= \mu + \frac{R}{rRo}\hat{\mu}U'\frac{\partial u}{\partial z} + \frac{R}{rRo}\hat{\mu}V'\frac{\partial v}{\partial z},
\end{aligned}
$$

where

$$\hat{\mu} = \frac{k^2(n-1)\mu}{\{1 + k^2[(U')^2 + (V')^2]\}} = k^2(n-1)\{1 + k^2[(U')^2 + (V')^2]\}^{(n-3)/2}.$$

The derivatives of the viscosity and disturbance viscosity functions are given by

$$\frac{\partial \mu}{\partial z} = \mu',$$

$$\frac{\partial \hat{\mu}}{\partial z} = \frac{k^2(n-3)\mu'}{\{1+k^2[(U')^2+(V')^2]\}},$$

$$\frac{\partial \mu}{\partial r} = \frac{1}{r}\frac{k^2(n-1)\mu[(U')^2+(V')^2]}{\{1+k^2[(U')^2+(V')^2]\}},$$

$$\frac{\partial \hat{\mu}}{\partial r} = \frac{2}{r}\frac{k^2(n-1)\mu}{\{1+k^2[(U')^2+(V')^2]\}} + \frac{1}{r}\frac{k^2(n-3)\mu'[(U')^2+(V')^2]}{(U'U''+V'V'')\{1+k^2[(U')^2+(V')^2]\}}.$$

The r-momentum equation becomes

$$\frac{\partial}{\partial t}\left[\frac{rRoU(z)}{R}+u(r,z,\theta,t)\right] + \left[\frac{rRoU(z)}{R}+u(r,z,\theta,t)\right]\frac{\partial}{\partial r}\left[\frac{rRoU(z)}{R}+u(r,z,\theta,t)\right]$$

$$+\frac{1}{r}\left[\frac{rRoV(z)}{R}+v(r,z,\theta,t)\right]\frac{\partial}{\partial \theta}\left[\frac{rRoU(z)}{R}+u(r,z,\theta,t)\right]$$

$$+\left[\frac{RoW(z)}{R}+w(r,z,\theta,t)\right]\frac{\partial}{\partial z}\left[\frac{rRoU(z)}{R}+u(r,z,\theta,t)\right]$$

$$-\frac{1}{r}\left[\frac{rRoV(z)}{R}+v(r,z,\theta,t)\right]^2 - \frac{Co}{R}\left[\frac{rRoV(z)}{R}+v(r,z,\theta,t)\right]$$

$$=-\frac{\partial}{\partial r}\left[\frac{Ro^2P(z)}{R^2}+p(r,z,\theta,t)\right]+\frac{X_1}{R},$$

$$\implies \frac{\partial u}{\partial t}+\frac{rU^2Ro^2}{R^2}+\frac{rURo}{R}\frac{\partial u}{\partial r}+\frac{RoUu}{R}$$

$$+\frac{VRo}{R}\frac{\partial u}{\partial \theta}+\frac{rU'WRo^2}{R^2}+\frac{WRo}{R}\frac{\partial u}{\partial z}+\frac{rRoU'w}{R}-\frac{rV^2Ro^2}{R^2}-\frac{2VvRo}{R}-\frac{Cov}{R}$$

$$=-\frac{\partial p}{\partial r}+\frac{X_1}{R}.$$

where

$$X_1 = \frac{\partial}{\partial z}\left(\left(\mu + \frac{R}{rRo}\hat{\mu}U'\frac{\partial u}{\partial z} + \frac{R}{rRo}\hat{\mu}V'\frac{\partial v}{\partial z}\right)\left\{\frac{\partial}{\partial z}\left[\frac{rRoU(z)}{R} + u(r,z,\theta,t)\right]\right\}\right),$$

$$= \frac{\partial}{\partial z}\left\{\left(\mu + \frac{R}{rRo}\hat{\mu}U'\frac{\partial u}{\partial z} + \frac{R}{rRo}\hat{\mu}V'\frac{\partial v}{\partial z}\right)\left[\frac{rRoU'}{R} + \frac{\partial u}{\partial z}\right]\right\},$$

$$= \frac{\partial}{\partial z}\left[\frac{rRo\mu U'}{R} + \mu\left(\frac{\partial u}{\partial z}\right) + \hat{\mu}U'\left(U'\frac{\partial u}{\partial z} + V'\frac{\partial v}{\partial z}\right)\right],$$

$$= \frac{rRo(\mu U')'}{R} + \mu\left(\frac{\partial^2 u}{\partial z^2}\right) + \mu'\left(\frac{\partial u}{\partial z}\right) + \frac{k^2(n-3)\mu'}{\{1+k^2[(U')^2+(V')^2]\}}U'\left(U'\frac{\partial u}{\partial z} + V'\frac{\partial v}{\partial z}\right)$$

$$+ \frac{k^2(n-1)\mu}{\{1+k^2[(U')^2+(V')^2]\}}U''\left(U'\frac{\partial u}{\partial z} + V'\frac{\partial v}{\partial z}\right) + \frac{k^2(n-1)\mu}{\{1+k^2[(U')^2+(V')^2]\}}U'\left(U'\frac{\partial u}{\partial z} + V'\frac{\partial v}{\partial z}\right)',$$

$$= \frac{rRo(\mu U')'}{R} + \mu\left(\frac{\partial^2 u}{\partial z^2}\right) + \mu'\left(\frac{\partial u}{\partial z}\right) + \frac{k^2[(n-1)\mu U'' + (n-3)\mu'U']}{\{1+k^2[(U')^2+(V')^2]\}}\left(U'\frac{\partial u}{\partial z} + V'\frac{\partial v}{\partial z}\right)$$

$$+ \frac{k^2(n-1)\mu}{\{1+k^2[(U')^2+(V')^2]\}}U'\left(U'\frac{\partial u}{\partial z} + V'\frac{\partial v}{\partial z}\right)',$$

$$\implies \frac{X_1}{R} = \frac{rRo(\mu U')'}{R^2} + \frac{1}{R}\frac{\partial}{\partial z}\left[\mu\frac{\partial u}{\partial z} + \hat{\mu}U'\left(U'\frac{\partial u}{\partial z} + V'\frac{\partial v}{\partial z}\right)\right].$$

Apply parallel-flow approximation, we have

$$\frac{\partial u}{\partial t} + U\frac{\partial u}{\partial r} + \frac{Ro}{R}V\frac{\partial u}{\partial \theta} + \frac{Ro}{R}W\frac{\partial u}{\partial z} + \frac{Ro}{R}Uu + U'w$$
$$- \left(2\frac{Ro}{R}V + \frac{Co}{R}\right)v = -\frac{\partial p}{\partial r} + \frac{1}{R}\frac{\partial}{\partial z}\left[\mu\frac{\partial u}{\partial z} + \hat{\mu}U'\left(U'\frac{\partial u}{\partial z} + V'\frac{\partial v}{\partial z}\right)\right], \quad \text{(A.24)}$$

where

$$\hat{\mu} = \frac{k^2(n-1)\mu}{\{1+k^2[(U')^2+(V')^2]\}}. \quad \text{(A.25)}$$

The θ-momentum equation becomes

$$\frac{\partial}{\partial t}\left[\frac{rRoV(z)}{R}+v(r,z,\theta,t)\right]+\left[\frac{rRoU(z)}{R}+u(r,z,\theta,t)\right]\frac{\partial}{\partial r}\left[\frac{rRoV(z)}{R}+v(r,z,\theta,t)\right]$$

$$+\frac{1}{r}\left[\frac{rRoV(z)}{R}+v(r,z,\theta,t)\right]\frac{\partial}{\partial\theta}\left[\frac{rRoV(z)}{R}+v(r,z,\theta,t)\right]$$

$$+\left[\frac{RoW(z)}{R}+w(r,z,\theta,t)\right]\frac{\partial}{\partial z}\left[\frac{rRoV(z)}{R}+v(r,z,\theta,t)\right]$$

$$+\frac{1}{r}\left[\frac{rRoU(z)}{R}+u(r,z,\theta,t)\right]\left[\frac{rRoV(z)}{R}+v(r,z,\theta,t)\right]+\frac{Co}{R}\left[\frac{rRoU(z)}{R}+u(r,z,\theta,t)\right]$$

$$=-\frac{1}{r}\frac{\partial}{\partial\theta}\left[\frac{Ro^2P(z)}{R^2}+p(r,z,\theta,t)\right]+\frac{X_2}{R},$$

$$\Longrightarrow\frac{\partial v}{\partial t}+\frac{rUVRo^2}{R^2}+\frac{rURo}{R}\frac{\partial v}{\partial r}+\frac{RoVu}{R}$$

$$+\frac{VRo}{R}\frac{\partial v}{\partial\theta}+\frac{rV'WRo^2}{R^2}+\frac{RoW}{R}\frac{\partial v}{\partial z}+\frac{rV'wRo}{R}+\frac{rUVRo^2}{R^2}+\frac{Ro\,(Uv+Vu)}{R}+\frac{rCoRoU}{R^2}+\frac{Cou}{R}$$

$$=-\frac{1}{r}\frac{\partial p}{\partial\theta}+\frac{X_2}{R},$$

where

$$X_2=\frac{\partial}{\partial z}\left(\left(\mu+\frac{R}{rRo}\hat{\mu}U'\frac{\partial u}{\partial z}+\frac{R}{r}\hat{\mu}V'\frac{\partial v}{\partial z}\right)\left\{\frac{\partial}{\partial z}\left[\frac{rRoV(z)}{R}+v(r,z,\theta,t)\right]\right.\right.$$

$$\left.\left.+\frac{1}{r}\frac{\partial}{\partial\theta}\left[\frac{RoW(z)}{R}+w(r,z,\theta,t)\right]\right\}\right)$$

$$=\frac{\partial}{\partial z}\left[\left(\mu+\frac{R}{rRo}\hat{\mu}U'\frac{\partial u}{\partial z}+\frac{R}{rRo}\hat{\mu}V'\frac{\partial v}{\partial z}\right)\left(\frac{rRoV'}{R}+\frac{\partial v}{\partial z}+\frac{1}{r}\frac{\partial w}{\partial\theta}\right)\right],$$

$$=\frac{\partial}{\partial z}\left[\frac{rRo\mu V'}{R}+\mu\frac{\partial v}{\partial z}+\frac{\mu}{r}\frac{\partial w}{\partial\theta}+\hat{\mu}V'\left(U'\frac{\partial u}{\partial z}+V'\frac{\partial v}{\partial z}\right)\right],$$

$$=\frac{rRo(\mu V')'}{R}+\mu\frac{\partial^2 v}{\partial z^2}+\mu'\frac{\partial v}{\partial z}+\frac{\mu}{r}\frac{\partial^2 w}{\partial\theta\partial z}+\frac{\mu'}{r}\frac{\partial w}{\partial\theta}$$

$$+\frac{k^2[(n-1)\mu V''+(n-3)\mu'V']}{r\{1+k^2[(U')^2+(V')^2]\}}\left(U'\frac{\partial u}{\partial z}+V'\frac{\partial v}{\partial z}\right)$$

$$+\frac{k^2(n-1)\mu}{r\{1+k^2[(U')^2+(V')^2]\}}V'\left(U'\frac{\partial u}{\partial z}+V'\frac{\partial v}{\partial z}\right)',$$

$$\Longrightarrow\frac{X_2}{R}=\frac{r(\mu V')'}{R^2}+\frac{\mu}{R}\frac{\partial^2 v}{\partial z^2}+\frac{\mu'}{R}\frac{\partial v}{\partial z}+\frac{\mu}{rR}\frac{\partial^2 w}{\partial\theta\partial z}+\frac{\mu'}{rR}\frac{\partial w}{\partial\theta}+\frac{1}{R}\frac{\partial}{\partial z}\left[\mu\frac{\partial v}{\partial z}+\hat{\mu}V'\left(U'\frac{\partial u}{\partial z}+V'\frac{\partial v}{\partial z}\right)\right],$$

Apply parallel-flow approximation, we have

$$
\frac{\partial v}{\partial t} + U\frac{\partial v}{\partial r} + \frac{Ro}{R}V\frac{\partial v}{\partial \theta} + \frac{Ro}{R}W\frac{\partial v}{\partial z} + \frac{Ro}{R}Uv + V'w
$$
$$
+ \left(2\frac{Ro}{R}V + \frac{Co}{R}\right)u = -\frac{Ro}{R}\frac{\partial p}{\partial \theta} + \frac{1}{R}\frac{\partial}{\partial z}\left(\mu\frac{\partial v}{\partial z} + \hat{\mu}V'\left(U'\frac{\partial u}{\partial z} + V'\frac{\partial v}{\partial z}\right)\right), \quad \text{(A.26)}
$$

The *z*-momentum equation becomes

$$
\frac{\partial}{\partial t}\left[\frac{RoW(z)}{R} + w(r,z,\theta,t)\right] + \left[\frac{rRoU(z)}{R} + u(r,z,\theta,t)\right]\frac{\partial}{\partial r}\left[\frac{RoW(z)}{R} + w(r,z,\theta,t)\right]
$$
$$
+ \frac{1}{r}\left[\frac{rRoV(z)}{R} + v(r,z,\theta,t)\right]\frac{\partial}{\partial \theta}\left[\frac{RoW(z)}{R} + w(r,z,\theta,t)\right]
$$
$$
+ \left[\frac{RoW(z)}{R} + w(r,z,\theta,t)\right]\frac{\partial}{\partial z}\left[\frac{RoW(z)}{R} + w(r,z,\theta,t)\right]
$$
$$
= -\frac{\partial}{\partial z}\left[\frac{Ro^2 P(z)}{R^2} + p(r,z,\theta,t)\right] + \frac{X_3}{R},
$$

$$
\implies \frac{\partial w}{\partial t} + \frac{rURo}{R}\frac{\partial w}{\partial r} + \frac{VRo}{R}\frac{\partial w}{\partial \theta} + \frac{WW'Ro^2}{R^2} + \frac{WRo}{R}\frac{\partial w}{\partial z} + \frac{W'wRo}{R} = -\frac{P'Ro^2}{R^2} - \frac{\partial p}{\partial z} + \frac{X_3}{R}
$$

where

$$
X_3 = \frac{\partial}{\partial z}\left(\left(\mu + \frac{R}{rRo}\hat{\mu}U'\frac{\partial u}{\partial z} + \frac{R}{rRo}\hat{\mu}V'\frac{\partial v}{\partial z}\right)\left\{\frac{\partial}{\partial z}\left[\frac{RoW(z)}{R} + w(r,z,\theta,t)\right]\right\}\right),
$$
$$
= \frac{\partial}{\partial z}\left[\left(\mu + \frac{R}{rRo}\hat{\mu}U'\frac{\partial u}{\partial z} + \frac{R}{rRo}\hat{\mu}V'\frac{\partial v}{\partial z}\right)\left(\frac{RoW'}{R} + \frac{\partial w}{\partial z}\right)\right],
$$
$$
= \frac{\partial}{\partial z}\left[\frac{Ro\mu W'}{R} + \mu\frac{\partial w}{\partial z} + \frac{k^2(n-1)\mu W'}{r\{1 + k^2[(U')^2 + (V')^2]\}}\left(U'\frac{\partial u}{\partial z} + V'\frac{\partial v}{\partial z}\right)\right],
$$
$$
= \frac{Ro(\mu W')'}{R} + \mu\frac{\partial^2 w}{\partial z^2} + \mu'\frac{\partial w}{\partial z} + \frac{k^2[(n-1)\mu W'' + (n-3)\mu'W']}{r\{1 + k^2[(U')^2 + (V')^2]\}}\left(U'\frac{\partial u}{\partial z} + V'\frac{\partial v}{\partial z}\right)
$$
$$
+ \frac{k^2(n-1)\mu}{r\{1 + k^2[(U')^2 + (V')^2]\}}W'\left(U'\frac{\partial u}{\partial z} + V'\frac{\partial v}{\partial z}\right)',
$$
$$
\implies \frac{X_3}{R} = \frac{(\mu W')'}{R^2} + \frac{\mu}{R}\frac{\partial^2 w}{\partial z^2} + \frac{\mu'}{R}\frac{\partial w}{\partial z} + \frac{1}{rR}\frac{\partial}{\partial z}\left[\hat{\mu}W'\left(U'\frac{\partial u}{\partial z} + V'\frac{\partial v}{\partial z}\right)\right].
$$

Apply parallel-flow approximation, we have

$$\frac{\partial w}{\partial t} + U\frac{\partial w}{\partial r} + \frac{Ro}{R}V\frac{\partial w}{\partial \theta} + \frac{Ro}{R}W\frac{\partial w}{\partial z} + \frac{Ro}{R}W'w = -\frac{\partial p}{\partial z} + \frac{1}{R}\frac{\partial}{\partial z}\left(\mu\frac{\partial w}{\partial z}\right).$$

Therefore, we have the following perturbation equations

$$\frac{\partial u}{\partial r} + \frac{Ro}{R}\left(u + \frac{\partial v}{\partial \theta}\right) + \frac{\partial w}{\partial z} = 0, \tag{A.27a}$$

$$\frac{\partial u}{\partial t} + U\frac{\partial u}{\partial r} + \frac{Ro}{R}\left(V\frac{\partial u}{\partial \theta} + W\frac{\partial u}{\partial z} + Uu\right) + U'w - \frac{(2RoV + Co)v}{R}$$
$$= -\frac{\partial p}{\partial r} + \frac{1}{R}\frac{\partial}{\partial z}\left[\mu\frac{\partial u}{\partial z} + \hat{\mu}U'\left(U'\frac{\partial \hat{u}}{\partial z} + V'\frac{\partial \hat{v}}{\partial z}\right)\right], \tag{A.27b}$$

$$\frac{\partial v}{\partial t} + U\frac{\partial v}{\partial r} + \frac{Ro}{R}V\frac{\partial v}{\partial \theta} + \frac{Ro}{R}W\frac{\partial v}{\partial z} + \frac{Ro}{R}Uv + V'w + \left(2\frac{Ro}{R}V + \frac{Co}{R}\right)u$$
$$= -\frac{Ro}{R}\frac{\partial p}{\partial \theta} + \frac{1}{R}\frac{\partial}{\partial z}\left[\mu\frac{\partial v}{\partial z} + \hat{\mu}V'\left(U'\frac{\partial \hat{u}}{\partial z} + V'\frac{\partial \hat{v}}{\partial z}\right)\right],$$

$$\frac{\partial w}{\partial t} + U\frac{\partial w}{\partial r} + \frac{Ro}{R}V\frac{\partial w}{\partial \theta} + \frac{Ro}{R}W\frac{\partial w}{\partial z} + \frac{Ro}{R}W'w = -\frac{\partial p}{\partial z} + \frac{1}{R}\frac{\partial}{\partial z}\left(\mu\frac{\partial w}{\partial z}\right). \tag{A.27c}$$

Assume the disturbances have the normal mode form:

$$u = \hat{u}(\eta;\alpha,\beta,\omega;R,Ro,k)e^{i(\alpha r + \widetilde{\beta}\theta - \omega t)}, \tag{A.28a}$$

$$v = \hat{v}(\eta;\alpha,\beta,\omega;R,Ro,k)e^{i(\alpha r + \widetilde{\beta}\theta - \omega t)}, \tag{A.28b}$$

$$w = \hat{w}(\eta;\alpha,\beta,\omega;R,Ro,k)e^{i(\alpha r + \widetilde{\beta}\theta - \omega t)}, \tag{A.28c}$$

$$p = \hat{p}(\eta;\alpha,\beta,\omega;R,Ro,k)e^{i(\alpha r + \widetilde{\beta}\theta - \omega t)}, \tag{A.28d}$$

where $\widetilde{\beta} = \beta/Ro$.

Set $\omega = 0$ so that

$$\alpha\left(i\hat{u}\right) + \frac{Ro}{R}\hat{u} + i\bar{\beta}\hat{v} + \hat{w}' = 0,$$

$$\left(i\alpha U + i\bar{\beta}V + \frac{Ro}{R}U\right)\hat{u} + \frac{Ro}{R}W\hat{u}' - \frac{(2RoV + Co)\hat{v}}{R} + U'\hat{w} = -i\bar{\alpha}\hat{p} + \frac{1}{R}\{\mu\hat{u}'' + \mu'\hat{u}'$$

$$+ \hat{u}'[\hat{\mu}'U'U' + \hat{\mu}(U'U'' + U'U'')] + \hat{v}'[\hat{\mu}'U'V' + \hat{\mu}(V'U'' + U'V'')]$$

$$+ \hat{u}''\hat{\mu}U'U' + \hat{v}''\hat{\mu}U'V'\},$$

$$\left(i\alpha U + i\bar{\beta}V + \frac{Ro}{R}U\right)\hat{v} + \frac{Ro}{R}W\hat{v}' + \frac{(2RoV + Co)\hat{u}}{R} + V'\hat{w} = -i\bar{\beta}\hat{p} + \frac{1}{R}\{\mu\hat{v}'' + \mu'\hat{v}'$$

$$+ \hat{u}'[\hat{\mu}'U'V' + \hat{\mu}(U'V'' + V'U'')] + \hat{v}'[\hat{\mu}'V'V' + \hat{\mu}(V'V'' + V'V'')]$$

$$+ \hat{u}''\hat{\mu}U'V' + \hat{v}''\hat{\mu}V'V'\},$$

$$\left(i\alpha U + i\bar{\beta}V + \frac{Ro}{R}W'\right)\hat{w} + \frac{Ro}{R}W\hat{w}' = -\hat{p}' + \frac{1}{R}\{\mu\hat{w}'' + \mu'\hat{w}'\}.$$

Rearranging the equations in a way that it makes easy to solve by using the Chebyshev spectral method as in the following form

$$\alpha\left(i\hat{u} + \frac{Ro}{R}\right)\hat{u} + i\bar{\beta}\hat{v} + \hat{w}' = 0, \tag{A.29a}$$

$$\alpha\left[i\left(U\hat{u} + \hat{p}\right)\right] + r_0 = 0, \tag{A.29b}$$

$$\alpha(iU\hat{v}) + \theta_0 = 0, \tag{A.29c}$$

$$\alpha\left(iU\hat{w}\right) + z_0 = 0. \tag{A.29d}$$

Here

$$r_0 = \left(i\bar{\beta}V + \frac{Ro}{R}U\right)\hat{u} + \frac{1}{R}\left[RoW - \mu' - \hat{\mu}'\left(U'\right)^2 - 2\hat{\mu}U'U''\right]\hat{u}' - \frac{(2RoV + Co)}{R}\hat{v}$$

$$-\frac{1}{R}\left[\hat{\mu}'U'V' + \hat{\mu}\left(U'V'' + V'U''\right)\right]\hat{v}' - \frac{1}{R}\left[\mu + \hat{\mu}\left(U'\right)^2\right]\hat{u}'' - \frac{1}{R}\left(\hat{\mu}U'V'\right)\hat{v}'' + U'\hat{w},$$

$$\theta_0 = \left[\frac{(2RoV + Co)}{R}\right]\hat{u} - \frac{1}{R}\left[\hat{\mu}'U'V' + \hat{\mu}\left(U'V'' + V'U''\right)\right]\hat{u}' + \left(i\bar{\beta}V + \frac{Ro}{R}U\right)\hat{v}$$

$$+\frac{1}{R}\left[RoW - \mu' - \hat{\mu}'\left(V'\right)^2 - 2\hat{\mu}V'V''\right]\hat{v}' - \frac{1}{R}\left(\hat{\mu}U'V'\right)\hat{u}'' - \frac{1}{R}\left[\mu + \hat{\mu}\left(V'\right)^2\right]\hat{v}''$$

$$+V'\hat{w} + i\bar{\beta}\hat{p},$$

$$z_0 = \left(i\bar{\beta}V + \frac{Ro}{R}W'\right)\hat{w} + \frac{1}{R}\left(RoW - \mu'\right)\hat{w}' - \frac{\mu}{R}\hat{w}'' + \hat{p}',$$

where $\hat{\eta} = \eta\frac{(1-n)}{(n+1)}$ and $\hat{\mu} = \frac{k^2(n-1)\mu}{\left\{1 + k^2[(U')^2 + (V')^2]\right\}}$.

Appendix B

Numerical method for solving perturbation equations

In this appendix we present an overview of the spectral methods in §B.1. The implementation of the Chebyshev collocation method and the eigenvalue problems for power-law and Carreau fluids are described in §B.2.

B.1 Fundamental background of the spectral methods

Spectral methods are considered as a general class of weighted residual methods where the approximation solutions are defined as a truncated series expansion (Peyret, 2013). The error or residual of the approximations should be zero.

The truncated series expansion of the function $u(x)$ defined on the interval $[a,b]$ is given by

$$u_N(x) = \sum_{k=0}^{N} \hat{c}_k \varphi_k(x), \quad a \leq x \leq b, \tag{B.1}$$

where $u_N(x)$ is the approximation solution, $\hat{c}_k$ is the expansion coefficient and $\varphi_k(x)$ is the

orthogonal basis functions.

For periodic problems, the trigonometric functions e^{ikx} are used as orthogonal basis functions while Chebyshev $T_k(x)$ or Legendre $L_k(x)$ polynomials are applied for non-periodic problems.

If the function $u(x)$ is given, then the residual is defined in the following form

$$R_N(x) = u - u_N. \tag{B.2}$$

If $u_N(x)$ is an approximate solution to the differential equation $\mathscr{L}u - f = 0$, then the residual R_N is given by

$$R_N(x) = \mathscr{L}u_N - f, \tag{B.3}$$

where $\mathscr{L}$ is a partial differential operator subject to the appropriate boundary conditions.

Now, the following scalar product is set to zero in order to force the residual to be approximately zero

$$(R_N, \psi_i)_{w_*} = \int_a^b R_N \psi_i w_* dx = 0, \quad i \in I_N. \tag{B.4}$$

Note that $\psi_i(x)$ are the weighting functions, w_* is the weight and I_N is the discrete set where its dimension is the number of the collocation points x_i. If the weighting functions ψ_i are complex, then the functions in the integral is replaced by its complex conjugate $\bar{\psi}_i$.

The type of the spectral method used is identified by the selection of the weighting functions and the weight. For the case of Galerkin and tau formulations, it is required that the choice of weighting functions are equal to basis functions and the weight should be associated with the orthogonality of the basis functions such that

$$\psi_i = \varphi_i \quad \text{and} \quad w_* = w \tag{B.5}$$

For the Chebyshev collocation method, both weighting functions and weight are chosen in the following form

$$\psi_i(x) = \delta(x - x_i) \quad \text{and} \quad w_* = 1, \tag{B.6}$$

where δ is the Dirac delta-function and x_i are selected collocation points in $[a, b]$.

From (B.4) and (B.6) we have

$$R_N(x_i) = 0, \tag{B.7}$$

which gives with the definition of the residual (B.2)

$$u_N(x_i) = u(x_i), \quad i = 0, \dots, N, \tag{B.8}$$

therefore, from the truncated series expansion (B.1) we obtain an algebraic system of $N+1$ coefficients $\hat{c}_k$ given by

$$\sum_{k=0}^{N} \hat{c}_k \varphi_k(x_i) = u(x_i), \quad i = 0, \dots, N. \tag{B.9}$$

B.2   Implementation of Chebyshev collocation method

The Chebyshev collocation method is used by Appelquist (2014) and Alveroglu et al. (2016) to solve linear governing perturbation equations for the Newtonian fluids. We use this method to solve the governing equations for the generalised Newtonian fluids. The Chebyshev polynomials of the first kind are defined in terms of trigonometric function as follows

$$T_k(y_i) = \cos\left(k \cos^{-1}(y_i)\right), k = 0, 1, \dots, N, \tag{B.10}$$

where N is the number of collocation points and $y_i \in [-1, 1]$ is the Gauss-Lobatto points

defined by

$$y_i = \cos\left(i\pi/N\right), \quad i = 0, 1, \ldots, N, \tag{B.11}$$

then the Chebyshev polynomials recursively are given as

$$
\begin{aligned}
T_0\left(y_i\right) &= 1, \\
T_1\left(y_i\right) &= y_i, \\
T_{k+1}\left(y_i\right) &= 2y T_k\left(y_i\right) - T_{k-1}\left(y_i\right).
\end{aligned} \tag{B.12}
$$

Furthermore, the derivatives of Chebyshev polynomials are defined by

$$
\begin{aligned}
T_0^{(n)}\left(y_i\right) &= 0, \\
T_1^{(n)}\left(y_i\right) &= T_0^{(n-1)}\left(y_i\right), \\
T_2^{(n)}\left(y_i\right) &= 4y T_1^{(n-1)}\left(y_i\right), \\
T_k^{(n)}\left(y_i\right) &= 2k T_{k-1}^{(n-1)}\left(y_i\right) + \frac{k}{k-2} T_{k-1}^{(n)}\left(y_i\right), \quad k = 3, 4, \ldots, N,
\end{aligned} \tag{B.13}
$$

where n is the order of the derivative.

The type of governing perturbation equations (4.5) and (5.5) for both power-law and Carreau fluids, respectively is a second order ordinary differential equation. Therefore, the first and the second derivatives of the Chebyshev polynomials are only required in order to implement Chebyshev collocation method as follows

$$
\begin{aligned}
T_0'(y_i) &= 0, \quad T_0''(y_i) = 0, \\
T_1'(y_i) &= 0, \quad T_1'(y_i) = 1, \\
T_2'(y_i) &= 4T_1'(y_i), \quad T_2'(y_i) = 4T_1'(y_i), \\
T_k'(y_i) &= 2T_{k-1}(y_i) + 2y_i T_{k-1}'(y_i) - T_{k-2}(y_i), \\
T_k''(y_i) &= 4T_{k-1}'(y_i) + 2y_i T_{k-1}''(y_i) - T_{k-2}''(y_i), \quad k = 3,4,\ldots,N,
\end{aligned}
\tag{B.14}
$$

where superscripts $'$ and $''$ indicate the first and second derivatives with respect to y_i.

The Chebyshev expansions of these quantities are determined in order to solve the eigenvalue problems (4.5) and (5.5) for power-law and Carreau fluids, respectively. A transformation of the Gauss-Lobatto collocation points y_i defined in (B.11) is required at $N+1$ number of points in the interval $[-1,1]$ in to physical domain $[0,\eta_\infty]$ and $[0,z_\infty]$ for power-law and Carreau fluids, respectively. New collection points in the physical domain are calculated by using an exponential mapping transformation function defined in (B.15). These points is used to distribute collocation points $N = 100$ between the lower disk surface $\eta = 0$ and the top of the domain $\eta_{max} = 20$.

$$
\begin{aligned}
\eta_i &= -4\log\left((y_i - A)/B\right), \\
A &= -1 - B, \\
B &= 2/\left(e^{-(\eta_\infty/4)} - 1\right).
\end{aligned}
\tag{B.15}
$$

In the physical space of the rotating flows, the Chebyshev polynomials and their derivatives are introduced by using the chain rule as

$$
\begin{aligned}
S_k(\eta_i) &= T_k(y_i), \\
S_k'(\eta_i) &= \frac{dT_k(y_i)}{d\eta_i} = T_k'(y)\frac{dy_i}{d\eta_i}, \\
S_k'(\eta_i) &= \frac{d^2T_k(y_i)}{d\eta_i^2} = T_k''(y)\left(\frac{dy_i}{d\eta_i}\right)^2 + T_k'(y_i)\frac{dy_i^2}{d\eta_i^2}.
\end{aligned}
\tag{B.16}
$$

Here, Superscripts $'$ and $''$ denote the first and the second derivatives of $S_k(\eta_i)$ and $T_k(y_i)$ with respect to η_i and y_i, respectively.

The eigenfunctions of the perturbation components $(\hat{u}, \hat{v}, \hat{w}, \hat{p})$ and their derivatives are expanded in truncated series at collocation points η_i as follows

$$
\begin{aligned}
\hat{u}(\eta_i) &= \sum_{k=0}^{N} \hat{c}_k^{\hat{u}} S_k(\eta_i), \quad \hat{v}(\eta_i) = \sum_{k=0}^{N} \hat{c}_k^{\hat{v}} S_k(\eta_i), \\
\hat{w}(\eta_i) &= \sum_{k=0}^{N} \hat{c}_k^{\hat{w}} S_k(\eta_i), \quad \hat{p}(\eta_i) = \sum_{k=0}^{N} \hat{c}_k^{\hat{p}} S_k(\eta_i),
\end{aligned}
\tag{B.17}
$$

$$
\begin{aligned}
\hat{u}'(\eta_i) &= \sum_{k=0}^{N} \hat{c}_k^{\hat{u}} S_k'(\eta_i), \quad \hat{v}'(\eta_i) = \sum_{k=0}^{N} \hat{c}_k^{\hat{v}} S_k'(\eta_i), \\
\hat{w}'(\eta_i) &= \sum_{k=0}^{N} \hat{c}_k^{\hat{w}} S_k'(\eta_i), \quad \hat{p}'(\eta_i) = \sum_{k=0}^{N} \hat{c}_k^{\hat{p}} S_k'(\eta_i),
\end{aligned}
\tag{B.18}
$$

$$
\begin{aligned}
\hat{u}''(\eta_i) &= \sum_{k=0}^{N} \hat{c}_k^{\hat{u}} S_k''(\eta_i), \quad \hat{v}''(\eta_i) = \sum_{k=0}^{N} \hat{c}_k^{\hat{v}} S_k''(\eta_i), \\
\hat{w}''(\eta_i) &= \sum_{k=0}^{N} \hat{c}_k^{\hat{w}} S_k''(\eta_i), \quad \hat{p}''(\eta_i) = \sum_{k=0}^{N} \hat{c}_k^{\hat{p}} S_k''(\eta_i).
\end{aligned}
\tag{B.19}
$$

Regarding to the boundary conditions, all the perturbations quantities are equal to zero at the disk surface η_0 and the top of the domain η_N. It is noted that the domain η used in the previous equations for power-law fluids. Regarding to the Carreau fluids, η is replaced by z in the equations.

The following eigenvalue problem for the wavenumber α for power-law fluids is obtained by substituting the Chebyshev expansions of the perturbation quantities into the linearised perturbation equations (4.5)

$$\left(A_1^{PL}\alpha + A_0^{PL}\right)V = 0. \tag{B.20}$$

where V is the matrix of the eigenfunctions, A_1^{PL} and A_0^{PL} are the matrices defined in the following form

$$A_1^{PL} = \begin{bmatrix} \varepsilon S_N(\eta_0) & 0 & 0 & 0 & \dots \\ 0 & \varepsilon S_N(\eta_0) & 0 & 0 & \dots \\ 0 & 0 & \varepsilon S_N(\eta_0) & 0 & \dots \\ 0 & 0 & 0 & \varepsilon S_N(\eta_0) & \dots \\ iUS_0(\eta_1) & 0 & 0 & iS_0(\eta_1) & \dots \\ 0 & iUS_0(\eta_1) & 0 & 0 & \dots \\ 0 & 0 & iUS_0(\eta_1) & 0 & \dots \\ iS_0(\eta_1) & 0 & 0 & 0 & \dots \\ \vdots & \vdots & \vdots & \vdots & \dots \\ \varepsilon S_N(\eta_N) & 0 & 0 & 0 & \dots \\ 0 & \varepsilon S_N(\eta_N) & 0 & 0 & \dots \\ 0 & 0 & \varepsilon S_N(\eta_N) & 0 & \dots \\ 0 & 0 & \varepsilon S_N'(\eta_N) & 0 & \dots \end{bmatrix}, \tag{B.21}$$

$$
A_0^{PL} = \begin{bmatrix}
\varepsilon S_N(\eta_0) & 0 & 0 & 0 & \dots \\
0 & \varepsilon S_N(\eta_0) & 0 & 0 & \dots \\
0 & 0 & \varepsilon S_N(\eta_0) & 0 & \dots \\
0 & 0 & 0 & \varepsilon S_N(\eta_0) & \dots \\
A_{51} & A_{52} & A_{53} & A_{54}U & \dots \\
A_{61} & A_{62} & A_{63} & A_{64} & \dots \\
0 & 0 & A_{73} & A_{74} & \dots \\
A_{81} & A_{82} & A_{83} & 0 & \dots \\
\vdots & \vdots & \vdots & \vdots & \dots \\
\varepsilon S_N(\eta_N) & 0 & 0 & 0 & \dots \\
0 & \varepsilon S_N(\eta_N) & 0 & 0 & \dots \\
0 & 0 & \varepsilon S_N(\eta_N) & 0 & \dots \\
0 & 0 & \varepsilon S_N'(\eta_N) & 0 & \dots
\end{bmatrix} . \tag{B.22}
$$

Here

$$
\begin{aligned}
A_{51} &= \left(i\bar{\beta}V + U\frac{Ro}{R} + \frac{Ro\hat{\eta}}{R}U' \right) S_0(\eta_1) + \frac{1}{R}\Big[RoW + Ro\hat{\eta}U - \mu' - \hat{\mu}'(U')^2 \\
&\quad - 2\hat{\mu}U'U'' \Big] S_0'(\eta_1) - \frac{1}{R}\Big[\mu + \hat{\mu}(U')^2 \Big] S_0''(\eta_1), \\
A_{52} &= -\frac{1}{R}(2RoV + Co)S_0(\eta_1) - \frac{1}{R}\Big[\hat{\mu}'U'V' + \hat{\mu}(U'V'' + V'U'') \Big] S_0'(\eta_1) \\
&\quad - \frac{1}{R}(\hat{\mu}U'V')S_0''(\eta_1), \\
A_{53} &= U'S_0(\eta_1), \qquad\qquad A_{54} = \frac{Ro}{R}\hat{\eta}S_0'(\eta_1), \\
A_{61} &= \frac{1}{R}(2RoV + Co + Ro\hat{\eta}V')S_0(\eta_1) - \frac{1}{R}\Big[\hat{\mu}'U'V' + \hat{\mu}(U'V'' + V'U'') \Big] S_0'(\eta_1) \\
&\quad - \frac{1}{R}(\hat{\mu}U'V')S_0''(\eta_1), \\
A_{62} &= \left(i\bar{\beta}V + \frac{Ro}{R}U \right) S_0(\eta_1) + \frac{1}{R}\Big[RoW + Ro\hat{\eta}U - \mu' - \hat{\mu}'(V')^2 - 2\hat{\mu}V'V'' \Big] S_0'(\eta_1) \\
&\quad - \frac{1}{R}\Big[\mu + \hat{\mu}(V')^2 \Big] S_0''(\eta_1),
\end{aligned}
$$

$$
\begin{aligned}
A_{63} &= V'S_0(\eta_1), & A_{64} &= i\bar{\beta}S_0(\eta_1), \\
A_{73} &= \left(i\bar{\beta}V + \frac{Ro}{R}W'\right)S_0(\eta_1) + \frac{1}{R}\left(RoW + Ro\hat{\eta}U - \mu'\right)S_0'(\eta_1) - \frac{1}{R}\mu S_0''(\eta_1), \\
A_{74} &= S_0'(\eta_1), \\
A_{81} &= \frac{Ro}{R}S_0(\eta_1) + \frac{Ro}{R}\hat{\eta}S_0'(\eta_1), & A_{82} &= i\bar{\beta}S_0(\eta_1), & A_{83} &= S_0'(\eta_1).
\end{aligned}
$$

where $\hat{\eta} = \eta\frac{(1-n)}{(n+1)}$ and $\hat{\mu} = \frac{(n-1)\mu}{(U')^2+(V')^2}$.

Regarding to the Carreau fluids, substituting the Chebyshev expansions of the perturbation quantities into the linearised perturbation equations (5.5) gives the the following eigenvalue problem

$$
\left(A_1^C\alpha + A_0^C\right)V = 0, \tag{B.23}
$$

where V is the matrix of the eigenfunctions, and

$$
A_1^C = \begin{bmatrix}
\varepsilon S_N(z_0) & 0 & 0 & 0 & \cdots \\
0 & \varepsilon S_N(z_0) & 0 & 0 & \cdots \\
0 & 0 & \varepsilon S_N(z_0) & 0 & \cdots \\
0 & 0 & 0 & \varepsilon S_N(z_0) & \cdots \\
iUS_0(z_1) & 0 & 0 & iS_0(z_1) & \cdots \\
0 & iUS_0(z_1) & 0 & 0 & \cdots \\
0 & 0 & iUS_0(z_1) & 0 & \cdots \\
iS_0(z_1) & 0 & 0 & 0 & \cdots \\
\vdots & \vdots & \vdots & \vdots & \cdots \\
\varepsilon S_N(z_N) & 0 & 0 & 0 & \cdots \\
0 & \varepsilon S_N(z_N) & 0 & 0 & \cdots \\
0 & 0 & \varepsilon S_N(z_N) & 0 & \cdots \\
0 & 0 & \varepsilon S_N'(z_N) & 0 & \cdots
\end{bmatrix}, \tag{B.24}
$$

$$A_0^C = \begin{bmatrix} \varepsilon S_N(z_0) & 0 & 0 & 0 & \ldots \\ 0 & \varepsilon S_N(z_0) & 0 & 0 & \ldots \\ 0 & 0 & \varepsilon S_N(z_0) & 0 & \ldots \\ 0 & 0 & 0 & \varepsilon S_N(z_0) & \ldots \\ A_{51} & A_{52} & A_{53} & 0 & \ldots \\ A_{61} & A_{62} & A_{63} & A_{64} & \ldots \\ 0 & 0 & A_{73} & A_{74} & \ldots \\ A_{81} & A_{82} & A_{83} & 0 & \ldots \\ \vdots & \vdots & \vdots & \vdots & \ldots \\ \varepsilon S_N(z_N) & 0 & 0 & 0 & \ldots \\ 0 & \varepsilon S_N(z_N) & 0 & 0 & \ldots \\ 0 & 0 & \varepsilon S_N(z_N) & 0 & \ldots \\ 0 & 0 & \varepsilon S_N'(z_N) & 0 & \ldots \end{bmatrix}. \tag{B.25}$$

Here

$$
\begin{aligned}
A_{51} &= \left(i\bar{\beta}V + U\frac{Ro}{R} \right) S_0(z_1) + \frac{1}{R}\left[RoW - \mu' - \hat{\mu}'\left(U'\right)^2 - 2\hat{\mu}U'U'' \right] S_0'(z_1) \\
&\quad - \frac{1}{R}\left[\mu + \hat{\mu}\left(U'\right)^2 \right] S_0''(z_1), \\
A_{52} &= -\frac{1}{R}\left(2RoV + Co \right) S_0(z_1) - \frac{1}{R}\left[\hat{\mu}'U'V' + \hat{\mu}\left(U'V'' + V'U'' \right) \right] S_0'(z_1) \\
&\quad + \frac{1}{R}\left(\hat{\mu}U'V' \right) S_0''(z_1), \\
A_{53} &= U'S_0(z_1), \\
A_{61} &= \frac{1}{R}\left(2RoV + Co \right) S_0(z_1) - \frac{1}{R}\left(\hat{\mu}'U'V' + \hat{\mu}\left(U'V'' + V'U'' \right) \right) S_0'(z_1) \\
&\quad - \frac{1}{R}\left(\hat{\mu}U'V' \right) S_0''(z_1), \\
A_{62} &= \left(i\bar{\beta}V + \frac{Ro}{R}U \right) S_0(z_1) + \frac{1}{R}\left(RoW - \mu' - \hat{\mu}'\left(V'\right)^2 - 2\hat{\mu}V'V'' \right) S_0'(z_1) \\
&\quad - \frac{1}{R}\left[\mu + \hat{\mu}\left(V'\right)^2 \right] S_0''(z_1),
\end{aligned}
$$

$$
\begin{aligned}
A_{63} &= V' S_0(z_1), \qquad\qquad A_{64} = i\bar{\beta} S_0(z_1), \\
A_{73} &= \left(i\bar{\beta} V + \frac{Ro}{R} W' \right) S_0(z_1) + \frac{1}{R}\left(RoW - \mu'\right) S_0'(z_1) - \frac{1}{R}\mu S_0''(z_1), \\
A_{74} &= S_0'(z_1), \\
A_{81} &= \frac{Ro}{R} S_0(z_1), \qquad\qquad A_{82} = i\bar{\beta} S_0(z_1), \qquad\qquad A_{83} = S_0'(z_1),
\end{aligned}
$$

where

$$
\hat{\mu} = \frac{k^2(n-1)\mu}{\{1 + k^2[(U')^2 + (V')^2]\}}.
$$

The size of the matrices in (B.20) and (B.23) is $4(N+1)\text{x}4(N+1)$, where N is the number of collection points and 4 is the number of the perturbation quantities $\hat{u}, \hat{v}, \hat{w}$ and $\hat{p}$. The complex parameter ε in the matrices is selected to $\varepsilon = -1680i$, where i is $\sqrt{-1}$. This value is to ensure that the boundary conditions are suitably imposed for perturbing the matrix.

The eigenvalue problem is solved by using MATLAB solver function (**polyeig**) in the spectral code to compute the solutions and the eigenvalues α for fixed values of R and various values of β iteratively. The branch point is selected with very smallest imaginary part of eigenvalue $\text{Im}(\alpha_i)$ for each β such that the next imaginary part for the iteration of β is zero. The same procedure is continued for wide range of Reynolds number to obtain branch points required to plot the entire neutral curve of convective instability for power-law and Carreau fluids.

Appendix C

Steady mean flow profiles and neutral curves

In this appendix we show the mean flow profiles and the neutral curves that were not presented in the main text of this thesis. The mean flow velocities of the BEK family flows for shear-thinning and shear-thickening fluids with $k = ko$ are shown in §C.1. The numerical values of these mean flow profiles are reported in C.2. In §C.3 we present the neutral curves for shear-thinning and shear-thickening Carreau fluids with $k = 100$ while the neural curves for $k = ko$ are presented in §C.4. Finally, the comparative results between power-law and Carreau fluids are showed in §C.5.

C.1   Mean flow profiles of BEK family of flows for Carreau fluids

Figures C.1-C.4 present the neutral curves of BEK family flows for shear-thinning while Figures C.5-C.8 show the neutral curves for shear-thickening Carreau fluids when $k = ko$.
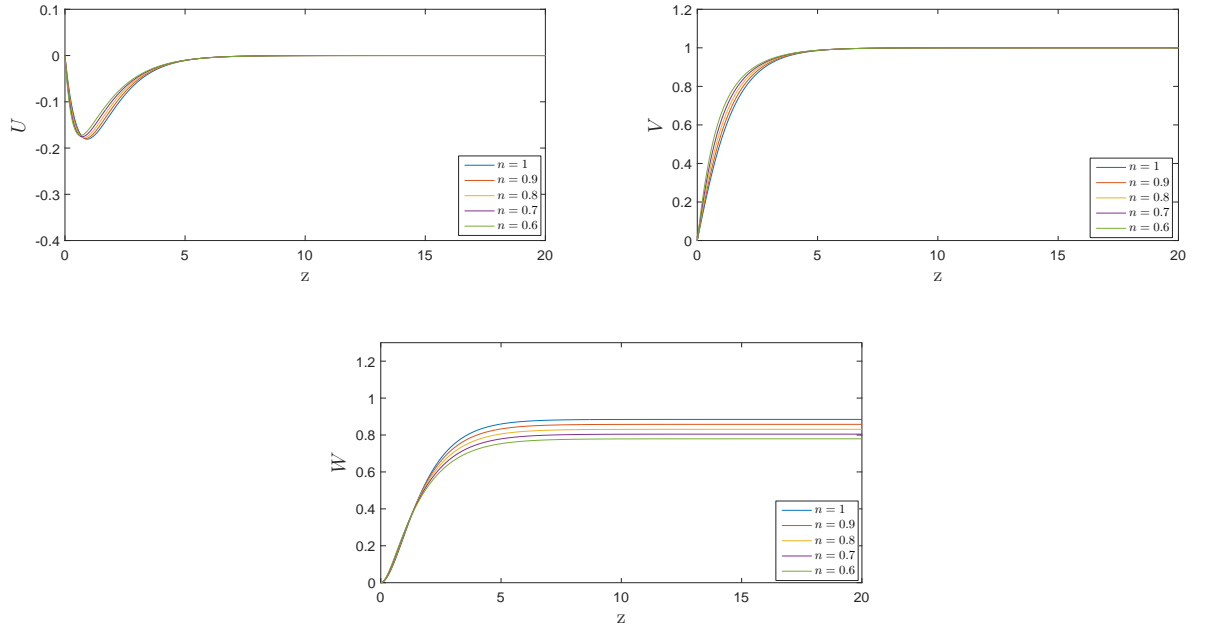
Figure C.1: Steady mean flow profiles U, V and W versus for Newtonian $(n = 1)$ and shear-thinning Carreau fluids with $n = 0.9, 0.8, 0.7, 0.6$ and $k = ko$ at $Ro = -1$.
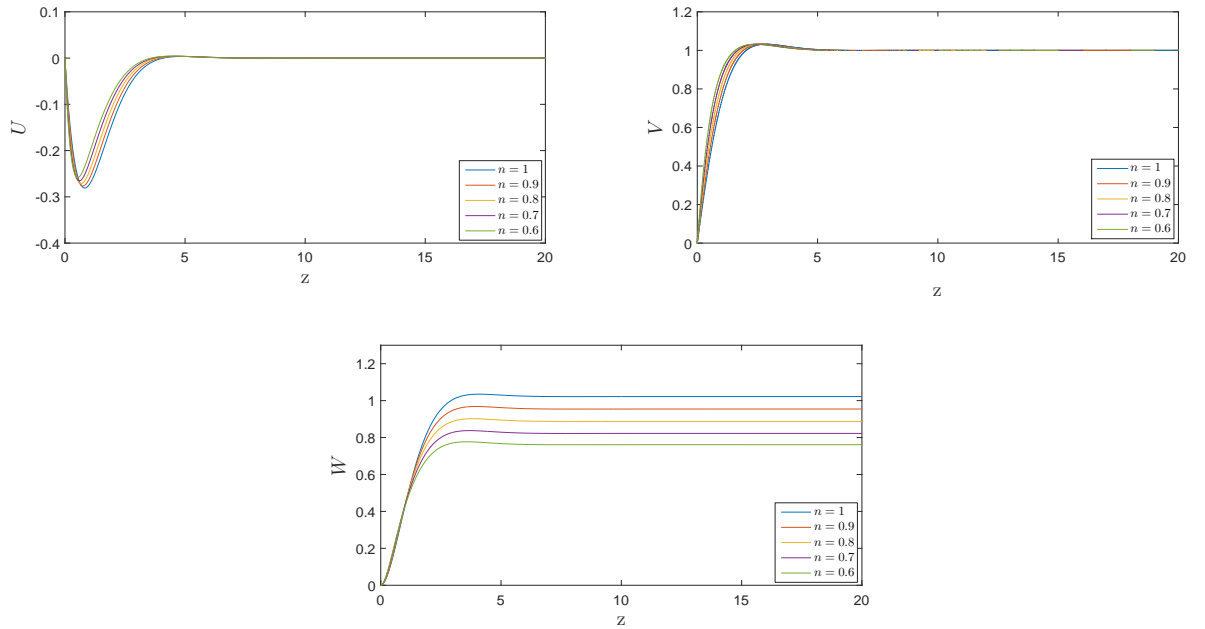

Figure C.2: Steady mean flow profiles U, V and W versus for Newtonian $(n = 1)$ and shear-thinning Carreau fluids with $n = 0.9, 0.8, 0.7, 0.6$ and $k = ko$ at $Ro = -0.5$.
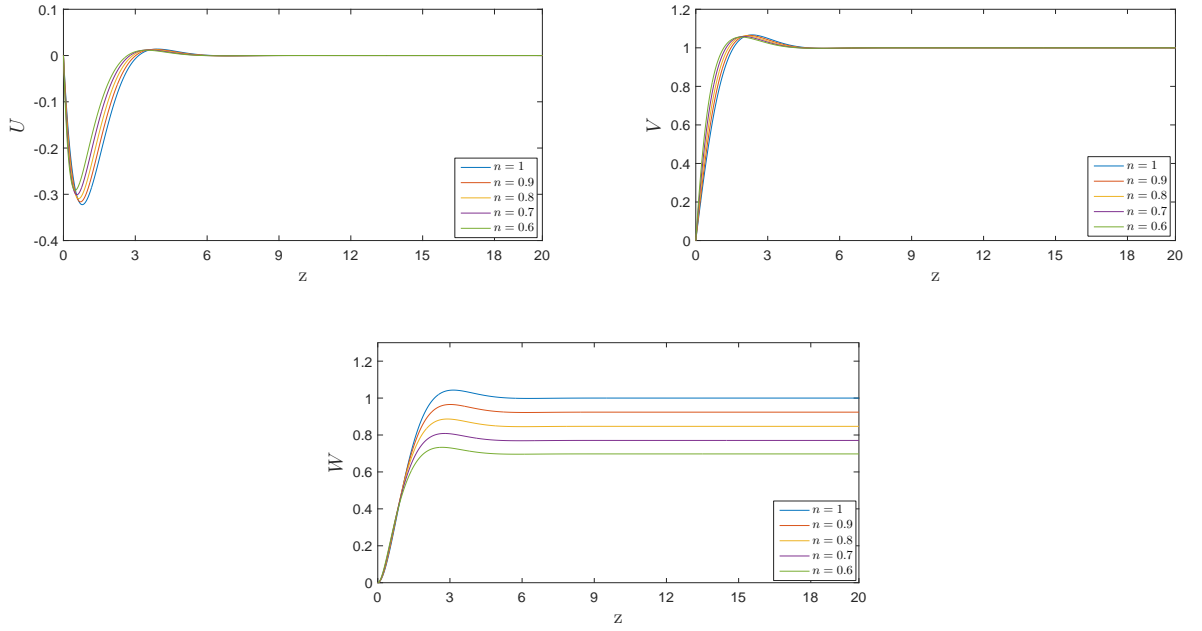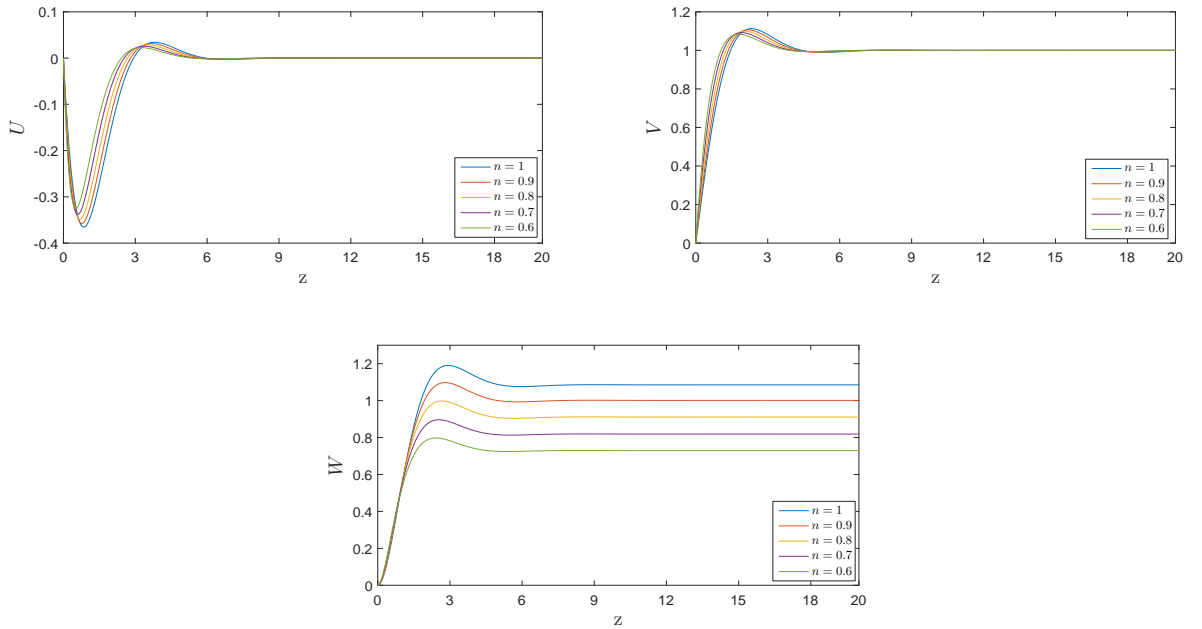
Figure C.3: Steady mean flow profiles U, V and W versus for Newtonian $(n = 1)$ and shear-thinning Carreau fluids with $n = 0.9, 0.8, 0.7, 0.6$ and $k = ko$ at $Ro = 0$.

Figure C.4: Steady mean flow profiles U, V and W versus for Newtonian $(n = 1)$ and shear-thinning Carreau fluids with $n = 0.9, 0.8, 0.7, 0.6$ and $k = ko$ at $Ro = 0.5$.
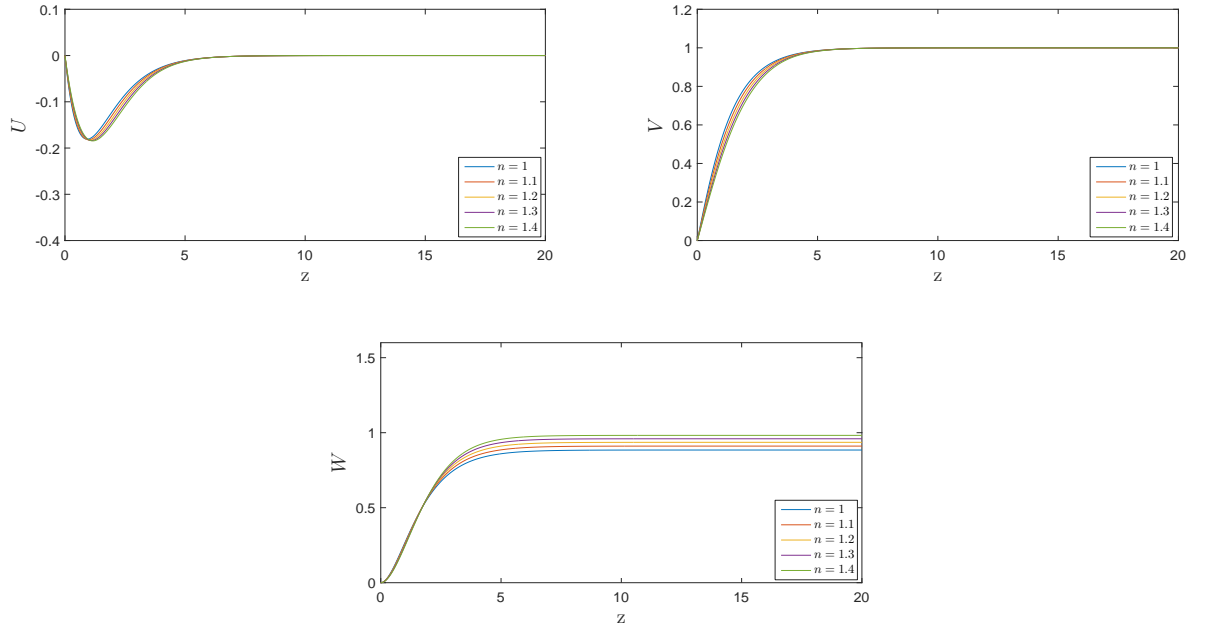
Figure C.5: Steady mean flow profiles U, V and W versus for Newtonian $(n = 1)$ and shear-thickening Carreau fluids with $n = 1.1, 1.2, 1.3, 1.4$ and $k = ko$ at $Ro = -1$.
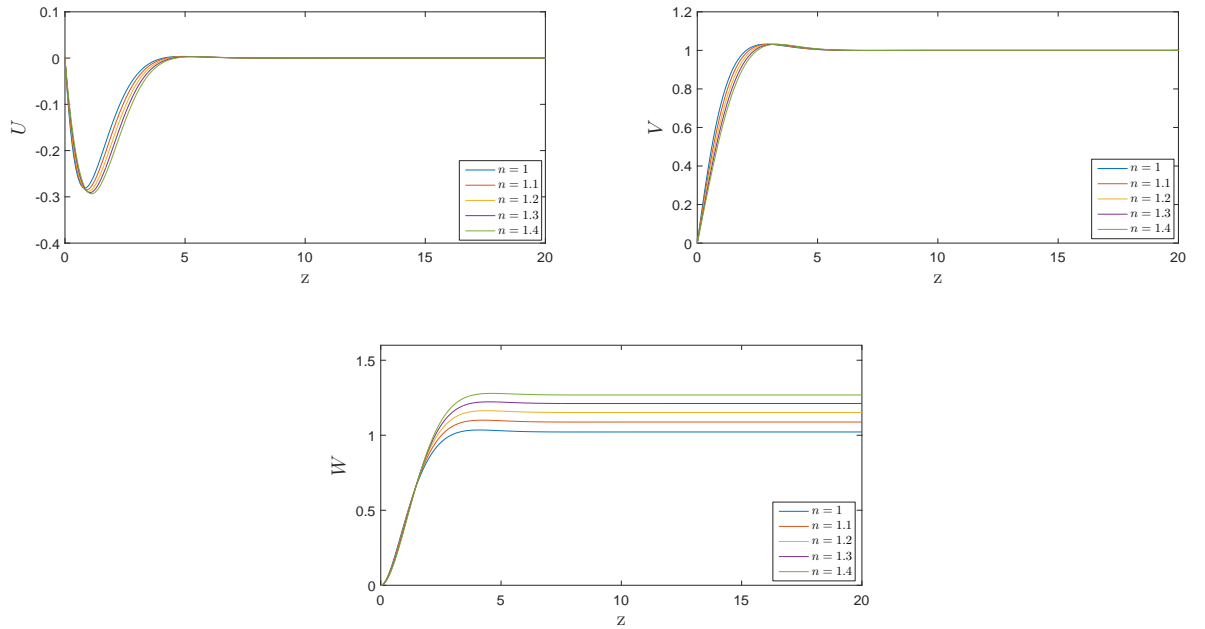

Figure C.6: Steady mean flow profiles U, V and W versus for Newtonian $(n = 1)$ and shear-thickening Carreau fluids with $n = 1.1, 1.2, 1.3, 1.4$ and $k = ko$ at $Ro = -0.5$.
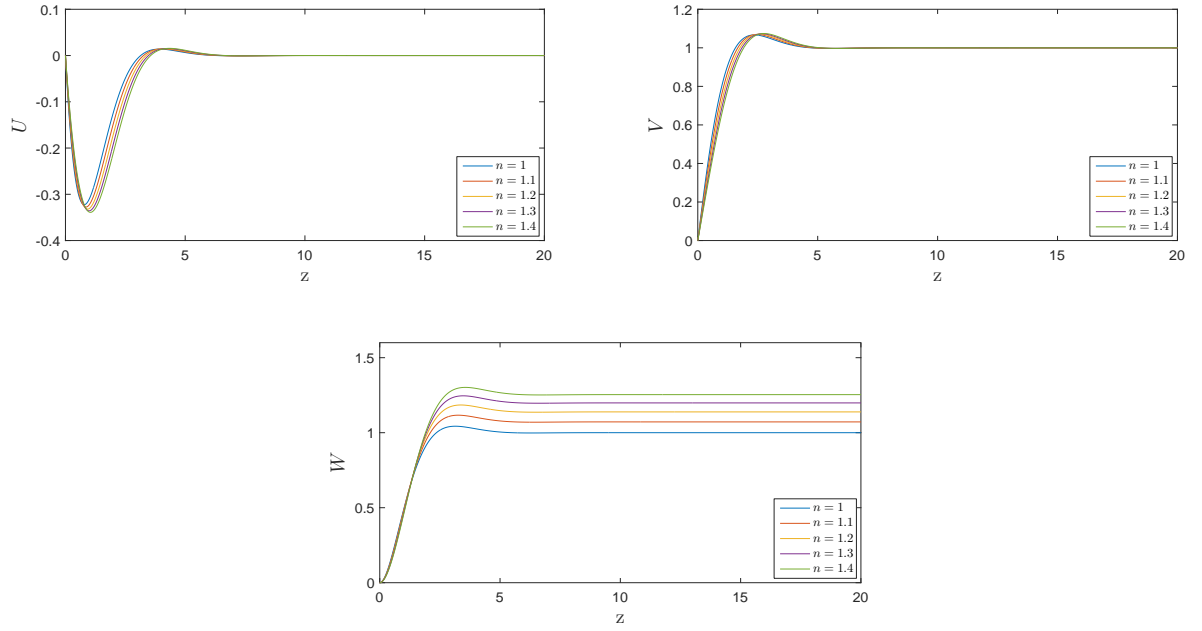
Figure C.7: Steady mean flow profiles U, V and W versus for Newtonian $(n = 1)$ and shear-thickening Carreau fluids with $n = 1.1, 1.2, 1.3, 1.4$ and $k = ko$ at $Ro = 0$.
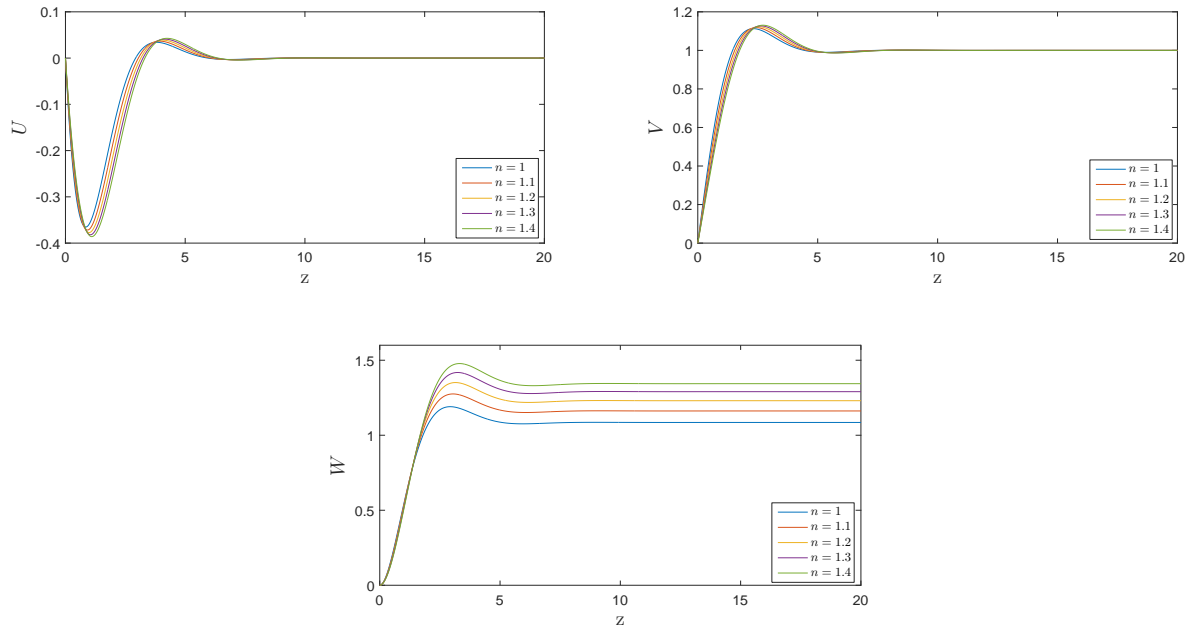

Figure C.8: Steady mean flow profiles U, V and W versus for Newtonian $(n = 1)$ and shear-thickening Carreau fluids with $n = 1.1, 1.2, 1.3, 1.4$ and $k = ko$ at $Ro = 0.5$.

C.2   Numerical values of the mean velocity flow velocities

Table C.1 shows the numerical values of the mean flow velocities for shear-thinning while Table C.2 presents the numerical values for shear-thickening fluids when $k = ko$.

n	$-U'(0)$	$V'(0)$	$W(z_\infty)$	ko
1	0.5102	0.6159	0.8845	-
0.9	0.5585	0.6887	0.8578	6.42
0.8	0.6182	0.7820	0.8309	6.40
0.7	0.6925	0.9033	0.8047	6.30
0.6	0.7870	1.0661	0.7794	6.16

(a) $Ro = -1$

n	$-U'(0)$	$V'(0)$	$W(z_\infty)$	ko
1	0.8570	0.9073	1.0219	-
0.9	0.9529	1.0349	0.9545	5.75
0.8	1.0705	1.1982	0.8876	5.59
0.7	1.2158	1.4106	0.8225	5.38
0.6	1.3955	1.6913	0.7614	5.09

(b) $Ro = -0.5$

n	$-U'(0)$	$V'(0)$	$W(z_\infty)$	ko
1	1.000	1.000	1.0000	-
0.9	1.1122	1.1415	0.9238	5.17
0.8	1.2517	1.3248	0.8469	5.11
0.7	1.4272	1.5676	0.7706	5.01
0.6	1.6473	1.8934	0.6976	4.82

(c) $Ro = 0$

n	$-U'(0)$	$V'(0)$	$W(z_\infty)$	ko
1	1.0176	0.9612	1.0853	-
0.9	1.1256	1.0911	1.0013	4.75
0.8	1.2662	1.2663	0.9112	4.96
0.7	1.4477	1.5035	0.8190	5.06
0.6	1.6789	1.8266	0.7294	5.01

(d) $Ro = 0.5$

Table C.1: Numerical values of the mean velocity flow parameters U', V' and W for shear-thinning Carreau fluids with $n = 1, 0.9, 0.8, 0.7, 0.6$ and $k = ko$ at various Ro.

n	$-U'(0)$	$V'(0)$	$W(z_\infty)$	ko
1	0.5102	0.6159	0.8845	-
1.1	0.4707	0.5581	0.9107	6.40
1.2	0.4382	0.5116	0.9358	6.32
1.3	0.4114	0.4740	0.9595	6.20
1.4	0.3887	0.4427	0.9822	6.11

(a) $Ro = -1$

n	$-U'(0)$	$V'(0)$	$W(z_\infty)$	ko
1	0.8570	0.9073	1.0219	-
1.1	0.7787	0.8066	1.0881	5.85
1.2	0.7147	0.7264	1.1518	5.81
1.3	0.6623	0.6623	1.2116	5.71
1.4	0.6184	0.6096	1.2685	5.63

(b) $Ro = -0.5$

n	$-U'(0)$	$V'(0)$	$W(z_\infty)$	ko
1	1.000	1.000	1.0000	-
1.1	0.9112	0.8914	1.0719	4.90
1.2	0.8403	0.8067	1.1386	4.73
1.3	0.7840	0.7406	1.1985	4.52
1.4	0.7376	0.6871	1.2537	4.35

(c) $Ro = 0$

n	$-U'(0)$	$V'(0)$	$W(z_\infty)$	ko
1	1.0176	0.9612	1.0853	-
1.1	0.9339	0.8630	1.1619	4.28
1.2	0.8685	0.7880	1.2302	4.03
1.3	0.8169	0.7296	1.2905	3.80
1.4	0.7752	0.6831	1.3438	3.60

(d) $Ro = 0.5$

Table C.2: Numerical values of the mean velocity flow parameters U', V' and W for shear-thickening Carreau fluids with $n = 1, 1.1, 1.2, 1.3, 1.4$ and $k = ko$ at various Ro.

C.3   Neutral curves of BEK family of flows for Carreau fluids with $k = 100$

Figures C.9-C.12 present the convective neutral curves of BEK family flows for shear-thinning Carreau fluids while Figures C.13-C.16 show the neutral curves for shear-thickening Carreau fluids when $k = 100$.
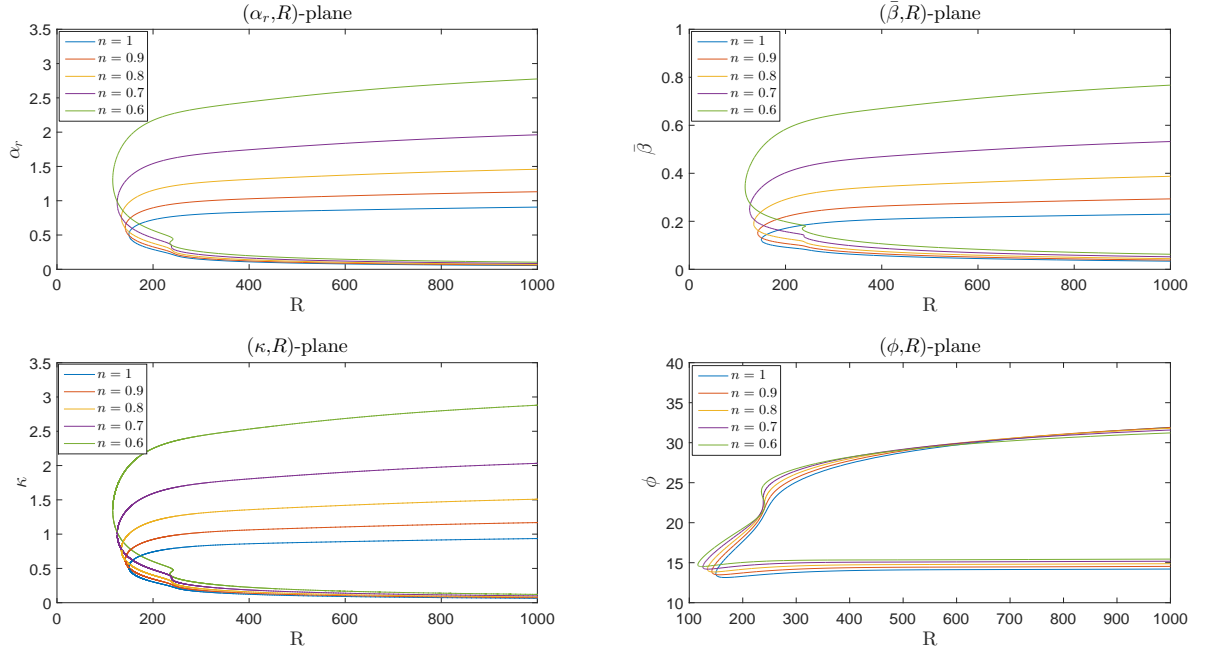
Figure C.9: Neutral curves of the flow at $Ro = -0.5$ for shear-thinning Carreau fluids with $n = 1, 0.9, 0.8, 0.7, 0.6$ and $k = 100$.
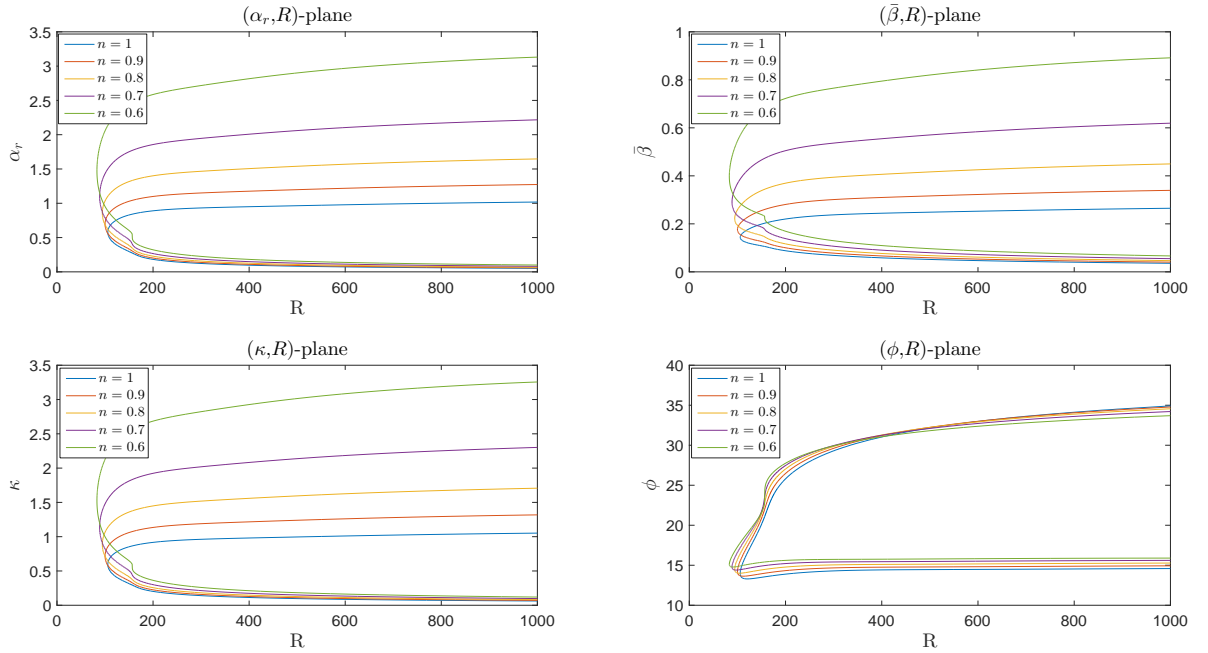

Figure C.10: Neutral curves of the Ekman flow, $Ro = 0$ for shear-thinning Carreau fluids with $n = 1, 0.9, 0.8, 0.7, 0.6$ and $k = 100$.
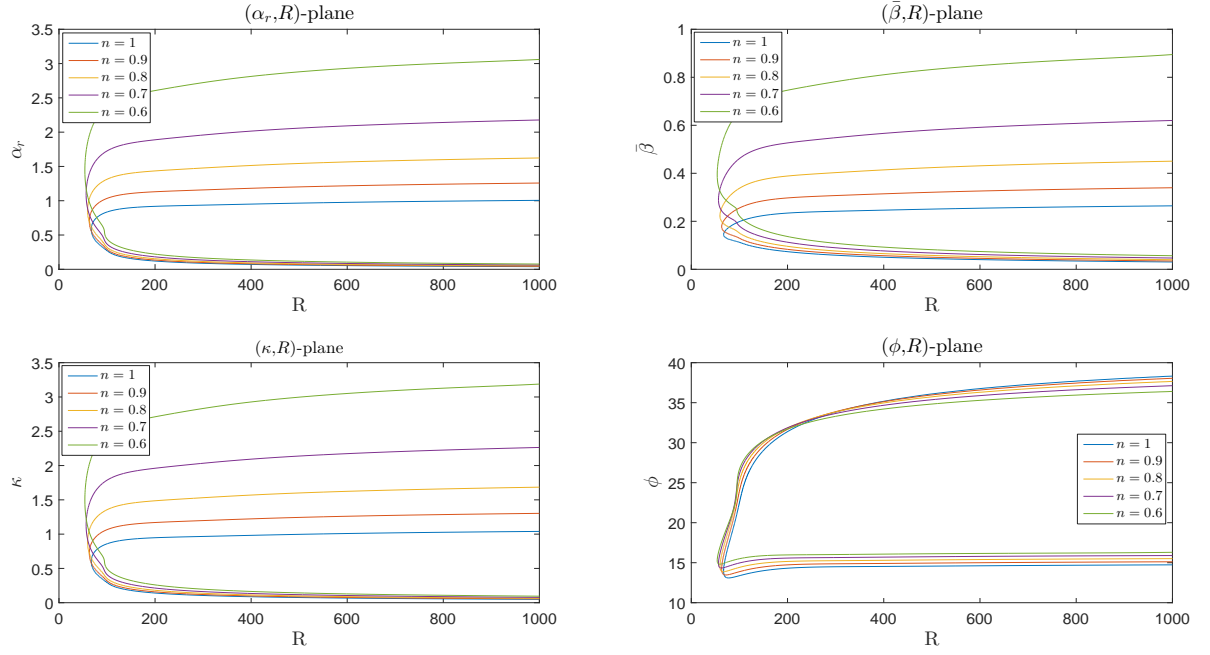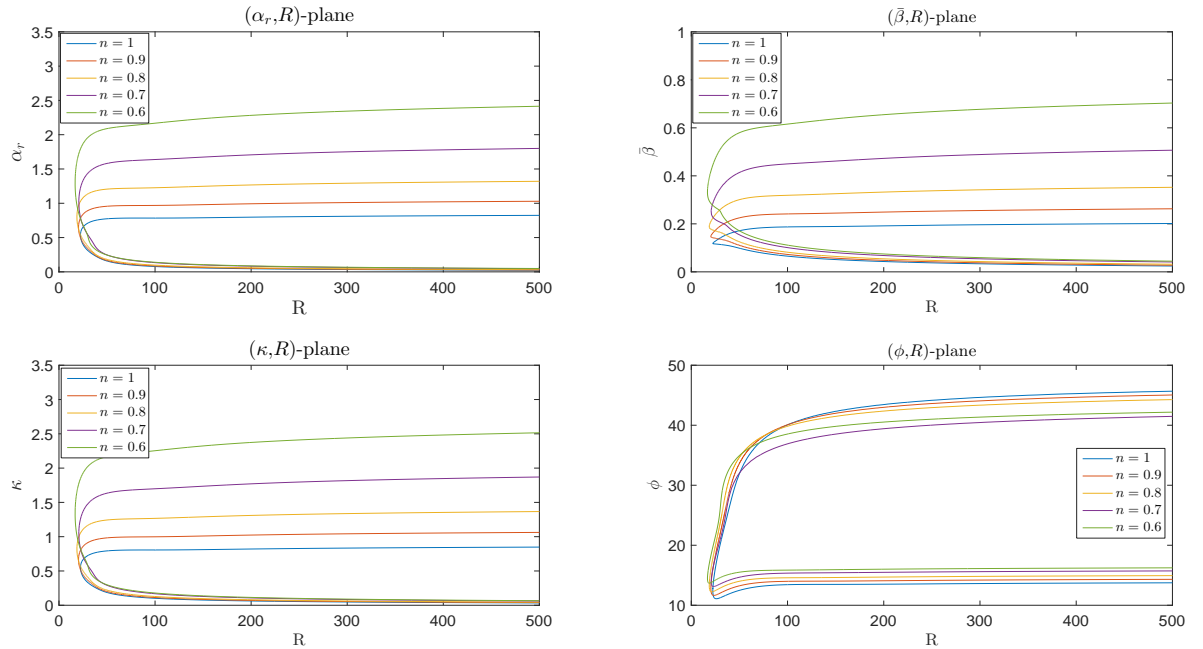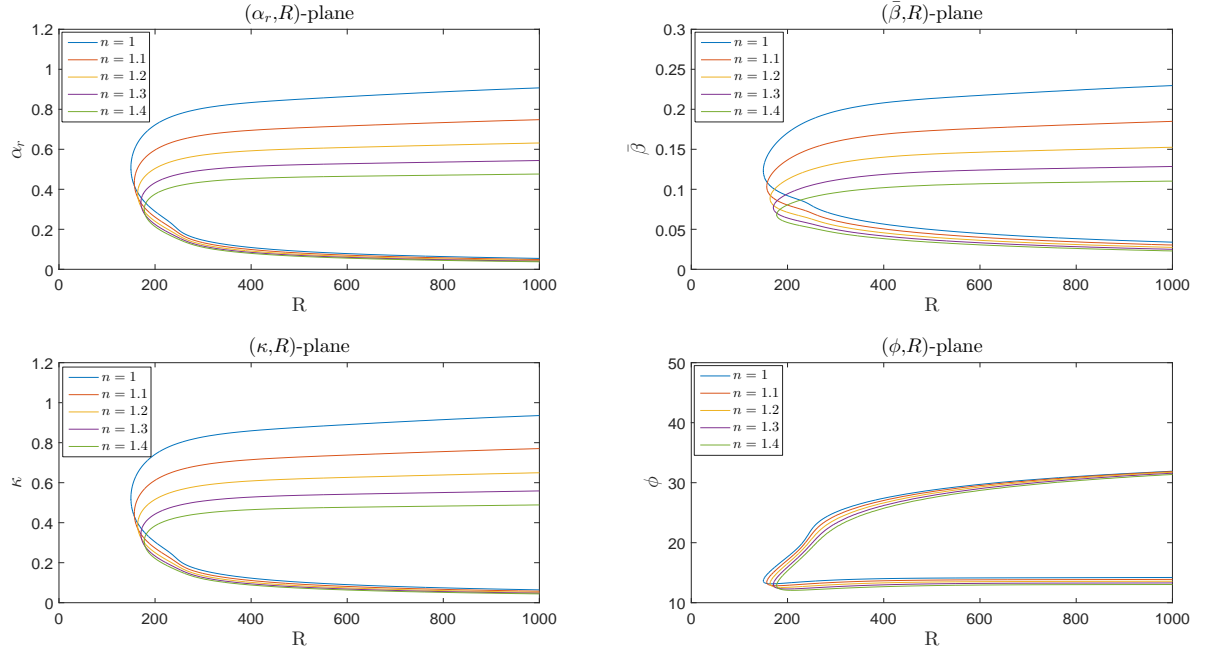
Figure C.11: Neutral curves of the flow at $Ro = 0.5$ for shear-thinning Carreau fluids with $n = 1, 0.9, 0.8, 0.7, 0.6$ and $k = 100$.

Figure C.12: Neutral curves of the Bödewadt flow, $Ro = 1$ for shear-thinning Carreau fluids with $n = 1, 0.9, 0.8, 0.7, 0.6$ and $k = 100$.

Figure C.13: Neutral curves of the flow at $Ro = -0.5$ for shear-thickening Carreau fluids with $n = 1, 1.1, 1.2, 1.3, 1.4$ and $k = 100$.
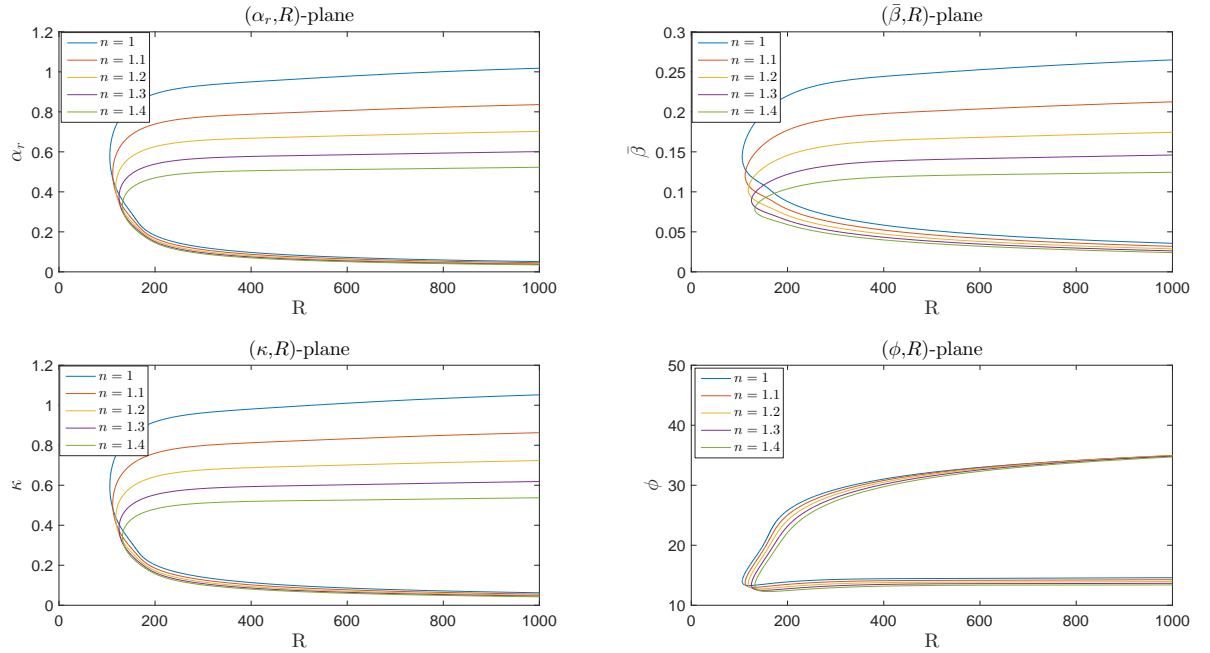

Figure C.14: Neutral curves of the Ekman flow, $Ro = 0$ for shear-thickening Carreau fluids with $n = 1, 1.1, 1.2, 1.3, 1.4$ and $k = 100$.
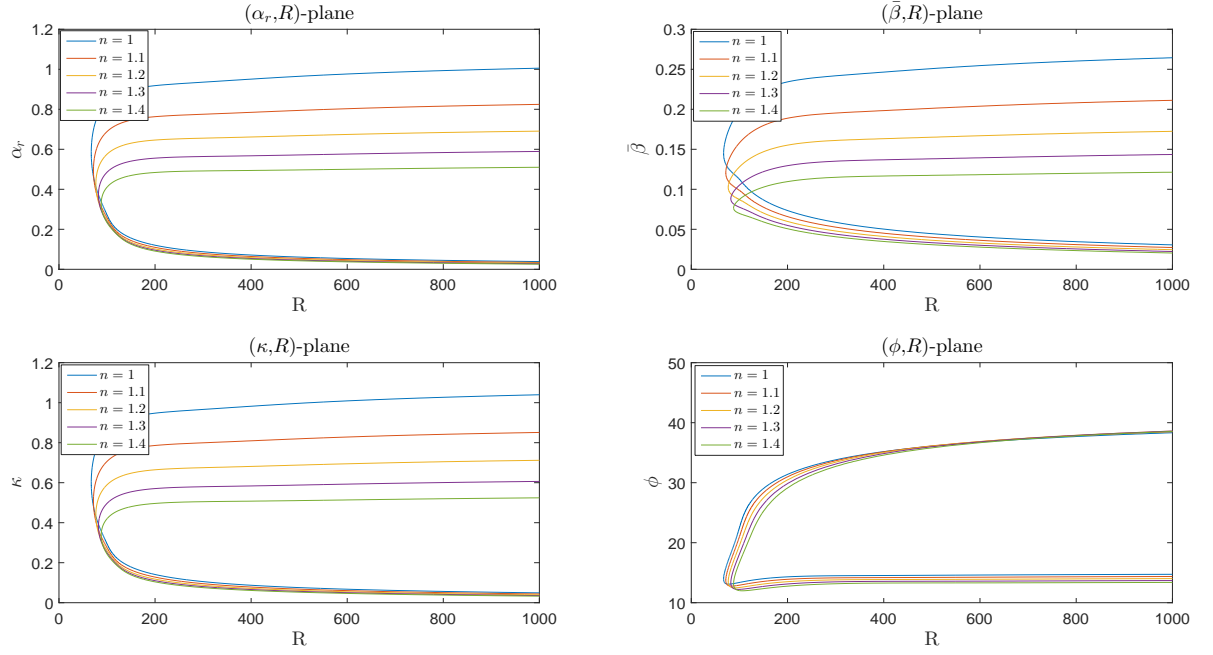
Figure C.15: Neutral curves of the flow at $Ro = 0.5$ for shear-thickening Carreau fluids with $n = 1, 1.1, 1.2, 1.3, 1.4$ and $k = 100$.
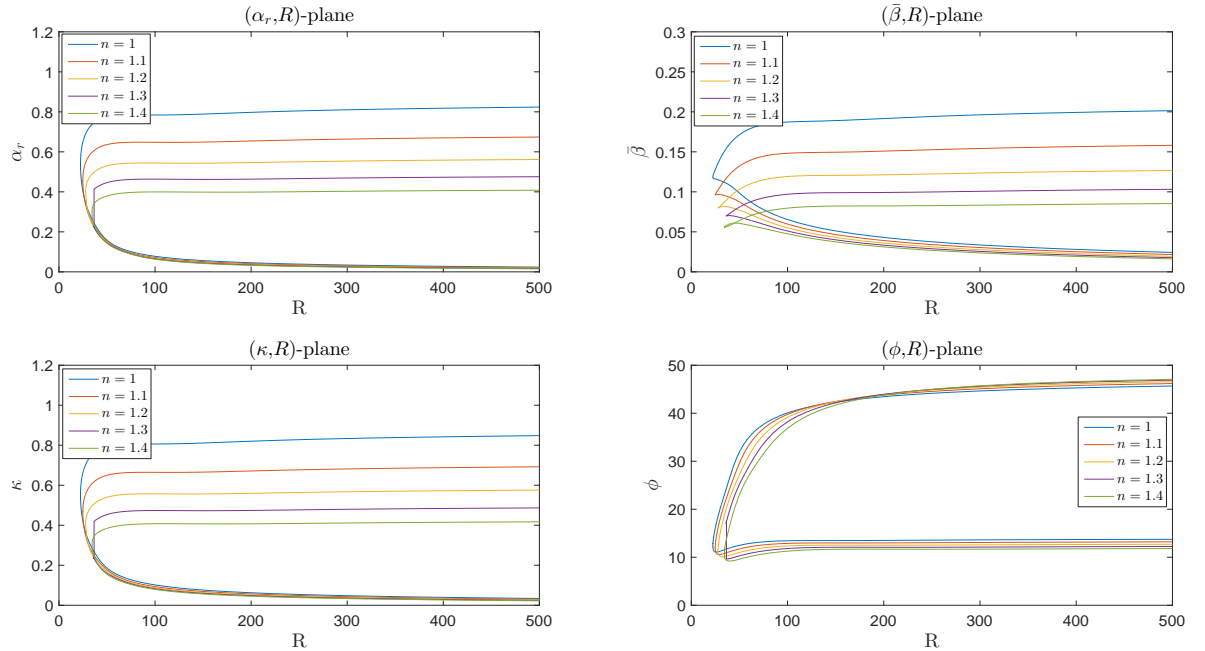

Figure C.16: Neutral curves of the Bödewadt flow, $Ro = 1$ for shear-thickening Carreau fluids with $n = 1, 1.1, 1.2, 1.3, 1.4$ and $k = 100$.

C.4 Neutral curves of BEK family of flows for Carreau fluids with $k = ko$

Figures C.17-C.19 show the convective neutral curves for shear-thinning Carreau fluids while Figures C.20-C.22 present the neutral curves for shear-thickening Carreau fluids when $k = ko$ at various values of Ro.
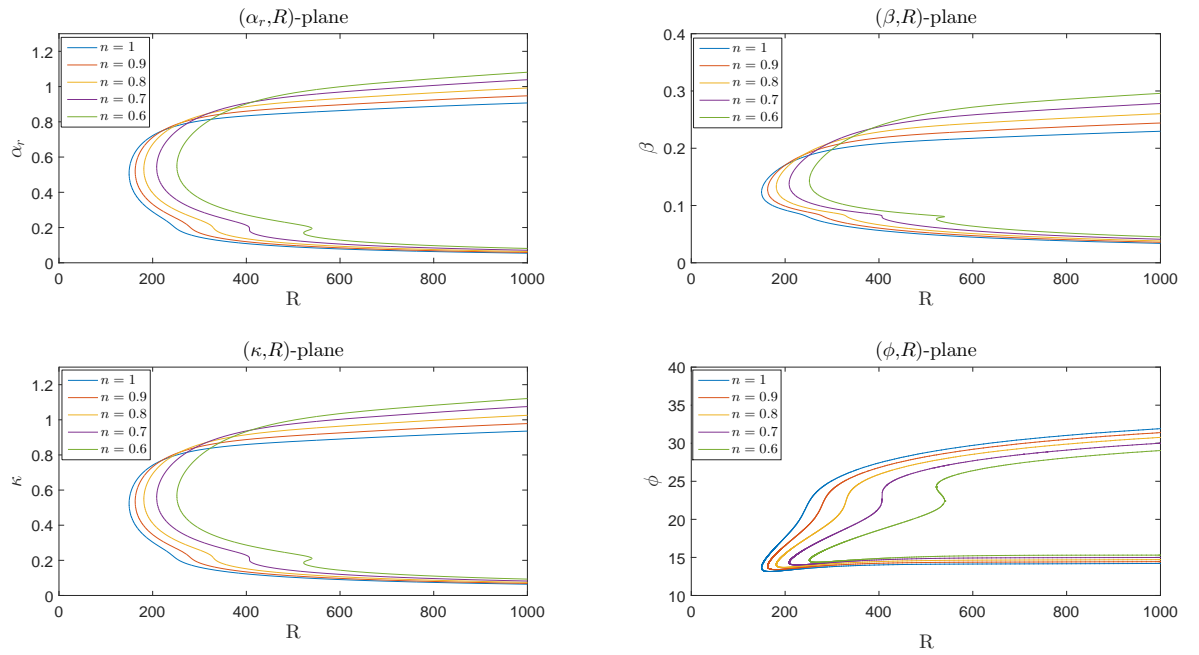

Figure C.17: Neutral curves of the flow at $Ro = -0.5$ for shear-thinning Carreau fluids with $n = 1, 0.9, 0.8, 0.7, 0.6$ and $k = ko$.
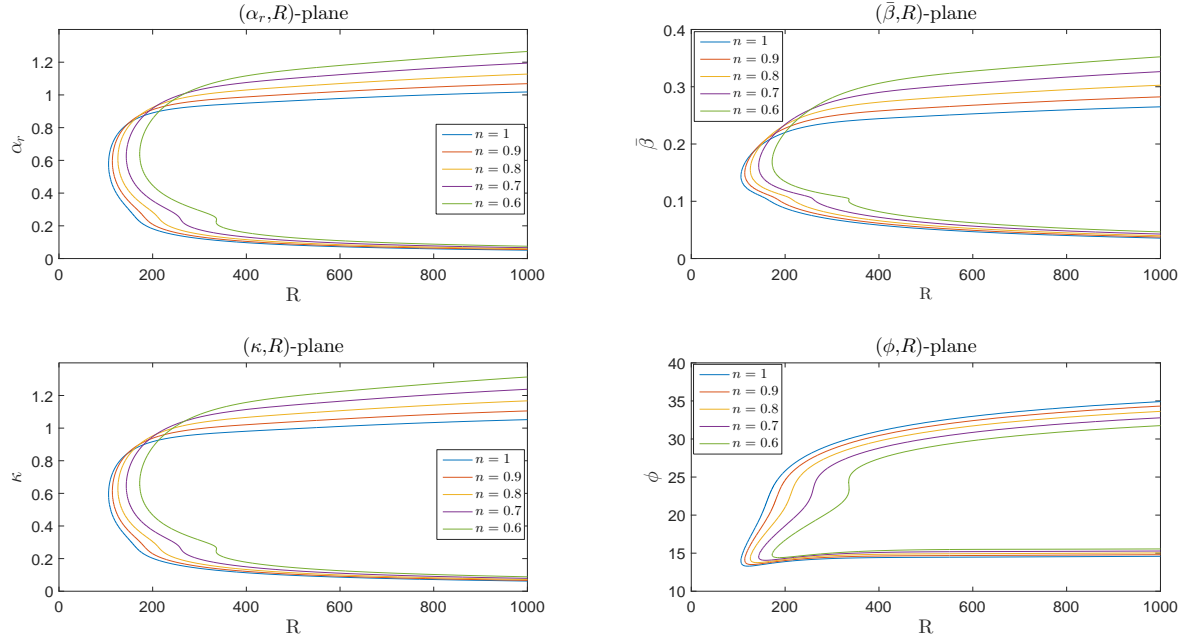
Figure C.18: Neutral curves of the Ekman flow, $Ro = 0$ for shear-thinning Carreau fluids with $n = 1, 0.9, 0.8, 0.7, 0.6$ and $k = ko$.
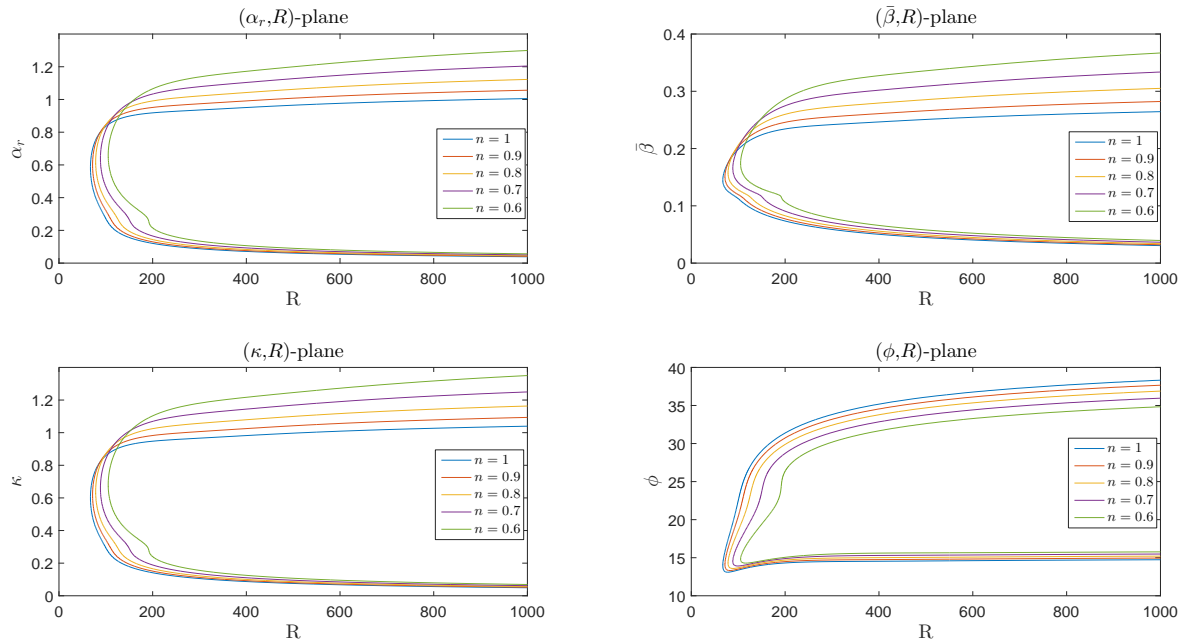

Figure C.19: Neutral curves of the flow at $Ro = 0.5$ for shear-thinning Carreau fluids with $n = 1, 0.9, 0.8, 0.7, 0.6$ and $k = ko$.
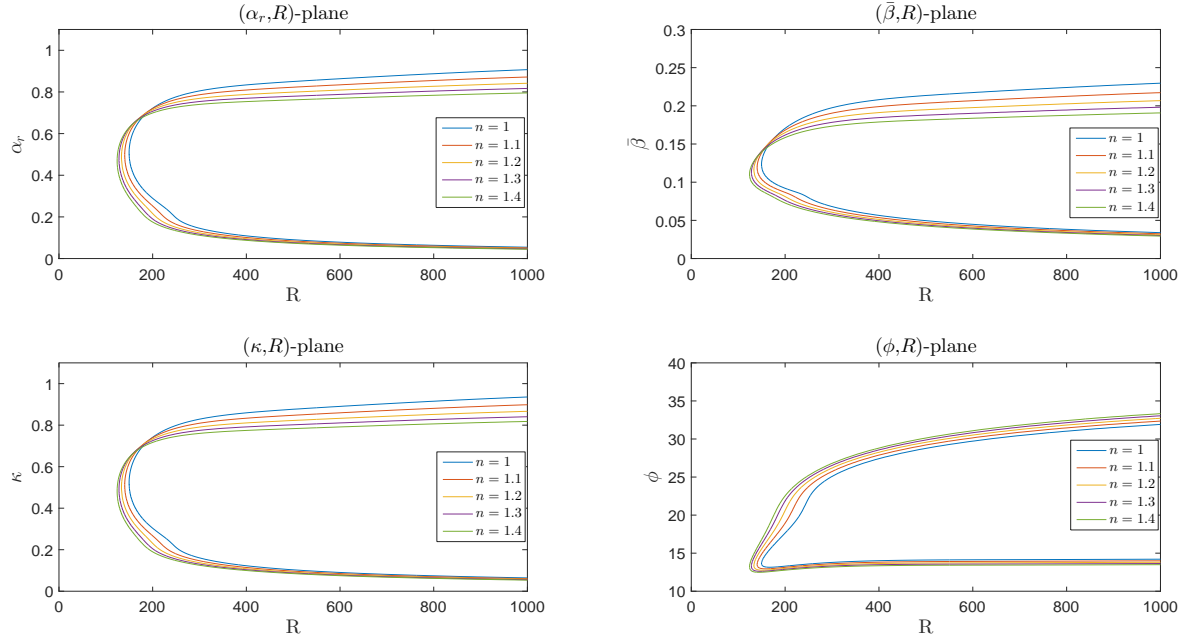
Figure C.20: Neutral curves of the flow at $Ro = -0.5$ for shear-thickening Carreau fluids with $n = 1, 1.1, 1.2, 1.3, 1.4$ and $k = ko$.
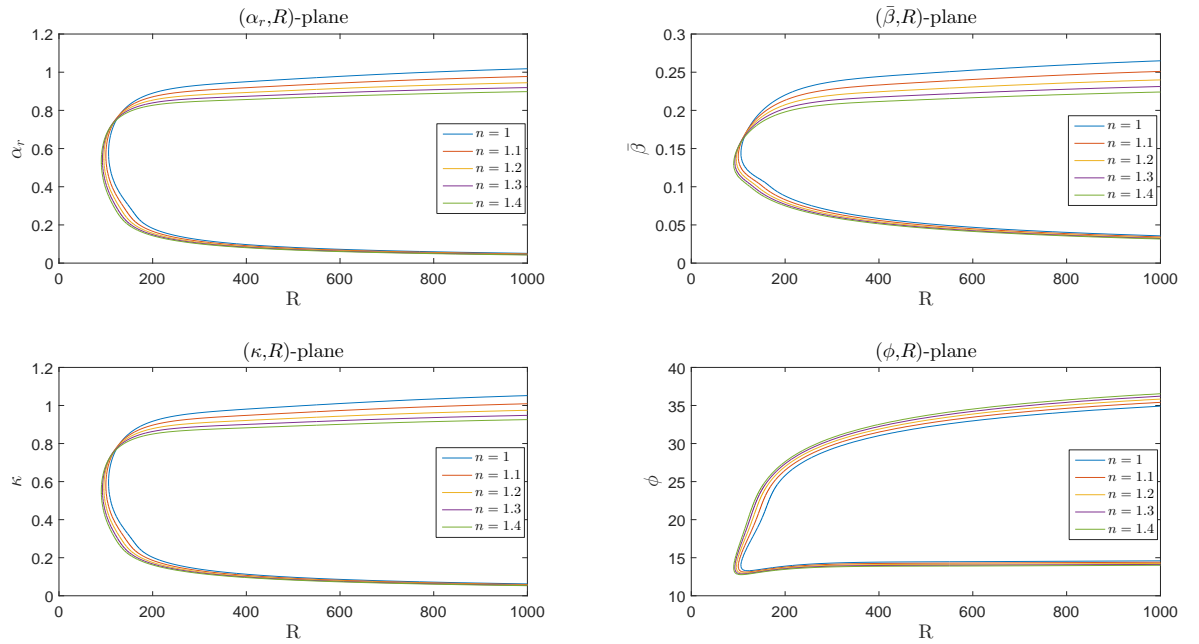

Figure C.21: Neutral curves of the Ekman flow, $Ro = 0$ for shear-thickening Carreau fluids with $n = 1, 1.1, 1.2, 1.3, 1.4$ and $k = ko$.

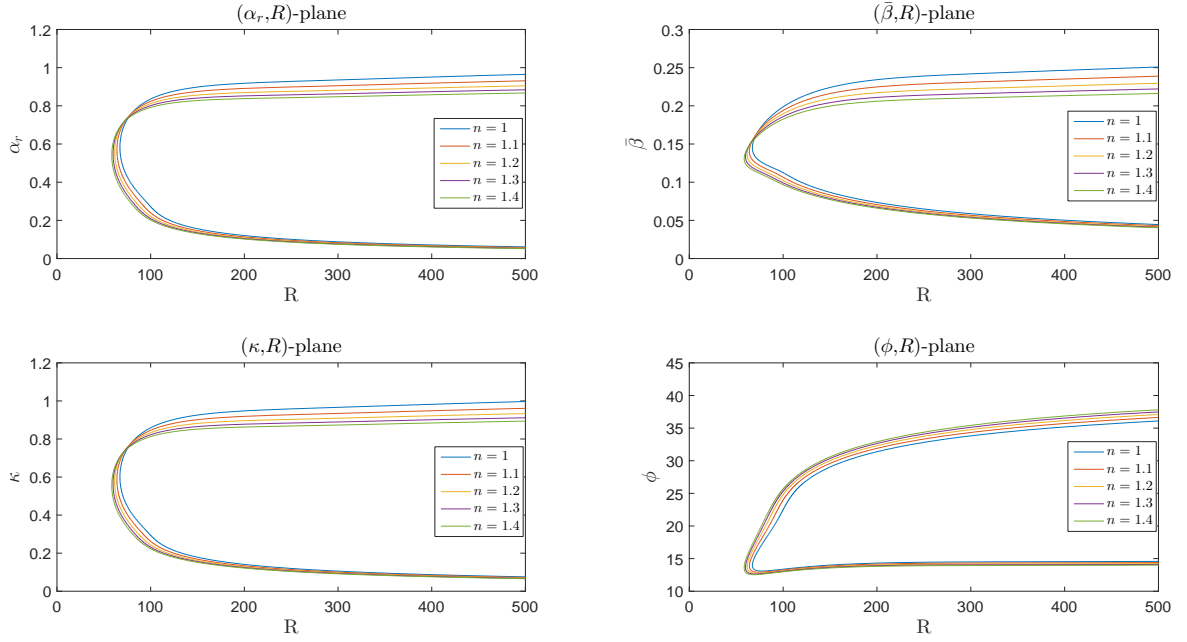Figure C.22: Neutral curves of the flow at $Ro = 0.5$ for shear-thickening Carreau fluids with $n = 1, 1.1, 1.2, 1.3, 1.4$ and $k = ko$.

C.5 Comparative results between the power-law and Carreau fluids

Figure C.23 present the comparative mean flow velocities, convective neutral curves, growth rates and energy balance between shear-thinning power-law and Carreau fluids for Ekman flow, $Ro = 0$.
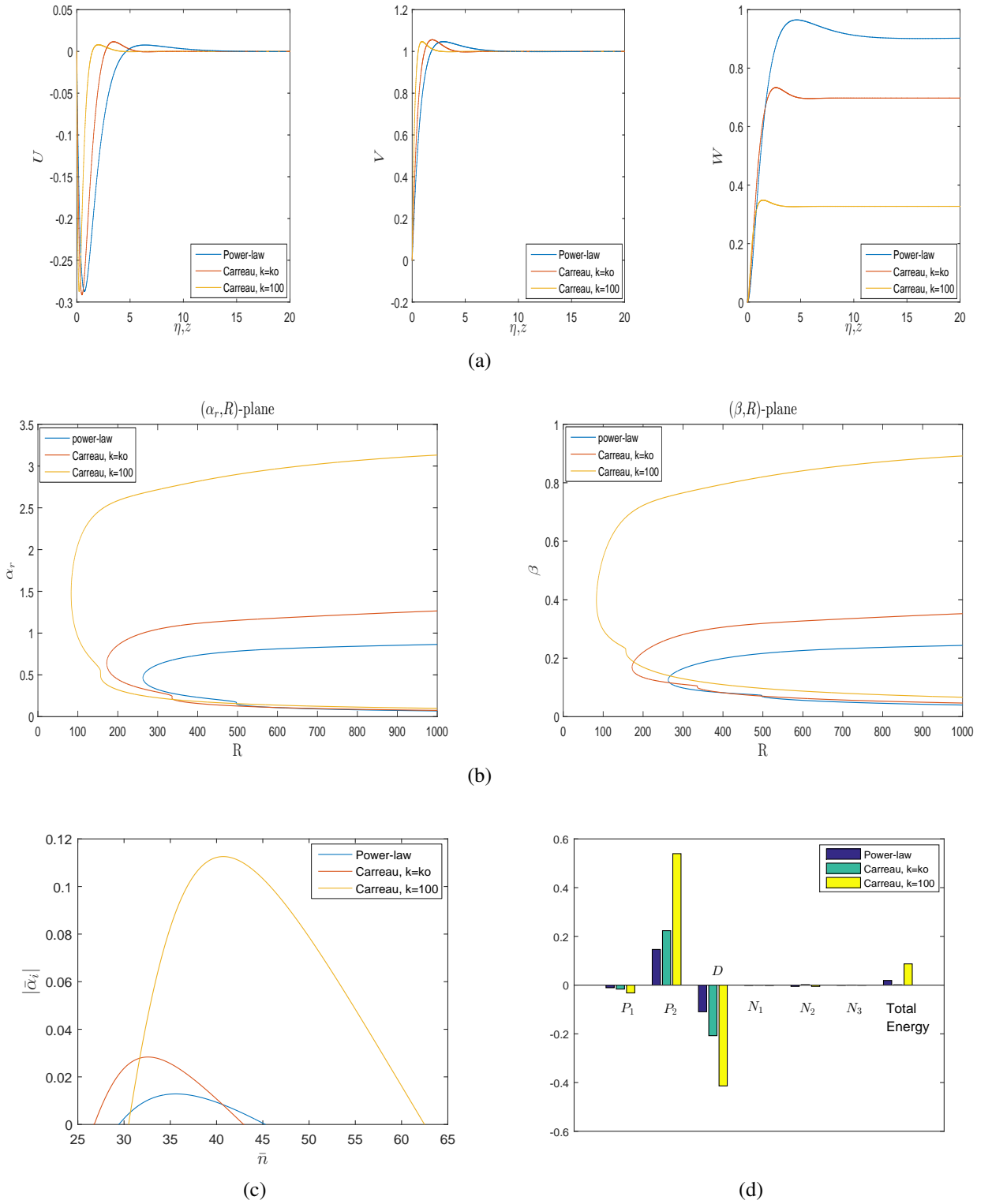
Figure C.23: Comparison of shear-thinning power-law and Carreau fluids for Ekman flow, $Ro = 0$ when $n = 0.6$ for (a) steady mean flow profiles, (b) neutral curves, (c) growth rates and (d) energy balance.

References

Abdulameer, M., Griffiths, P., Alveroğlu, B., Garrett, S. J., 2016. On the stability of the BEK family of rotating boundary-layer flows for power-law fluids. *Journal of Non-Newtonian Fluid Mechanics,* **236**, 63–72.

Alveroğlu, B., 2016. *The Convective Instability of the BEK System of Rotating Boundary-Layer Flows over Rough Disks*. Ph.D. thesis, Department of Mathematics.

Alveroglu, B., Segalini, A., Garrett, S. J., 2016. The effect of surface roughness on the convective instability of the BEK family of boundary-layer flows. *European Journal of Mechanics-B/Fluids,* **56**, 178–187.

Andersson, H., De Korte, E., Meland, R., 2001. Flow of a power-law fluid over a rotating disk revisited. *Fluid Dynamics Research,* **28** (2), 75–88.

Appelquist, E., 2014. *Direct Numerical Simulations of the Rotating-Disk Boundary-Layer Flow*. Ph.D. thesis, KTH Royal Institute of Technology.

Appelquist, E., Schlatter, P., Alfredsson, P., Lingwood, R., 2015. Global linear instability of the rotating-disk flow investigated through simulations. *Journal of Fluid Mechanics,* **765**, 612–631.

Balakumar, P., Malik, M., 1990. Traveling disturbances in rotating-disk flow. *Theoretical and Computational Fluid Dynamics,* **2** (3), 125–137.

Barnes, H. A., Hutton, J. F., Walters, K., 1989. *An Introduction to Rheology*. Vol. **3**. Elsevier.

Batchelor, G. K., 1951. Note on a class of solutions of the Navier-Stokes equations representing steady rotationally-symmetric flow. *The quarterly journal of mechanics and applied mathematics,* **4** (1), 29–41.

Bers, A., 1975. Linear waves and instabilities. In: *Plasma physics–les houches 1972*.

Bingham, E. C., 1916. An investigation of the laws of plastic flow.

Bird, R. B., Armstrong, R. C., Hassager, O., Curtiss, C. F., 1977. *Dynamics of Polymeric Liquids*. Vol. **1**. Wiley New York.

Böedewadt, v. U., 1940. Die drehströmung über festem grunde. *ZAMM-Journal of Applied Mathematics and Mechanics/Zeitschrift für Angewandte Mathematik und Mechanik,* **20** (5), 241–253.

Briggs, R. J., 1964. Electron-stream interaction with plasmas.

Carreau, P. J., 1972. Rheological equations from molecular network theories. *Transactions of the Society of Rheology,* **16** (1), 99–127.

Cochran, W., 1934. The flow due to a rotating disc. In: *Mathematical Proceedings of the Cambridge Philosophical Society*. Vol. **30**. Cambridge University Press, pp. 365–375.

Cooper, A., Carpenter, P. W., 1997. The stability of rotating-disc boundary-layer flow over a compliant wall. Part 1. Type I and II instabilities. *Journal of Fluid Mechanics,* **350**, 231–259.

Cooper, A., Harris, J., Garrett, S. J., Özkan, M., Thomas, P., 2015. The effect of anisotropic and isotropic roughness on the convective stability of the rotating disk boundary layer. *Physics of Fluids,* **27** (1), 014107.

Dabrowski, P. P., 2009. *Boundary-Layer Flows in Non-Newtonian Fluids.* Ph.D. thesis.

Davies, C., Carpenter, P. W., 2003. Global behaviour corresponding to the absolute instability of the rotating-disc boundary layer. *Journal of Fluid Mechanics,* **486**, 287–329.

De Waele, A., 1923. Viscometry and plastometry. *Oil Color Chem Assoc J,* **6**, 33–88.

Denier, J. P., Hewitt, R. E., 2004. Asymptotic matching constraints for a boundary-layer flow of a power-law fluid. *Journal of Fluid Mechanics,* **518**, 261–279.

Ekman, V. W., 1905. On the influence of the earth's rotation on ocean-currents.

Faller, A. J., 1963. An experimental study of the instability of the laminar Ekman boundary layer. *Journal of Fluid Mechanics,* **15** (4), 560–576.

Faller, A. J., 1991. Instability and transition of disturbed flow over a rotating disk. *Journal of Fluid Mechanics,* **230**, 245–269.

Faller, A. J., Kaylor, R. E., 1966. A numerical study of the instability of the laminar Ekman boundary layer. *Journal of the Atmospheric Sciences,* **23** (5), 466–480.

Garrett, S. J., Cooper, A., Harris, J., Özkan, M., Segalini, A., Thomas, P., 2016. On the stability of von kármán rotating-disk boundary layers with radial anisotropic surface roughness. *Physics of Fluids,* **28** (1), 014104.

Garrett, S. J., Hussain, Z., Stephen, S., 2009. The cross-flow instability of the boundary layer on a rotating cone. *Journal of Fluid Mechanics,* **622**, 209–232.

Garrett, S. J., Peake, N., 2002. The stability and transition of the boundary layer on a rotating sphere. *Journal of Fluid Mechanics,* **456**, 199–218.

Gray, W., 1952. The nature of the boundary layer flow at the nose of a swept wing. *Roy. Aircraft Est. TM,* **256**.

Gregory, N., Stuart, J., Walker, W., 1955. On the stability of three-dimensional boundary layers with application to the flow due to a rotating disk. *Philosophical Transactions of the Royal Society of London A: Mathematical, Physical and Engineering Sciences,* **248** (943), 155–199.

Griffiths, P., Garrett, S. J., Stephen, S., 2014a. The neutral curve for stationary disturbances in rotating disk flow for power-law fluids. *Journal of Non-Newtonian Fluid Mechanics,* **213**, 73–81.

Griffiths, P., Stephen, S., Bassom, A., Garrett, S. J., 2014b. Stability of the boundary layer on a rotating disk for power-law fluids. *Journal of Non-Newtonian Fluid Mechanics,* **207**, 1–6.

Griffiths, P. T., 2015. Flow of a generalised Newtonian fluid due to a rotating disk. *Journal of Non-Newtonian Fluid Mechanics,* **221**, 9–17.

Griffiths, P. T., 2016. *Hydrodynamic Stability of Non-Newtonian Rotating Boundary-Layer Flows*. Ph.D. thesis, University of Birmingham.

Hall, P., 1986. An asymptotic investigation of the stationary modes of instability of the boundary layer on a rotating disc. In: *Proceedings of the Royal Society of London A: Mathematical, Physical and Engineering Sciences*. Vol. **406**. The Royal Society, pp. 93–106.

Hussain, Z., Garrett, S. J., Stephen, S., 2011. The instability of the boundary layer over a disk rotating in an enforced axial flow. *Physics of Fluids,* **23** (11), 114108.

Hussain, Z., Garrett, S. J., Stephen, S., 2014. The centrifugal instability of the boundary-layer flow over slender rotating cones. *Journal of Fluid Mechanics,* **755**, 274–293.

Imayama, S., Alfredsson, P. H., Lingwood, R. J., 2014. On the laminar–turbulent transition of the rotating-disk flow: the role of absolute instability. *Journal of Fluid Mechanics,* **745**, 132–163.

Imayama, S., Alfredsson, P. H., Lingwood, R. J., 2016. Experimental study of rotating-disk boundary-layer flow with surface roughness. *Journal of Fluid Mechanics,* **786**, 5–28.

Kierzenka, J., Shampine, L. F., 2001. A BVP solver based on residual control and the maltab PSE. *ACM Transactions on Mathematical Software (TOMS),* **27** (3), 299–316.

Kohama, Y., 1984. Behaviour of spiral vortices on a rotating cone in axial flow. *Acta mechanica,* **51** (3-4), 105–117.

Lilly, D. K., 1966. On the instability of Ekman boundary flow. *Journal of the Atmospheric Sciences,* **23** (5), 481–494.

Lingwood, R., 1996. An experimental study of absolute instability of the rotating-disk boundary-layer flow. *Journal of Fluid Mechanics,* **314**, 373–405.

Lingwood, R., 1997. Absolute instability of the Ekman layer and related rotating flows. *Journal of Fluid Mechanics,* **331**, 405–428.

Lingwood, R., Alfredsson, P., 2000. Experimental study of the stability of the Bödewadt layer. In: *Laminar-Turbulent Transition*. Springer, pp. 553–558.

Lingwood, R., Garrett, S., 2011. The effects of surface mass flux on the instability of the BEK system of rotating boundary-layer flows. *European Journal of Mechanics-B/Fluids,* **30** (3), 299–310.

Lingwood, R. J., 1995. Absolute instability of the boundary layer on a rotating disk. *Journal of Fluid Mechanics,* **299**, 17–33.

Mack, L. M., 1985. The wave pattern produced by a point source on a rotating disk. In: *AIAA, Aerospace Sciences Meeting*.

Malik, M. R., 1986. The neutral curve for stationary disturbances in rotating-disk flow. *Journal of Fluid Mechanics,* **164**, 275–287.

Miklavčič, M., Wang, C., 2004. The flow due to a rough rotating disk. *Zeitschrift für Angewandte Mathematik und Physik (ZAMP),* **55** (2), 235–246.

Ming, C., Zheng, L., Zhang, X., 2011. Steady flow and heat transfer of the power-law fluid over a rotating disk. *International Communications in Heat and Mass Transfer,* **38** (3), 280–284.

Mitschka, P., 1964. Nicht-Newtonsche flüssigkeiten II. Drehströmungen Ostwald-de Waelescher Nicht-Newtonscher Flüssigkeiten. *Collection of Czechoslovak Chemical Communications,* **29** (12), 2892–2905.

Mitschka, P., Ulbrecht, J., 1965. Nicht-Newtonsche flüssigkeiten IV. Strömung nicht-Newtonscher flüssigkeiten Ostwald-de-Waeleschen typs in der umgebung rotierender drehkegel und scheiben. *Collection of Czechoslovak Chemical Communications,* **30** (8), 2511–2526.

Ostwald, W., 1925. Ueber die geschwindigkeitsfunktion der viskosität disperser systeme. i. *Colloid & Polymer Science,* **36** (2), 99–117.

Peyret, R., 2013. Spectral Methods for Incompressible Viscous Flow. Vol. **148**. Springer Science & Business Media.

Pier, B., 2003. Finite-amplitude crossflow vortices, secondary instability and transition in the rotating-disk boundary layer. *Journal of Fluid Mechanics,* **487**, 315–343.

Saric, W., Reed, H., 2003. Crossflow instabilities-theory & technology. In: 41st Aerospace Sciences Meeting and Exhibit. p. 771.

Savaş, Ö., 1987. Stability of Bödewadt flow. *Journal of Fluid Mechanics,* **183**, 77–94.

Smith, N. H., 1947. Exploratory investigation of laminar-boundary-layer oscillations on a rotating disk.

Tatro, P. R., Mollo-Christensen, E., 1967. Experiments on Ekman layer instability. *Journal of Fluid Mechanics,* **28** (3), 531–543.

Thomas, C., 2007. *Numerical Simulations of Disturbance Development in Rotating Boundary-Layers*. Cardiff University (United Kingdom).

von Kármán, T., 1921. Über laminare und turbulente Reibung. *ZAMM-Journal of Applied Mathematics and Mechanics/Zeitschrift für Angewandte Mathematik und Mechanik,* **1** (4), 233–252.

Yoon, M. S., Hyun, J. M., Park, J. S., 2007. Flow and heat transfer over a rotating disk with surface roughness. *International journal of heat and fluid flow,* **28** (2), 262–267.